Genetic and Immunological Dissection of Host Susceptibility to *Cryptococcus neoformans* Infection

Mitra Shourian

Department of Experimental Medicine
McGill University
Montreal, QC, Canada

June 2017

A thesis submitted to McGill University in partial fulfillment of the requirements of the degree of Doctor of Philosophy

To my beloved parents, Parviz and Tahereh

To Mojtaba, Shaghaiegh and Mahla

I am blessed and grateful beyond words to have you in my life…

Acknowledgment

First, I would like to thank my supervisor Dr. Salman Qureshi. Thank you for giving me the opportunity to do research in your lab. Thank you for your support, knowledge and scientific guidance over the past years. Thank you for the peaceful workplace, independence and trust you offered which allowed me to think, plan, study, fail and accomplish. I also highly appreciate your understanding and support while I was writing my thesis.

Thank you to Isabelle Angers for scientific advice, assistance in performing experiments and lab management. A special thank you to Annie Beauchamp for breeding mice and helping me with long animal experiments. In addition, I would like to thank past lab members, Scott Carroll, Erin Lafferty and Adam Flaczyk for training me during my early years in the lab.

I thank my supervisory committee members, Dr. Silvia Vidal, Dr. Danielle Malo, Dr. Maziar Divangahi and Dr. Jacques Lapointe, for taking the time to attend yearly committee meetings and their scientific suggestions. I also thank the RI-MUHC and the Division of Experimental Medicine for their financial support.

Finally, I would like to thank all my friends and family members, who are essential parts of my happiness. I would like to express my gratitude and love to Damien, for invaluable support, love and encouragement especially while I was writing my thesis. A special thank you to Sedighe and Soroor my lovely friends for daily talks, support and friendship.

Table of Contents

Abstract

Cryptococcus neoformans, the major cause of human cryptococcosis, is an encapsulated yeast that is ubiquitously distributed in the environment. In individuals with a defective immune response, uncontrolled replication of *C. neoformans* in the lung may result in dissemination to other parts of the body with a tropism for the brain. Notably, not all immune compromised hosts develop disease following cryptococcoccal infection while some individuals deemed immune competent exhibit severe illness; therefore, it is believed that yet uncharacterized genetic factors play an important role in determining the susceptibility to progressive infection. The overall aim of this Ph.D. project was to dissect the genetic and immunological aspects of host susceptibility to *C. neoformans* by applying both forward and reverse genetic methods in a well-established and clinically relevant mouse model of infection.

Our laboratory previously identified *Cnes2* on mouse chromosome 17 (31.1 Mb) as a region associated with susceptibility to progressive *C. neoformans* 52D infection, using genome-wide linkage analysis between susceptible C57BL/6N and resistant CBA/J mouse strains and lung fungal burden as a quantitative trait. By constructing a congenic strain on the C57BL/6N background (B6.CBA-*Cnes2*), I validated and characterized the role of *Cnes2* locus during the host response. Phenotypic analysis of B6.CBA-*Cnes2* mice 35 days after *C. neoformans* infection showed a significant reduction of fungal burden in the lung and spleen compared to C57BL/6N mice. The immune response of B6.CBA-*Cnes2* congenic mice was characterized by a significantly higher expression of type 1 cytokines and greater numbers of lung neutrophils, antigen-presenting cells, and Th1 $CD4^+$ lymphocytes compared to that in C57BL/6N mice. Taken together, these findings demonstrated that the *Cnes2* interval is a potent regulator of host defense and differential Th1/Th2 polarization following *C. neoformans* infection.

With the goal of identifying the underlying susceptibility genes encoded within the *Cnes2* locus that regulate the host response to *C. neoformans* infection, we generated four sub-congenic strains (*Cnes2.1*-*Cnes2.4*). Analysis of lung fungal burden, cell infiltration, and histopathology indicated that two sub-intervals within *Cnes2* regulate susceptibility to *C. neoformans* infection: *Cnes2.2 and Cnes2.4.* In addition, we conducted an extensive *in silico* candidate gene analysis using publicly available genome browsers and we identified 2 protein coding genes within *Cnes2.2*

(*Fpr3 and Fpr-rs4*) and 10 protein coding genes within *Cnes2.4* (*Notch3*, *Ager*, *H2-Ab1*, *Myo1f*, *Ubash3a, Tap1, H2-Eb1, H2-Oa, C5b and Lst1*) as potential candidate genes. This data provides a foundation for further detailed investigation of the causative genes and variants that mediate host resistance to cryptococcal infection.

IL-1α and IL-1β are pro-inflammatory cytokines that are highly induced following *C. neoformans* infection. The final goal of the last chapter of this thesis was to determine the role of IL-1RI (a common receptor for IL-1α and IL-1β) signaling in cryptococcal infection by applying reverse genetic approaches. Our findings demonstrate that IL-1RI$^{-/-}$ mice (on the BALB/c background) have a significantly higher fungal burden in the lungs and brain as well as a significantly higher mortality when compared to WT mice. In IL-1RI$^{-/-}$ mice, *C. neoformans* 52D infection is associated with lung eosinophilia, elevated airway mucus secretion, greater recruitment of M2 macrophages and CD4^{+} Th2 cells, as well as significantly fewer lung neutrophils and Th17 cells at early and late time points post-infection. Taken together, our analysis shows that IL-1R plays an essential role in protection against lethal *C. neoformans* infection by triggering a complex innate and adaptive immune response and raises the possibility that modulation of this signaling axis could be a potential therapeutic strategy.

Résumé

Cryptococcus neoformans, la principale cause de la cryptococcose humaine, est une levure encapsulée répartie de façon omniprésente dans l'environnement. Chez les individus atteints d'une réponse immunitaire défectueuse, la réplication incontrôlée de *C. neoformans* dans le poumon peut entraîner la dissémination dans d'autres parties du corps avec un tropisme pour le cerveau. Notamment, les hôtes immunodéprimés ne développent pas tous de maladie après une infection cryptococcique alors que certaines personnes avec un système immunitaire jugé compétent présentent une maladie grave; par conséquent, des facteurs génétiques encore non-caractérisés pourraient jouer un rôle important dans la détermination de la susceptibilité à une infection progressive. Le but général de ce projet de doctorat était de disséquer les aspects génétiques et immunologiques de la susceptibilité de l'hôte à *C. neoformans* en appliquant des méthodes d'investigations génétiques dans un modèle de souris bien établi et cliniquement approprié.

Notre laboratoire à précédemment identifier *Cnes2* sur le chromosome 17 de la souris (31,1 Mb) comme une région associée à la sensibilité à une infection progressive de *C. neoformans* 52D, en utilisant l'analyse de liaison génomique entre la souche de souris sensible C57BL/6N et la souche résistante CBA/J et le fardeau fongique pulmonaire comme caractéristique quantitative. En construisant une souche congénique à partir de la souche C57BL/6N (B6.CBA-*Cnes2*), j'ai validé et caractérisé le rôle du locus *Cnes2* pendant la réponse de l'hôte. L'analyse phénotypique des souris B6.CBA-*Cnes2* à 35 jours après l'infection à *C. neoformans* a montré une réduction significative du fardeau fongique dans le poumon et la rate par rapport aux souris C57BL/6N. La réponse immunitaire des souris congénitales B6.CBA-*Cnes2* a été caractérisée par une expression significativement plus élevée de cytokines de type 1 et d'un plus grand nombre de neutrophiles pulmonaires, de cellules présentatrices d'antigène et de lymphocytes Th1 $CD4^+$ comparés à ceux des souris C57BL/6N. Ensemble, ces résultats ont démontré que l'intervalle *Cnes2* est un régulateur puissant de la défense de l'hôte et de la polarisation différentielle Th1/Th2 suite à une infection par *C. neoformans*.

Dans le but d'identifier les gènes de susceptibilité sous-jacents codés dans le locus *Cnes2* qui régulent la réponse de l'hôte à une infection par *C. neoformans*, nous avons généré quatre souches sous-congéniques (*Cnes2.1*-*Cnes2.4*). L'analyse du fardeau fongique pulmonaire, de l'infiltration cellulaire et de l'histopathologie a indiqué que deux loci au sein de *Cnes2* régulent la sensibilité à

l'infection à *C. neoformans*: *Cnes2.2* et *Cnes2.4*. En outre, nous avons mené une vaste analyse de gènes candidats *in silico* à l'aide de navigateurs de génome accessibles au public et nous avons identifié 2 gènes de codage de protéines dans *Cnes2.2* (*Fpr3* et *Fpr-rs4*) et 10 gènes de codage de protéines dans *Cnes2.4* (*Notch3, Ager, H2 -Ab1, Myo1f, Ubash3a, Tap1, H2-Eb1, H2-Oa, C5b* et *Lst1*) en tant que gènes candidats potentiels. Ces données fournissent une base pour une étude détaillée approfondie des gènes responsables et des variantes qui servent de médiation à la résistance de l'hôte à une infection cryptococcique.

Enfin, l'objectif du dernier chapitre de cette thèse était de déterminer le rôle de la signalisation IL-1RI (récepteur commun pour IL-1α et IL-1β) dans une infection cryptococcique en appliquant des approches génétiques inverses. L'IL-1α et l'IL-1ß sont des cytokines pro-inflammatoires fortement induites suite à une infection par *C. neoformans*. Nos résultats démontrent que les souris IL-1RI$^{-/-}$ (souche BALB/c) ont un fardeau fongique significativement plus élevé dans les poumons et le cerveau ainsi qu'une mortalité significativement plus élevée en comparaison aux souris WT. Chez les souris IL-1RI$^{-/-}$, l'infection par *C. neoformans* 52D est associée à l'éosinophilie pulmonaire, à la sécrétion de mucus des voies respiratoires élevées, à un recrutement plus important de macrophages M2 et de cellules CD4^{+} Th2, ainsi qu'à un nombre significatif de neutrophiles et de cellules Th17 à des points-temps précoces et tardifs post-infection. Notre analyse montre que l'IL-1R joue un rôle essentiel dans la protection contre l'infection létale de *C. neoformans* en déclenchant une réponse immunitaire innée et adaptative complexe et soulève la possibilité que la modulation de cet axe de signalisation puisse être une stratégie thérapeutique potentielle.

Contribution of Authors and Statement of Originality

This thesis is structured based on a manuscript format, consisting of one published (chapter 2), one under review (chapter 4) and one will be submitted later (chapter 3).

Unless otherwise stated, Mitra Shourian designed and performed all experiments, analyzed and interpreted the data, and wrote the manuscripts. Dr. Salman Qureshi conceived the studies, contributed to the design of experiments and interpretation of the data, provided crucial guidance and advice, and extensively edited all manuscripts.

Chapter 2 – The *Cnes2* locus on mouse chromosome 17 regulates host defense against cryptococcal infection through pleiotropic effects on host immunity. *Infection and Immunity*
Authors: Mitra Shourian, Adam Flaczyk, Isabelle Angers, Barbara C. Mindt, Jörg H. Fritz, Salman T. Qureshi.
Contributions: Adam Flaczyk assisted in performing intracellular cytokine staining presented in Figure 2.8. Isabelle Angers conducted all congenic mouse breeding and genotyping, and Barbara C. Mindt performed ELISA of serum antibody presented in Figure 2.9. Jörg H. Fritz provided valuable feedback in drafting the manuscript.

Scientific contributions: For the first time, this work shows the significant role of the *Cnes2* locus on mouse chromosome 17 in regulating host response to *C. neoformans* infection.

Chapter 3 – Phenotypic analysis of *Cnes2* sub-congenic mice reveals two different intervals associated with resistance to *C. neoformans 52D* infection. *Manuscript in preparation*.

Authors: Mitra Shourian, Isabelle Angers, Salman T. Qureshi.
Contributions: Isabelle Angers conducted breeding and generation of sub-congenic mice, genotyping and assisted with *in silico* candidate gene analysis.
Scientific contributions: This work shows for the first time that two separate regions within *Cnes2* interval on mouse chromosome 17 regulate the host response to *C. neoformans* infection. Using *in silico* analysis, in total of 12 candidate genes are proposed for further investigations.

Chapter 4 – Essential role of IL-1RI signaling in protection against *Cryptococcus neoformans 52D* infection. *Under revision*

Authors:

Mitra Shourian, Ben Ralph, Isabelle Angers, Donald C. Sheppard, Salman T. Qureshi

Contributions: Isabelle Angers conducted breeding, generation, and genotyping of mice, Benjamin Ralph performed the IL-1 alpha ELISA assay presented in Figure 4.3.

Scientific contributions: For the first time this study indicates that IL-1RI-dependent signaling is necessary for host resistance against progressive cryptococcal infection. Deficient IL-1 signaling broadly impairs the innate and adaptive host immune response against *C. neoformans*.

Chapter 1

Introduction

1.1. *Cryptococcosis* as a global health threat

1.1.1. Importance of invasive fungal diseases

The incidence of invasive fungal diseases associated with more than 1.3 million global mortality has increased during the past several decades (2, 4, 5). This increase is attributable to the rising numbers of people with weakened immune systems who are at risk for the development of serious fungal infections. The risk factors for invasive mycoses include blood and marrow transplantation (BMT), solid-organ transplantation, major surgery (especially gastrointestinal surgery); AIDS, neoplastic disease, advanced age, prematurity, and immunosuppressive therapy (4, 5). More than 90% of all reported fungal-related deaths result from species that belong to one of the following four genera: *Cryptococcus*, *Candida*, *Aspergillus*, and *Pneumocystis*. Recently, it has been estimated that more people die from the 10 top invasive fungal diseases than tuberculosis or malaria (6). Because of similarities between eukaryotic fungi and humans, treatment of fungal infections is more difficult compared to bacterial and viral infections, and therefore fewer antifungal drugs are available (3). In addition to delays in diagnosis, antifungal therapy has been less successful because of toxicity, a narrow spectrum of activity, detrimental drug interactions, the development of drug resistance, and treatment cost (7). A better understanding of the key mechanisms of host immunity to fungi and greater knowledge of infection risk factors will be important for future development of new and more effective approaches to preventing and treating fungal diseases (3, 7).

1.1.2. Epidemiology of *Cryptococcus* sp.

Cryptococcosis, also known as cryptococcal disease, is mainly caused by *Cryptococcus neoformans* and *Cryptococcus gattii*. Human cryptococcosis was first identified in 1894 but the disease only became widely recognized with the onset of the AIDS pandemic in the 1980s, and it became a common AIDS-associated illness in patients with greatly reduced T-cell function (5-8% of HIV-infected persons) (8, 9). Cryptococcosis most commonly presents as a disseminated disease characterized by meningoencephalitis, skin lesions, and/or fungemia (10, 11). Isolated pneumonia that precedes these systemic manifestations can also occur; however, cryptococcal pneumonia is underdiagnosed because it manifests with nonspecific respiratory symptoms.

Pulmonary infection has been reported in 10-55% of patients with HIV-associated cryptococcal meningitis (12, 13). Development of pulmonary cryptococcosis as a sole manifestation of disease is more common in non-immunocompromised patients compared to immunocompromised hosts (14).

The advent of combination antiretroviral therapy along with fluconazole therapy in mid-1990s helped to reduce the incidence of cryptocccosis; however, in parts of the developing world where access to antiretroviral therapy (ART) and antifungal therapy are limited, it remains an important clinical problem (8, 15, 16). In addition, even with antifungal therapy, one-third of patients with cryptococcal meningitis still have a positive CSF culture at 10 weeks and acute mortality has remained at 35-40%, both in resource-rich and resource-poor settings (8, 17, 18). In 2009, the global burden of cryptococcal meningitis among persons living with HIV/AIDS was estimated to be 950,000 cases with approximately 625,000 deaths annually (9). The majority of disease burden is in sub-Saharan Africa where the mortality rate may exceed deaths from tuberculosis (720,000 cases; range, 144,000 to 1.3 million) (9). In Uganda, the prevalence of serum cryptococcal antigen among patients with a $CD4^+$ T cell count $\leq$100 cells/μL has been reported to be 8.8 percent (19). Significant morbidity and mortality has been also reported in Southeast Asia and the USA (20) (Figure 1.1). According to a report in 2015 by US Centers for Disease Control and Prevention, the annual incidence of cryptococcosis is currently 0.4-1.3 cases per 100,000 persons in the general population, 2 to 7 cases per 1,000 AIDS patients, and 0.3 to 5.3 cases per 100 transplant patients (1). Another report in 2015 from analysis of stored serum samples of HIV-infected persons during 1986-2012 indicated the overall prevalence of cryptococcal antigen was 2.9 percent (1, 21).

Although cryptococcosis is mainly caused by *C. neoformans* in individuals with cell-mediated immune deficiencies, *C. gattii* predominantly causes disease in persons with apparently normal immune systems (72 to 100%) (22). Worldwide, *C. gattii* infections have mainly occurred in Papua New Guinea, Australia, and South America. Recent outbreaks of *C. gattii* infection have occurred in British Columbia, Canada (218 cases reported during 1999 – 2007) and in the US Pacific Northwest (96 cases reported during 2004 – 2011) (22-27). In fact, in more developed countries, *C. gattii* infection occurs mainly in non-HIV infected individuals including transplant recipients, patients who are receiving immunosuppressive agents such as glucocorticosteroids, cytotoxic chemotherapy, TNF-α inhibitors, and other disease modifying agents, and a heterogeneous group

of patients with underlying disorders such as organ failure syndromes, innate immunologic problems, common variable immunodeficiency, and hematologic disorders (14). In addition, 17%-22% of cases of cryptococcosis occur in phenotypically normal or otherwise clinically non-immunocompromised patients (14, 28). Despite the development of antifungal therapy, cryptococcal disease in HIV-negative hosts continues to be associated with extensive morbidity and mortality. In a study of 207 patients from 2012, 86 (42%) were HIV-positive, 42 (20%) were transplant recipients, and 79 (38%) were HIV-negative/non-transplant (28, 29).

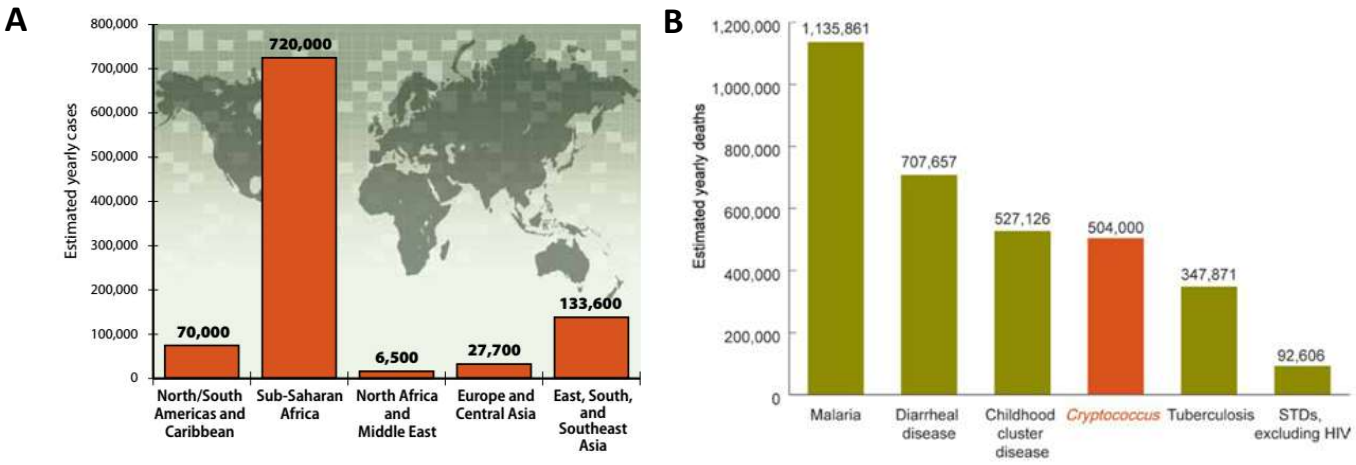

Figure 1.1. A: global burden of HIV-related cryptococcal meningitis**.** B: Causes of death in sub-Saharan Africa, excluding HIV/AIDS. Taken from Ref (1) with permission.

1.2. The pathogen *Cryptococcus*

1.2.1. Taxonomy

C. neoformans is a spherical yeast with a diameter of 4-6 µm that is classified in the phylum basidiomycota which also includes mushrooms, wood-rotting fungi, and several common plant pathogens (3). *Cryptococcus sp.* is surrounded by a thick polysaccharide capsule and is often referred to as "sugar-coated yeast" (30). It was first described as human pathogen in 1894 by pathologist Otto Busse and surgeon Abraham Buschke and given the name "*Saccharomyces-like"* and *Saccharomyces neoformans;* however, in 1901 Jean-Paul Vuillemin renamed the organism ~~to~~ *Cryptococcus neoformans* (31). The genus *Cryptococcus* contains around 37 species; however, the vast majority of human infections are caused by *Cryptococcus neoformans* and *Cryptococcus*

gattii. Based on antigenic specificity of the capsule, these two species are further classified into different varieties and serotypes. *C. neoformans* includes three varieties, *C. neoformans* var. *grubii* (serotype A), *C. neoformans* var. *neoformans* (serotype D), and a hybrid (serotype AD) while *Cryptococcus gattii* includes serotypes B and C (Figure 1.2) (32, 33). *C. neoformans* var. *grubii* (serotype A) and *C. neoformans* var. *neoformans* (serotype D) generally cause disease in immunocompromised patients and are responsible for 70-95% and 5-15% of clinical infections, respectively. *C. gattii (serotype B*) is responsible for less than 1% of infections, has a tropism for individuals with normal immune responses, and is believed to be clinically more virulent than *C. neoformans* (3, 34-36). Recently, based on whole genome sequence analysis, division of *C. neoformans* into two separate species (*C. neoformans* and *C. deneoformans*) and *C. gattii* into a total of five species (*C. gattii, C. bacillisporus*, *C. deuterogattii, C. tetragatti,* and *C. decagattii*) has been proposed (8). Nevertheless, it is currently recommended to use "*C. neoformans* species complex" and "*C. gattii* species complex" as these seven species are not yet known to be clinically distinguishable, and more detailed studies with a larger number of isolates are needed to identify the clinical and biological relevance of the new species (37).

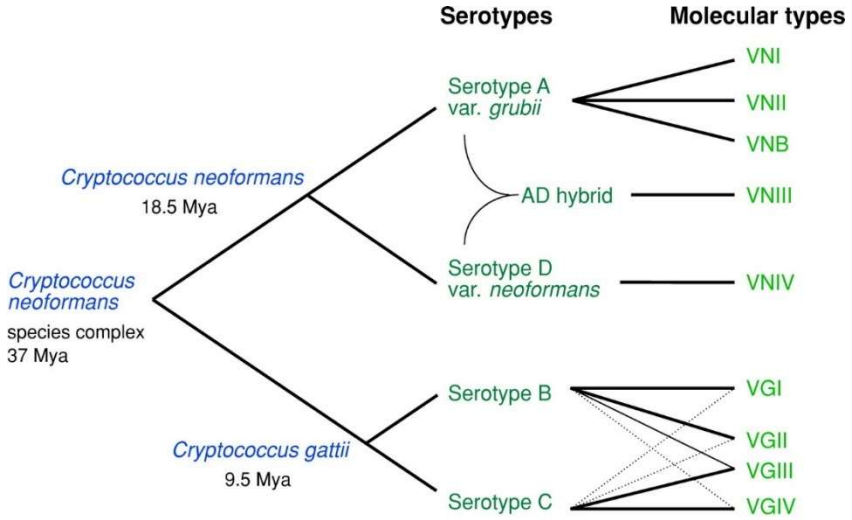

Figure 1.2. Evolution of the *C. neoformans* species complex. The *Cryptococcus* species complex contains at least two subspecies, *C. neoformans* and *C. gattii*, which diverged from a common ancestor. They are further divided into four serotypes consisting of at least nine molecular types. Solid, thin, and dashed lines indicate the prevalence of the respective serotype in each molecular type. Taken from Ref (2) with permission.

C. neoformans does not require a host to reproduce or survive in the environment, and therefore it is considered as an accidental human pathogen (10, 38). In the environment, *C. neoformans* has been found distributed worldwide and mainly associated with soils, several tree species, pigeon droppings, and urban environments. In contrast, *C. gattii* is mainly found in tropical and sub-tropical areas on decaying material and wood from eucalyptus trees; although recently it has been also isolated from other tree species, environmental sources, and geographical areas (2, 39-41). Both *C. neoformans* and *C. gattii* can survive and replicate in free-living amoebae and soil nematodes and many of the *C. neoformans* genes that are required for human disease are also required for infection, survival, and killing of amoebae, nematodes, and insects (8). Cryptococcosis occurs in domestic animals such as cats, dogs, cattle, pigs, guinea pigs, rabbits, horses, sheep, and goats, and also in wild animals such as birds, koalas, ferrets, mice, and foxes (42). In both animals and humans, *Cryptococcus* can reside in organs such as the skin, eyes, heart, bones, joints, lungs, prostate gland, urinary tract, and central nervous system. With some rare exceptions, animal to animal or human to human transmission has not been described (2).

1.2.3. Life cycle

C. neoformans is mainly isolated from the environment as a poorly encapsulated cell and from patients as a budding yeast; however, it can also undergo dimorphic transition to a filamentous growth form with two different differentiation pathways: mating and monokaryotic fruiting. *C. neoformans* cells isolated from the environment and cultured in the laboratory have two forms, MATa and MATα. MATα is the mating type isolated from clinical samples and is more virulent than MATa. The filamentous cell type that is generated from mating between MATa and MATα contains both nuclei as a dikaryon and produces chains of haploid spores following nuclear fusion, meiosis, and sporulation. In contrast, sexual reproduction between the same mating type can also produce a filamentous cell as a monokaryon, which also generates spores. Monokaryotic fruiting is observed mainly in MATα type (2, 3, 8, 27, 43) (Figure 1.3).

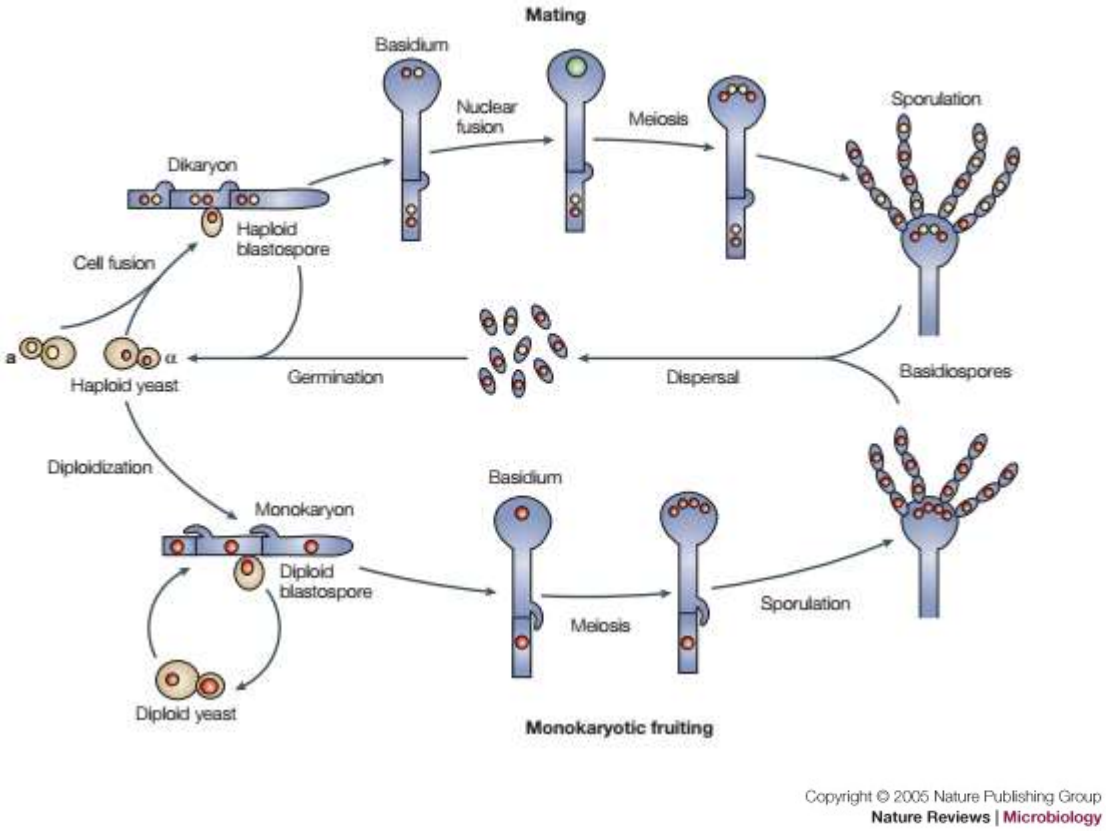

Figure 1.3. Model of *C. neoformans* life cycle. In response to nutrient limitation, a and α yeast cells secrete peptide pheromones that trigger cell–cell fusion. The resulting dikaryon initiates filamentous growth. The two parental nuclei migrate coordinately in the dikaryotic hyphae and as each septum forms to separate the cells, one nucleus is transferred to the penultimate hyphal cell through a clamp connection. At the stage of basidium development, the two nuclei fuse and undergo meiosis to produce four meiotic products that undergo mitosis and bud from the surface of the basidium to produce chains of basidiospores. During monokaryotic fruiting, cells of one mating type, for example, α cells, become diploid cells α/α, either by endoduplication or by nuclear fusion following fusion of two cells. The diploid monokaryotic hyphae form rudimentary clamp connections, but these are not fused to the preceding cell. At the stage of basidium development, meiosis occurs and haploid basidiospores are produced in four chains. Taken from Ref (3) with permission.

1.2.4. Virulence factors

Cryptococcus contain several virulence factors that are required to reside in the environment and survive within the host. The principal virulence factors are a polysaccharide capsule, melanin production, the ability to grow physiological temperature and low pH, and the secretion of extracellular enzymes (11, 44) (Table1.1). It has been shown that *Cryptococcus* virulence factors are exported to the host environment by extracellular vesicles (EVs), also named as "virulence bags" (45). EVs contain capsule components, nucleic acids, and many virulence-associated proteins and enzymes including laccase and urease. Cryptococcal EVs have shown to be biologically and immunologically active and are important for cell-cell communication, pathogenesis and regulation of the host response (45-49).

Morphological adaptation and formation of "Titan cells" is also one of virulence-associated characteristic of *C. neoformans*. *Cryptococcus sp.* can enlarge its capsule size during infection which helps to avoid phagocytosis and the stressful intracellular host environment. Titan cells with a diameter of 12-100 μm have been observed mainly in the lungs of infected mice by different cryptococcal strains (both serotype A and D, including standard laboratory strains such as H99 or 24067, and clinical isolates). These enlarged cells have been detected in polypoid and uninucleate forms, meaning that they are result of DNA replication without cell division (27, 50-53). In addition to well-known cryptococcal virulence factors, recent studies have found the transcription regulation networks and new enzymes associated with cryptococcal virulence, resistance, and survival in the host and environment including a zinc transporter *(Zip1)*, isopropyl malate dehydrogenase *(Leu1)*, inositol polyphosphate kinase *(Kcs1)*, membrane high affinity Cch1-Mid1 calcium channel *(CMC)* and C_2H_2 zinc finger transcription factor *(Usv101)* (54-57).

Table 1.1. *C. neoformans* Virulence Factors.

Characteristic		Description/function	Refs
Polysaccharide Capsule		The most distinctive feature of *C. neoformans*, mostly composed of glucuronoxylomannan (GXM) and galactoxylomannan (GalXM); it prevents phagocytosis, quenches free radical bursts, interferes with immune responses and protects the fungus from desiccation.	**(44, 58-65)**
Melanin		Accumulates in the *C. neoformans* cell wall; considered to be a powerful antioxidant that also protects against UV radiation, heat and cold, and contributes to acquired resistance against to the antifungal drugs.	**(44, 66-68)**
Growth at physiological temperature and tolerance of low pH		Survival and persistence in the host and environment.	**(69-74)**
Extracellular Enzymes	**Urease**	Benefits the fungus in the environment by converting urea to a usable nitrogen source and plays a role in fungal migration across the blood-brain barrier.	**(44, 75, 76)**
	Superoxide dismutase	Facilitates growth within macrophages by protection of the fungus against superoxide.	**(44, 77)**
	Phospholipases	Promote fungal invasion of host tissue by hydrolysis of phospholipids in lung surfactant and the plasma membrane; contributes to fungal survival by maintenance of cell wall integrity and provision of nutrients.	**(78, 79)**
	Proteases	Proteolytic activity; degrade immunologically important proteins, contribute to tissue invasion, colonization, and suppression of host immune response.	**(80, 81)**

1.3. Human *Cryptococcosis*

1.3.1. Pulmonary infection

Exposure to *C. neoformans* is common because most people develop cryptococcal antibodies by school age (82). It is hypothesized that the initial exposure occurs through inhalation of spores or small desiccated yeast cells also known as propagules (1–5 μm in size) that enter the lower respiratory tract (8). In mouse models of infection there is some evidence that spores could be effective infectious particles and cause morbidity and mortality equivalent to parental yeast strains, but the interaction of spores and yeast cells with the host immune cells are different (83). In contrast to *C. neoformans* yeast cells, spores can be phagocytosed by macrophages in culture in the absence of opsonization; however, opsonized yeast that are phagocytosed by activated macrophages are more resistant to macrophage killing mechanisms compared to phagocytosed spores (83-85).

In an immunocompetent host, *Cryptococcus sp.* may be cleared by immune cells or stay in the lung inside macrophages and multinucleated giant cells in granulomas and establish latent infection until the host immune status changes from immunocompetent to immunocompromised (53, 72, 86). Most patients with pulmonary cryptococcosis are asymptomatic or have non-specific signs and symptoms of pneumonia with cough, scant mucoid sputum, pleuritic chest pain, fever, and dyspnea; however, life-threatening pneumonia with respiratory failure can occur, mainly in immunocompromised individuals (39, 87).

1.3.2. Cryptococcal meningitis (CM)

Although *Cryptococcus sp.* can infect any organ in the body, it shows a clear preference for the central nervous system (CNS). Cryptococcal meningitis can occur following a primary infection of the lung or by reactivation and dissemination of latent pulmonary infection upon subsequent immunosuppression. The reasons for the CNS tropism are not known; however, the brain may provide preferred substrates for *C. neoformans* growth and survival or it may function as a niche that protects the organism from certain elements of the host immune response. In addition, during systemic infection specific receptors on neuronal cells may preferentially attract *Cryptococcus sp.* to the brain and divert them from other tissues (2). Based on experimental observations, *C.*

neoformans can cross the Blood Brain Barrier (BBB) by three different mechanisms: 1) Paracytosis: *C. neoformans* uses enzymes such as protease and urease to enhance migration through endothelial cell tight junctions 2) Transcytosis: Endothelial cells lining the blood vessels in the brain internalize the fungus and transmigrate it through the cytoplasm to reach the brain tissue. 3) Trojan horse: Phagocytic cells that have engulfed *C. neoformans* cross the endothelium and transfer the organism to the brain by a hitch-hiking mechanism (8, 27). Meningoencephalitis is the main clinical presentation for *C. neoformans* infections, occurring in 90% of HIV-positive and 70% of HIV-negative individuals (88). In the HIV-positive patient, cryptococcal meningitis is a late opportunistic infection that usually occurs when the $CD4^+$ T-lymphocyte count falls below 50-100 cells/mm^3. Overwhelming cryptococcal infection of the meninges and brain tissue results in high intracranial pressure and is universally fatal if not treated. The clinical signs and symptoms may vary; fever, headache, fatigue, and visual problems are more frequently observed in the HIV-positive subjects, while altered mental status is more common among HIV-negative individuals (8, 15, 39, 89).

1.3.3. Diagnosis and treatment

Conventional diagnosis of cryptococcosis in suspected individuals is achieved by direct examination and identification of the fungus by microscopy and culture of infected tissues and detection of cryptococcal antigen (CrAg) in body fluids such as sputum, CSF and urine. Rapid diagnostic methods include detection of cryptococcal antigen by Latex Agglutination test, lateral flow immunochromatographic assay (LFA), or enzyme immunoassay (EIA) on cerebral spinal fluid or serum (90, 91). A positive CrAg result may precede clinical signs or symptoms by several weeks to months and has potential utility for screening of high-risk individuals or for initiation of pre-emptive therapy. The antifungal drug regimen that is recommended for the initial treatment of cryptococcal meningitis is a combination of intravenous liposomal amphotericin B and flucytosine. If flucytosine is unavailable, the combination of amphotericin B and a high dose of fluconazole is a recommended alternative (90, 92, 93). The fungicidal effect of amphotericin B is mediated by binding to ergosterol; this interaction creates pores that results in leakiness of the fungal cell membrane and induction of cell death through oxidative damage (8). Amphotericin B is expensive and not easily available in resource-limited areas; in addition, it may cause life-threatening and toxic side effects such as renal failure which requires further monitoring and

hospitalization (94). AmBisome® is an alternative liposomal formulation of amphotericin B with less toxic effects; however, it is more expensive (78, 95). Fluconazole is less effective than the combination of amphotericin B and flucytosine, but it is important for maintenance treatment to prevent recurrence of cryptococcal meningitis in recovering patients (15). Sertraline, which is an antidepressant drug, has recently been shown to have *in vitro* antifungal activity and is effective during experimental cryptococcosis. It is now in clinical trials, either alone or as an adjuvant, and could be a potentially inexpensive alternative for therapy of cryptococcal infection (96-99). Finally, monoclonal antibodies such as GXM IgG1 and recombinant interferon gamma have been used as adjuvants in clinical trials of cryptococcal meningitis therapy in HIV-infected patients (10, 93, 100). Administration of recombinant interferon in addition to standard treatment resulted in improved cryptococcal clearance; however, no significant difference in mortality has been observed (101, 102).

1.4. Immune response to cryptococcal infection

1.4.1. Innate immune response

When *Cryptococcus sp.* enters the lung, its first interaction is with pulmonary epithelial cells. *In vitro* studies have shown that cryptococci can adhere to pulmonary epithelial cells, be internalized and activate them to release cytokines and chemokines such as IL-8 and CXCL1 (103-106) Alveolar macrophages are most likely the first phagocytes and antigen presenting cells (APCs) that encounter *Cryptococcus sp.* in the lung (107-109). Macrophages alone are unable to clear the infection and an adaptive immune response and granuloma formation is required in protective response against cryptococcal infection (110). Depending on the immune status of the host and cytokine milieu, macrophages can polarize to M1 or M2 phenotypes (10, 111-113). IFN-γ, TNF-α and LPS are the most responsible stimuli for M1 macrophage polarization (114). M1-polarized macrophages (classically activated), produce high levels of reactive oxygen and nitrogen species and pro-inflammatory cytokines, promote protective Th1 immune responses, and have stronger fungicidal properties compared to the M2 phenotype. The hallmark of M1 activation is the production of inducible nitric oxide synthase (iNOS) which acts on arginine and reduces it to citrulline and nitric oxide (NO). Exposure to Th2-type cytokines such as IL-4 and IL-13 leads to the differentiation of M2 (alternatively activated) macrophages which are less fungicidal and non-

protective against cryptococcal infection. The classical markers of M2 macrophage activation are chitinase-like 3 (*Ym1*), found in inflammatory zone (*Fizz1*), mannose receptor (*Cd206)* and arginase-1 (*Arg1*) (111-113, 115, 116). In general, experimental pulmonary infection with highly virulent *Cryptococcus* strains result in induction of strong Th2-type responses and polarization of M2 skewed macrophages (10).

The complex interaction of macrophages with *Cryptococcus sp.* leads to a variety of different outcomes: 1) intracellular killing of the fungus, 2) lysis of macrophages and release of the fungus, 3) nonlytic exocytosis of *Cryptococcus sp.* and survival of macrophages (72). Once phagocytosed, an ingested *Cryptococcus* is placed into a phagosome that is formed through the invagination of the surface membrane. *Cryptococcus sp.* can regulate phagosomal maturation which facilitates its intracellular survival and proliferation. Pathogen degradation is mediated by fusion of the phagosome with host lysosomes. *Cryptococcus sp.* can damage the phagolysosome; the exact mechanism is not well understood but may involve phospholipase enzymes and mechanical damage from capsule enlargement (72, 117). Rapid replication of virulent *C. gattii* in phagocytes is a virulence trait that contributes to the development of disease in immune competent individuals (8, 27). Nonlytic escape of *Cryptococcus* from phagocytes, named "vomocytosis" or phagosome extrusion/expulsion, occurs by merging of the phagosomal and plasma membranes which result in lateral transfer of *Cryptococcus* between host cells (118-120). It has been shown that repeated cycles of actin polymerization (actin flashes), which are dependent on classical WASP-Arp2/3 complex-mediated actin filament nucleation, form dynamic actin cages around the phagosome and inhibit cryptococcal expulsion in response to phagosome permeabilization (121). Vomocytosis has been observed *in vivo* and facilitates release of *Cryptococcus sp.* once it has crossed the BBB (110, 118-120, 122). It is hypothesized that *Cryptococcus sp.* disseminates to the CNS via the bloodstream and crosses the BBB within macrophages using a Trojan Horse mechanism (123-127).

Dendritic Cells (DCs) are the most efficient element of the host immune system for presentation of cryptococcal antigen to T cells and their activation is critical for host protection. DCs phagocytose and kill *Cryptococcus sp.* by oxidative and non-oxidative mechanisms (128, 129). Cathepsin B, a lysosomal enzyme, inhibits cryptococcal growth within DCs (130). *Cryptococcus sp.* can block DC maturation by shedding its polysaccharide capsule during infection and reduce

the secretion of proinflammatory cytokines (8). Internalization of *Cryptococcus sp.* by DCs occurs mainly through complement and antibody-mediated opsonization (131). The cryptococcal capsule activates the alternative pathway of complement; however, mannose binding lectin (MBL) can bind to the fungal cell wall and activate the lectin pathway (132-134). Mannose receptors on DCs can bind cryptococcal mannoproteins, trigger DC activation and maturation, induce the expression of MHC class and costimulatory molecules (CD40, CD80, and CD86), and mediate phagocytosis. TLR9 can recognize cryptococcal DNA and activate DCs to produce IL-12p40. TLR2 and TLR4 are not important for uptake of *C. neoformans* or activation of DCs by the fungus (108, 135-139). A protective immune response against pulmonary *C. neoformans* infection is also associated with recruitment and activation of $Ly6C^+$ monocyte-derived ($CD11b^+$) DCs in a CCR2-dependent manner (140-143).

In addition to macrophages and DCs, isolated neutrophils from human samples were shown to kill *C. neoformans* by oxidative and non-oxidative mechanism and enhance granuloma formation (144-146). Nevertheless, *in vivo* depletion of neutrophils during the early phase of infection in a mouse model resulted in less inflammatory damage and increased survival. In addition, neutrophil depletion in immunized mice did not affect the pulmonary fungal burden, indicating that neutrophils are not required for clearance (147, 148).

Eosinophilic infiltration of the lung has been observed both in humans and mouse models of cryptococcal infection and is associated with a failure of fungal clearance, increased lung pathology, and a non-protective immune response (149-151). Eosinophil recruitment during *C. neoformans* infection is dependent on IL-5 production (151, 152). Mice that are deficient in eosinophils display a reduced Th2 and an enhanced Th1/Th17 immune response following *C. neoformans* infection (153). In contrast, rat peritoneal eosinophils phagocytose opsonized *C. neoformans*, present cryptococcal antigen and might be involved in the protective immune response following infection (154, 155).

Natural Killer (NK) cells are important during the early phase of the immune response to *C. neoformans* and both human and mouse NK cells can kill *C. neoformans* using perforin (a calcium-dependent pore-forming cytolytic granzyme) rather than granulysin (156-158). NK cells have also been shown to be key in the immune response to cryptococcal granulomas with the ability to continue perforin degranulation in acidic environment (159). Expression of the NK receptor

(NKp30) is important for direct recognition of *C. neoformans* and its reduced expression in HIV-infected patients is associated with defective perforin secretion and diminished anticryptococcal activity (158, 160). The number of NKT cells is increased early in the lungs following intratracheal infection of mice with *C. neoformans*. NKT cell recruitment and accumulation in the lung is dependent on Monocyte Chemoattractant Protein-1 (MCP-1) and increases Th1 immune response by producing IFN-γ (161, 162).

1.4.2. Adaptive immune response:

$CD4^+$ T cells play a crucial role in cell-mediated immunity against *C. neoformans* in mice and humans. $CD4^+$ T cells kill *C. neoformans* by releasing granulysin and play a dominant role compared to $CD8^+$ T cells for macrophage and granulocyte recruitment to the lung and fungal clearance (16, 163-170). Patients with severe T-cell deficiency are at higher risk for development of *C. neoformans* infection (171, 172) and protection is associated with development of Th1 type $CD4^+$ cells (10, 16, 17, 168-170). Expression of IFN-γ and TNF-α by $CD4^+$ T cells of HIV+ patients with cryptococcal meningitis is related to survival and fungal clearance (173-175). In experimental models of cryptococcal infection, a Th1 type response characterized by secretion of IL-2, IL-12, IFN-γ, and TNF-α enhances internalization and killing of *Cryptococcus sp.* by phagocytes, induces M1 polarization of macrophages and promotes fungal clearance (176, 177). In contrast, a Th2 type response characterized by secretion of IL-4, IL-5, IL-10, and IL-13 is associated with eosinophilia, induction of M2 polarized macrophages, dissemination of the fungus and immunopathology (62). T regulatory cells are induced in the lung and suppress the deleterious effect of Th2 cells following *C. neoformans* infection (178). Compared to Th1, Th17-type responses characterized by IL-17A, IL-21, IL-22, IL-23, and TGF-β production have been suggested to play an important but secondary role in protection against *C. neoformans* (179). For example, inhibition of IL-17A expression and signaling has no effect on M1 macrophage polarization and survival of mice infected with *C. neoformans* (180, 181).

$CD8^+$ T cells also play an important role in the host immune response to *C. neoformans* infection by mediating an increase in pulmonary $CD4^+$ T cells, macrophages, and neutrophils (167). $CD8^+$ cells can kill *C. neoformans* through $CD4^+$-dependent upregulation and release of granulysin; however, recruitment of $CD8^+$ T cells to the lung occurs independently of $CD4^+$ cells (182, 183).

Production of IFN-γ by $CD8^+$ T cells also inhibits the growth and survival of *C. neoformans* within macrophages independently of $CD4^+$ T cells and depletion of $CD8^+$ T cells reduces survival in experimental models of cryptococcal infection (184, 185).

Gamma delta T-cells (γδ T) also have been shown to accumulate to the lung early after infection and play a down-modulatory role in the development of a Th1 response. Depletion of γδ T has resulted in increased IFN-γ synthesis by draining lymph node cells and enhanced cryptococcal clearance through induction of Th1-mediated responses in the lung (186). Increased expression of IL-17A by γδ T cells has been observed in neutrophil-depleted mice during pulmonary infection with *C. neoformans* strain H99γ. (147).

B cells also play an important role in protective immune response in experimental models of cryptococcal infection. X-linked immunodeficient (XID) mice, which lack B-1 cells and natural IgM, exhibit reduced yeast uptake by macrophages, increased dissemination to the brain, and significantly more enlarged extracellular *C. neoformans* cells in the lung during pulmonary infection compared to control mice. There is also evidence that HIV-infected patients that have lower serum levels of GXM-reactive IgM are more susceptible to cryptococcosis (187-191). In addition, IgG2 (the predominant GXM-binding IgG subclass) is also reduced in individuals with HIV/AIDS (10).

1.4.3. Immune Reconstitution Inflammatory Syndrome (IRIS)

A successful immune response to cryptococcal infection requires an intricate balance between Th1, Th17, and Th2 responses that regulates fungal growth and prevents immunopathology caused by dysregulated inflammation (8, 10). Cryptococcosis in HIV patients, solid organ transplant recipients, and pregnancy may be associated with the development of cryptococcal IRIS. Cryptococcal IRIS is caused by recovery of cryptococcus-specific immune responses and results in exaggerated host inflammation (192). There are two types of cryptococcal IRIS: 1) Paradoxical cryptococcal IRIS that occurs during immune recovery and presents as a deterioration or recurrence of clinical disease in the same or new site even with successful antifungal therapy, and 2) unmasking cryptococcal IRIS that begins shortly after initiation of ART in patients with no prior diagnosis of cryptococcosis and may be its first manifestation. Paradoxical cryptococcal IRIS has been reported in 10–45% of ART-naive HIV-positive patients with cryptococcal meningitis, and

approximately 60% of IRIS cases occur within the first month of ART (89). Earlier ART initiation has been associated with significant excess mortality (193). The exact immune response associated with poor outcomes is not well known; however, increased CSF cellular infiltrate, macrophage/microglial activation, and T helper 2 responses within the central nervous system have been associated with mortality (89, 194). A paradoxical immune response characterized by defects in macrophage activation and immune-mediated host cell damage can also occur in non-HIV cryptococcal meningitis and is associated with severe neurological disease (195, 196).

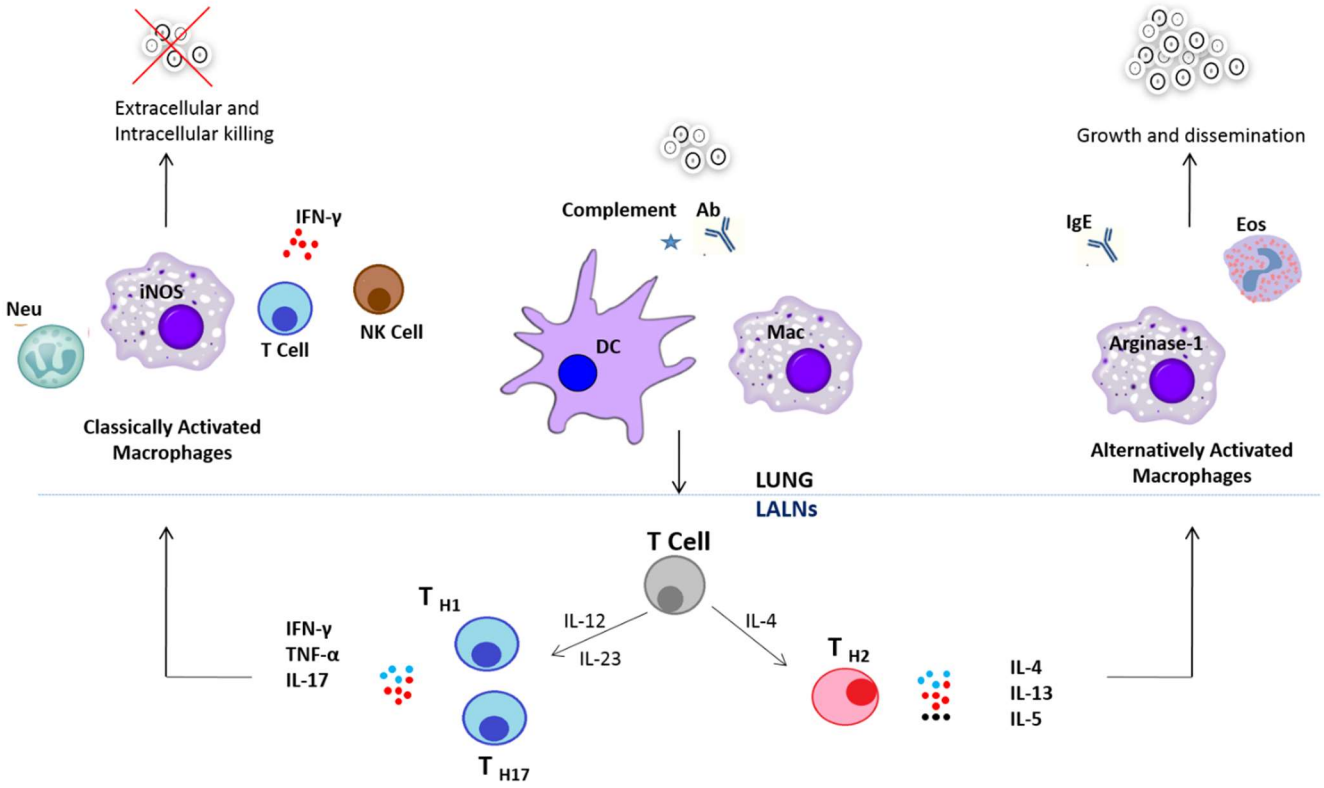

Figure 1.4: The immune response to *C. neoformans.* Opsonized *C. neoformans* is phagocytosed by macrophages and DCs in the lungs. DCs will kill *C. neoformans* by oxidative and non-oxidative mechanisms, undergo maturation to present cryptococcal antigens to $CD4^+$ T cells, and initiate a T-helper response. A Th1 response directs the protective host immunity against *C. neoformans.* Th1-type cytokines trigger enhanced uptake and killing by neutrophils and dendritic cells, induce macrophages to polarize to a classically activated M1 phenotype, and recruit monocytes to the site of infection where they promote clearance of the organism. A Th17 response also has been shown to be associated with protection against *C. neoformans*. A Th2 response is associated with significant chemotaxis of eosinophils to the lungs, the induction of alternately activated M2 macrophages, and dissemination of the pathogen.

1.5. Genetic Susceptibility to Cryptococcal Infection

Risk factors associated with cryptococcosis other than HIV infection include solid organ transplantation, $CD4^+$ T-cell lymphopenia, prolonged corticosteroid or immunosuppressive treatment, hematological malignancies, diabetes mellitus, cirrhosis, sarcoidosis, pregnancy, liver disease, and apparently immune competent individuals (10, 88, 197). Up to 20% of cases of cryptococcosis occur in phenotypically "normal" or apparently immunocompetent patients without any known risk factors for infection susceptibility (14). Recent *C. gattii* outbreaks in British Columbia and US Pacific Northwest has occurred mainly among non-HIV+ patients, emphasizing the importance of understanding risk factors for susceptibility to infection in healthy individuals (25, 198). Environmental exposure and genetic susceptibility could be the dominant risk factors and some studies have reported this possibility (199-213).

The contribution of human genetic variation and susceptibility to cryptococcosis has been analyzed in several cohorts. For example, mutations in CD40L that cause X-linked hyper-IgM syndrome have been associated with disseminated cryptococcosis (214-219). Mutations in interleukin-12R have been associated with susceptibility to cryptococcal infection (220) and a trend for susceptibility to *C. gattii* has been linked to the HLA B*5601 genotype (221). Fc gamma receptors (FcγR) and mannose-binding lectin (MBL) polymorphisms have been reported to increase susceptibility to cryptococcal meningitis (222-224) and a dectin-2 polymorphism is associated with pulmonary cryptococcosis in HIV-uninfected Chinese patients (225). In HIV-infected patients, humoral immunity in general and a polymorphism in FCGR3A are both associated with susceptibility to cryptococcal infection (226, 227).

1.6. Mouse Models of Infection

Investigation of genetic susceptibility in human has several limitations including the selection of comparable cases and controls to limit the effect of confounding variables, the requirements for a large sample size and independent replication, and the need to control for environmental factors (228, 229). Considering these limitations, an alternative approach to identification and validation of the genetic causes of susceptibility to infections such as cryptococcosis is the use of animal models. Several factors must be considered when choosing a suitable species for genetic

investigations including the potential for controlled breeding or other experimental manipulations, the associated expenses, the ability to perform tissue and time-specific molecular phenotyping, the availability of gene-editing tools and the similarity or relevance to humans (230). Compared to other animal species, there are several advantages of a mouse model including the availability of numerous well-characterized inbred and genetically engineered strains with reproducible responses to infection that are relatively inexpensive to purchase and maintain, extensive immunologic and genetic tools and databases for detailed phenotypic and genotypic analysis, and virtually complete conservation of orthologous protein coding sequences with humans (42, 231-235). The use of laboratory mice has been extremely successful for dissection of host response to various infectious diseases including the identification of causal susceptibility genes and their variants (236, 237).

Two major strategies, termed forward and reverse genetic analysis, have been used in mouse models to identify molecules and biochemical pathways that affect the host response to infection with viral, parasitic, fungal, and bacterial pathogens.

1.6.1. Forward genetic analysis

In forward genetics, a variable phenotype in natural populations or randomly mutagenized stocks is measured and the causal sequence variants are identified by positional cloning or candidate gene analysis (230, 238). Propelled by rapid technological development, forward genetic dissection and functional analysis of clinically relevant mouse models of infection has been established as a powerful and highly tractable approach to analyze the role of genetic susceptibility in host immune defense (204, 236, 239). This approach has been successful for the study of a variety of infectious diseases and has uncovered novel genes, proteins, and signaling pathways that play critical roles in the immune response to a diverse array of microbial pathogens (236).

QTL mapping

Quantitative trait locus (QTL) analysis is a statistical method that associates complex traits of interest with genotypic data that segregates in an experimental cross to identify and localize specific chromosomal regions that regulate the observed phenotypic variation. Several types of molecular markers are used in QTL analysis, including single nucleotide polymorphisms (SNPs),

simple sequence repeats (SSRs, or microsatellites), restriction fragment length polymorphisms (RFLPs), and transposable element positions. To perform QTL analysis using inbred mice, homozygous parental strains that differ in one or more traits of interest are crossed to generate heterozygous (F1) individuals that are subsequently intercrossed to produce an F2 generation that is amenable to genetic and phenotypic analysis. Markers that are linked to a QTL that influences the trait of interest will segregate more frequently with the trait values, whereas unlinked markers will not show a significant association with the phenotype(s) under consideration (240).

Interval Specific Congenic Strains

Although the QTL mapping approach occasionally identifies a single causal gene or other single structural, regulatory, or functional element that controls the phenotypic trait under study, in most cases additional genetic and functional studies are needed. Biological validation and dissection of the QTL in Interval Specific Congenic Strains (ISCS; also termed congenic strains) is one the most frequent methods used for the purpose (241). Congenic mouse strains have played a pivotal role in the genetic analysis of complex diseases including phenotypes that may be under the control of both environmental and multiple genetic factors such as type 1 diabetes, multiple sclerosis, obesity, and cancer (242). Congenic strains are derived by repeated backcrossing of the donor strain to the recipient strain with selection for the differential chromosomal segment corresponding to the mapped QTL and continuing until the integrity of the host strain background has been restored. Prior to establishing homozygosity of the desired congenic interval through brother-sister mating, a genome scan is conducted to determine if further backcrossing is required to remove any contaminating genomic fragments. The result of congenic breeding is to create a mosaic structure with a segment of genetic material from one parent on the genetic background of the other parent. The amount of donor strain genome is reduced by 50% with each generation, therefore after a minimum of 10 backcross generation a congenic strain is 99.90% identical to the recipient inbred strain except for the loci of interest (241). Marker-assisted selection also known as "speed congenics" can be used to reduce the number of backcross generations as few as five generations by selection of appropriate breeders (243). Congenic strains will normally carry differential regions of 10-20 Mb in size unless specific efforts are made to reduce the size of the differential segment. The genetic interval of a congenic line can be reduced and refined by identification of new recombinants during further backcrossing. The availability of sub-phenotypes for

characterization is often critical to the fine dissection of the trait of interest. Analysis often starts with the most robust and basic phenotype before proceeding to more subtle analysis of sub-phenotypes. Phenotyping methods often employed range from histology, behavioral studies, and the evaluation of physiological parameters to metabolomics and transcriptional profiling (242, 244-246).

Forward genetic approaches to cryptococcal infection

Genetic regulation of susceptibility to progressive cryptococcal infection among inbred mice has been reported in several forward genetic studies. For example, at the hemolytic complement (*Hc*) locus on chromosome 2, inbred mouse strains with the Hc^0 allele that encodes a defective form of complement component 5 have decreased survival following intravenous cryptococcocal challenge (247). Mutation of the X-linked Bruton Tyrosine Kinase (Btk^{xid}) in CBA/N mice causes absence of the mature B cell population and agammaglobulinemia and confers susceptibility to intravenous *C. neoformans* infection. Susceptibility in CBA/N mice was associated with increased spleen and brains weights, increased fungal burden in liver and spleen, and shorter survival time following infection (248). Immunoglobulin heavy chain (IgH) -linked genes on the telomeric region of mouse chromosome 12 have been associated with effectiveness of the host response against *C. neoformans* infection. The less resistant phenotype of BALB/c compared to C.B-17 mice (BALB/c strain congenic for C57BL/6 Immunoglobulin heavy chain) was associated with higher lung fungal burden, lower levels of IFN-γ, higher levels of the Th2 cytokines and significantly greater serum levels of IgM, IgG1, IgG2a, and IgG3 anti-cryptococcal Abs (249). Using MHC congenic mice, liver-specific susceptibility to intraperitoneal injection of the H99 cryptococcal strain has been linked to the H-$2^{k/k}$ haplotype (250). Spontaneous mutation of the *nu* locus on mouse chromosome 11, which encodes a member of the winged-helix domain family of transcription factors, results in hairless athymic mice with T cell-deficiency and has been associated with increased fungal burden and dissemination following intratracheal and intraperitoneal *C. neoformans* infections (166, 251). Finally, inbred mice with the beige mutation on mouse chromosome 13 have shown increased susceptibility to *C. neoformans* infection. The beige mutation in mice models human Chediak-Higashi syndrome and leads to defective and reduced bactericidal activity of granulocytes and severe deficiency of natural killer NK cell function (252).

In our laboratory, a well-established and clinically relevant model of intratracheal infection with the *C. neoformans* 52D strain has been used to investigate the genetic determinants of susceptibility to progressive cryptococcal pneumonia in susceptible C57BL/6J and resistant CBA/J inbred mice. A QTL analysis for cryptococcal pneumonia susceptibility in a segregating F2 population identified two significant QTL in the female F2 intercross that are located on chromosome 1 (*Cnes1*), and chromosome 17 (*Cnes2*), respectively and a third QTL on distal chromosome 17 in the male F2 intercross (*Cnes3*) (207). Two additional QTL associated with susceptibility to progressive cryptococcal pneumonia have been identified on chromosome 1 (*Cnes4*) and chromosome 9 (*Cnes5*) in a separate F2 population derived from susceptible C3H/HeN and resistant CBA/J mice that share the same *H-2*^{k} haplotype (253).

1.6.2. Reverse genetic analysis

Reverse genetic analysis starts with the identification of one or more sequences that are amenable to modification by genetic engineering techniques such as homologous recombination in embryonic stem cells. Modification of specific nucleotide sequences is followed by analysis of the impact of these changes on the phenotypes of interest (230, 238). To analyze host-pathogen interactions, the gene(s) of interest are usually chosen using direct or indirect evidence that links the sequence to pathogenesis or immune response to infection. The role of an individual gene in phenotypes of interest may be tested by infecting mice carrying a desired modification (usually a loss-of-function mutation due to deletion) at the corresponding locus.

Reverse genetic approaches to cryptococcal infection

Susceptibility to progressive cryptococcal infection has been extensively studied using reverse genetic approaches in mouse models (Table 1.3). These investigations have greatly increased our understanding of the contribution of individual cytokines, chemokines, and cell populations to a protective immune response. The overall conclusion arising from these studies indicates a crucial role for pro-inflammatory innate and Th1 adaptive cell-mediated immune response for protection and clearance of cryptococcal infection. Some of the major findings using reverse genetic approaches to analyze host resistance in cryptococcal infection are listed in Table 1.3.

Table1.2. Reverse genetic studies in *Cryptococcus* infection using knockout mice.

Knockout Gene	Description	Refs
MyD88	Decreased survival correlating with increased numbers of lung CFU and serum and lung GXM levels.	(254, 255)
TLR2/4	Diminished cryptococcal clearance associated with reduced TNF-alpha, IL-12 and IFN-gamma expression in TLR2$^{-/-}$ but not TLR4$^{-/-}$ mice.	(139, 254, 255)
TLR9	Profoundly impaired pulmonary clearance during the adaptive phase of the immune response, defects in Th polarization, diminished macrophage accumulation and activation.	(256)
CCR2	Prolonged pulmonary infection, significant dissemination to the spleen and brain, markedly impaired recruitment of cDCs and macrophages, development features of Th2 responses.	(142, 143, 257, 258)
MCP1	Diminished recruitment of NKT and NK cells to the lungs.	(161)
MIP-1α	Dramatically decreased survival, increased *C. neoformans* burden in the lungs, greater number of eosinophils, extremely high levels of serum IgE, switch of immune response to a Th2 phenotype.	(259)
CCR5	Defects in leukocyte recruitment to the brain, decreased elimination of cryptococcal polysaccharide from the brain, no defects in lung leukocyte recruitment, pulmonary clearance, or delayed-type hypersensitivity.	(260)
IFN-γ/R	Increased susceptibility associated with increased pulmonary and brain fungal burden.	(261) (262)
IL-12p35/40	Decreased survival; infected IL-12p40$^{-/-}$ mice died earlier and developed higher organ burdens than IL-12p35$^{-/-}$ mice. Susceptibility of both IL-12p35$^{-/-}$ and IL-12p40$^{-/-}$ mice was associated with Th2 polarization.	(263)
IL-1/18R	Decreased survival time in IL-18R$^{-/-}$ mice.	(264)
TNF-α	Reduced survival, increased fungal burden, reduced polymorphonuclear leukocyte infiltrate in the brain, lower levels of IL-6 in lungs and brain, IL-1β and KC in brain and spleen.	(265)

IL-4/10	Decreased fungal burden, absent of pulmonary eosinophilia.	(266)
IL-4R	Reduced delayed-type hypersensitivity responses, lower fungal burden in the lung.	(267)
IL-4Rα	Decreased fungal control during the early phase of infection.	(268)
IL-17A	Impaired late fungal clearance, reduced intracellular containment of the organism within lung macrophages, reductions in $CD11c^+$ $CD11b^+$ myeloid cells, B cells, and $CD8^+$ T cells, nonsignificant trend in the reduction of lung neutrophils.	(269)
IL23p19 **IL-17RA**	No effect on pulmonary or brain fungal burden; however, reduced survival of *IL-23p19*$^{-/-}$ mice compared to *IL-17RA*$^{-/-}$ mice.	(180)
STAT1	Increased pulmonary fungal burden and brain dissemination, increased mortality, shift from Th1 to Th2 cytokine bias, pronounced lung inflammation, and defective classical macrophage activation, inability to control intracellular cryptococcal proliferation by macrophages.	(270, 271)
Scavenger RA	Improved fungal clearance, decreased accumulation of eosinophils and greater accumulation of $CD4^+$ T cells and $CD11b^+$ dendritic cells, decreased expression of Th2 cytokines in lung, diminished serum IgE, increased hallmarks of classical pulmonary macrophage activation.	(272)
Dectin-2	Increased Th2 response and mucin production.	(273)
Mannose R	Decreased survival, higher lung fungal burden.	(136)
sIgM	Increased mortality and higher blood and brain CFUs, comparable lung CFU, reduced Th1 polarization	(191)
γδ T cells	Promote fungal clearance, increased serum levels of IFN-γ.	(186)
Surfactant PR D	Longer mean time to death and decreased fungal burden.	(151, 274)
T1/ST2	Improved survival, decreased fungal burden in the lungs, spleen, and brain, decreased early production of IL-5 and IL-13 by lung type 2 innate lymphoid cells.	(275, 276)
C3/factor B	Increased fungal burden, decreased survival.	(277)

1.7. Thesis rationale and specific aims

The general goal of my thesis is to dissect the genetic and immunological aspects of host susceptibility to the fungal pathogen *C. neoformans*. I have approached this objective by applying both forward and reverse genetic methods followed by immunological characterization of immune responses in an established mouse model of infection.

Chapter 2: The *Cnes2* locus on mouse chromosome 17 was previously associated with susceptibility to *C. neoformans* infection. The aim of this chapter is to confirm the role of *Cnes2* interval on host susceptibility to *C. neoformans* infection. To reach this goal, *Cnes2* congenic mice were generated by transferring the *Cnes2* chromosomal interval from the resistant CBA/J donor to the susceptible C57BL/6 recipient background by repeated backcrossing. The host resistance phenotype and immune responses were analyzed following infection.

Chapter 3: The aim of this chapter is to dissect the *Cnes2* interval into the underlying smaller genetic regions which regulate the host response to *C. neoformans* infection. To reach this goal, a panel of sub-congenic mice were generated. The host resistance phenotype and immune response of each sub-congenic line were analyzed following infection. An extensive *in silico* analysis using publicly available genome browsers was conducted to identify the most possible candidate genes in implicated regions.

Chapter 4: IL-1 alpha (IL-1α) and IL-1 beta (IL-1β) are pro-inflammatory cytokines that are highly induced following *C. neoformans* infection. The aim of this chapter is to determine the role of IL-1RI signaling, a common receptor for IL-1α and IL-1β, in cryptococcal infection using a reverse genetic approach. IL-1RI-deficient mice (IL-1RI$^{-/-}$) were generated on the Balb/c background and the host resistance phenotype and immune responses of IL-1RI$^{-/-}$ and wild type mice were analyzed following cryptococcal infection.

Chapter 2

The *Cnes2* locus on mouse chromosome 17 regulates host defense against cryptococcal infection through pleiotropic effects on host immunity.

Infection and Immunity, 2015

Mitra Shourian,[a,b] Adam Flaczyk,[a,b] Isabelle Angers,[a,b] Barbara C. Mindt,[c] Jörg H. Fritz,[c] Salman T. Qureshi[a,b]#

Meakins-Christie Laboratories, Department of Medicine and Division of Experimental Medicine, McGill University, Montréal, Québec, Canada[a]

Department of Critical Care and Research Institute of the McGill University Health Centre, Montréal, Québec, Canada[b]

Complex Traits Group, Departments of Microbiology and Immunology, and Physiology, McGill University, Montréal, Québec, Canada[c]

Running Head: *Cnes2* regulates host defense against *Cryptococcus*

#Address correspondence to Salman T. Qureshi, salman.qureshi@mcgill.ca

Preface to Chapter 2

To identify the underlying factors that regulate the progression and outcome of *C. neoformans* infection, quantitative trait locus (QTL) analysis in an experimental cross between susceptible C57BL/6 and resistant CBA/J mice was used to define three significant chromosomal intervals (*Cnes1, Cnes2,* and *Cnes3*) that are associated with control of lung fungal burden (207). In this chapter, to validate and characterize the role of *Cnes2* during the host response, we constructed a congenic strain on the C57BL/6 background (B6.CBA-*Cnes2*) and analyzed the host susceptibility phenotype and immune response following *C. neoformans* Infection.

2.1. Abstract

The genetic basis of natural susceptibility to progressive *Cryptococcus neoformans* infection is not well understood. Using C57BL/6 and CBA/J inbred mice we previously identified three chromosomal regions associated with *C. neoformans* susceptibility (*Cnes1, Cnes2, Cnes3)*. To validate and characterize the role of *Cnes2* during the host response we constructed a congenic strain on the C57BL/6 background (B6.CBA-*Cnes2*). Phenotypic analysis of B6.CBA-*Cnes2* mice 35 days after *C. neoformans* infection showed a significant reduction of fungal burden in the lungs and spleen with higher pulmonary expression of IFN-γ and IL-12, lower expression of IL-4, IL-5, and IL-13, and an absence of airway epithelial mucus production compared to C57BL/6. Multi-parameter flow cytometry of infected lungs also showed a significantly higher number of neutrophils, exudate macrophages, $CD11b^+$ dendritic cells, and $CD4^+$ cells in B6.CBA-*Cnes2* compared to C57BL/6 mice. The activation state of recruited macrophages and dendritic cells was also significantly increased in B6.CBA-*Cnes2* mice. Taken together these findings demonstrate that the *Cnes2* interval is a potent regulator of host defense, immune responsiveness, and differential Th1/Th2 polarization following *C. neoformans* infection.

2.2. Introduction

Cryptococcus neoformans is a basidiomycete fungus that can cause severe and potentially life-threatening pneumonia, meningitis, and disseminated disease in the immunocompromised host with an estimated annual death toll of 625,000 (9, 27, 278). The pulmonary manifestations of *C. neoformans* infection vary from asymptomatic nodular disease to severe acute respiratory distress syndrome and are strongly influenced by the quality and magnitude of the immune response (279). Notably, not all immune compromised hosts develop disease following cryptococcal infection while some immune competent individuals exhibit severe illness (29, 280, 281); therefore, it is believed that genetic factors play an important role in determining the susceptibility to progressive infection. Case-control studies in mainly non-HIV infected patients have associated mannose-binding lectin (MBL) deficiency and functional polymorphisms in members of the low-affinity Fc-gamma receptor family with cryptococcal infection (222-224, 226). Nonetheless, such variation was observed in a minority of cases, signifying an important gap in the knowledge of heritable factors that predispose the host to cryptococcal disease. Comprehensive elucidation of the genetic basis for cryptococcal susceptibility would facilitate the identification of individuals at high risk for infection and increase our understanding of the underlying mechanisms of disease pathogenesis but is hindered by the requirement for large, homogenous study cohorts and adequate clinical sample acquisition.

Spontaneous mutation or naturally occurring variation involving several genetic loci that are crucial to host immunity have been reported to confer increased susceptibility to murine cryptococcal disease. For example, the Hc^0 allele on mouse chromosome 2 that causes a deficiency of the C5 complement component was among the first mutations to be associated with severe *C. neoformans* infection (247, 282). Another study showed that CBA/N XID mice that lack a late-maturing B cell population due to a mutation of the X-linked Bruton agammaglobulinemia tyrosine kinase (*Btk*) are also highly susceptible to intravenous *C. neoformans* infection (248). Conversely, the C.B-17 congenic strain that bears the Ig H chain-containing region of chromosome 12 from C57BL/Ka mice on a BALB/c background exhibited enhanced pulmonary clearance of *C. neoformans* following intratracheal infection (249). A spontaneous mutation of the *nu* locus on mouse chromosome 11 that encodes the forkhead box N1 transcription factor results in a hairless athymic state with abrogation of T cell-mediated immunity and has also been associated with

increased fungal burden and dissemination following intraperitoneal *C. neoformans* infection (166, 283). Finally, a potential role for the histocompatibility complex (H-2) in murine susceptibility to intraperitoneal *C. neoformans* infection has also been reported using congenic mice (250).

Susceptibility to progressive cryptococcal infection has been extensively studied using reverse genetic approaches in mouse models and these investigations have greatly increased our understanding of the host response to this pathogen (62, 284, 285). For example, genetically engineered defects of a variety of cytokines, chemokines or their receptors, as well as several microbial pattern recognition receptors have been shown to alter the activation, recruitment, and differentiation of leukocytes during cryptococcal infection (286). Following inhalation, resident lung dendritic cells (DC) and alveolar macrophages (AM) are the first immune cells that encounter *C. neoformans,* and several studies have shown they are able to phagocytose *C. neoformans in vivo* (129, 287). Upon contact with *Cryptococcus*, DC and AM also produce pro-inflammatory cytokines such as tumor necrosis factor (TNF)- α, Interleukin (IL)-1β and IL-6 that are required for the generation of protective immunity (177, 288, 289). Resistance to cryptococcal infection is dependent on recruitment of antigen-specific $CD4^+$ T lymphocytes to the site of infection, and T-helper 1 (Th1)/T-helper 17 (Th17) polarization of the adaptive immune response characterized by the cytokines interferon-γ, IL-12, IL-17(A), and IL-22 (269, 290-294). Effector cells such as NK cells and $CD8^+$ T cells also produce perforin/granulysin that kills extracellular *C. neoformans* as well as host cells bearing intracellular cryptococci (183, 295). Equally important to host defense is a classical pattern of macrophage activation that aids in the elimination of cryptococcal cells (270, 296, 297). In contrast, susceptibility to progressive cryptococcal disease is characterized by a Th2 pattern of cytokine expression, lung eosinophilia, goblet cell metaplasia, and alternative macrophage activation (153, 275, 298).

Beyond the well-characterized contribution of spontaneous mutations or specifically engineered defects that alter immunity against *C. neoformans*, there is emerging evidence that genetic susceptibility to cryptococcal infection in the apparently normal host is a complex trait (207, 253). For example, a previous study demonstrated that C57BL/6 mice develop a lung fungal burden that is 1000-fold higher than the CBA/J inbred strain five weeks following direct intratracheal infection with moderately virulent *C. neoformans* 52D (152). Infected C57BL/6 mice subsequently develop disseminated disease and succumb to the infection while CBA/J mice can progressively clear the

fungus. Detailed analysis of susceptible C57BL/6 mice following experimental pulmonary infection clearly demonstrated a distinct Th2 pattern of adaptive immunity that contrasts with the Th1 response of resistant CBA/J mice (299). To identify the underlying factors that regulate the progression and outcome of *C. neoformans* infection, quantitative trait locus (QTL) analysis in an experimental cross between susceptible C57BL/6 and resistant CBA/J mice was used to define three significant chromosomal intervals (*Cnes1, Cnes2,* and *Cnes3*) that are associated with control of lung fungal burden (207).

A tractable approach to confirm the biological validity of a quantitative trait locus is to generate interval specific congenic mice (ISCS) that bear the corresponding chromosomal segment from a donor strain on the recipient background (246). Comparative analysis of the ICSC and recipient strain can then be used to confirm the autonomous contribution of the congenic segment to the phenotype of interest. Here we report that the *Cnes2* QTL derived from chromosome 17 of the CBA/J inbred strain has a major effect on control of lung fungal burden and disseminated cryptococcal infection in the C57BL/6 background. Specifically, at day 35 post-infection B6.CBA-*Cnes2* mice had a lung fungal burden that was more than 100-fold lower than that of C57BL/6 inbred mice. Compared to C57BL/6, the immune response of B6.CBA-*Cnes2* congenic mice was characterized by a significantly higher expression of Type 1 cytokines and greater numbers of lung neutrophils, antigen-presenting cells, and Th1-polarized $CD4^+$ T lymphocytes. Taken together, these data demonstrate that one or more genes within the *Cnes2* locus regulate pulmonary host defense through pleiotropic effects on the inflammatory and immune response following *C. neoformans* infection (253, 300).

2.3. Materials and Methods

Mice

C57BL/6 and CBA/J mice were purchased from Harlan Laboratories (Indianapolis, IN, USA), and subsequently bred and maintained in our SPF facility. The B6.CBA-*Cnes2* congenic line was created by intercrossing C57BL/6 and CBA/J inbred mice to generate F1 progeny that were successively backcrossed to C57BL/6 for 7 generations. Breeder mice for each backcross were selected for CBA alleles in the *Cnes2* interval and a high percentage of C57BL/6 alleles throughout the rest of the genome as determined by a low-density genome scan. The *Cnes2* SNP markers rs13482444 (6.9 Mb), rs13482930 (26.8 Mb) and rs13460774 (35.1 Mb) were genotyped by Taqman real-time PCR (Life Technologies) using the ABI Prism 7500 Real-Time PCR System (Life Technologies). The genome scans were carried out by TCAG (The Center for Applied Genomics, Toronto, ON) using the Illumina's Mouse Low-Density Linkage panel. At the 7^{th} generation, mice with a 100% C57BL/6 background were intercrossed to obtain a homozygous congenic line (Supplementary Figure 2.1). All animals were maintained in compliance with the Canadian Council on Animal Care and all experiments were approved by the McGill University animal care and use committee. All experimental groups in this report include an equal number of male and female mice.

Cultures of *C. neoformans*

C. neoformans 52D (ATCC no. 24067) was grown and maintained on Sabouraud dextrose agar (SDA; BD, Becton Dickinson and Company). To prepare an infectious dose, a single colony was suspended in Sabouraud dextrose broth (BD) and grown to early stationary phase (48 h) at room temperature on a rotator. The stationary culture was then washed with sterile phosphate-buffered saline (PBS), counted on a hemacytometer and diluted to 2×10^5 CFU per ml in sterile PBS. The fungal concentration of the experimental dose was confirmed by plating a dilution of the inoculum on SDA and counting the CFU after 72 hours of incubation at room temperature.

Intratracheal infection with *C. neoformans*

For intratracheal administration of *C. neoformans,* mice were anesthetized with 150 mg/kg of ketamine (Ayerst Veterinary Laboratories) and 10 mg/kg of xylazine (Bayer) intraperitoneally. A small skin incision was made below the jaw along the trachea, and the underlying glands and

smooth muscle were separated. Infection was performed by intratracheal injection of 50 ul PBS with 10^4 *C. neoformans* suspension (2×10^5 CFU/ml) through a 22-gauge catheter via a 1-ml tuberculin syringe. The incision was closed using the 9mm EZ Clip wound closing kit (Stoelting) and mice were monitored daily following surgery.

Organ isolation and CFU assay

After mice were euthanized by CO_2, their infected lungs, spleen and brain were excised and placed in sterile, ice-cold PBS. Tissues were then weighed and homogenized using a glass tube and pestle attached to a mechanical tissue homogenizer (Glas-Col) and then plated at various dilutions on Sabouraud dextrose agar. Plates were incubated at 37ºC for 72 hours and CFU were counted.

Histopathological analysis

Following euthanasia, lungs were perfused with ice-cold PBS via the right ventricle of the heart. Using 10% buffered formalin acetate (Fisher Scientific) the lungs were inflated to a pressure of 25 cm H_2O and fixed overnight. Subsequently lungs were embedded in paraffin, sectioned at 5 μm, and stained with hematoxylin-eosin (H&E), periodic acid-Schiff (PAS) or mucicarmine reagents at the Histology Facility of the Goodman Cancer Research Centre (McGill University). Representative photographs of lung sections were taken using a BX51 microscope (Olympus), QICAM Fast 1394 digital CCD camera (QImaging) and Image-Pro Plus software version 7.0.1.658 (Media Cybernetics).

Bronchoalveolar lavage harvest

At the designated time points, an incision was made below the jaw to expose the trachea. A 22-gauge catheter was inserted into the airway and secured in place by a string. A total of 4 volumes of 500 μL of ice-cold PBS were instilled via the catheter and subsequently aspirated. The bronchoalveolar lavage fluid was then spun at 1200 rpm for 10 minutes and the supernatants were stored at -80ºC for subsequent analysis. The cell pellet was counted using a Beckman Coulter particle counter (Beckman Coulter), and spun onto slides at a concentration of 5 x 10^5 cells/slide using a cytospin (Shandon). Following Diff-Quik staining (Dade Behring), differential cell counts of macrophages, lymphocytes, neutrophils, and eosinophils were obtained by counting a total of 300 cells per slide in duplicate. The average percentage was multiplied by the total cell count to obtain the total cell number for each leukocyte population.

Flow cytometry

Lungs were excised using sterile technique and placed in RPMI (Gibco, Invitrogen) supplemented with 10% fetal bovine serum (Wisent). Subsequently lungs were minced using surgical blades, and incubated with 1 mg/mL collagenase (Sigma) at 37^{o}C for one hour. Following incubation, lung pieces were passed through a 16G needle and filtered through a 70 μm cell strainer (BD). Red blood cells were removed using 1X ACK lysis buffer before counting the cells using a Beckman Coulter Z1 particle counter. Fc receptors were blocked with the addition of unlabeled anti-CD16/32 antibodies (93; eBioscience, eBio) and single cell suspensions were stained with the following fluorescence-conjugated anti-mouse monoclonal antibodies purchased from eBio, BD, and BioLegend (BL): CD45-V500 (30-F11; BD), B220-FITC (RA3-6B2; eBio), CD3e-FITC (145-2C11; eBio), CD4-V450 (GK1.5; eBio), CD8-PerCP (53-6.7; BD), CD11b-APC (M1/70; BD), CD11c-FITC (N418; eBio), MHCII-PE-Cy7 (M5/114.15.2; eBio), Ly6G-V450 (clone 1A8; BL), F4/80-PE (clone BM8; eBio), CD86-PE (GL1; eBio), CD40-PerCp/Cy5.5 (3/23; BL), CD80-PE (16-10A1; eBio), CD69-PE/Cy7 (H1.2F3; BL), CD44-PE (IM7; eBio) and CD25-APC (PC61; BL). Nonviable cells were excluded using fixable viability dye eFluor780 reagent (eBio). Data were acquired using a FACS LSR-II flow cytometer (BD) and analyzed using Flow Jo version X software (Tree Star).

Pulmonary macrophage isolation

The leukocyte population was enriched for macrophages by positive selection using magnetic beads labeled with F4/80 antibody (Stemcell Technologies) according to the manufacturer's recommendations. Fungal burden was determined by lysis of the macrophages using sterile deionized water, followed by serial dilution and plating on SDA agar for 48 h at 37˚C.

Intracellular flow cytometry

For intracellular cytokine staining of T cells, lungs were processed as above and lymphocytes were isolated using a 40/70 Percoll gradient (Sigma). Cells were plated and stimulated for 4 hours with 0.1 μL/mL Phorbol 12-Myristate 13-Acetate (PMA) and 1 μL/mL calcium ionophore (Ionomycin; BD) in the presence of Brefeldin A (GolgiPlug; BD) for the final three hours. Cells were then washed and blocked with α-CD16/32 antibodies (93; eBio) and stained with a surface antibody cocktail consisting of α-CD3-PE-Cy7 (145-2C11; BD), α-CD4-V450 (GK1.5; eBio), α-CD8-

PerCP (53-6.7; BD) and α-CD45-V500 (30-F11; BD). The cells were then fixed, permeabilized, and stained with IL-13-PE-Cyanine7 (eBio13A), IL-5-PE (TRFK5; BL) IFN-γ (XMG1.2; BL) and IL-4-APC (11B11; BL). Data were acquired using a FACS LSR-II flow cytometer (BD) and analyzed using Flow Jo software (Tree Star) with gating determined by fluorescence-minus-one (FMO) controls.

Total lung cytokine and chemokine production

Mice were euthanized and lungs flushed with 10 mL of ice-cold PBS. Whole lungs were homogenized in 2 mL PBS with Halt Protease and Phosphatase Inhibitor Cocktail (Fisher Scientific) using a sterilized glass tube and pestle attached to a mechanical tissue homogenizer (Glas-Col) and spun at 12,000 rpm for 20 minutes. Supernatants were collected and aliquots were stored at -80ºC for further analysis. Cytokine and chemokine contents of whole lung protein samples were analyzed using DuoSet ELISA kits (R & D Systems): TNF-α (DY410), IL-6 (DY406), IL-1β (DY401), CCL2/MCP-1 (DY479), IL-12/IL-23P40 (DY2398), IFN-γ (DY485), CXCL1/KC (DY453), CCL3/MIP-1α (DY450), CXCL2/MIP-2α (DY452), IL-4 (DY404), IL-5 (DY405), IL-13 (DY413) and IL-17A (DY421).

Quantitative PCR

For lung RNA extraction, 4 mm diameter lung pieces were collected in RNAlater solution (Life Technologies), homogenized in lysis buffer using a tissue homogenizer (Fisher Scientific) and processed using an RNeasy kit. Using 40 ng of RNA, a reverse transcription reaction was performed using the ABI high capacity cDNA reverse transcription kit (Life Technologies). Quantitative real-time PCR (qRT-PCR) was performed with an ABI Prism 7500 Real time PCR system (Life Technologies). Each reaction well contained 10 µL TaqMan Genotyping Master Mix (Life Technologies), 5 µL RNase-free water (Wisent), 1 µL of Taqman probes (Life Technologies) and 40 ng of cDNA template in 4 µL of water. The probes used were *IL4 (*Mm00445259_m1)*, Arg1* (Mm00475988_m1), *Retnla/Fizz1* (Mm00445109_m1), *Nos2* (Mm00440502_m1) and *β-actin* (Part no. 401846) as a housekeeping gene. Results were calculated using the change-in-cycling-threshold method ($2^{-\Delta\Delta Ct}$) relative to the expression of *β-actin* and presented as fold induction relative to unstimulated samples.

Determination of serum antibody levels

Blood was harvested via cardiac puncture and spun down in a gel tube to obtain serum. The concentration of total serum IgE, IgG subclasses, and IgM was determined by ELISA (BL) according to the manufacturer's instructions.

Statistical analysis

For all experiments the mean and standard error of mean (SEM) are shown. To test the significance of single comparisons, an unpaired Student's t-test was applied (with a threshold P value of <0.05), unless otherwise stated. All statistical analysis was performed with GraphPad Prism software version 5 (GraphPad Software Inc).

2.4. Results

B6.CBA-*Cnes2* mice display a decreased fungal burden in the lung, brain, and spleen following *C. neoformans* infection.

To evaluate the influence of the *Cnes2* congenic segment derived from CBA/J mice on *C. neoformans* infection (Figure 2.1A), we first analyzed the pulmonary fungal burden of B6.CBA-*Cnes2* and C57BL/6 mice at weekly intervals after intratracheal infection (Figure 2.1B). Comparable growth of *C. neoformans* was observed at day 7 post-infection in both strains of mice, suggesting that the *Cnes2* congenic segment did not have a marked effect the initial host response to *C. neoformans*. In C57BL/6 mice the cryptococcal load reached a plateau of 10^7 CFU at day 14 post-infection and remained stable up to day 35 post-infection. In contrast, a significant reduction in pulmonary fungal burden was observed in B6.CBA-*Cnes2* mice beginning at day 21 post-infection and was more pronounced at day 35 post-infection (Figure 2.1B). Remarkably, the lung CFU in B6.CBA-*Cnes2* mice was more than 100-fold lower compared to C57BL/6 mice at day 35 post-infection (Log_{10} CFU 4.68 ± 0.20 vs. 6.87 ± 0.22, $p < 0.001$) and was similar to the published phenotype of the CBA inbred strain (207). Collectively, these data show that the *Cnes2* congenic interval makes a significant contribution to the control of cryptococcal growth in mouse lungs.

As infection of the brain and other organs is a serious and potentially fatal consequence of pulmonary cryptococcal disease, we also examined whether the *Cnes2* congenic segment derived from CBA/J altered the dissemination rate to these extrapulmonary sites. Analysis of CFU from infected C57BL/6 and B6.CBA-*Cnes2* mice showed a comparable rate of dissemination to the brain at day 7 to day 21 post infection (data not shown); however, at day 35 post-infection B6.CBA-*Cnes2* mice demonstrated a trend towards reduction in the rate of brain dissemination (4/12 vs. 6/12; Figure 2.1C) and cerebral fungal burden (Log_{10} CFU 1.02 ± 0.44 vs. 1.95 ± 0.59, $p = 0.22$; Figure 2.1C) compared to C57BL/6 mice. Dissemination of *C. neoformans* from the lung to the spleen was also comparable between inbred and congenic strains at day 14 post-infection (data not shown). At day 21 post-infection, all of the C57BL/6 and B6.CBA-*Cnes2* mice had detectable fungal growth in the spleen, however, the CFU values were significantly lower in B6.CBA-*Cnes2* strain compared to C57BL/6 mice (Log_{10} CFU 2.29 ± 0.21 vs. 3.00 ± 0.09, $p < 0.05$) and this difference was also observed at day 35 post-infection (Log_{10} CFU 1.69 ± 0.32 vs. 2.80 ± 0.07, $p < 0.05$; Figure 2.1C). Therefore, at later time points, B6.CBA-*Cnes2* mice have a

highly resistant lung phenotype and a reduction of fungal growth in extrapulmonary target organs compared to C57BL/6 mice.

B6.CBA-*Cnes2* mice have an altered pattern of pulmonary inflammation following *C. neoformans* infection.

In order to determine the effect of *Cnes2* on lung pathology after *C. neoformans* challenge, we analyzed tissue sections from B6.CBA-*Cnes2* and C57BL/6 mice at serial time points after infection. Staining with H&E at day 7 and day 14 post-infection demonstrated no clear differences between the two strains (data not shown). At day 35 post-infection, H&E staining revealed diffusely increased inflammatory infiltration in B6.CBA-*Cnes2* mice compared to C57BL/6 mice (Figure 2.2C, D). Mucicarmine staining of C57BL/6 lungs at day 35 post-infection revealed numerous extracellular *C. neoformans* that were heavily encapsulated (Figure 2.2E) while only a few intracellular cryptococci could be observed in B6.CBA-*Cnes2* lungs (Figure 2.2F). Finally, at day 14 post-infection abundant mucus secretion and goblet cell metaplasia were observed in the airways of C57BL/6 mice (Figure 2.2A) but were notably absent from B6.CBA-*Cnes2* airways (Figure 2.2B). Collectively, the lung histology demonstrates that B6.CBA-*Cnes2* mice have enhanced leukocyte recruitment and diminished signs of type 2 airway inflammation that is associated with markedly fewer extracellular cryptococci at day 35 post-infection.

Differential mucosal inflammatory response of C57BL/6 and B6.CBA-*Cnes2* mice following *C. neoformans* infection

To determine if the enhanced fungal clearance was associated with an altered mucosal inflammatory response, leukocytes in the bronchoalveolar lavage fluid (BALF) of C57BL/6 and B6.CBA-*Cnes2* mice were enumerated at day 3, 7, 14, and 21 post-infection. Comparison of both strains showed a similar increase in the total number of leukocytes from day 3 to day 14 and a similar decline at day 21 (Figure 2.3A). Differential staining showed that B6.CBA-*Cnes2* mice had a significantly higher number of BALF macrophages at day 21 post-infection relative to the C57BL/6 strain (Figure 2.3B). Furthermore, B6.CBA-*Cnes2* mice exhibited a significantly higher

number of neutrophils at day 7 and day 14 post-infection (Figure 2.3C) while C57BL/6 mice had a significant higher number of eosinophils at day 14 and day 21 (Figure 2.3D).

Cnes2 regulates pulmonary cytokine and chemokine expression following *C. neoformans* challenge

Several studies have shown that susceptible C57BL/6 mice develop a Th2 pattern of adaptive immunity following *C. neoformans* infection while resistant CBA/J mice mount a Th1 response associated with classical macrophage activation that is crucial for fungal clearance (152, 166, 301, 302). Therefore, we sought to determine if B6.CBA-*Cnes2* mice display a heritable tendency towards Th1 or Th2 immune polarization following *C. neoformans* infection. Accordingly, we quantified the expression of pro-inflammatory mediators (IL-1β, IL-6 and TNF-α), Th1-type cytokines (IL-12 and IFN-γ), chemokines (KC, MIP-1α, and MIP-2α) and Th2-type cytokines (IL-4, IL-5, and IL-13) in total lung homogenates of C57BL/6 and B6.CBA-*Cnes2* mice after cryptococcal challenge. At day 3 post-infection, there were no significant differences in the expression of these mediators between the two strains; however, at day 7 and day 14 the expression of pro-inflammatory cytokines (IL-1β, IL-6, and TNF-α) was significantly higher in B6.CBA-*Cnes2* compared to C57BL/6 mice (Figure 2.4A and data not shown). At day 14 post-infection a significantly higher expression of both Th1-associated cytokines (IL-12 and IFN-γ) (Figure 2.4B) and chemokines (KC, MIP-1α, and MIP-2α) (Figure 2.4C) as well as a significantly lower expression of Th2-associated cytokines (IL-4, IL-5, and IL-13) (Figure 2.4D) was detected in lung homogenates of B6.CBA-*Cnes2* mice compared to C57BL/6 mice. Pulmonary expression of IL-17A did not differ between the resistant B6.CBA-*Cnes2* and the susceptible C57BL/6 mice at day 14 post-infection (Figure 2.4B). Taken together, these findings demonstrate that the *Cnes2* congenic interval regulates the expression of inflammatory cytokines and chemokines that are associated with the development of a Th1-associated pattern of adaptive immunity following *C. neoformans* infection.

B6.CBA-Cnes2 mice exhibit increased recruitment of neutrophils, exudate macrophages and dendritic cells to the lung during *C. neoformans* infection

To characterize the effect of *Cnes2* congenic interval on the cellular immune response during *C. neoformans* infection, flow cytometry analysis of whole-lung digests was performed on C57BL/6 and B6.CBA-*Cnes2* mice at serial time points. Comparison of uninfected C57BL/6 and B6.CBA-*Cnes2* mice showed relatively few inflammatory cells in the lungs with no significant differences between the strains (Figure 2.5E-H, day 0). The total number of resident AM (identified as auto-fluorescent $CD11c^{+}CD11b^{-}MHCII^{low}$ cells) was also comparable between C57BL/6 and B6.CBA-*Cnes2* mice prior to infection and at all time points post-infection (data not shown). Quantification of $CD11b^{+}Ly6G^{+}$ neutrophils (Figure 2.5A) showed a significant increase in B6.CBA-*Cnes2* mice relative to C57BL/6 at day 7 and day 14 after *C. neoformans* infection with an equivalent reduction in both strains at day 21 and day 28 (Figure 2.5E). In contrast, C57BL/6 mice had a significantly greater number of $CD11b^{+}SSC^{high}$ eosinophils (Figure 2.5B) in the lung at day 7 compared to B6.CBA-*Cnes2* mice and this strain-dependent difference was sustained up to day 28 post-infection (Figure 2.5F). Inflammatory monocyte-derived $CD11c^{+}CD11b^{+}$ macrophages, otherwise referred to as ExM, and inflammatory DC are both recruited to the mouse lung following *C. neoformans* infection and have crucial roles in pathogen elimination and antigen presentation (142, 296). These two myeloid cell populations may be distinguished by flow cytometry since ExM are inherently autofluorescent and have intermediate surface expression of MHCII while inflammatory DC lack autofluorescence and express high levels of MHCII (296, 303). Compared to C57BL/6 mice, the B6.CBA-*Cnes2* strain had a significantly higher number of lung ExM at day 21 and day 28 post-infection. In addition, B6.CBA-*Cnes2* mice had a higher number of lung inflammatory DC compared to C57BL/6 mice at day 14 post-infection and this difference was sustained up to day 28 post-infection. Taken together, these findings indicate that the *Cnes2* congenic segment has a significant effect on lung recruitment of inflammatory myeloid cell subsets after *C. neoformans* infection including ExM and DC that are both crucial to cryptococcal clearance. In contrast, C57BL/6 lungs are characterized by the development of a persistent eosinophilia that is associated with an inability to clear cryptococcal infection (152, 167).

Exudate macrophages and inflammatory DC from B6.CBA-*Cnes2* mice display enhanced activation and effector phenotypes following *C. neoformans* infection

To determine the activation status of $CD11c^+CD11b^+$ macrophage and DC populations that had been recruited to the site of cryptococcal infection, comparative flow cytometry analysis of isolated lung cell preparations from C57BL/6 and B6.CBA-*Cnes2* mice was performed at day 21 post-infection. After gating on $CD11c^+CD11b^+$ macrophage and DC populations, the surface expression of costimulatory molecules (CD40, CD80, and CD86) was determined by analysis of fluorescence intensity plots (Figure 2.6A). Consistent with a robust Th1 response, B6.CBA-*Cnes2* mice developed higher surface expression of the CD40 and CD80 maturation markers, with similar expression of CD86, compared to C57BL/6 mice (Figure 2.6B). To evaluate the pattern of pulmonary macrophage polarization in infected C57BL/6 and B6.CBA-*Cnes2* mice, the expression of the classical activation marker nitric oxide synthase (*Nos2*) and the alternative activation markers arginase-1 (*Arg1*) and found in inflammatory zone-1 (*Fizz1)* was compared by quantitative reverse transcription PCR analysis. At day 14 post-infection, significantly higher induction of *Fizz1* and a trend towards higher *Arg1* expression was observed in C57BL/6 relative to B6.CBA-*Cnes2* mice; in contrast, a significantly greater expression of *Nos2* was observed in B6.CBA-*Cnes2* mice compared to C57BL/6 (Figure 2.6C). To characterize the antifungal activity of macrophages at the primary site of *C. neoformans* infection, $F4/80^+$ cells were isolated from the lungs of C57BL/6 and B6.CBA-*Cnes2* mice by positive selection using antibody labeled magnetic beads at day 21 post-infection and subsequently lysed for determination of fungal burden. Interestingly, a significantly lower growth of cryptococci was observed in macrophage lysates derived from B6.CBA-*Cnes2* mice compared to the lysates derived from C57BL/6 mice (Figure 2.6D).

B6.CBA-*Cnes2* mice have an increased number of lung $CD4^+$ and $CD8^+$ T cells following *C. neoformans* infection

As lymphocytes are necessary for effective clearance of *C. neoformans*, we sought to compare B- and T-cell populations in the lungs of infected C57BL/6 and B6.CBA-*Cnes2* mice. No differences in the number of pulmonary B cells were observed between the two strains at any time point post-infection (data not shown). Conversely, B6.CBA-*Cnes2* mice showed a higher number of

pulmonary $CD4^+$ T lymphocytes relative to C57BL/6 at day 21 and day 28 post-infection (Figure 2.7A). No difference in the frequency or absolute number of lung $CD8^+$ T cells was observed between the two strains at day 21 post-infection; however, B6.CBA-*Cnes2* mice had a significant increase in this population at day 28 post-infection (Figure 2.7B). Expression of the surface markers CD25 and CD44 (for activated/memory T cells), CD69 (for early activation) and CD62L (for naive T cells) at day 21 post-infection was similar between B6.CBA-*Cnes2* and C57BL/6 mice (Figure 2.7C).

Pulmonary CD4+ T cells from B6.CBA-*Cnes2* mice show diminished Th2 cytokine production in response to *C. neoformans* infection

Analysis of whole lung lysates from B6.CBA-*Cnes2* and C57BL/6 mice showed significant differences in the expression of Th1- and Th2-associated cytokines during *C. neoformans* infection (Figure 2.4). To determine whether altered T-cell polarization could explain this difference, analysis of cytokine production by $CD4^+$ cells was performed at day 21 post-infection. Single-cell suspensions from infected C57BL/6 and B6.CBA-*Cnes2* lungs were restimulated with PMA and ionomycin to increase cytokine production and stained for intracellular IFN-γ, IL-4, IL-5, and IL-13. B6.CBA-*Cnes2* mice had a significantly lower frequency of $IL\text{-}4^+CD4^+$, $IL\text{-}5^+CD4^+$, and $IL\text{-}13^+CD4^+$ cells compared to C57BL/6, while the frequency of $IFN\text{-}\gamma^+CD4^+$ cells was comparable between the two strains (Figure 2.8B).

B6.CBA-*Cnes2* mice have a selective increase of serum IgG_3 antibody following *C. neoformans* infection

To determine whether B6.CBA-*Cnes2* mice develop an altered humoral response to *C. neoformans*, the total serum IgM, IgE, and IgG subclasses was determined at day 21 post-infection. The level of IgG_3 was significantly increased in B6.CBA-*Cnes2* mice compared to C57BL/6 while the level of all other antibodies was comparable between the two strains (Figure 2.9).

2.5. Discussion

The host genetic factors that underpin natural susceptibility to *C. neoformans* infection are poorly characterized (304). A precise understanding of the molecular and cellular mechanisms of protective immunity against this invasive fungal pathogen would advance the understanding of disease pathogenesis and could also be valuable for the development of prevention strategies as well as prediction of disease risk and response to therapy. Previous studies using a well-established model of intratracheal infection with *C. neoformans* 52D demonstrated that C57BL/6 mice developed a lung fungal load that was over 1000 times greater than that of CBA/J mice at day 35 post-infection (152). The wide spectrum of naturally occurring resistance was subsequently demonstrated for a panel of 10 inbred mouse strains (253). Further analysis showed that susceptibility to progressive fungal infection in C57BL/6 mice was associated with lung eosinophilia and a Th2-biased adaptive immune response while resistance in CBA/J mice was characterized by Th1-mediated immunity (152, 207). Forward genetic analysis of this strain combination demonstrated that host resistance segregated as a complex trait that was regulated by three significant *C. neoformans* susceptibility loci (*Cnes1, Cnes2, Cnes3*) (207).

To determine whether the *Cnes* loci that segregate between C57BL/6 and CBA/J mice have an autonomous biological effect on resistance against pulmonary cryptococcal infection, we have generated interval specific congenic mouse strains by introgression of each of the linked chromosomal regions from resistant CBA/J mice onto the susceptible C57BL/6 genetic background. The *Cnes2* QTL was prioritized for further analysis based on a highly significant peak LOD score of 7.30 that was estimated to explain 15.9% of the overall phenotypic variance in lung fungal burden among female mice. Comprehensive phenotypic and functional analysis of the host response clearly demonstrates that the B6.CBA-*Cnes2* congenic strain is highly resistant to cryptococcal infection and mounts a robust immune response that resembles the parental CBA/J phenotype. Nonetheless, comparison of the predicted effects of *Cnes2* locus and the observed phenotype of B6.CBA-*Cnes2* mice also revealed two notable differences. First, the host resistance phenotype of B6.CBA-*Cnes2* was equally evident in both males and females in the current study. Second, at 35 days post-infection the marked reduction in lung fungal burden of this congenic strain was similar to that of resistant inbred CBA/J mice that encodes the *Cnes1, Cnes2, and Cnes3* QTLs. These two interesting observations are not entirely surprising, since the penetrance and

phenotypic effects of a donor strain congenic interval may be influenced by complex interactions with the recipient genetic background (305). Accordingly, both the presence of an extremely resistant phenotype and its expression in female as well as male B6.CBA-*Cnes2* mice may be attributable to the absence of interacting or epistatic factors from the CBA/J background that suppress *Cnes2* function in males, or the presence of *Cnes2* modifier genes in the C57BL/6 background (306).

It is interesting to note that pulmonary growth and organ dissemination of *C. neoformans* was comparable between C57BL/6 and B6.CBA-*Cnes2* mice during the early phase of infection. This contrasts with later time points when B6.CBA-*Cnes2* mice had significantly diminished growth of *C. neoformans* in the lungs and spleen as well as a trend towards reduced growth in the brain. Clinical observations and experimental data have shown that uncontrolled infection of the respiratory tract precedes the development of disseminated infection and/or meningitis. The mechanisms by which *C. neoformans* reaches and actually enters the brain following its escape from the lung are complex and not fully understood; these include intravascular trapping followed by paracellular or transcellular migration or transmigration within circulating phagocytes (307). The data presented here suggest that *Cnes2* restricts progressive infection by enhancing the pulmonary and systemic immune response. Despite the recognized pattern of disease progression, control of cryptococcal growth in the lung does not always correlate with reduced brain dissemination, as was observed in IL-4/IL-13 knockout mice that mounted an effective Th1/Th17 pulmonary immune response but were not protected against cryptococcal meningitis (294).

The host mounts a highly complex immune response to cryptococcal infection that begins with phagocytosis by resident AM (308, 309). Subsequent production of inflammatory cytokines and chemokines leads to recruitment of activated ExM and antigen-presenting DC that facilitate the selection, activation, and differentiation of $CD4^+$ T cells. A variety of other cell types including granulocytes, innate lymphoid cells, and B cells have also been implicated in the host response to *C. neoformans* (286). To gain insight into the mechanisms that underlie the protective effects of the *Cnes2* interval on host defense, we performed a comparative analysis of inflammatory mediator expression and immune cell recruitment, activation, and differentiation during the course of pulmonary cryptococcal infection between C57BL/6 and B6.CBA-*Cnes2* mice.

Analysis of bronchoalveolar lavage and whole lung cell preparations showed that B6.CBA-*Cnes2* mice have fewer eosinophils and more neutrophils compared to C57BL/6 at day 7 post-infection with the greatest strain difference at day 14. C57BL/6 mice continued to have significantly more lung eosinophils at day 28; however no differences were observed in neutrophil numbers after day 14. Following intratracheal *C. neoformans* infection, genetically susceptible C57BL/6 mice were shown to have marked IL-5 dependent eosinophil recruitment that was associated with crystal deposition and airway epithelial damage (152). Eosinophils were also shown to produce IL-4 that promotes Th2 responses and contributes to immunopathology during pulmonary cryptococcal infection (153). Conversely, despite the ability to internalize and kill *C. neoformans in vitro* (146, 310), there is relatively little evidence that neutrophils contribute to protective host defense. In one study, antibody-mediated neutrophil depletion was associated with higher levels of Th1- and Th2-associated cytokines and prolonged survival after pulmonary infection (148). A more recent report showed that neutrophil depletion was dispensable for fungal clearance and was associated with higher levels of production of IL-17A production by $\gamma\delta^+$ T cells (147). Thus, it is possible that the reduction in pulmonary eosinophils, rather than the transient increase in neutrophil recruitment, may contribute to the resistant phenotype of in B6.CBA-*Cnes2* mice.

Non-resident ExM are derived from circulating Ly-$6C^{high}$ monocytes in a CCR2-dependent manner. These $CD11b^+$ cells have a classical activation phenotype and are highly fungicidal compared to AM (296). In addition, DC are considered to be primary antigen presenting cells and have been shown to promote T cell proliferation and activation during cryptococcal infection (128, 129, 141). At day 21 post-infection, the number of DC and ExM was higher in B6.CBA-*Cnes2* lungs compared to C57BL/6 mice and both of these myeloid cell subsets showed higher expression of the surface activation markers CD40 and CD80. Comparative analysis of lung macrophage polarization at day 14 showed significantly higher expression of the classical activation marker *Nos2* in B6.CBA-*Cnes2* mice*,* while C57BL/6 exhibited a significant increase in *Fizz1* expression and a trend towards higher *Arg1* expression. *Ex vivo* analysis at day 21 post-infection also showed a significant reduction of viable cryptococci in isolated lung macrophages from B6.CBA-*Cnes2* mice compared to C57BL/6. The reduced intracellular fungal burden suggests that ExM from B6.CBA-*Cnes2* mice directly contribute to improved host defense; however, it is likely that several distinct myeloid and lymphoid cell populations are collectively responsible for the overall reduction in whole lung CFU at this time point. Nevertheless, compared to C57BL/6, the resistant

phenotype of B6.CBA-*Cnes2* mice can be attributed, at least in part, to its positive influence on the recruitment, activation, and polarization of monocyte-derived macrophages. These results are also consistent with other studies demonstrating that increased recruitment of classical activated lung ExMs correlates with improved fungal clearance and a reduction in fungal dissemination (269, 270, 296, 297, 311, 312).

Following *C. neoformans* infection it has been shown that early cytokine signals produced by innate cells such as resident AM are crucial to the development of effective adaptive immune responses (313). Specifically, a Th1/Th17 cytokine profile is shown to activate macrophage anti-cryptococcal activities while a Th2 profile is associated with cryptococcal dissemination and host damage (113, 116, 166, 297). Comparison of lung cytokine and chemokine profiles showed that the B6.CBA-*Cnes2* strain had higher expression of pro-inflammatory mediators (IL-6, IL-1β, and TNF-α) compared to C57BL/6 mice at day 7 and day 14 post-infection. B6.CBA-*Cnes2* mice also expressed higher levels of Th1-associated cytokines (IFN-γ and IL-12) and chemokines (KC, MIP-1α, and MIP-2α) compared to the C57BL/6 strain at day 14 post-infection. Both $CD4^+$ and $CD8^+$ T cells produce pro-inflammatory cytokines in response to cryptococcal exposure (314). Compared to C57BL/6, the lungs of B6.CBA-*Cnes2* mice also contained a greater number of $CD4^+$ T cells at day 21 and day 28 post-infection and higher number of $CD8^+$ T cells at day 28 post-infection. Intracellular staining at day 14 and day 21 post-infection also showed that $CD4^+$ T cells in C57BL/6 lungs produced significantly higher Th2-associated cytokines (IL-4, IL-5 and IL-13) compared to those in B6.CBA-*Cnes2* lungs. No significant difference in the frequency of IFN-γ^+CD4 T cells was observed between two strains nor was there any difference in the number of B cells between the two strains (data not shown). Accordingly, it appears that *Cnes2* congenic interval regulates the number and function of $CD4^+$ T cells but does not significantly affect total B cell accumulation in the lungs of mice that have been infected with *C. neoformans* 52D. The current observations do not exclude a functional role for B lymphocytes in cryptococcal host defense since previous studies have shown an association between B cell responses and fungal clearance (187, 191). In fact, quantification of serum antibody levels at day 21 post-infection showed a selective increase in the level of IgG_3 in B6.CBA-*Cnes2* compared to C57BL/6 mice. Although the mechanism of antibody-mediated protection against *C. neoformans* is extremely complex, this observation is consistent with a previous report showing a protective effect of a IgG_3

monoclonal antibody against glucuronoxylomannan in C57BL/6 x 129/Sv mice (315). Despite the fact that IgE antibody levels generally reflect the balance between Th1 and Th2 responses, the equivalent serum levels between C57BL/6 and B6.CBA-*Cnes2* mice was not unexpected since the CBA/J inbred strain does not regulate this isotype during *C. neoformans* infection (316).

Taken together, the data presented in this report demonstrates pleiotropic effects of the *Cnes2* locus on the host immune response to pulmonary *C. neoformans* infection. Although the exact regulatory mechanisms remain to be defined, based on the observation that the phenotypic differences between B6.CBA-*Cnes2* and C57BL/6 mice are most evident between day 7 and day 21 post-infection, we hypothesize that the underlying genetic factors encoded by the *Cnes2* locus function during the afferent phase of the host response. We speculate that the enhanced recruitment of ExM and DC may arise from key differences in the inflammatory microenvironment of the infected lung and that these activated myeloid cell subsets may directly facilitate cryptococcal clearance while promoting lymphocyte polarization to a sterilizing Th1 pattern (111).

The *Cnes2* region spans 31.1 Mb of mouse chromosome 17 and contains 482 annotated protein coding genes. A comparative analysis of the C57BL/6 and CBA/J mouse genome sequences indicates that 128 of these genes contain either a non-synonymous single nucleotide polymorphism (SNP) in the protein coding region, a stop codon variation, or a splice-site SNP. There are several genes with a clearly recognized role in the immune response including tumor necrosis factor (*Tnf*), lymphocyte antigen 6 complex (*Ly6g*), chemokine C-C motif receptor 6 (*Ccr6*), complement factor B (*Cfb*), lymphotoxin A and B (*Lta*, *Ltb*), peptidoglycan recognition protein 2 (*Pglyrp2*), formyl peptide receptor 1 (*Fpr1*); however, none of these have a difference in the predicted protein sequence between C57BL/6 and CBA/J. It is possible that the *Cnes2* interval contains one or more regulatory variants that affect the level or pattern of gene expression and modulate immune function (317). Well-known mechanisms of transcriptional regulation include non-coding DNA variation within *cis*-regulatory elements such as proximal promoters and distal enhancers or expression of a variety of non-coding RNA species (318, 319). Regulatory variants have a diverse mode of action and may act locally or at a distance to modulate a range of epigenetic processes, often in a highly context-specific manner (320). Such complexity makes functional characterization of regulatory variants a challenging pursuit; nevertheless, indirect evidence for their role in differential *C. neoformans* susceptibility could be obtained by comparative gene

expression analysis at serial time points following infection in purified C57BL/6 and B6.CBA-*Cnes2* lung cell populations that have been implicated in host defense by this study. Genes with a significantly different spatial/temporal pattern or level of expression could provide an entry point for identification of causal regulatory variants and their mechanism of action through further molecular experimentation. The mouse major histocompatibility complex (*H-2)* is a highly polymorphic region that encodes molecules responsible for antigen presentation, and a portion of this complex is located at the telomeric end of the *Cnes2* congenic interval (207). Using a panel of congenic mice the $H\text{-}2^{k/k}$ haplotype was associated with susceptibility to intraperitoneal cryptococcal infection; however, this route of infection does not necessarily reflect the pulmonary host response and the role of genes that are linked to the *H-2* complex could not be excluded in this study (250). The peak LOD score position of the *Cnes2* locus is approximately 20Mb proximal to the *H-2* (290) and suggests that the causative genes are not located in this complex; nevertheless, it is theoretically possible that polymorphic sequences encoded at the distal end of the congenic CBA/J segment could contribute to the resistant phenotype of B6.CBA-*Cnes2* mice. Thus, it is clear that further studies, including the creation of B6.CBA-*Cnes2* sub-congenic mice, will be required to identify the strongest candidate genes for host resistance to progressive cryptococcal infection.

Figures

Figure 2.1: The *Cnes2* chromosomal interval restricts *C. neoformans* pulmonary infection and dissemination to the brain and spleen. (A) Schematic representation of the *Cnes2* congenic interval on chromosome 17 flanked by marker rs13460774 (3.4Mb) and marker 13482963 (35.5Mb). C57BL/6 and B6.CBA-*Cnes2* mice were infected intratracheally with 10^4 CFU of *C. neoformans* 52D and fungal burden in the (B) lungs at 7, 14, 21, and 35 dpi and (C) brain and spleen at 35 dpi was determined by plating tissue homogenates on Sabouraud dextrose agar. Data are shown as mean ± SEM with n = 6–8 mice/group and are representative of two independent experiments. $^{**}p < 0.01$, $^{***}p < 0.001$, using an unpaired Student's t-test (B) and Mann–Whitney U test (C).

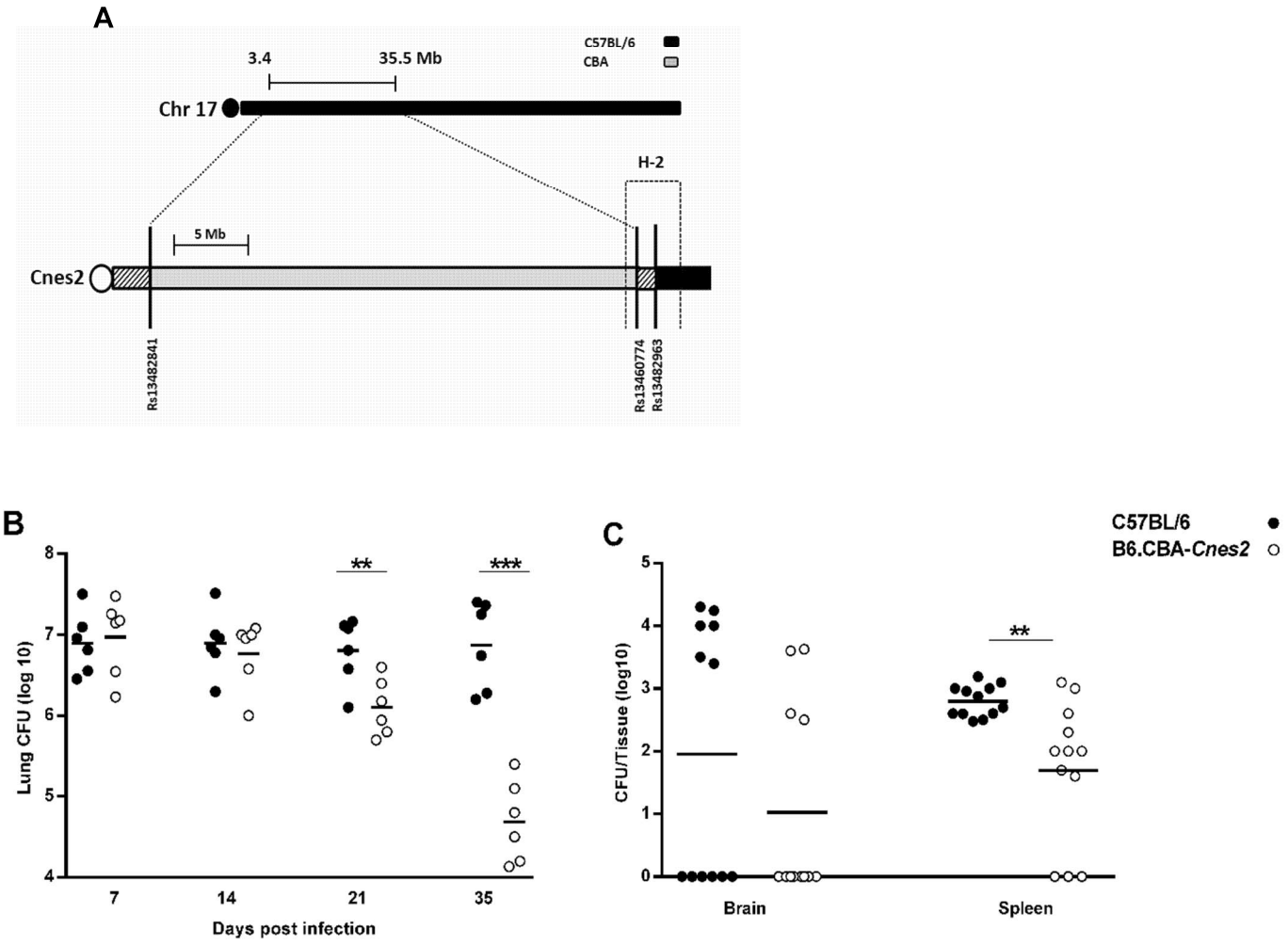

Figure 2.2: B6.CBA-*Cnes2* mice develop an altered pattern of pulmonary inflammation following *C. neoformans* infection. C57BL/6 and B6.CBA-*Cnes2* mice were infected with 10^4 CFU of *C. neoformans* 52D. At 35 dpi lungs were fixed, excised, embedded in paraffin, and stained with PAS (A and B), H&E (C and D), or mucicarmine (E&F). The airway epithelial mucus stains red with PAS. The cryptococcal cell wall stains red with mucicarmine. Each image is representative of n=3 mice/group.

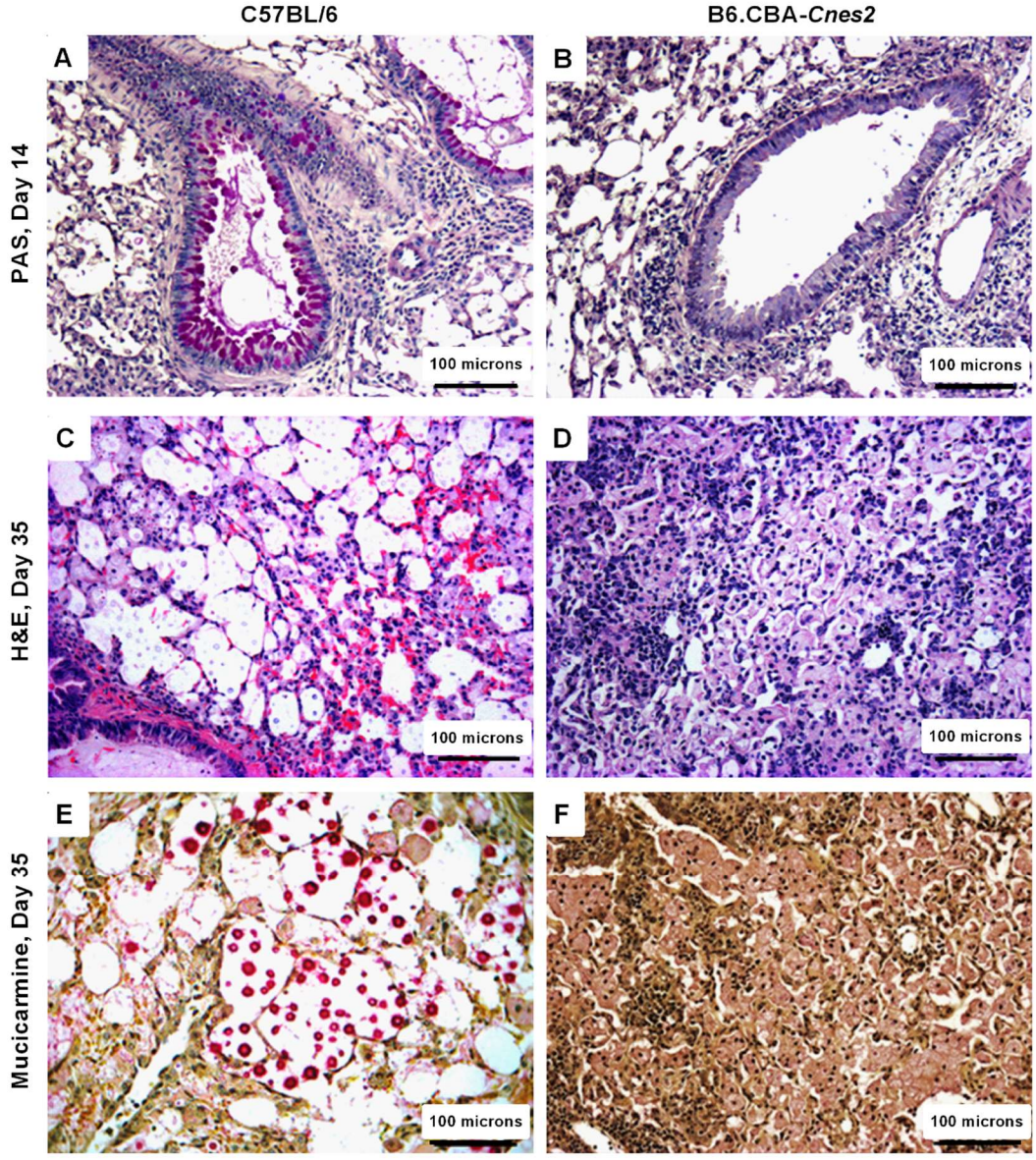

Figure 2.3: Increased airway neutrophilia, decreased eosinophilia, and enhanced macrophage accumulation in C57BL/6.CBA-*Cnes2* airways following *C. neoformans* infection. Airway leukocytes were isolated by bronchoalveolar lavage (BAL) from C57BL/6 and B6.CBA-*Cnes2* mice at 3, 7, 14, and 21 dpi following intratracheal infection with 10^4 CFU of *C. neoformans* 52D and the total cell number was determined by a Z1 particle counter (A). Leukocyte subsets were identified by Diff-Quik staining of BALF cell suspensions on cytospin slides and the absolute number of cells for each leukocyte subset (B-D) was determined by multiplying the percentage of each cell type by the total number of leukocytes. n = 4-6 mice/strain/time point; $^{**}p < 0.01$, $^{***}p < 0.001$.

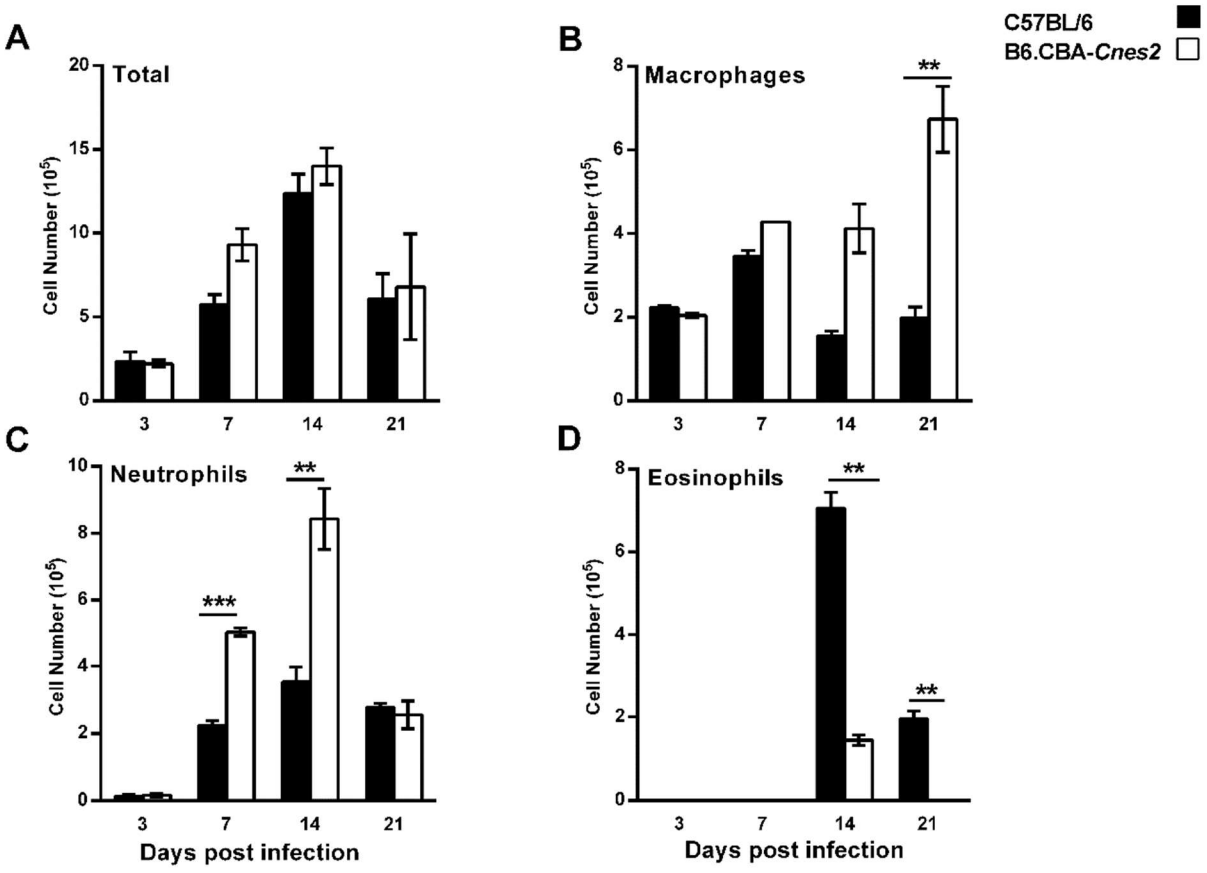

Figure 2.4: B6.CBA-*Cnes2* lungs have a heightened inflammatory response to *C. neoformans* infection characterized by increased expression of Th1 cytokines and chemokines. Whole lung protein was collected at 7 (A) or 14 (B-D) dpi with 10^4 CFU of *C. neoformans* 52D. ELISA was performed to determine the level of (A) pro-inflammatory mediators, (B) Th1/Th17-type cytokines, (C) chemokines, and (D) Th2-type cytokines. The expression of lung IL-4 mRNA was determined by quantitative RT-PCR (E). Data are shown as mean ± SEM with n = 4-6 mice per group and are representative of two independent experiments. *$p < 0.05$, ** $p < 0.01$, ***$p < 0.001$ using an unpaired Student's t-test.

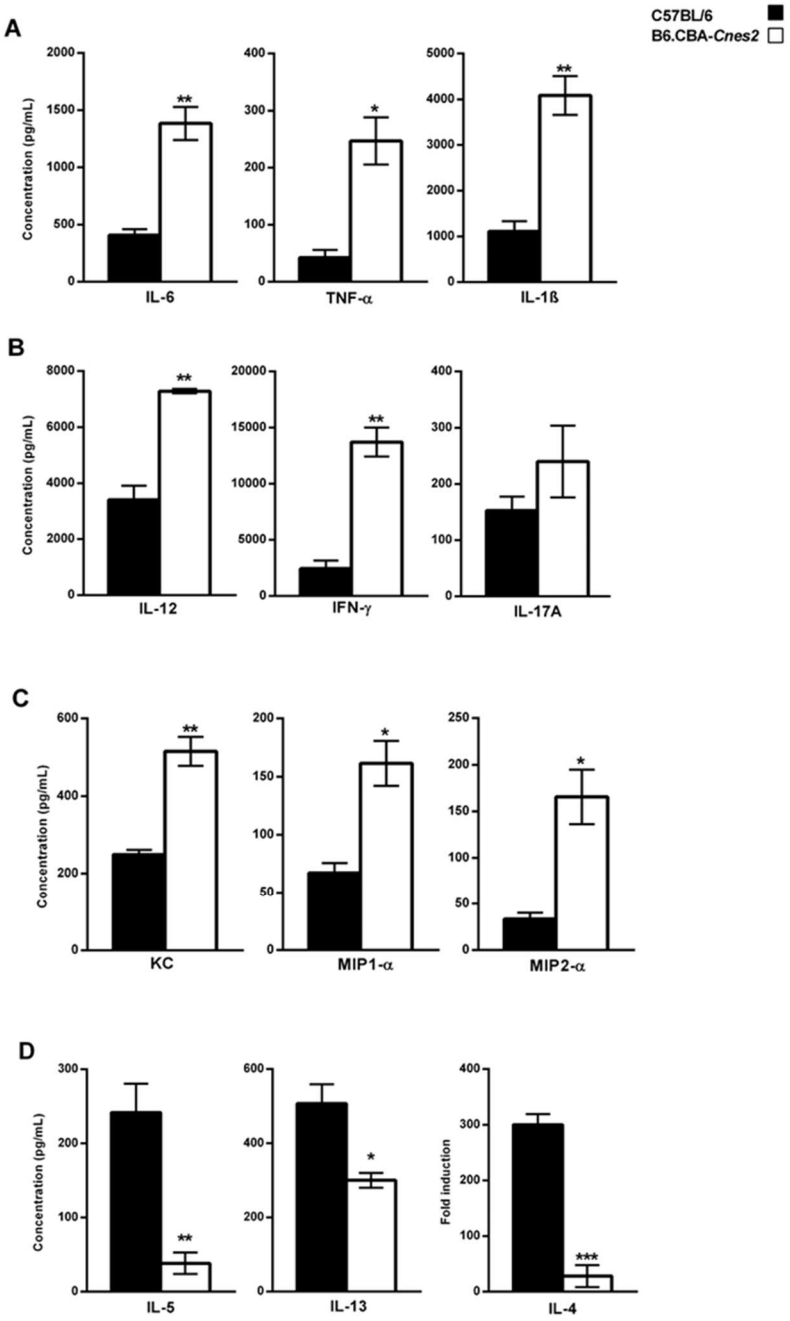

Figure 2.5: B6.CBA-*Cnes2* mice display greater accumulation of neutrophils, exudate macrophages, and CD11b$^+$ dendritic cells in the lungs following *C. neoformans* infection. Lung cell suspensions from infected C57BL/6 and B6.CBA-*Cnes2* mice were stained with fluorochrome-labeled antibodies and analyzed by flow cytometry as described in Materials and Methods. The gating strategy for (A) neutrophils (CD11b$^+$Ly6G$^+$), (B) eosinophils (CD11b$^+$SSC^{hi}), (C) ExM (autofluorescence$^+$CD11b$^+$CD11c$^+$) and (D) DC (autofluorescence$^-$ CD11b$^+$CD11c$^+$) at 14 dpi is shown. Absolute numbers of neutrophils, eosinophils, ExM, and DC in the lung at 0, 7, 14, 21, and 28 dpi are displayed (E-H). Values represent the mean ± SEM (n = 4-6 mice/group/time point). Data were pooled from two independent experiments. *$p < 0.05$, **$p < 0.01$, ***$p < 0.001$, using an unpaired Student's t-test.

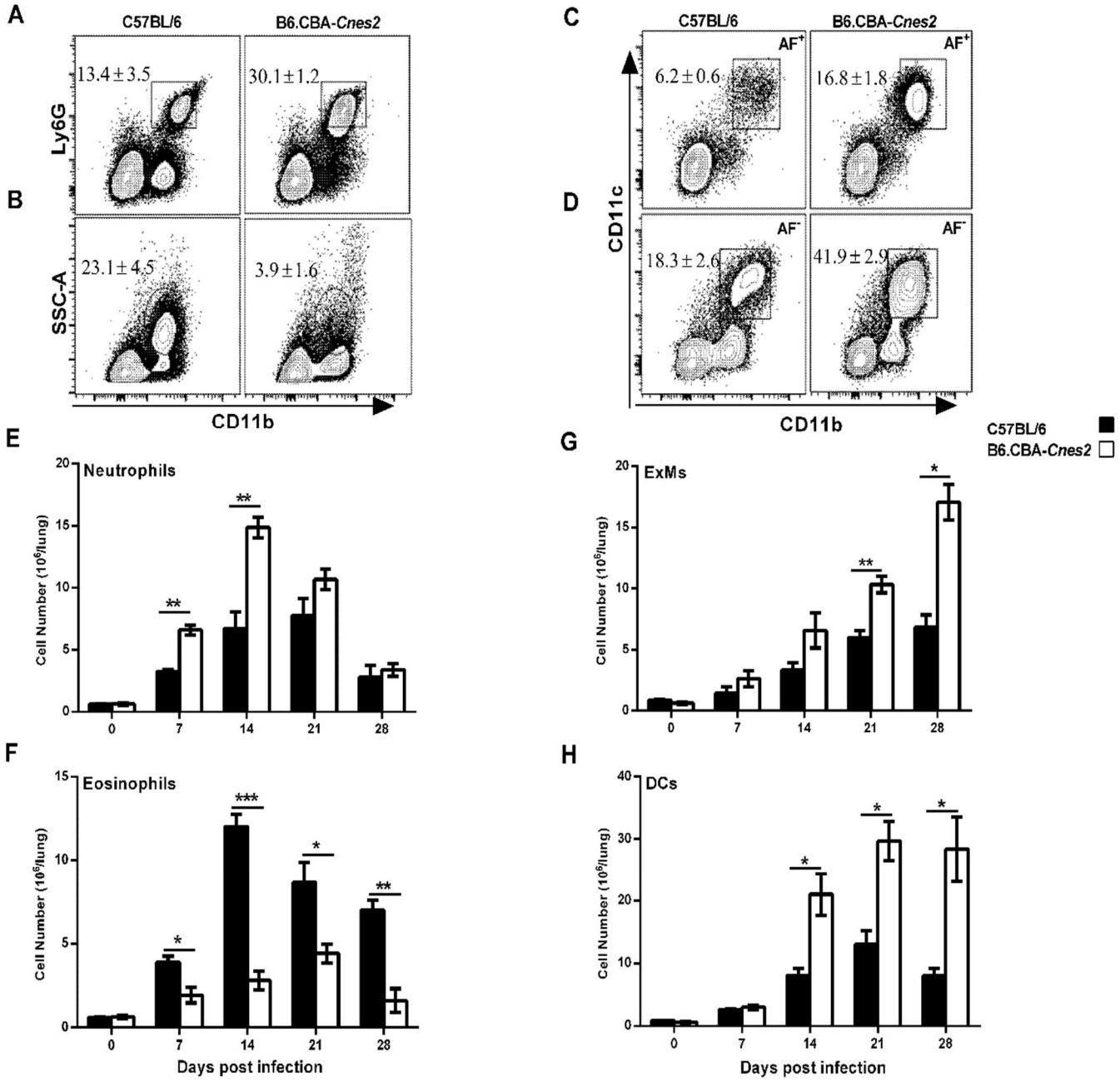
A
C57BL/6
B6.CBA-Cnes2
13.4±3.5
30.1±1.2
Ly6G
B
23.1±4.5
3.9±1.6
SSC-A
CD11b
C
AF+
6.2±0.6
16.8±1.8
D
CD11c
AF-
18.3±2.6
41.9±2.9
CD11b
C57BL/6
B6.CBA-Cnes2
E
Neutrophils
Cell Number (10⁶/lung)
G
ExMs
F
Eosinophils
Days post infection
H
DCs
Days post infection

Figure 2.6: Pulmonary macrophages and dendritic cells of B6.CBA-*Cnes2* mice develop a stronger classical activation phenotype in response to *C. neoformans* infection. (A) The surface expression of costimulatory molecules by ExM (autofluorescence^{+}CD11c^{+}CD11b^{+}) and pulmonary DC (autofluorescence^{-}CD11c^{+}CD11b^{+}) were analyzed at 21 dpi using flow cytometry. C57BL/6, gray filled lines; B6.CBA-*Cnes2*, white filled solid lines; uninfected mice, dashed lines. (B) The bar graph displays the mean fluorescence intensity of positive cells derived from total CD11c^{+} CD11b^{+} macrophages and DC (C) The expression of classical (*Nos2*) and alternative (*Arg1*, *Fizz1*) activation markers by total adherent pulmonary macrophages was evaluated by qRT-PCR at 14 dpi. Values represent the mean ± SEM (n = 4-6 mice). (D) Macrophages were isolated from the lungs of C57BL/6 and B6.CBA-*Cnes2* mice at 21 dpi and intracellular cryptococci enumerated. Data were pooled from two independent experiments. *$p < 0.05$, ** $p < 0.01$, *** $p < 0.001$, using an unpaired Student's t-test.

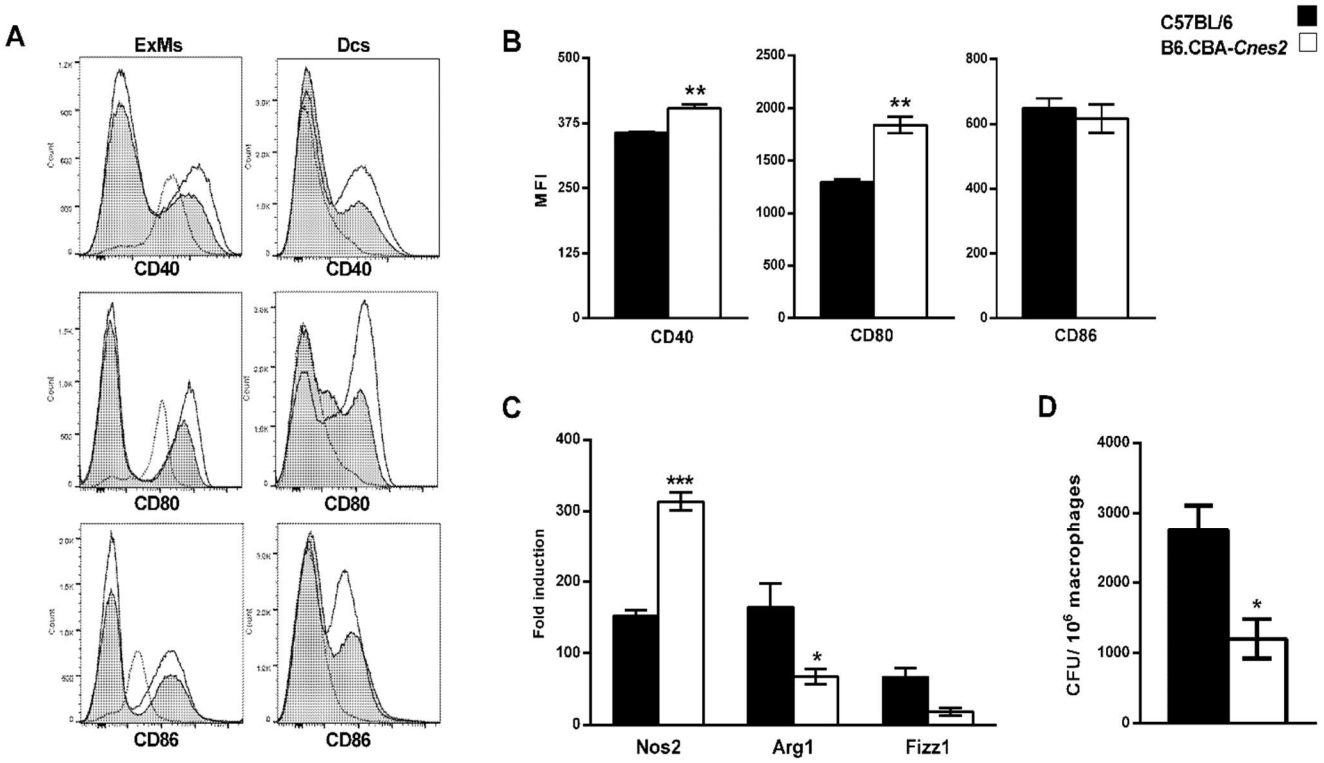

Figure 2.7: The lungs of B6.CBA-*Cnes2* mice contain a greater number of T lymphocytes during the adaptive immune response against *C. neoformans*. Lung cell suspensions from infected mice were stained with fluorochrome-labeled antibodies and analyzed by flow cytometry as described in Materials and Methods. (A, B) The total number of $CD4^+$ and $CD8^+$ cells in the lungs at 0, 7, 14, 21, and 28 dpi is shown. (C) Surface expression of effecter (CD44), early activation (CD69), and naïve (CD62L) markers on $CD4^+$ and $CD8^+$ cells are displayed at 21 dpi; C57BL/6, gray filled dashed lines; B6.CBA-*Cnes2*, white filled solid lines. Values represent the mean ± SEM (n = 4-6 mice/group). Data were pooled from two independent experiments. *$p < 0.05$, **$p < 0.01$, using an unpaired Student's t-test.

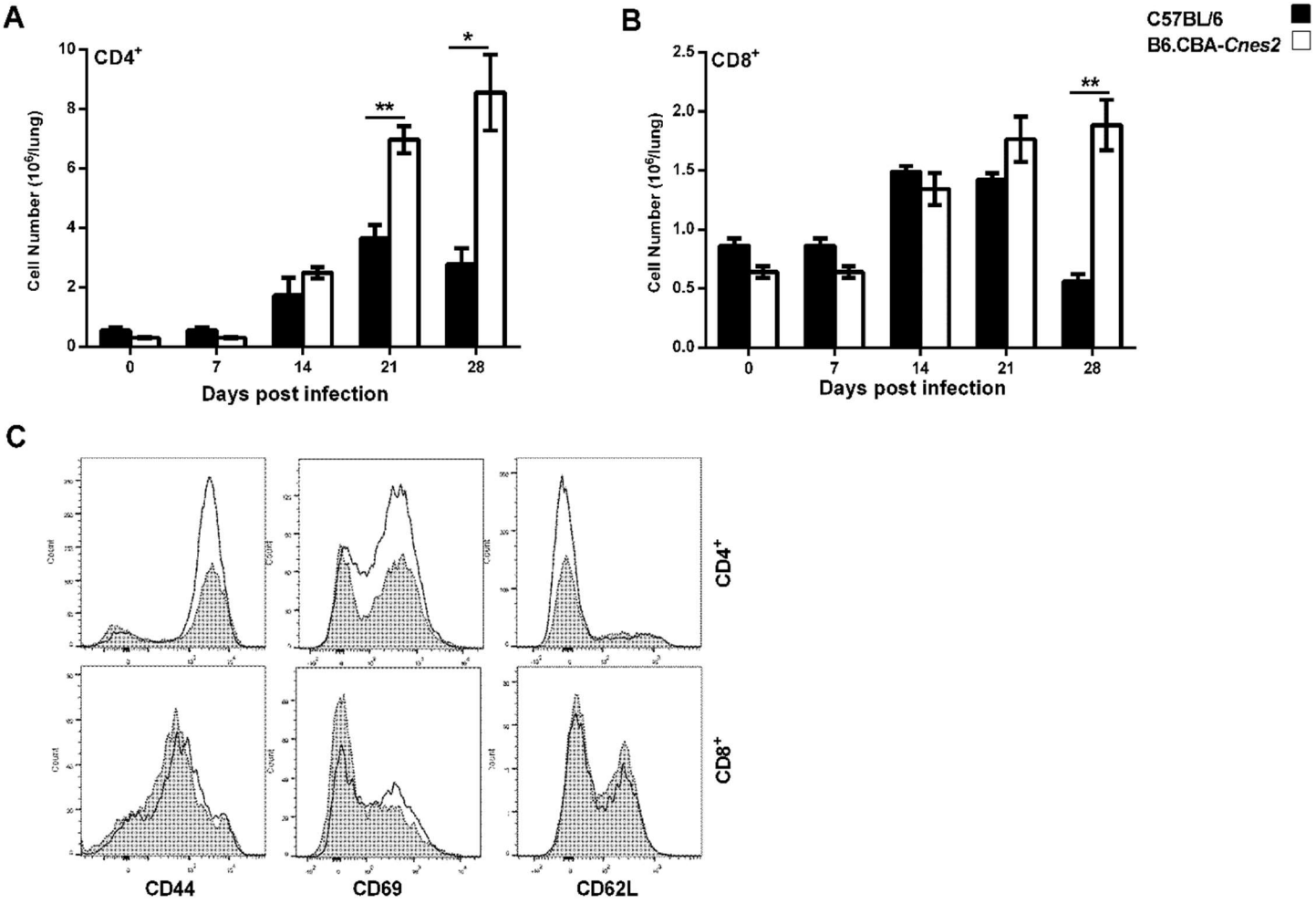

Figure 2.8: Decreased Th2 type cytokine expression by CD4$^+$ T cells from B6.CBA-*Cnes2* lungs infected with *C. neoformans*. (A) Representative flow cytometry plots of lung lymphocytes from individual mice harvested at 21 dpi and restimulated with PMA/ionomycin followed by intracellular staining for IFN-γ, IL-4, IL-5, and IL-13. Numbers shown are the percentage of cells in each gate relative to total cells in each plot and are expressed as mean ± SEM with n = 4-6 mice/group. **(B)** The frequency of CD4$^+$ T cells expressing IFN-γ, IL-4, IL-5, and IL-13 per mouse at 21 dpi is shown. Values represent means ± SEM with n = 4-6 mice. Data were pooled from two independent experiments. *$p < 0.05$, using an unpaired Student's t-test.

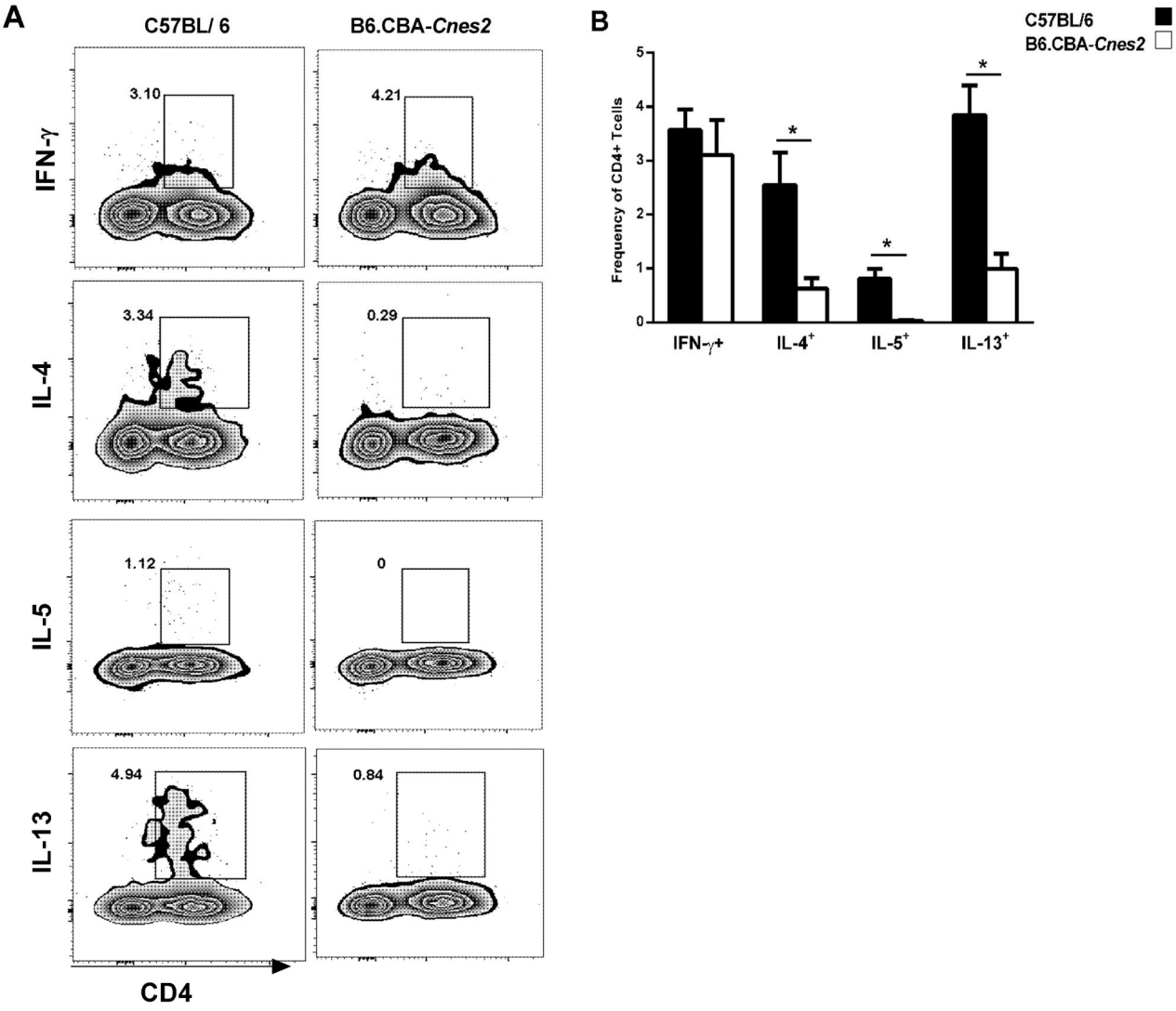

Figure 2.9: Characterization of serum antibody responses following *C. neoformans* infection of C57BL/6 and B6.CBA-*Cnes2* mice. The level of total IgE, IgG subclasses, and IgM is shown at 21 dpi. Data were pooled from two independent experiments. *$p < 0.05$, using an unpaired Student's t-test.

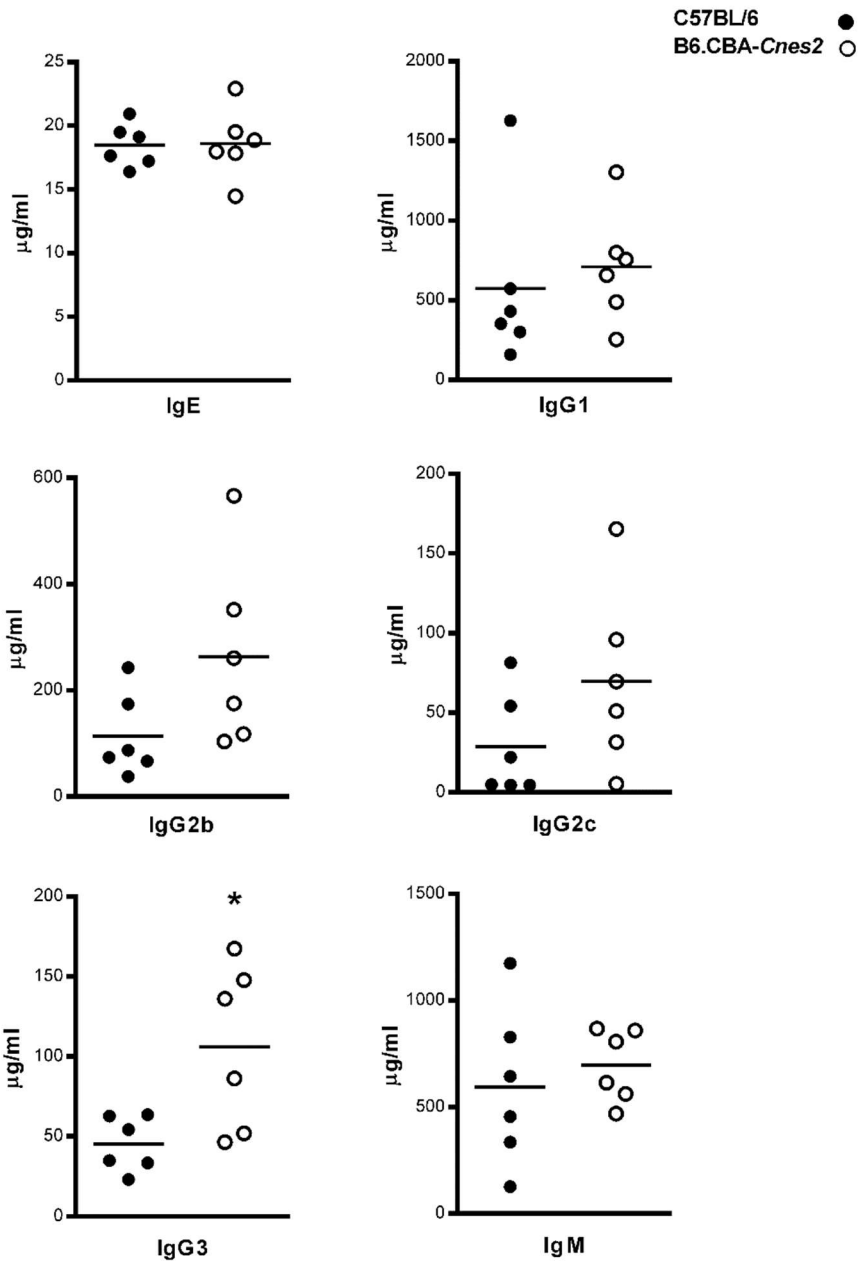

Supplementary Figure 2.1. Breeding strategy for congenic mice.

A) Schematic representation of the sequential backcrossing of CBA/J donor alleles (in white) onto the C57BL/6 recipient background (in black). At each generation, the genomic DNA of at least 2 males was sent for a low density genome scan. The male with the best background percentage was selected for the next generation. B) Time course required to obtain 100% B6 background for the B6.CBA-*Cnes2* congenic lines. Each generation required an average of 70 days (21days gestation period and 49 days for maturation of the male). (adapted from www.jax.org)

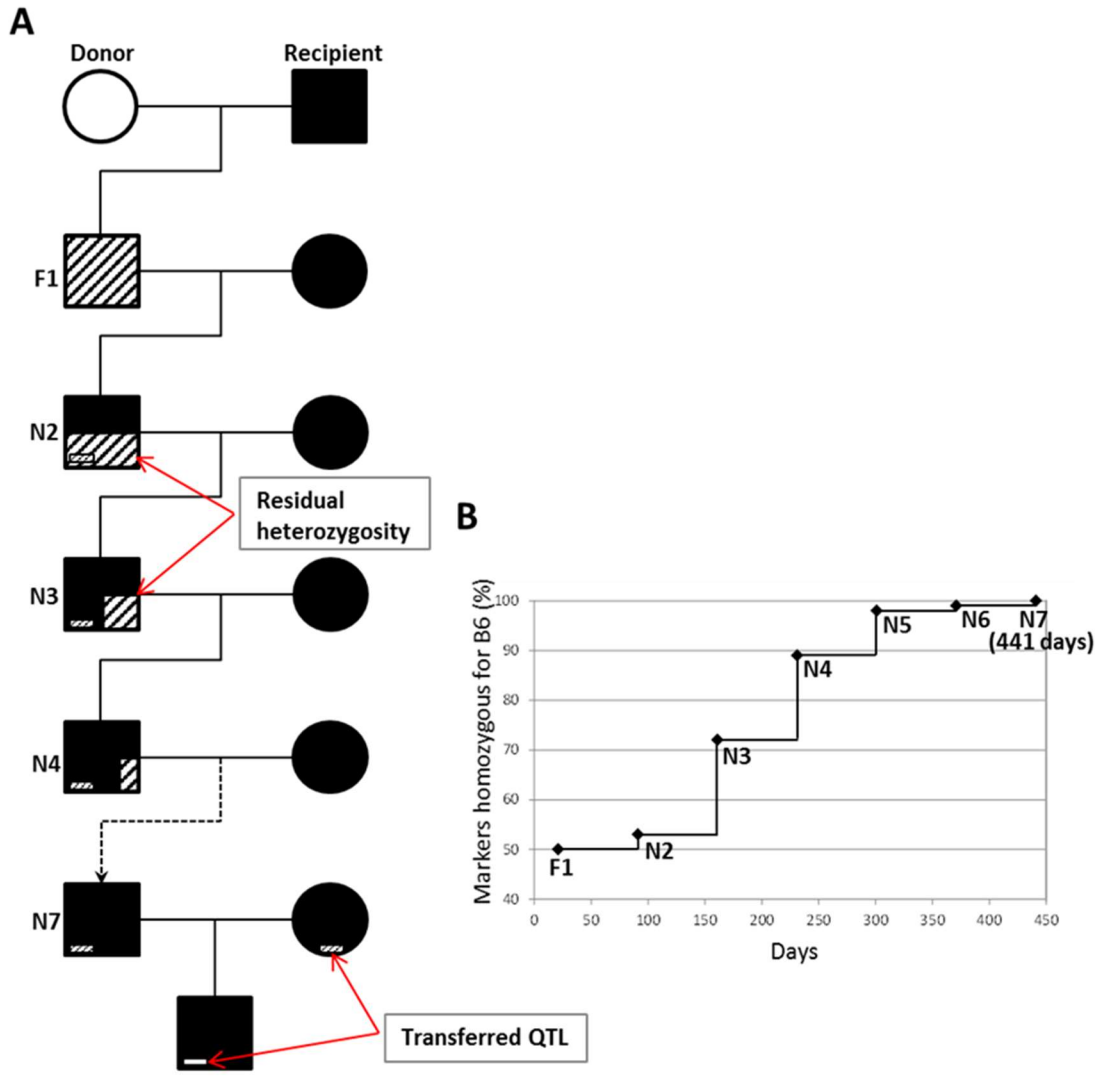

Supplementary Figure 2.2: Gating strategy used for flow cytometry analysis.

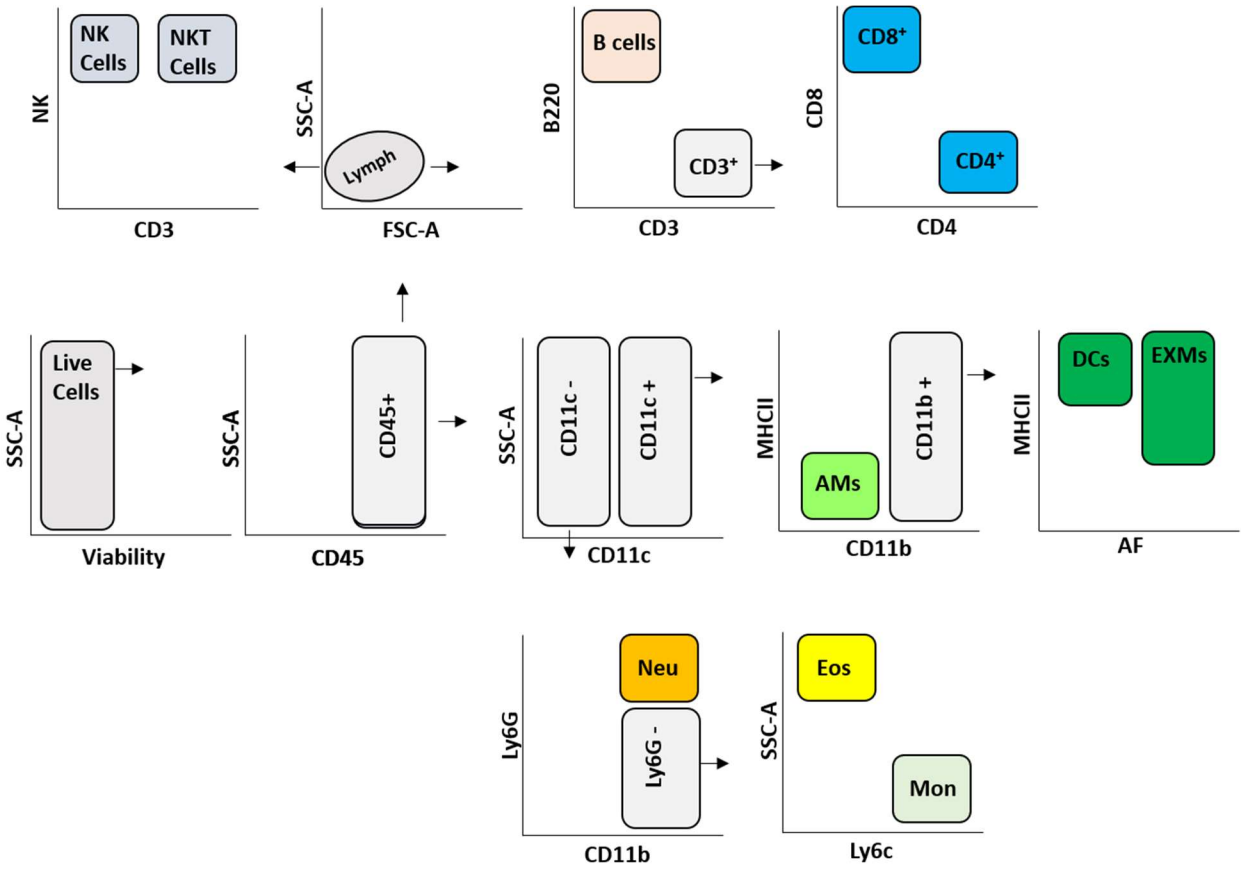

Chapter 3

Phenotypic analysis of *Cnes2* sub-congenic mice reveals two different intervals associated with resistance to *C. neoformans* infection

Mitra Shourian,[a,b] Isabelle Angers,[a,b] Salman T. Qureshi[a,b]

Meakins-Christie Laboratories, Department of Medicine and Division of Experimental Medicine, McGill University, Montréal, Québec, Canada[a]

Department of Critical Care and Research Institute of the McGill University Health Centre, Montréal, Québec, Canada[b]

Preface to Chapter 3

Using genome-wide linkage analysis between susceptible C57BL/6N and resistant CBA/J mouse strains and lung fungal burden as a quantitative trait, we previously identified a significant association between the *Cnes2* locus on mouse chromosome 17 and susceptibility to progressive *C. neoformans* 52D infection. Subsequently, to confirm the biological role of this QTL, we created a unique interval specific congenic mouse strain by transferring the *Cnes2* locus from CBA/J to the C57BL/6N background by repeated backcrossing. We then characterized the immune response of *Cnes2* mice following cryptococcal infection at different time intervals. Analysis of lung fungal burden, cell infiltration, cytokine/chemokine expression, and histopathology confirmed a strong and pleiotropic effect of the *Cnes2* locus on host susceptibility to cryptococcal infection (321). The *Cnes2* locus spans 31.1 Mb of mouse chromosome 17 and contains 482 annotated protein-coding genes which poses a challenge for identification of the causal candidate genes and variants that regulate host resistance. In this chapter, we aimed to reduce the complexity of the *Cnes2* interval by further development and characterization of sub-congenic strains.

3.1. Abstract

With the goal of definitively identifying the underlying susceptibility genes encoded within the *Cnes2* locus that regulate the host response to *C. neoformans* infection, we generated four sub-congenic strains (*Cnes2.1-Cnes2.4*) that contain overlapping CBA donor regions on a C57BL/6N background. Phenotypic analysis of fungal burden and cell recruitment allowed us to reduce the size of underlying QTL to 20 Mb by elimination of 17.5 Mb from the centromeric portion of the *Cnes2* interval, as the presence of this segment did not confer any significant differences in host resistance compared to control C57BL/6N mice. In addition, we found that two separate chromosomal intervals, *Cnes2.2* and *Cnes2.4*, independently regulate lung fungal burden and cell recruitment at day 35 post-infection with *C. neoformans* (Log_{10}: 6.520 ± 0.088 in C57BL/6N vs 5.796 ± 0.081, $p<0.0001$ in *Cnes2.2* and 5.434 ± 0.121, $p<0.0001$ in *Cnes2.4*). Flow cytometry analysis demonstrated that the total number of $CD45^+$ cells was higher in both sub-congenic strains at day 21 post-infection. At this timepoint the *Cnes2.2* and *Cnes2.4* subcongenic strains both showed significantly higher lung DCs and ExMs compared to control mice. In *Cnes2.4* mice ExMs and DCs expressing the M1 phenotype ($iNOS^+$) were significantly higher compared to control mice. Furthermore, *Cnes2.4* mice showed significantly higher numbers of neutrophils and $CD4^+$ cells compared to control mice. Surprisingly, we observed that the *Cnes2.4* strain had a 30% mortality by day 35 post-infection despite a significantly lower fungal burden in the lung at 21 and 35 days post-infection. Taken together, these data indicate that *Cnes2* locus harbors at least two distinct intervals that regulate susceptibility to *C. neoformans* infection. To complement the functional data, we conducted an extensive *in silico* analysis using publicly available genome browsers. Based on the identification of single nucleotide polymorphisms within conserved protein coding regions or exon splice sites that are predicted to have a deleterious functional consequence, we identified 2 protein coding genes within *Cnes2.2* (*Fpr3 and Fpr-rs4*) and 10 protein coding genes within *Cnes2.4* (*Notch3*, *Ager, H2-Ab1*, *Myo1f*, *Ubash3a, Tap1, H2-Eb1, H2-Oa, C5b and Lst1*) as plausible candidates. This data provides a foundation for further detailed investigation of the causative genes and variants that mediate host resistance to cryptococcal infection.

3.2. Introduction

Based on recent data, infection with *Cryptococcus sp.* represents the most prevalent life-threatening fungal infection in the world, killing up to 600000 individuals each year, mainly in Sab-Saharan Africa (9, 15). Although cryptococcosis occurs mainly in immunocompromised patients, up to 20% of cases develop phenotypically normal or non-immunocompromised individuals (14, 28). The incidence of cryptococcosis in immunocompetent individuals, coupled with the fact that not all HIV-infected patients develop the disease, signifies the importance of investigating other risk factors for susceptibility. Such knowledge will improve the ability to predict which populations are predisposed to infection and could facilitate the development of targeted therapeutic interventions. A handful of case reports and cohort studies have investigated the role of human genetic susceptibility to cryptococcal infection (10, 208-210), but very few human population-based studies have directly investigated this issue (227). For example, in HIV-negative individuals, FCγR (FCGR2A, 3A and 3B genes) and mannose-binding lectin (MBL) polymorphisms have been reported to increase susceptibility to cryptococcal infection (222-224). In HIV-infected patients, allelic polymorphisms of FCγRIII were correlated with a 20-fold increased risk of *Cryptococcus sp.* infection in homozygous individuals (226). Conversely, a study in the Papua New Guinean population did not reveal a significant association of HLA genotype with susceptibility to cryptococcal infection (221). These epidemiologic studies are a valuable approach for identifying inherited factors that may influence immunity to infectious diseases but their scope is quite limited.

In most cases, host resistance to infection is recognized to be a highly complex trait under multigenic control (236). Accordingly, comprehensive elucidation of the factors that underlie susceptibility to infection requires several complementary approaches. Forward genetic analysis using mouse models is a powerful and well-established strategy to study the fundamental basis of natural variation in complex phenotypic traits and disease (reviewed in chapter 1). Among the classical inbred strains, C57BL/6 mice are one of the most susceptible, and the CBA/J strain has been reported to be highly resistant, to cryptococcal infection. To model the process of human infection, we have used a direct intratracheal method for administration of *C. neoformans* 52D and conducted genome-wide linkage analysis in a [C57BL/6N X CBA/J] F2 population using lung fungal burden as a complex trait. This analysis revealed two significant Quantitative Trait

Loci (QTL) in the female F2 population: *Cnes1* on chromosome 1, and *Cnes2* on chromosome 17 (207). To confirm the role of each QTL on host susceptibility, we developed interval-specific congenic mice for *Cnes1* and *Cnes2* on the C57BL/6 genetic background. As quantification of lung fungal burden reflects the overall outcome of an innate and adaptive immune response, we also measured other phenotypes such as lung cell recruitment and cytokine/chemokine expression following infection to fully elucidate the potential role of each identified QTL on host resistance. Compared to C57BL/6N mice, the B6.CBA-*Cnes1* congenic strain had a significantly lower lung fungal burden at 35 days post-infection; however, no significant differences in several inflammatory phenotypes were detected at various time intervals (data not shown). In contrast, transfer of the *Cnes2* locus (B6.CBA-*Cnes2)* was sufficient to reduce fungal burden in the lung by more than 100-fold (log_{10} CFU, 4.68± 0.20 versus 6.87± 0.22; $p \leq 0.001$) compared to the inbred C57BL/6N strain. Further detailed phenotypic analysis of B6.CBA-*Cnes2* mice revealed a strong and pleiotropic effect of the *Cnes2* segment on host immune response (321). The *Cnes2* region spans 31.1 Mb of mouse chromosome 17 and contains 482 annotated protein-coding genes that make it extremely challenging to efficiently identify causal sequences and variants. The aim of the present study was to reduce the complexity of the *Cnes2* interval by further development and characterization of sub-congenic strains. Here we report the confinement of the *Cnes2* segment to a ~23 Mb interval using a panel of unique sub-congenic strains and have identified two sub-intervals (*Cnes2.2* and *Cnes2.4*) that act separately to confer resistance to infection. Furthermore, we have refined the list of candidate genes by extensive *in silico* analysis using publicly available genome browsers. Uncovering the causal genes that regulate host susceptibility has the potential to guide the development of new management strategies for human cryptococcal disease.

3.3. Material and Methods

Generation of sub-congenic lines: C57BL/6 mice were purchased from Harlan Laboratories (Indianapolis, IN, USA) and subsequently bred and maintained in our specific-pathogen-free (SPF) facility. The B6.CBA-*Cnes2* congenic strain was generated as previously described (16). A series of overlapping sub-congenic strains were created by crossing a homozygous *Cnes2* mouse with C57BL/6 to generate F1 progeny that were intercrossed or backcrossed to C57BL/6 mice. The resulting F2 or N2 mice were genotyped for a series of single nucleotide polymorphisms (SNPs) in the interval to identify recombination events. Mice that showed recombination within the *Cnes2* interval were selectively outcrossed to C57BL/6 to generate males and females that were subsequently mated to create homozygous sub-congenic lines for phenotypic analysis. All the known SNPs in the *Cnes2* region between the C57BL/6N and CBA/J strains were identified by searching dbSNPs using the MGI online tool (http://www.informatics.jax.org/snp). This list was compared to the list of commercially available Mouse TaqMan Pre-Designed SNP Genotyping Assays from Applied Biosystems (ABI) to select the markers that would be used to genotype the progeny. The SNP markers were genotyped by TaqMan (Life Technologies) using the ABI Prism 7500 real-time PCR system (Life Technologies). A schematic representation of sub-congenic lines (B6.CBA-*Cnes2*.1 to -*Cnes2.4*) and the markers used for genotyping are shown in Figure 3.1. All experiments were performed with 7- to 9-week old gender matched mice. All animals were maintained in compliance with the Canadian Council on Animal Care and all experimental protocols were reviewed and approved by the McGill University Animal Care Committee.

Cultures of *C. neoformans*

C. neoformans 52D (ATCC 24067) was grown from glycerol stocks and maintained on Sabouraud dextrose agar (SDA) (Becton Dickinson). To prepare an infectious dose, a single colony was suspended in Sabouraud dextrose broth and grown to early stationary phase (48 h) at room temperature on a rotator. The stationary phase culture was then washed with sterile phosphate-buffered saline (PBS), counted on a hemacytometer, and diluted to 2×10^5 CFU per ml in sterile PBS. The fungal concentration of the experimental dose was confirmed by plating a dilution of the inoculum on SDA and counting the CFU after 72 h of incubation at room temperature.

Intratracheal infection with *C. neoformans*. For intratracheal administration of *C. neoformans*, mice were anesthetized with 150 mg/kg of ketamine (Ayerst Veterinary Laboratories) and 10

mg/kg of xylazine (Bayer) intraperitoneally. A small skin incision was made below the jaw along the trachea, and the underlying glands and smooth muscle were separated. Infection was performed by intratracheal injection of 50µl of sterile PBS containing 10^4 or 10^5 CFU (for survival experiments) of *C. neoformans* through a 22-gauge catheter mounted on a 1ml tuberculin syringe. The incision was closed using the 9-mm EZ clip wound closing kit (Stoelting), and mice were monitored daily following surgery.

Tissue isolation and CFU assay. After mice were humanely euthanized with CO_2, the lungs, spleen, and brain were excised and placed in sterile, ice-cold PBS. The tissues were then homogenized using a glass tube and pestle attached to a mechanical tissue homogenizer (Glas-Col), and plated at various dilutions on Sabouraud dextrose agar. Agar plates were incubated at 37°C for 72 h, and CFU were counted. For survival analyses, mice were inoculated as stated above and monitored twice daily for up to 120 days post-infection.

Histopathological analysis. Following euthanasia, lungs were perfused with ice-cold PBS via the right ventricle of the heart. The lungs were inflated to a pressure of 25 cm H_2O and fixed overnight in 10% buffered formalin acetate (Fisher Scientific). Subsequently lungs were embedded in paraffin, sectioned at 5µm, and stained with hematoxylin-eosin (H&E), periodic acid-Schiff (PAS), or mucicarmine reagents at the Histology Facility of the Goodman Cancer Research Centre (McGill University). Representative photographs of lung sections were taken using a BX51 microscope (Olympus), QICAM Fast 1394 digital charge-coupled device (CCD) camera (QImaging), and Image-Pro Plus software version 7.0.1.658 (Media Cybernetics).

Flow cytometry. Lungs were excised using sterile technique and placed in RPMI (Gibco, Invitrogen) supplemented with 10% fetal bovine serum (Wisent). Subsequently lungs were minced using surgical blades and incubated with 1 mg/ml collagenase (Sigma) at 37°C for 1 h. Following incubation, lung pieces were passed through a 16-gauge needle and filtered through a 70µm cell strainer (BD). Red blood cells were removed using ACK lysis buffer before the cells were counted using a Beckman Coulter Z1 particle counter. Fc receptors were blocked with the addition of unlabeled anti-CD16/32 antibodies (93; eBioscience [eBio]) and single-cell suspensions were stained with the following fluorescence-conjugated anti-mouse monoclonal antibodies purchased from eBio, BD, and BioLegend (BL): CD45-V500 (30-F11; BD), B220-fluorescein isothiocyanate (FITC) (RA3-6B2; eBio), CD3e-FITC (145-2C11; eBio), CD4-V450 (GK1.5; eBio), CD8-

peridinin chlorophyll protein (PerCP) (53-6.7; BD), CD11b-allophycocyanin(APC)(M1/70; BD),CD11c-FITC(N418; eBio), MHCII-phycoerythrin (PE)-Cy7 (M5/114.15.2; eBio), Ly6G-V450 (clone 1A8; BL), F4/80-PE (clone BM8; eBio), CD86-PE (GL1; eBio), CD40- PerCp/Cy5.5 (3/23; BL), CD80-PE (16-10A1; eBio) (add TFs, iNos, CD206). Non- viable cells were excluded using fixable viability dye eFluor780 reagent (eBio). Data were acquired using a fluorescence-activated cell sorter (FACS) LSR-II flow cytometer (BD) and analyzed using Flow Jo versionX software (TreeStar).

Intracellular flow cytometry. For intracellular cytokine staining of T-cells, lungs were processed as described above. Cells were plated and stimulated for 4h with 0.1 µl/ml phorbol 12-myristate 13-acetate (PMA) and 1 µl/ml calcium ionophore (Ionomycin; BD) in the presence of brefeldin A (GolgiPlug; BD) for the final 3h. Cells were then washed, blocked with anti-CD16/32 antibodies (93; eBio), and stained with a surface antibody cocktail consisting of anti-CD3-PE-Cy7 (145-2C11; BD), anti-CD4-V450 (GK1.5; eBio), anti-CD8-PerCP (53-6.7; BD), and anti-CD45-V500 (30- F11; BD). Cells were then fixed, permeabilized, and stained with IL-13-PE-Cyanine7 (eBio13A), IFNγ (XMG1.2; BL), and IL-17-APC (17B7; BL). Data were acquired using a FACS LSR-II flow cytometer (BD) and analyzed using Flow Jo software (TreeStar), with gating determined with fluorescence-minus-one (FMO) controls.

Statistical analysis. For all experiments, the mean and standard error of mean (SEM) are shown. To test the significance of single comparisons, an unpaired Student t test was applied (with a threshold P value of ≤ 0.05), unless otherwise stated. All statistical analysis was performed with GraphPad Prism software version 6 (GraphPad Software Inc.).

Candidate gene prioritization in the *Cnes2.2* and *Cnes2.4* intervals

Initially, a list of all variants including SNPs, indels and SVs with polymorphisms between C57BL/6NJ and CBA/J were acquired from Wellcome Trust Sanger Institute Mouse SNP viewer (https://www.sanger.ac.uk/sanger/Mouse/SnpViewer/rel-1303). Subsequently, reference SNP ID numbers (rs#) in separate lists for SNPs and indels were entered in input form to Variant Effect Predictor (VeP); http://www.ensembl.org/info/docs/tools/vep/index.html. The data from Vep were categorized based on variant impact level (high, moderate, low and modifier) and consequence (missense variant, start/stop lost variant, splice donor/acceptor variant, frameshift variant, synonymous variant, etc.). Variants with high impact and variants with moderate impact and a

deleterious effect (SIFT score ≤0.05) were chosen for further analysis. Finally, protein coding genes affected by deleterious variants were prioritized as candidate genes. The top candidates were chosen based on the expression pattern and functional information acquired from various databases (MGI, NCBI, Genecards, PubMed).

3.4. Results

Generation of sub-congenic mice and fungal burden analysis following *C. neoformans* infection: Previously we showed that the *Cnes2* locus clearly regulates lung fungal burden and susceptibility to progressive *C. neoformans* infection (321). To precisely identify the chromosomal segments that encode causative alleles underlying *Cnes2*, a series of four overlapping sub-congenic strains were created, as described in the material and methods section: B6.CBA-*Cnes2.1* (*Cnes2.1*) that spans from 3.4 to 16.2 Mb (length = 17.5 Mb), B6.CBA-*Cnes2.2* (*Cnes2.2*) that spans from 16.2 to 27.6 Mb (length = 11.4 Mb), B6.CBA-*Cnes3* (*Cnes2.3*) that spans from 22.8 to 27.6 Mb (length = 4.8 Mb), and B6.CBA.*Cnes2.4* (*Cnes2.4*) that spans from 27.6 to 35.5 Mb (length = 7.9 Mb) and includes part of H-2 complex (Figure 3.1). In the current study, we first evaluated the homozygous sub-congenic lines for lung fungal burden at 35 days post-infection as this was the phenotypic trait used for QTL mapping in the original study that had been validated in *Cnes2* congenic mice (207, 321). To accomplish this, mice were intratracheally infected with 10^4 CFU of *C. neoformans* 52D and lungs, brains and spleens were harvested for CFU enumeration (Figure 3.2). Our results revealed that the *Cnes2.1* interval at the centromeric region of *Cnes2* has no effect on lung fungal burden. *Cnes2.3* mice also showed no meaningful differences in lung CFU compared to C57BL/6; however, *Cnes2.2* had a significantly reduced lung fungal burden compared to C57BL/6 mice ($\log_{10}$ CFU: 5.79 ± 0.08 vs 6.52 ± 0.08, $p<0.0001$) (Figure 3.2A). *Cnes2.2* also showed a trend towards reduced brain dissemination compared to C57BL/6 mice at day 35 (2/11 vs 6/12 mice, $\log_{10}$ CFU: 0.7679 ± 0.51 vs 1.954 ± 0.59) (Figure 3.2B). Therefore, by excluding a contribution of the *Cnes2.3* segment to host defense, we refined the critical interval for *Cnes2.2* from 11.4 Mb to 6.6 Mb. In addition to *Cnes2.2*, mice with the *Cnes2.4* sub-congenic interval also showed a significantly lower lung fungal burden at day 35 post-infection compared to C57BL/6 mice ($\log_{10}$ CFU: 5.43 ± 0.12 vs 6.52 ± 0.08, $p<0.0001$). CFU analysis showed no significant differences in brain fungal load or proportion of mice with brain dissemination between *Cnes2.4* and C57BL/6 mice (Figure 3.2B). The fact that individual sub-congenic intervals did not have a significant effect on brain dissemination at 35 days post-infection was not surprising, as the entire *Cnes2* interval also did not change the pattern of brain dissemination compared to C57BL/6 mice at this time point (Figure 3.2B). Notably, *Cnes2.4* mice had a 30% mortality rate by day 35 post-infection despite having a significantly lower fungal burden in the lungs and spleen (Figure 3.2C, D). No mortality was seen in *Cnes2.2* and C57BL/6 mice; however, previously we had also

noticed a 13% mortality rate in *Cnes2* mice at 35 days post-infection (Figure 3.2D) despite having a lower fungal burden in the lungs, brain and spleen (321). To determine whether the observed mortality in *Cnes2.4* mice was associated with impaired pathogen control, we investigated tissue fungal burden at 18 days post-infection, just before the onset of mortality. Interestingly, fungal burden analysis showed significantly fewer CFU in the lungs of the *Cnes2.4* sub-congenic strain compared to C57BL/6 mice (Figure 3.2E). CFU analysis of the brain and spleen showed no significant differences between the two strains, although a higher proportion of *Cnes2.4* mice developed brain dissemination compared to C57BL/6 mice (4/7 vs 2/8 mice) (Figure 3.2F, G).

In summary, using fungal burden analysis we identified the presence of two non-overlapping sub-congenic intervals that contribute to the enhanced host resistance phenotype of the *Cnes2* congenic mice: *Cnes2.2* located between 16.2 Mb and 22.8 Mb and *Cnes2.4* that spans 27.6 Mb to 35.5 Mb. Each of these sub-congenic intervals regulates lung fungal burden but does not significantly alter brain dissemination at day 35 post-infection. Interestingly, the enhanced host defense phenotype of *Cnes2.4* sub-congenic mice is associated with an increased mortality rate compared to C57BL/6.

Flow cytometry analysis of myeloid lung cell recruitment and activation in sub-congenic mice following *C. neoformans* infection

We previously showed that the *Cnes2* congenic interval has a significant effect on lung cell recruitment and activation following *C. neoformans* infection. *Cnes2* congenic mice displayed greater accumulation of neutrophils, exudate macrophages, and $CD11b^+$ dendritic cells in the lungs following *C. neoformans* infection compared to C57BL/6 mice. In contrast, eosinophils were significantly lower in *Cnes2* congenic compared to control mice. As the myeloid cell difference between congenic *Cnes2* and control mice was mainly seen 14 and 21 days after infection, we decided to analyze the lung cell recruitment pattern in sub-congenic mice at 14 and 21 days post-infection with *C. neoformans* (Figure 3.3 and 3.4). At 14 days post-infection, flow cytometry analysis showed no significant differences in the total number of $CD45^+$ cells, neutrophils, or eosinophils between the *Cnes2.2* or *Cnes2.4* sub-congenic strains and control mice; however, the *Cnes2.4* strain did show a trend towards a higher number of neutrophils and lower eosinophils compared to C57BL/6 mice. The total number of DCs and ExMs were also similar between both sub-congenic strains and control mice at day 14 post-infection. To evaluate the activation state of

recruited DCs and ExMs, the surface expression of costimulatory molecules (CD40, CD80, CD86) was characterized by flow cytometry. Compared to C57BL/6 controls, DCs from *Cnes2.4* sub-congenic mice showed a trend towards higher expression of CD80 but not CD40 or CD86. No differences were observed in the expression of costimulatory molecules on ExMs from *Cnes2.4* and control mice at day 14 post-infection. No significant differences in lymphocyte recruitment were observed between either sub-congenic strain and control mice except for a higher number of $CD8^+$ cells in mice. Taken together, these data indicate that there were modest differences in cell recruitment and activation in the *Cnes2.2* and *Cnes2.4* sub-congenic strains compared to control mice at day 14 post-infection. Similar to *Cnes2* mice, both *Cnes2.2* and *Cnes2.4* sub-congenic strains had a significantly higher number of $CD45^+$ cells in the lung compared to C57BL/6 at 21 days post-infection. Specifically, the *Cnes2.4* strain had a significantly higher number of lung neutrophils ($CD11b^+$ $Ly6G^+$) while both sub-congenic strains had significantly fewer lung eosinophils ($CD11c^-$ $CD11b^+$ $Ly6G^-$ SSC^{hi}). The number of DCs ($CD11c^+$ $CD11b^+$ $MHCII^+$ AF^-) and ExMs ($CD11c^+$ $CD11b^+$ $MHCII^+$ AF^+) was also significantly higher in both *Cnes2.2* and *Cnes2.4* sub-congenic strains compared to C57BL/6 mice; however, the difference was more prominent for *Cnes2.4*. By qRT-PCR analysis we previously showed that *Cnes2* macrophages express higher classical (M1; *Nos2*) and lower alternative (M2; *Arg1*, *Fizz1*) activation markers compared to control mice. Here we examined the expression of iNOS and CD206 as representative M1 vs M2 markers by flow cytometry (Figure 3.5). Like the *Cnes2* congenic strain, the frequency and total number of DCs and ExMs that expressed iNOS (M1 phenotype) was significantly higher in *Cnes2.4* compared to control mice. In contrast, the frequency, but not the total number, of DCs and ExMs that expressed CD206 (M2 phenotype) was significantly lower in both *Cnes2.2* and *Cnes2.4* mice. Expression of these markers on AMs was similar among all strains; however, C57BL/6 mice showed a trend towards more CD206-expressing AMs compared to congenic mice at day 21 post-infection.

Flow cytometry analysis of lymphoid lung cell recruitment and polarization in sub-congenic mice following *C. neoformans* infection

We previously showed that *Cnes2* mice display a significantly higher number of $CD4^+$ cells at 21 days post-infection. Flow cytometry analysis at 21 days post-infection showed a significantly

higher number of $CD4^+$ and $CD8^+$ cells in the lungs of *Cnes2.4* mice that resembled the phenotype of *Cnes2* congenic mice (Figure 3.6). PMA/Ionomycin stimulation of leukocytes isolated from infected lungs followed by intracellular cytokine staining showed a significantly higher number of $CD4^+IFN\gamma^+$ T-cells in *Cnes2.4* compared to control mice; however, there was no difference in the number of Th2 or Th17 cells. Finally, there was also significantly fewer $B220^+$ cells in *Cnes2.4* compared to control mice. The *Cnes2.2* sub-congenic strain did not show any significant differences in the lung lymphoid cell populations compared to control mice.

In summary, the flow cytometry analysis revealed increased myeloid cell recruitment in both *Cnes2.2* and *Cnes2.4* (DCs and ExMs) and increased lymphoid cell recruitment in *Cnes2.4* mice. No significant alterations in cell recruitment were observed in the *Cnes2.1* or *Cnes2.3* strains that failed to exhibit a reduction in lung fungal burden.

Lung histological analysis of sub-congenic mice following *C. neoformans* infection.

Following infection with *C. neoformans,* histopathological analysis of *Cnes2* lungs showed more inflammation compared to C57BL/6 mice. Here, we analyzed differences in lung histopathology between *Cnes2.2* and *Cnes2.4* sub-congenic mice and the C57BL/6 strain at day 35 post-infection (Figure 3.7). Staining with H&E did not show clear differences between *Cnes2.2* and C57BL/6 mice; however, the lungs of *Cnes2.2* mice had slightly more cell infiltration in certain areas. In contrast, the *Cnes2.4* strain showed confluent cellular inflammation throughout most of the lung which resembled *Cnes2* congenic mice. Staining with mucicarmine identified numerous heavily encapsulated extracellular *C. neoformans* organisms in the lung parenchyma and airways of C57BL/6 mice with only a few, mainly intracellular, organisms in the lungs of *Cnes2.4* sub-congenic mice; these findings were consistent with the significant difference in lung fungal burden between these two strains. *Cnes2.2* lung sections also showed less extracellular *C. neoformans* in the tissue compared to control mice, however the difference was not as pronounced as *Cnes2.4* mice. PAS staining did not demonstrate a significant difference in mucus secretion between *Cnes2.2* or *Cnes2.4* sub-congenic and C57BL/6 mice at 35 days post-infection (data not shown).

Candidate gene prioritization in the *Cnes2.2* and *Cnes2.4* intervals

Based on tissue fungal burden and lung cell recruitment/polarization analysis, the host resistance phenotypes in the *Cnes2.2* and *Cnes2.4* sub-congenic strains were attributable to non-overlapping 6.6 Mb (16.2 - 22.8) and 7.9 Mb (27.6 - 35.5) segments of *Cnes2* locus (Figure 3.1). According to the mouse genome informatics website (MGI), there are total of 103 genes, including 77 protein coding genes and 23 non-coding RNA genes, in the *Cnes2.2* interval. The *Cnes2.4* interval contains a total of 380 genes, including 228 protein coding genes and 124 non-coding RNA genes. A list of protein coding genes in the *Cnes2.2* and *Cnes2.4* intervals with functional or expression annotations that are related to the immune system is summarized in supplementary Table 3-2, respectively. Several QTLs associated with other immune phenotypes and disease susceptibility/resistance have also been mapped to these intervals, suggesting that the underlying genes or variants encoded within *Cnes2.2* and/or *Cnes2.4* may have broad regulatory functions (Supplementary Table 3.3 and 3.4).

The integration of comprehensive bioinformatics resources including public sequence and expression databases with experimental forward genetic data is a powerful way to narrow a QTL interval (322). Identifying the genetic polymorphisms in the region of interest between parental strains used in QTL mapping is a useful approach to find the candidate genes underlying a QTL (323). Thus, to characterize the known genetic variation between resistant CBA/J and susceptible C57BL/6 strains within the *Cnes2.2* and *Cnes2.4* intervals, we conducted an extensive *in silico* analysis using publicly available mouse genome databases. A schematic overview of the approach used to find potential candidate genes is shown in Figure 3.8. As described in material and methods, a list of all variants including SNPs, indels and SVs with polymorphisms between C57BL/6NJ and CBA/J was obtained from Wellcome Trust Sanger Institute Mouse SNP viewer. No major structural variants were found in the *Cnes2.2* or *Cnes2.4* regions. All reference (rs) SNPs were stratified and filtered according to their predicted functional consequence and location using Ensembl Variant Effect Predictor (VeP). The VeP determines the effect of any variants (SNPs, insertions, deletions, copy number structural variants) on genes, transcripts, and protein sequence, as well as regulatory regions. Based on the VeP analysis, among a total of 12140 uploaded SNPs in the *Cnes2.2* interval (including intronic and intergenic variants), 8677 were transcript and 399 were regulatory feature variants. In the *Cnes2.4* interval, among a total of 155767 uploaded SNPs,

146798 were transcript and 6034 were regulatory feature variants. A summary of the VeP analysis for *Cnes2.2* and *Cnes2.4* variants (SNPs and indels) is shown in supplementary Figure 3.2.

As determined by Ensembl, variants are categorized into four groups based on severity of the predicted consequence: High, Moderate, Low and Modifier. High impact variants are expected to have a disruptive impact on the protein structure or function and include splice acceptor/donor, stop gained/lost, start lost, transcript amplification/ablation and frameshift variants. Moderate impact variants are non-disruptive variants that might alter protein function and include in-frame insertion/deletion and missense variants. For missense mutations, the SIFT algorithm predicts whether the amino acid substitution is damaging to the protein structure; a score of >0.05 is considered tolerated and a score of ≤0.05 is deleterious (324).

A list of variants with high and moderate impact in *Cnes2.2* and *Cnes2.4* and their affected genes is shown in supplementary Table 3.5 and 3.6, respectively. Moderate impact variants with a SIFT score lower than or equal to 0.05 are highlighted as variants with deleterious effect. In summary, the candidate gene analysis indicated that the *Cnes2.2* interval contains 3 high impact variants (stop gained) in 3 genes and 12 missense variants with deleterious effect in a total of 12 genes (supplementary Table 3.5A). In addition, there are 2 high impact indels affecting 2 genes, and 1 in-frame deletion in the *Cnes2.2* interval (supplementary Table 3.5B). Among a total of 14 protein coding genes that are affected by these variants, 2 could be considered as top candidate genes based on their annotated expression and function: *Fpr3* and *Fpr-rs4* (Table 3.1 and Table 3.3)

The *Cnes2.4* interval contains 10 variants with high impact (among 10 genes) and 46 missense variants with a deleterious effect (among 31 genes). In addition, it has 3 indels (among 3 genes) with high impact (splice acceptor and frameshift) and 5 in-frame deletion variants (among 4 genes) (supplementary Table 3.6). In total, 36 protein coding genes were affected by these variants of which 10 could be considered as top candidate genes based on their expression pattern and predicted function related to the immune system: *Notch3*, Ager, *H2-Ab1*, *Myo1f*, *Ubash3a, Tap1, H2-Eb1, H2-Oa, C5b and Lst1* (Table 3.2 and Table 3.3).

3.5. Discussion

We previously associated the *Cnes2* locus on mouse chromosome 17 with susceptibility to *C. neoformans* infection (321). Since the chromosomal region spanned by this locus was extremely broad (3.4-35.5 Mb; 611 protein coding genes) and not easily amenable to focused candidate gene analysis, in this study we narrowed the *Cnes2* interval by developing and analyzing sub-congenic mouse strains. The sub congenic lines were created by backcrossing *Cnes2* mice to the C57BL/6J background with marker-assisted selection of *Cnes2* sub-intervals for 7 generations. Four homozygous sub-congenic lines were phenotypically analyzed following *C. neoformans* infection. Compared to C57BL/6J mice we didn't observe any significant difference in fungal burden or lung cell infiltration in either the *Cnes2.1* or the *Cnes2.3* sub-congenic line (Figure 2 and data not shown). Therefore, these phenotypic analyses helped us to reduce the length of the *Cnes2* segment from 32 to 14 Mb which decreased the number of protein coding genes under consideration from 611 to 351 (Figure 8).

Furthermore, based on our phenotypic analysis, we identified two non-overlapping intervals in *Cnes2* segment that independently control susceptibility to *C. neoformans* infection. These intervals were designated as *Cnes2.2* (defined by markers at 16.2 to 23.8 Mb) and *Cnes2.4* (defined by markers at 26.8 and 35.5 Mb). In both *Cnes2.2* and *Cnes2.4* lines we did not observe any significant differences in lung fungal burden and cell recruitment at 14 days post-infection; however, *Cnes2.4* showed a trend towards more neutrophils and fewer eosinophils in the lungs compared to C57BL/6J mice at this time point (Figure 3). At 21 days post-infection, there were significantly fewer eosinophils in both *Cnes2.2* and *Cnes2.4* compared to C57BL/6 mice and *Cnes2.4* displayed a significantly higher number of neutrophils in the lung compared to C57BL/6J mice (Figure 4). Antigen-presenting cells including ExMs and inflammatory DCs, which are considered one of the most important cell types recruited to the lung following infection (142, 296), were significantly higher in both sub-congenic lines compared to C57BL/6J strain at 21 days post-infection (Figure 4). Notably, our analysis indicates that the influence of the *Cnes2.4* on both lung fungal burden and cell recruitment is much greater compared to the *Cnes2.2* interval. Importantly, for all phenotypes that were analyzed, none of the sub-congenic lines displayed the complete resistant phenotype of *Cnes2* mice following infection (Figure 2.6). While the *Cnes2* congenic region from the CBA/J strain reproduced the donor background phenotypes faithfully

(321), reduction in the length of the congenic interval attenuated such phenotypic effects. This observation is not entirely surprising since it has been observed that phenotypic effects often diminish as the genetic interval is reduced, particularly when the original effect is due to a combination of several genes (325).

Remarkably, following infection with 10^4 CFU of *C. neoformans*, a 30% mortality was observed in *Cnes2.4* mice at 35 days post-infection. *Cnes2* mice also display 13% mortality at the same time point. Importantly, fungal burden analysis at 18 days post-infection suggested that morbidity and mortality was not associated with increased pathogen load, as *Cnes2.4* mice had significantly fewer CFU in the lung compared to C57BL/6J mice with 100% survival rate (Figure 3.2). In contrast to *Cnes2* and *Cnes2.4* mice, we did not observe any mortality in the CBA/J parental strain infected with 10^4 CFU of *C.neoformans* 52D (data not shown); this could be explained by the fact that genetic background interactions may lead to the suppression of the mortality phenotype in CBA/J mice while generation of sub-congenic strains is accompanied by an increase in the penetrance of the trait caused by genes within the donor interval (325). In summary, both the *Cnes2.2* and *Cnes2.4* sub-congenic intervals regulate lung fungal burden but have a limited effect on spleen and brain dissemination. This is consistent with a previous report showing that the robust Th1/Th17 immune responses and classically activated macrophages are not sufficient to provide protection against lethal dissemination of *C. neoformans* into the CNS (294). Clarification of the exact relationship between pathogen load and/or dissemination and mortality in the *Cnes2* and *Cnes2.4* strains will require further analysis of the spleen and brain fungal burden combined with detailed immunological characterization among a larger number of mice with signs of illness just before mortality (18-21 days post-infection).

The observed mortality in both *Cnes2* and *Cnes2.4* mice could be explained by dysregulated inflammation in the lung and/or brain following cryptococcal infection. Indeed, an excessive host immune response to infection could be harmful and may cause significant tissue damage and pathology (326, 327). Although we have no direct evidence of tissue injury, the fact that these mice controlled the lung fungal load suggests that mortality is a consequence of the host immune response. Histological and flow cytometry analysis of the lung tissue from infected *Cnes2* and *Cnes2.4* mice revealed a significant increase in the influx of highly reactive inflammatory cells including DCs and ExMs (Figure 3.4). In influenza, monocyte-derived dendritic cells and exudate

macrophages produce induced pulmonary immune pathology and mortality (328). Interestingly, $CCR2^{-/-}$ mice that have reduced recruitment of monocyte-derived DCs and ExMs are protected from pulmonary fibrosis, weight loss and death in the acute lung injuries caused by fluorescein isothiocyanate and bleomycin (329, 330). Excessive recruitment and presence of phagocytic cells, particularly macrophages, could also lead to cryptococcal brain dissemination. It has been suggested that cryptococci may require macrophages or monocytes to cross the blood-brain barrier (BBB) through a "Trojan horse" mechanism. Increased phagocytic uptake of *Cryptococcus* is a potential mechanism for fungal spread and some studies have provided evidence for the role of these cells in fungal dissemination (123, 125, 226, 307, 331-334). Despite these findings, the exact mechanism of "Trojan horse" dissemination is still unknown and needs further investigation using *in vivo* models.

The heightened inflammation in *Cnes2* and *Cnes2.4* congenic mice infected with *C. neoformans* could be a model for immune reconstitution inflammatory syndrome (IRIS). This life-threatening inflammatory reaction occurs in some HIV-infected patients during antiretroviral therapy (ART) and is caused by an overreaction of the newly reconstituted immune system to residual pathogen antigen (8, 195, 335, 336). In non-HIV cryptococcal meningitis, a highly-activated antigen-presenting dendritic cell population within the CSF, accompanied by a highly active T-lymphocyte population with potentially damaging inflammatory cytokine responses has been identified (195). Further investigations will be required to prove that excessive tissue damage and immunopathology caused by inflammatory cells and heightened cytokine/chemokine responses are responsible for the observed mortality in *Cnes2* and *Cnes2.4* mice.

In summary, this study identified two distinct sub-congenic intervals within *Cnes2* that mediate host resistance against *C. neoformans* infection. It is likely that genes within *Cnes2.2* and *Cnes2.4* regulate different aspects of the host immune response. Compared to C57BL/6J mice the *Cnes2.2* strain has a moderate inflammatory response that leads to a significantly lower lung fungal burden. Based on the phenotypic and candidate gene analysis, the *Cnes2.2* interval regulates the function or migration of phagocytic leukocytes. In contrast, *Cnes2.4* mice display a vigorous inflammatory response that leads to more effective pathogen clearance from the lung; however, this outcome is associated with subsequent mortality.

In silico analysis of the *Cnes2.2* and *Cnes2.4* intervals is one approach to facilitate the prioritization of potential candidate genes for further analysis. In this study protein-coding genes were chosen based on the high and moderate impact variants; however, this does not exclude other variants, such as synonymous mutations or those in regulatory regions, from future consideration (337, 338). Haplotype analysis to identify common polymorphisms in the *Cnes2* interval between known resistant and susceptible strains to *C. neoformans* infection could also help to prioritize allelic variants for further analysis. The next critical step in candidate gene analysis is to perform a comparative gene expression studies of lung stromal tissue and infiltrating cell populations between parental C57BL/6N and CBA/J mice in addition to congenic *Cnes2*, *Cnes2.2,* and *Cnes2.4* strains, both before and at different time points after *C. neoformans* challenge. This comparative analysis will allow the identification expression differences for genes within the *Cnes2* congenic interval/sub-interval, as well as for genes that do not necessarily map to the congenic interval but are involved in downstream pathways that mediate host resistance. Finally, genes that exhibit significant nucleotide sequence and/or expression variation will be functionally characterized to confirm their role in host resistance using genetically modified mice with specific nucleotide substitutions or targeted mutations that confer a loss or gain of function. Sequences with definitive evidence for causality may provide a deeper understanding of host genetic susceptibility to cryptococcal, and potentially other fungal infections, and may lead to the discovery of targets for improved antifungal therapies.

Figures

Figure 3.1. Breakdown of B6.CBA-*Cnes2* into sub-congenic lines: Schematic outline of sub-congenic strains (B6.CBA-*Cnes2.1 to Cnes2.4*) which were generated by backcrossing the *Cnes2* mice to the parental C57BL/6J strain and subsequently intercrossing the offspring. Each bar represents a congenic line that defines the approximate mega base (Mb) position of the interval region. The black portions of each bar represent the regions homozygous for the B6 alleles (the background strain), the white portions represent the congenic regions for the CBA alleles (donor strain) and the gray portions represent the transitional regions that were not genotyped.

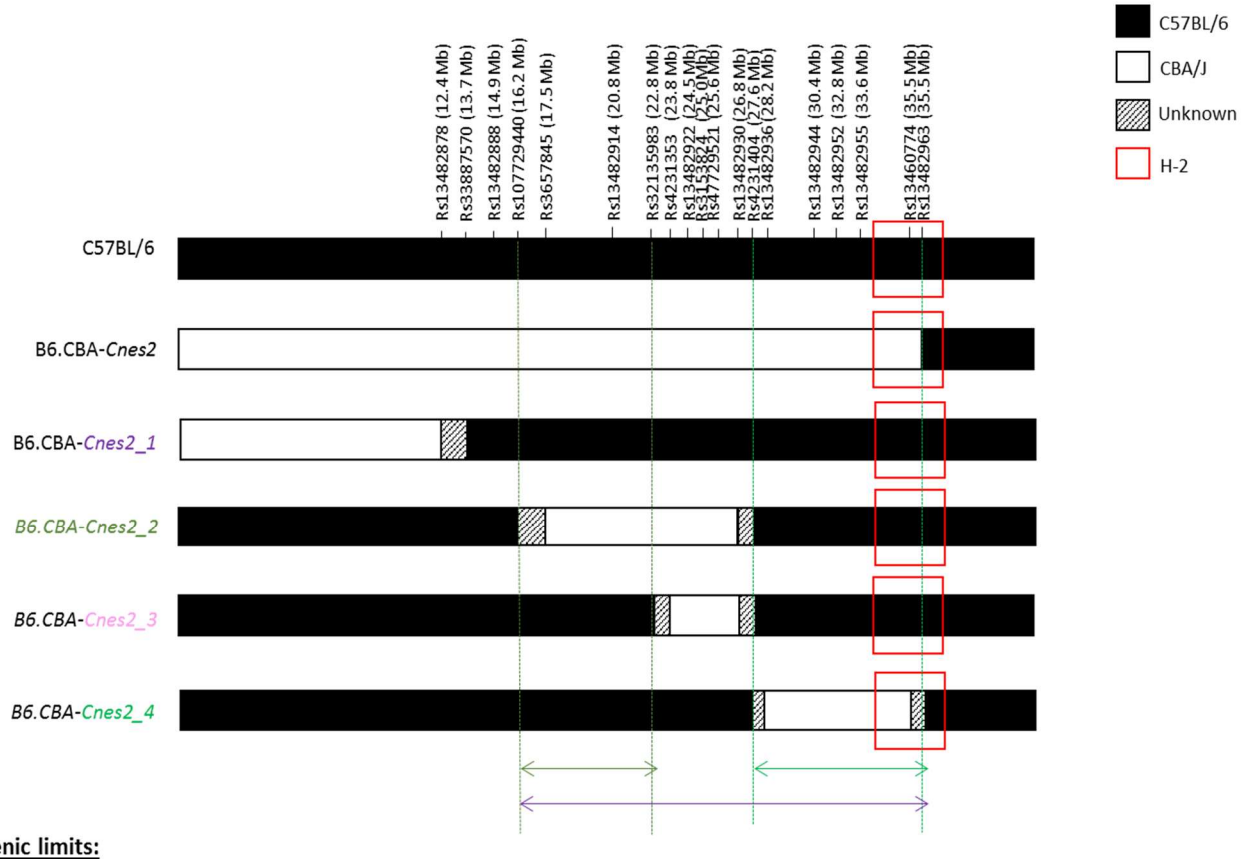

Sub-congenic limits:
Cnes2-1: centromere-rs33887570
Cnes2-2: rs107729440-rs4231404
Cnes2-3: rs32135983-rs4231404
Cnes2-4: rs4231404-rs13482963

Figure 3.2. Tissue fungal burden and survival analysis of sub-congenic mice following *C. neoformans* infection. C57BL/6 and B6.CBA-*Cnes2* sub-congenic mice were infected intratracheally with 10^4 CFU of *C. neoformans* 52D and fungal burden in the lungs, brains and spleens at 35 days post-infection (A-C) and 18 days post-infection (E-G) was determined by plating tissue homogenates on Sabouraud dextrose agar. Mice were observed for up to 35 days for survival analysis (D). Data are shown as mean ± SEM, *, $P \leq 0.05$; **, $P \leq 0.01$; ***, $P \leq 0.001$, using an unpaired Student's t-test (A, E, G), log-rank test (D) and Mann–Whitney U test (B, C, F).

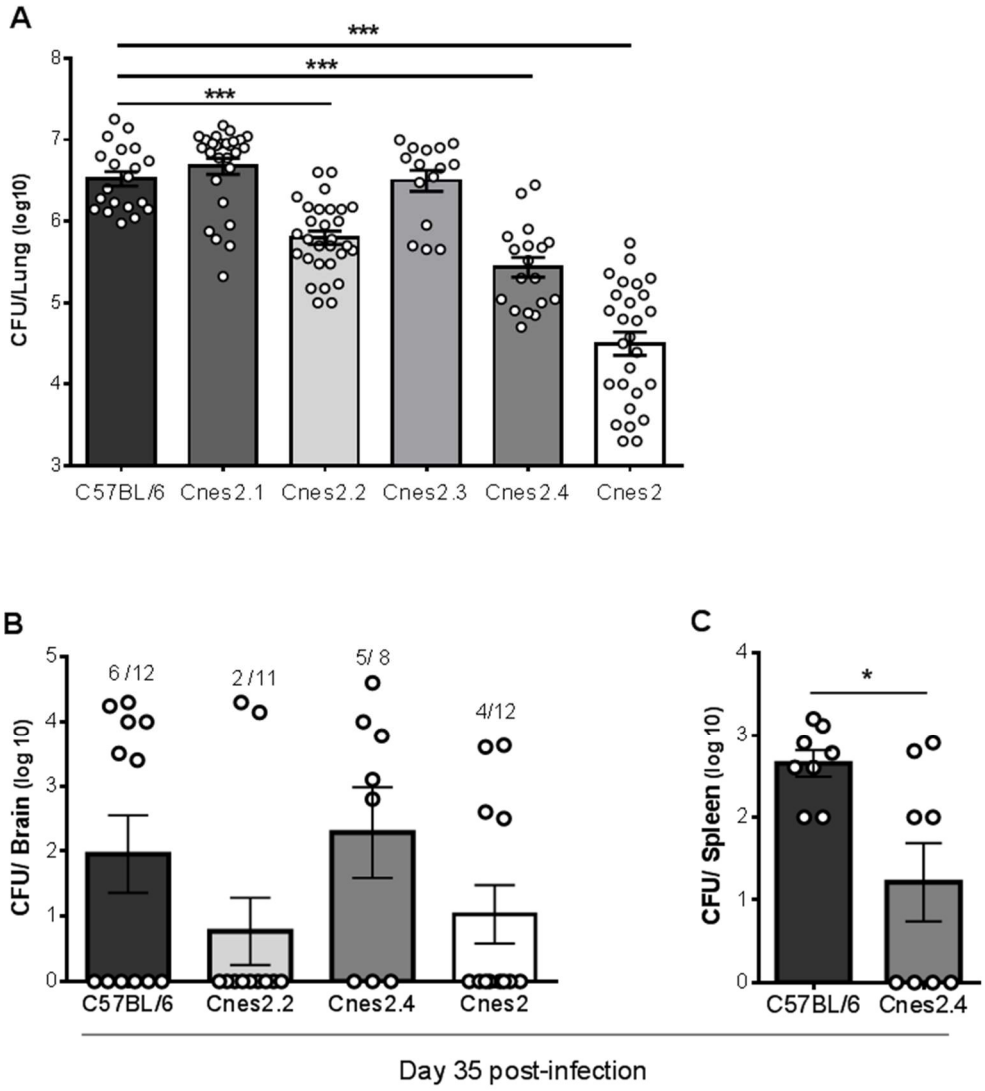

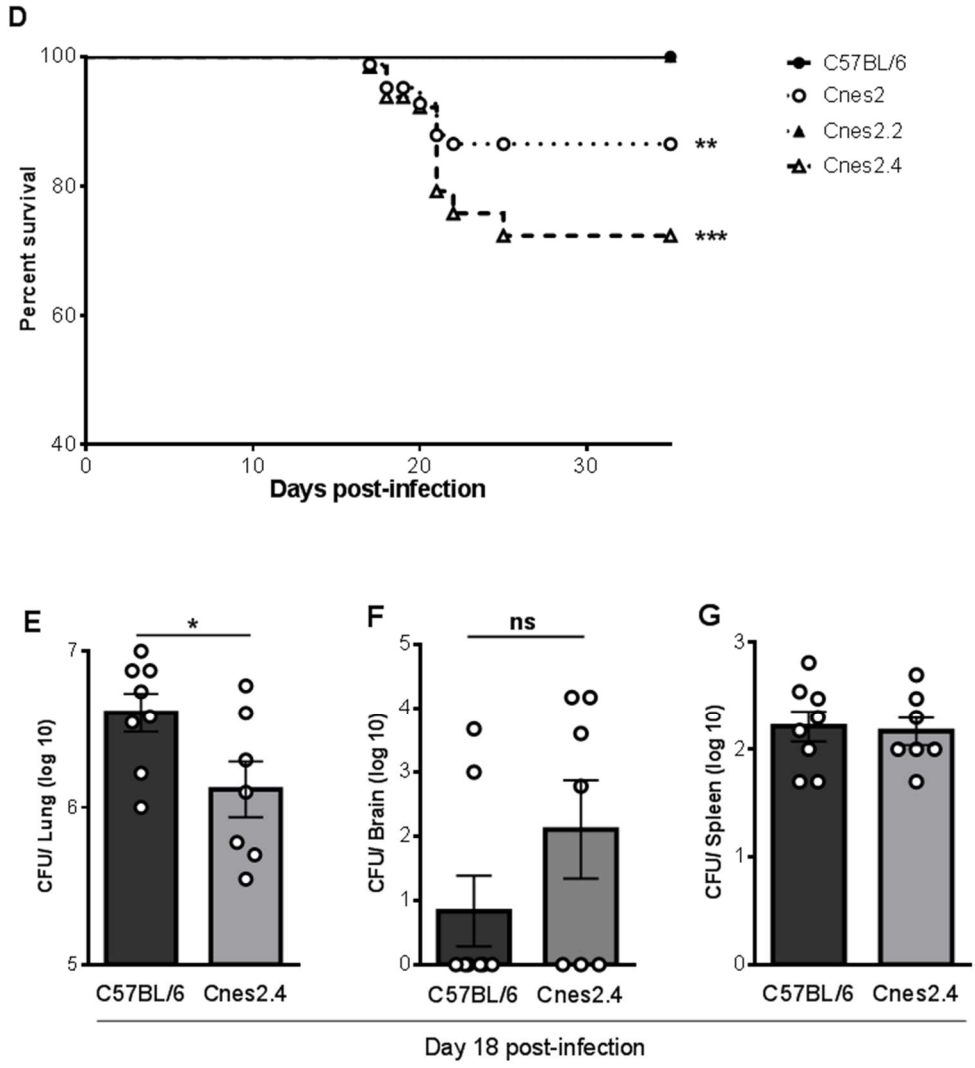
D
100
80
60
40
Percent survival
0
10
20
30
Days post-infection
C57BL/6
Cnes2
Cnes2.2
Cnes2.4
**
***
E
*
CFU/ Lung (log 10)
7
6
5
C57BL/6
Cnes2.4
F
ns
CFU/ Brain (log 10)
5
4
3
2
1
0
C57BL/6
Cnes2.4
G
CFU/ Spleen (log 10)
3
2
1
0
C57BL/6
Cnes2.4
Day 18 post-infection

Figure 3.3. FACS analysis of lung cell recruitment in sub-congenic mice at 14 days post-infection. C57BL/6 and B6.CBA-*Cnes2* sub-congenic mice were infected intratracheally with 10^4 CFU of *C. neoformans* 52D. At 14 days post-infection lung cell suspensions were stained with fluorochrome-labeled antibodies and analyzed by flow cytometry as described in materials and methods. Absolute number of $CD45^+$ cells, neutrophils, eosinophils, DCs and ExM in the infected lungs is shown (A-E). Surface expression of costimulatory molecules by total $CD11c^+CD11b^+$, DCs and ExM were examined. Mean fluorescence intensity (MFI) of positive cells is shown (F-H). Absolute number of $CD4^+$, $CD8^+$ and $B220^+$ lymphocytes is shown (I-K). Data are representative of two independent experiments (n= 4 to 6 mice/strain) and are shown as mean ± SEM. *, $P \leq 0.05$; **, $P \leq 0.01$; **, $P \leq 0.001$.

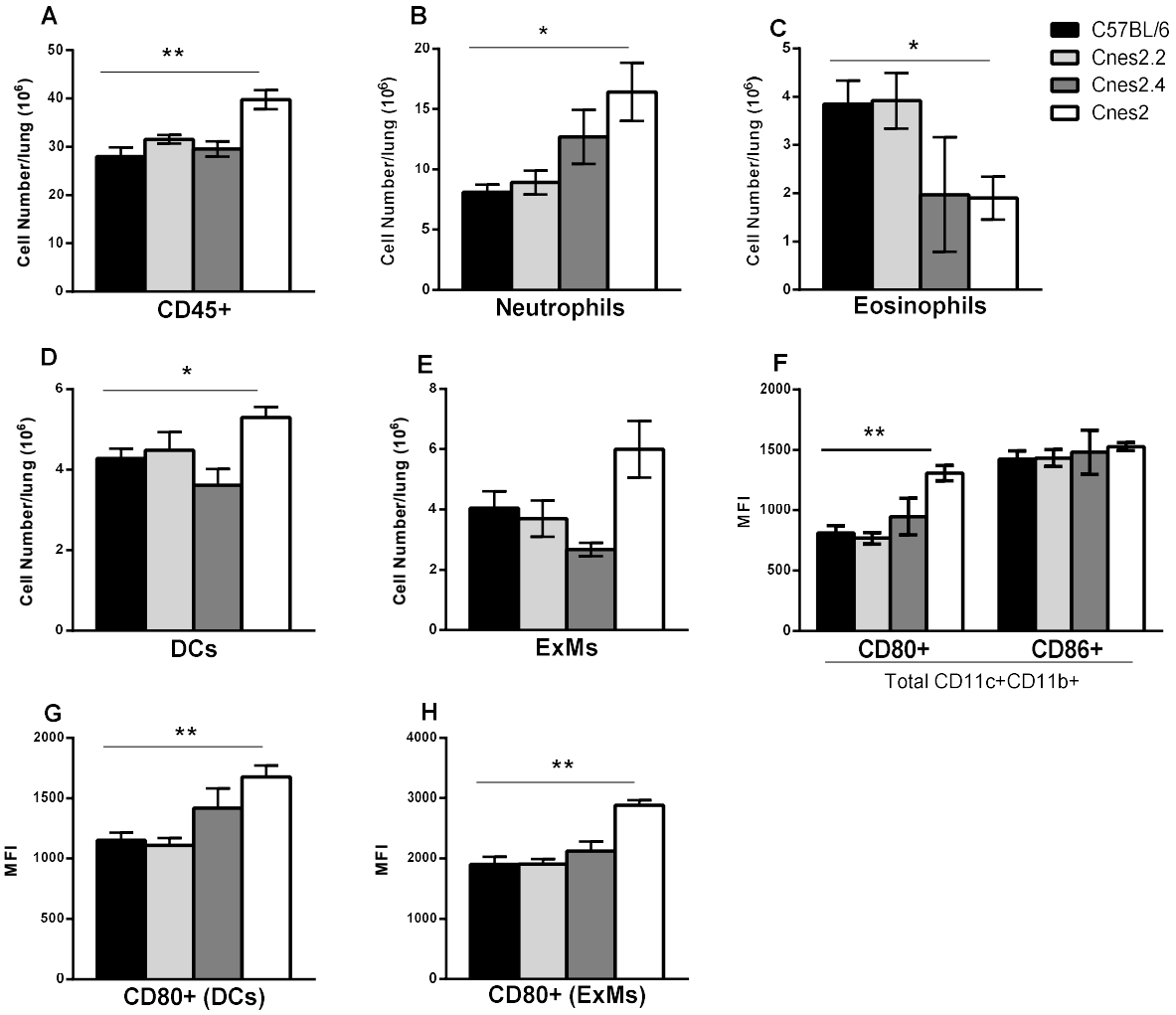

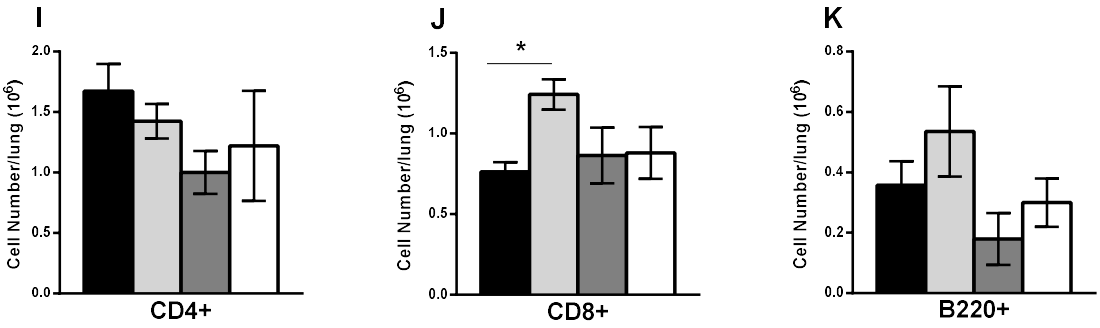
I
J
K
Cell Number/lung (10^6)
2.0
1.5
1.0
0.5
0.0
CD4+
*
1.5
1.0
0.5
0.0
CD8+
0.8
0.6
0.4
0.2
0.0
B220+

Figure 3.4. FACS analysis of lung myeloid cell recruitment in sub-congenic mice at 21 days post-infection. Absolute number of $CD45^+$ cells, eosinophils, neutrophils, DCs and ExM in the infected lungs at 21 days post-infection is shown (A-E). Representative plot for eosinophils ($CD11c^-CD11b^+Ly6G\text{-}SSC^{hi}$) (F), neutrophils ($CD11c^-CD11b^+Ly6G^+$) (G), and total inflammatory $CD11c^+MHCII^+$ DCs and ExMs (H) is shown. Data are representative of two independent experiments (n= 4 to 6 mice/strain) and are shown as mean ± SEM. *, $P \leq 0.05$; **, $P \leq 0.01$; **, $P \leq 0.001$.

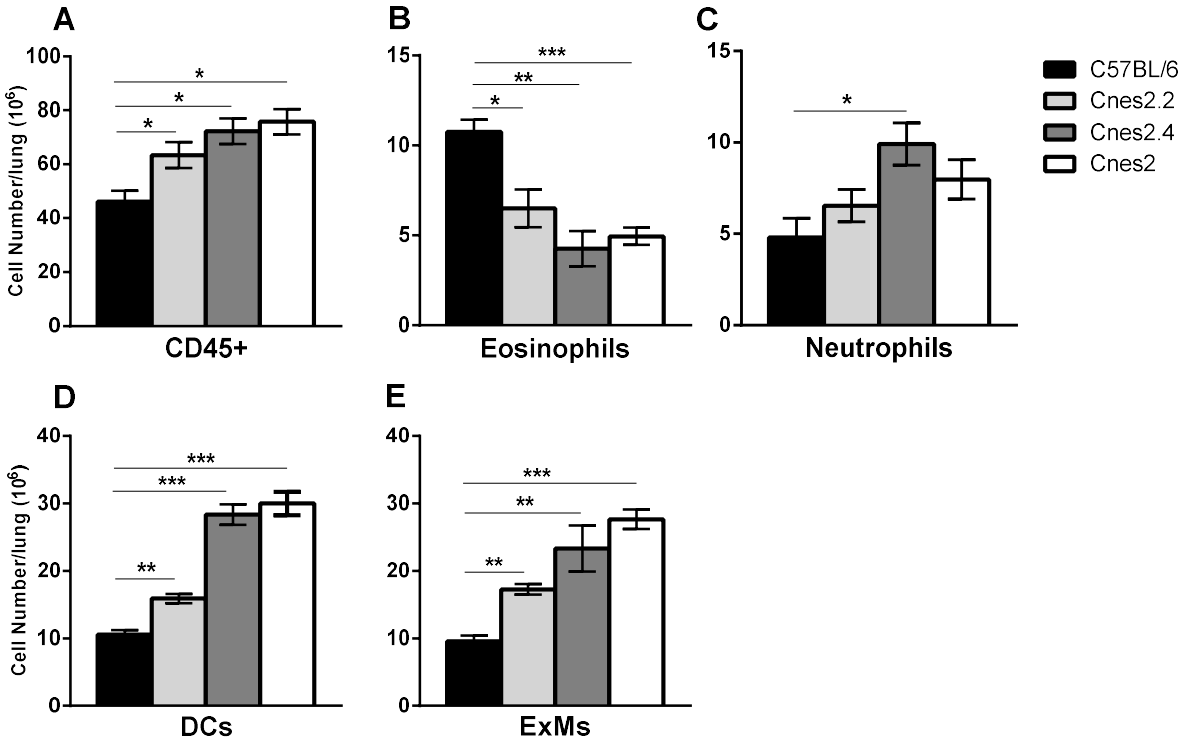

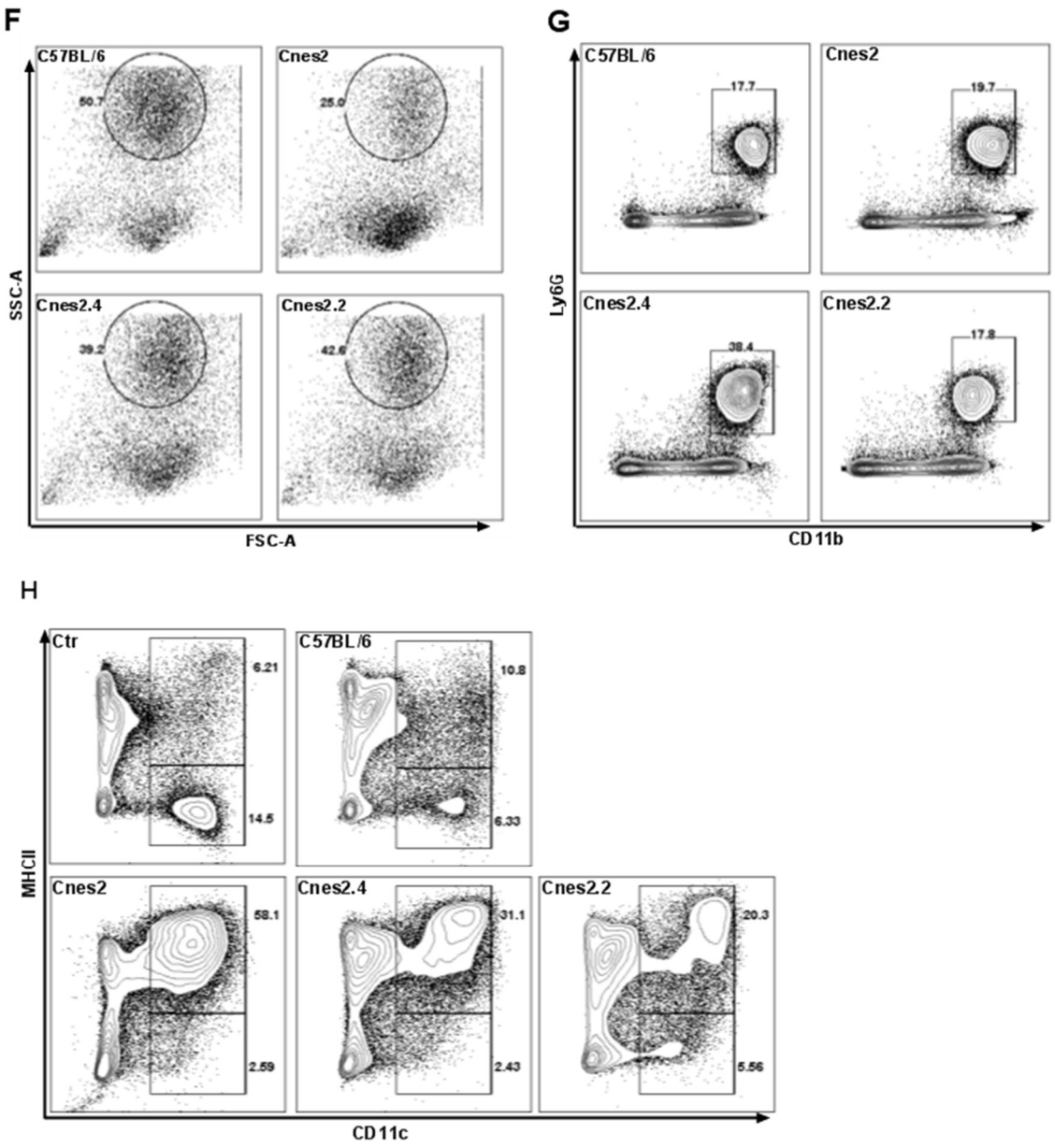
F
C57BL/6
50.7
Cnes2
25.0
Cnes2.4
39.2
Cnes2.2
42.6
SSC-A
FSC-A
G
C57BL/6
17.7
Cnes2
19.7
Cnes2.4
38.4
Cnes2.2
17.8
Ly6G
CD11b
H
Ctr
6.21
14.5
C57BL/6
10.8
6.33
Cnes2
58.1
2.59
Cnes2.4
31.1
2.43
Cnes2.2
20.3
5.56
MHCII
CD11c

Figure 3.5. Activation phenotype of lung AMs, ExMs and DCs in sub-congenic mice at 21 days post-infection. The expression of classical (iNos) and alternative (CD206) activation markers by macrophages and DCs was evaluated by flow cytometry at 21 days post-infection. Absolute number and frequency of DC, ExMs and AMs expressing CD206/iNOS is shown (A-F). A representative plot of $CD206^+$ and $iNOS^+$ cells gated on total $CD11c^+$ myeloid cells is presented (G). Data are representative of two independent experiments (n= 4 to 6 mice/strain) and are shown as mean ± SEM. *, $P \leq 0.05$; **, $P \leq 0.01$; **, $P \leq 0.001$.

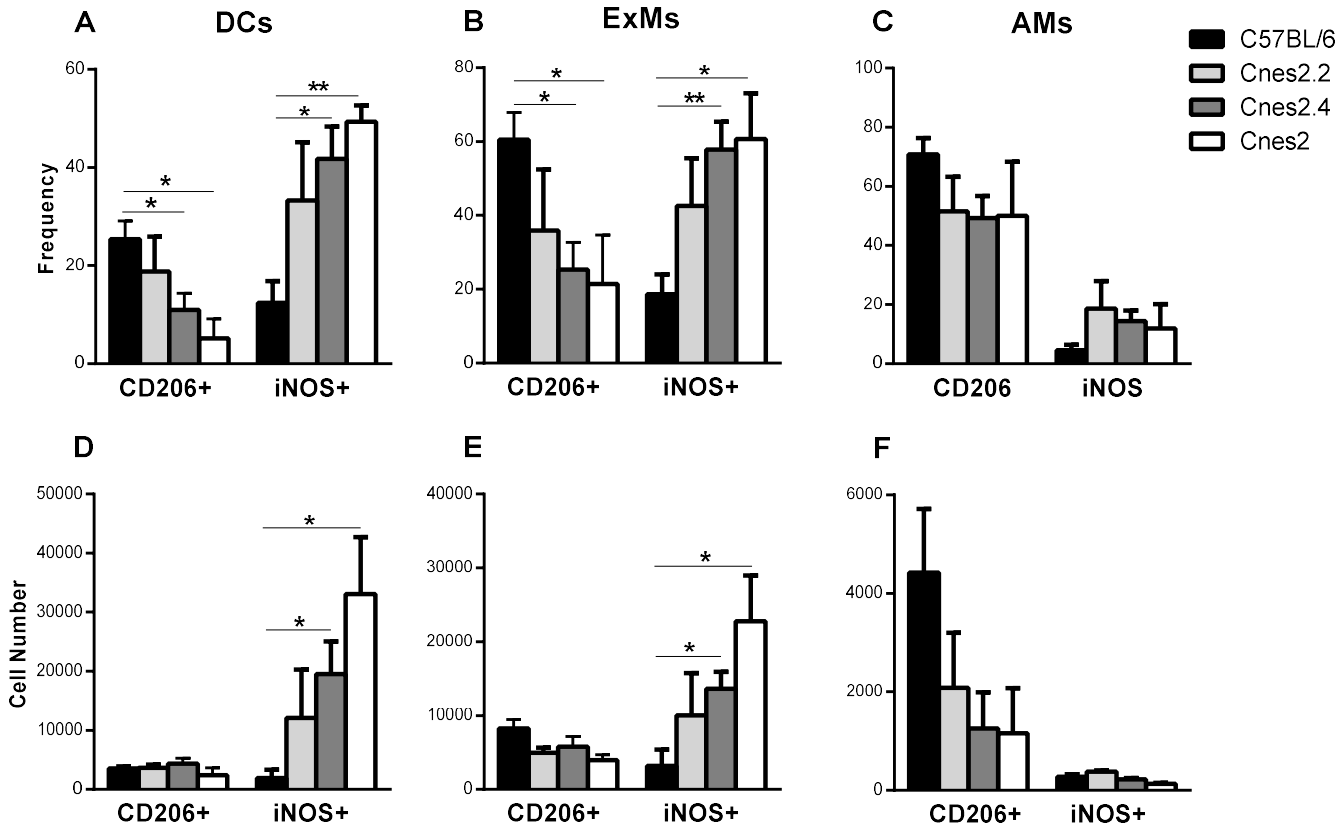

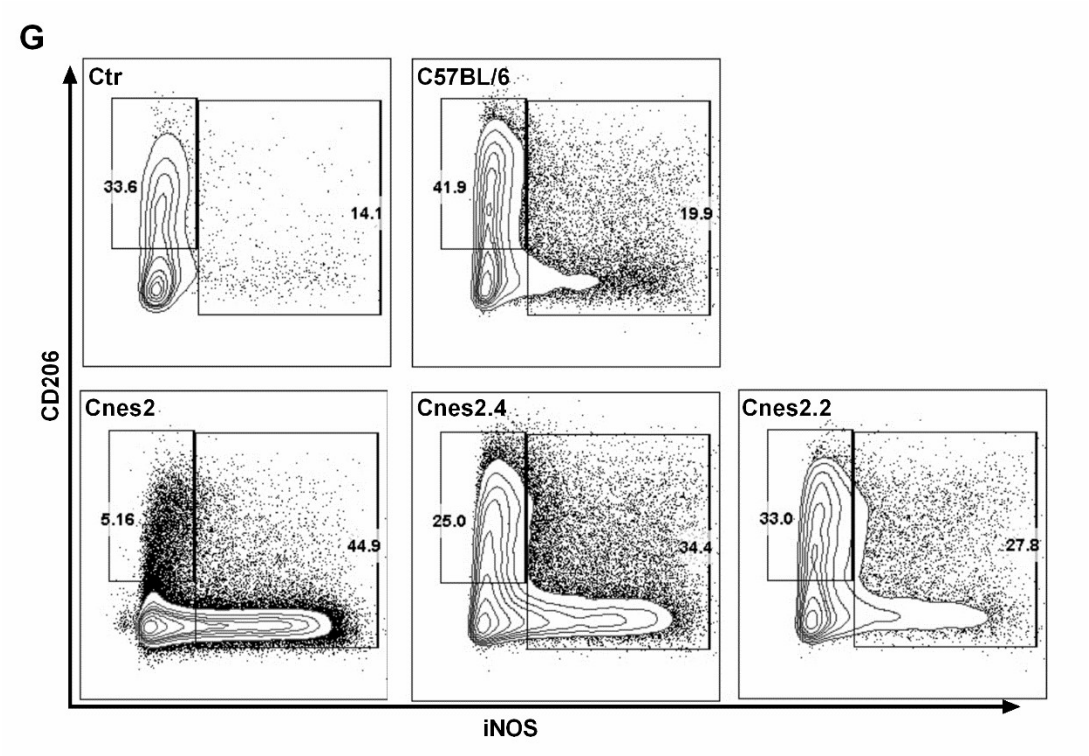
G
Ctr
33.6
14.1
C57BL/6
41.9
19.9
Cnes2
5.16
44.9
Cnes2.4
25.0
34.4
Cnes2.2
33.0
27.8
CD206
iNOS

Figure 3.6. Lung lymphoid cell recruitment and polarization in sub-congenic mice at 21 days post-infection. Lung cell suspensions from infected mice at 21 days post-infection were stimulated with PMA-ionomycin and analyzed with fluorochrome-labeled antibodies and intracellular cytokine staining as described in materials and methods. The absolute number of $CD3^+$ $CD4^+$, $CD3^+CD8^+$ and $B220^+$ cells is shown (A). Absolute number of $CD4^+$ T cells expressing IFN-γ, IL-13 and IL-17 at 21 days post-infection. Data are representative of two independent experiments (n= 4 to 6 mice/strain) and are shown as mean ± SEM. *, $P \leq 0.05$; **, $P \leq 0.01$; **, $P \leq 0.001$ (using an unpaired Student t test).

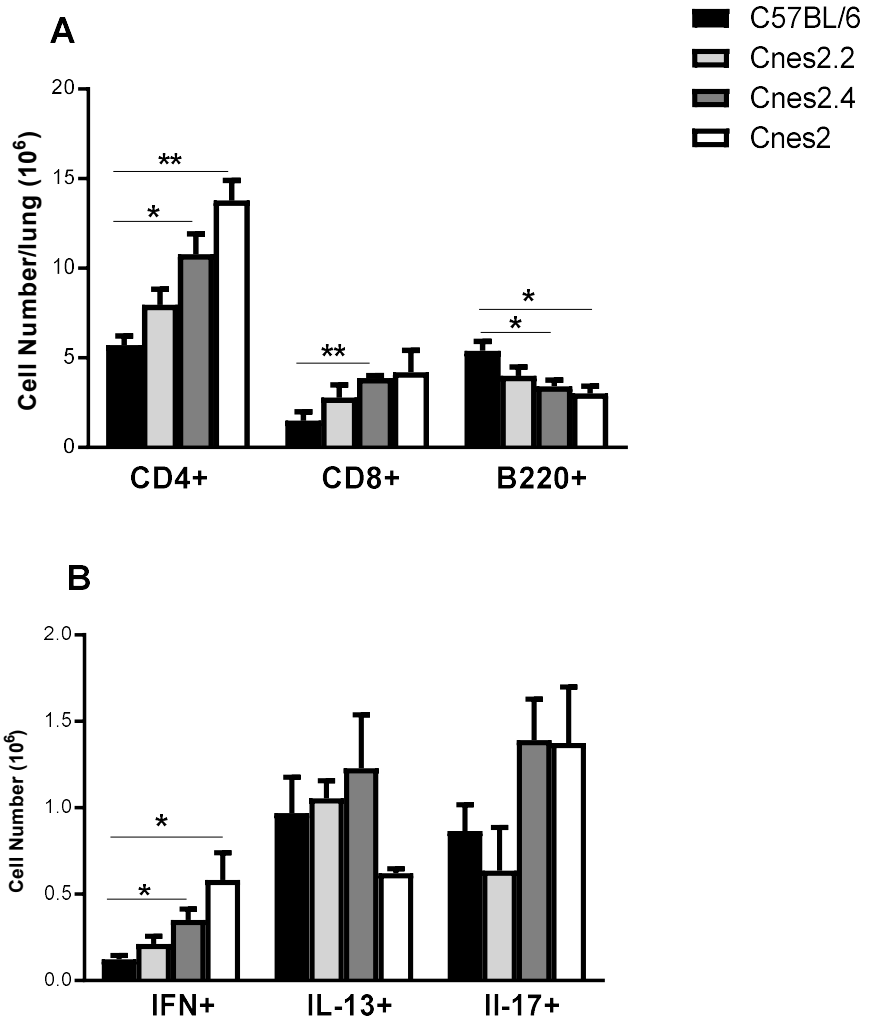

Figure 3.7. Histological analysis of C57BL/6, *Cnes2.2* and *Cnes2.4* infected lungs at 35 days post-infection. Mice were infected with 10^4 CFU of *C. neoformans* 52D, lungs were harvested at 35 days post-infection and paraffin fixed section were stained with mucicarmine (A) and H&E (B). Staining with mucicarmine, which specifically stains the cryptococcal cell wall, confirms lung fungal burden analysis at 35 days post infection. H&E staining revealed clearly increased inflammatory infiltration in *Cnes2.4* compared to C57BL/6 and *Cnes2.2* mice at 35 days post-infection.

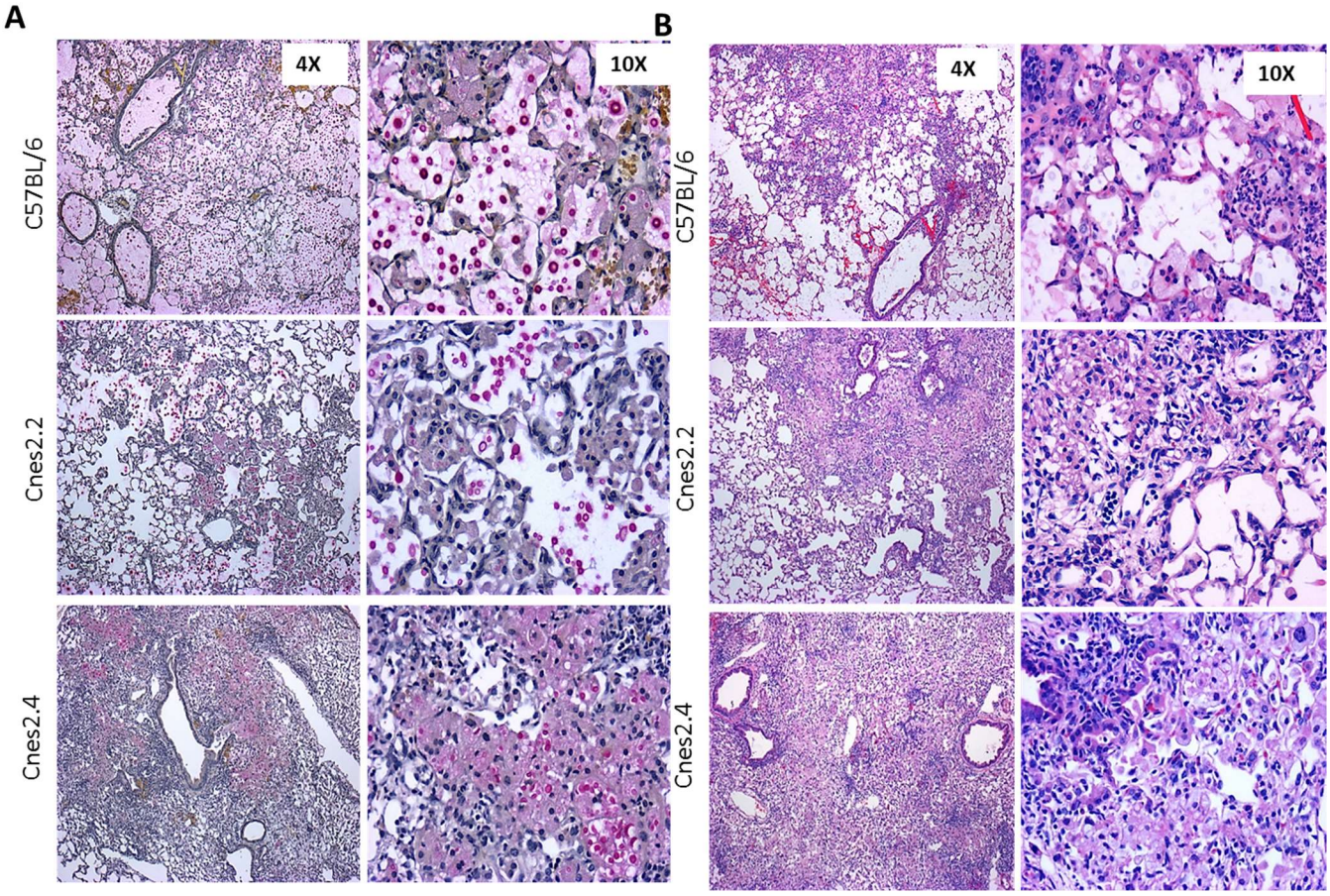

Figure 3.8: Schematic overview of the *in-silico* analysis used for identifying potential candidate genes in the *Cnes2.2* and *Cnes2.4* intervals. As described in material and methods, a list of all polymorphic variants between C57BL/6NJ and CBA/J mice in each interval was acquired from the Sanger SNP viewer. Using variant effect predictor (VeP), the data were categorized based on variant effects. Protein coding genes with high impact variants and deleterious effect were selected for further analysis. The top candidate genes were selected based on functional and expression information gained from gene databases (MGI, PubMed, etc.).

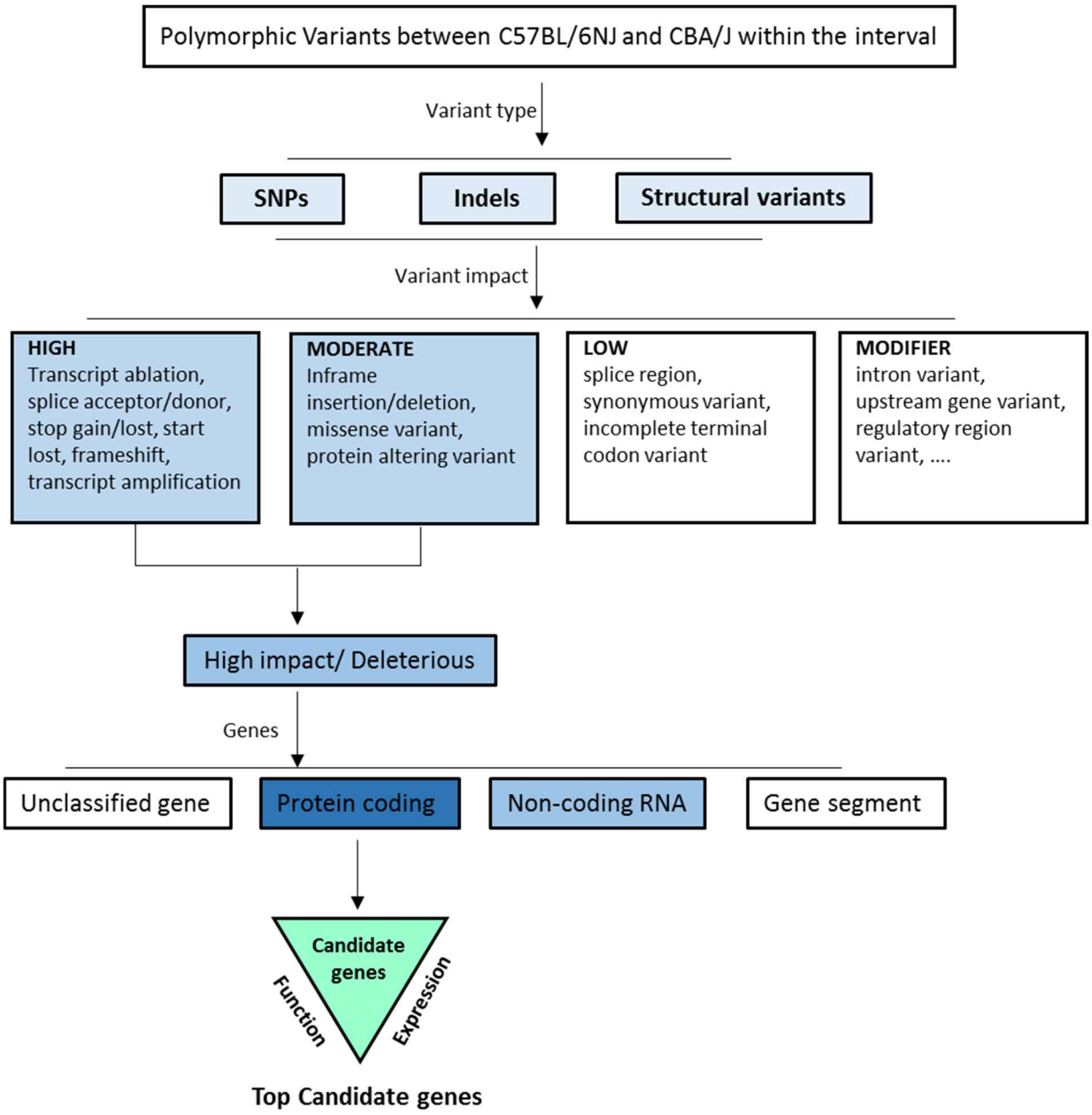

Table 3.1. List of protein coding genes in the *Cnes2.2* interval with deleterious or high impact variants. Genes with known expression/function related to immune system are highlighted in A (red).

SYMBOL	Name	A
Chd1	chromodomain helicase DNA binding protein 1	
Fpr3	formyl peptide receptor 3	
Fpr-rs4	formyl peptide receptor, related sequence 4	
Riok2	RIO kinase 2 (yeast)	
Vmn2r107	vomeronasal 2, receptor 107	
Vmn1r225	vomeronasal 1 receptor 225	
Vmn1r231	vomeronasal 1 receptor 231	
Vmn2r108	vomeronasal 2, receptor 108	
Vmn2r103	vomeronasal 2, receptor 103	
Vmn2r99	vomeronasal 2, receptor 99	
Vmn2r90	vomeronasal 2, receptor 90	
Vmn2r109	vomeronasal 2, receptor 109	
Zfp758	zinc finger protein 758	
Zfp97	zinc finger protein 97	

Table 3.2. List of protein coding genes in the *Cnes2.4* interval with deleterious or high impact variants. Genes with known expression/function related to immune system are highlighted in A (red).

Symbol	**Name**	**A**
Notch3	notch 3	
Ager	advanced glycosylation end product-specific receptor	
H2-Ab1	histocompatibility 2, class II antigen A, beta 1	
Notch4	notch 4	
Rgl2	ral guanine nucleotide dissociation stimulator-like 2	
Myo1f	myosin IF	
Btnl2	butyrophilin-like 2	
Col11a2	collagen, type XI, alpha 2	
Ly6g6d	lymphocyte antigen 6 complex, locus G6D	
Umodl1	uromodulin-like 1	
Cpne5	copine V	
Sapcd1	suppressor APC domain containing 1	
Btnl4	butyrophilin-like 4	
Btnl6	butyrophilin-like 6	
Tnxb	tenascin XB	
Ubash3a	ubiquitin associated and SH3 domain containing, A	
Mdga1	MAM domain containing glycosylphosphatidylinositol anchor 1	
Ly6g6e	lymphocyte antigen 6 complex, locus G6E	
C4a	complement component 4A (Rodgers blood group)	
Tap1	transporter 1, ATP-binding cassette, sub-family B (MDR/TAP)	
H2-Eb1	histocompatibility 2, class II antigen E beta	
H2-Eb2	histocompatibility 2, class II antigen E beta2	
H2-Ke6	H2-K region expressed gene 6	
H2-Oa	histocompatibility 2, O region alpha locus	
H2-Ob	histocompatibility 2, O region beta locus	
H2-Q2	histocompatibility 2, Q region locus 2	
Uhrf1bp1	UHRF1 (ICBP90) binding protein 1	
Zfp870	zinc finger protein 870	
Morc2b	microrchidia 2B	
Rab44	RAB44, member RAS oncogene family	
Msh5	mutS homolog 5	
Cfb	complement factor B	
Cyp4f	cytochrome P450, family 4, subfamily f	
Daxx	Fas death domain-associated protein	
Prrc2a	proline-rich coiled-coil 2A	
Lst1	leukocyte specific transcript 1	

Table 3.3. List of top candidate genes in the *Cnes2.2* and *Cnes2.4* intervals with description of KO mice phenotype and gene ontology. information are taken from MGI, Genecards and NCBI genes.

Symbol	Phenotype of KO mice/ disease	Gene Ontology
Cnes2.2		
Fpr3/ Fpr-rs4	The formyl peptide receptor family, Including Fpr1 are Gi-protein-coupled receptors that are expressed mainly by mammalian phagocytic leukocytes. FPRs are involved in antibacterial host defence and inflammation.	G-protein coupled receptor activity, complement receptor mediated signaling pathway, leukocyte migration.
Cnes2.4		
Notch 3	Thymus hyperplasia, increased thymocyte number, abnormal T cell differentiation, increased double-negative T cell number, enlarged spleen, enlarged lymph nodes.	Negative regulation of cell differentiation.
H2-Ab1	Homozygotes for targeted null mutations exhibit depletion of mature CD4+ T cells, deficiency in cell-mediated immune responses, and increased susceptibility to viral infections.	Antigen processing and presentation, B cell affinity maturation, positive regulation of T-helper 1 type immune response, etc.
Myo1f	Mice homozygous for a knock-out allele exhibit impaired neutrophil migration and adhesion.	Neutrophil mediated immunity, regulation of innate immune response.
Ubash3a	Homozygous null mice are viable and healthy with no abnormalities detected in any of the hematopoietic lineages.	Negative regulation of T cell receptor signaling pathway.
Tap1	Mice homozygous for targeted mutations that inactivate the gene are deficient in antigen presentation, surface class I antigens, and CD4-8+ T cells.	Adaptive immune response, protection from natural killer cell mediated cytotoxicity.
H2-Eb1	Increased granulocyte number, increased monocyte cell number.	Antigen processing and presentation of exogenous peptide antigen via MHC class II, response to interferon-gamma, etc.

H2-Oa	Homozygous inactivation of this gene results in abnormal antigen presentation via MHC class II. Mice homozygous for a knock-out allele show enhanced selection of CD4+ single positive thymocytes. Mice homozygous for a different knock-out allele show increased serum IgG1 levels.	Antigen processing and presentation, regulation of T cell differentiation.
Cfb	Homozygotes for targeted null mutations lack the alternative complement pathway, and have reduced overall complement activity.	Complement activation, immune system process.
Lst1	Mice homozygous for a knock-out allele are slightly more susceptible to viral infections.	Immune system process, regulation of lymphocyte proliferation.
Ager	Decreased dendritic cell number, abnormal cytokine secretion, abnormal immune system physiology.	Positive regulation of dendritic cell differentiation, positive regulation of activated T cell proliferation.

Supplementary Figure 3.1. Summary statistics and histogram of VeP analysis for uploaded *Cnes2.2* SNPs (A), *Cnes2.2* indels (B), *Cnes2.4* SNPs (C) and *Cnes2.4* indels (D).

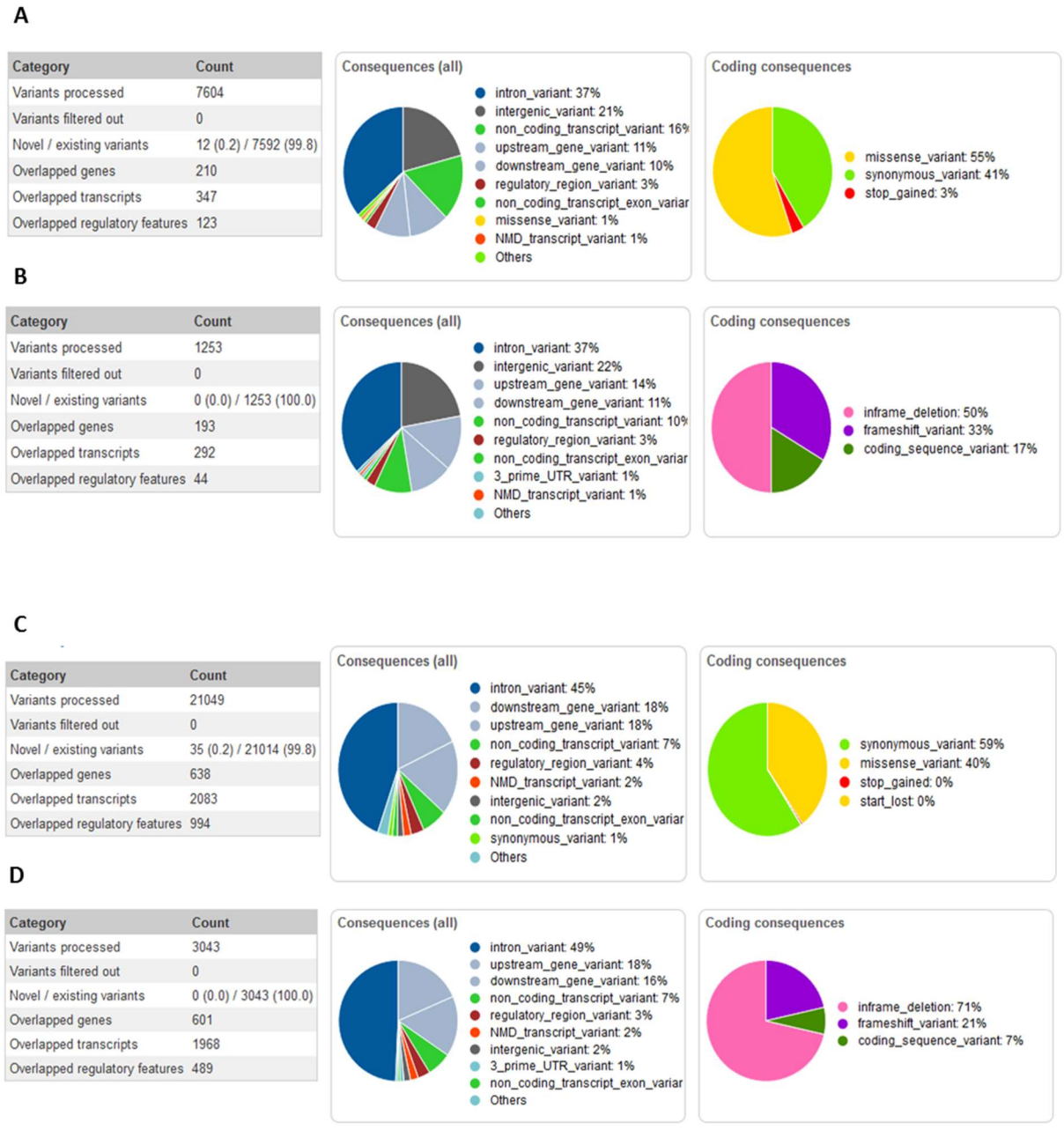

Supplementary Table 3.1. *Cnes2.2* protein coding gene list.

Symbol	Name	Immune system related
Fpr1	formyl peptide receptor 1	*
Fpr2	formyl peptide receptor 2	*
Fpr3	formyl peptide receptor 3	*
Fpr-rs4	formyl peptide receptor, related sequence 4	
Fpr-rs7	formyl peptide receptor, related sequence 7	
Pkmyt1	protein kinase, membrane associated tyrosine/threonine 1	
Ppp2r1a	protein phosphatase 2, regulatory subunit A, alpha	*
Riok2	RIO kinase 2 (yeast)	
Tnfrsf12a	tumor necrosis factor receptor superfamily, member 12a	*
Vmn1r	vomeronasal 1 receptor (genes)	
Vmn2r	vomeronasal 2, receptor (genes)	
Zfp	zinc finger protein (genes)	
Zscan10	zinc finger and SCAN domain containing 10	*

Supplementary Table 3.2. List of protein coding genes within *Cnes2.4*.

Symbol	Name	Immune system related
H2-Ab1	histocompatibility 2, class II antigen A, beta 1	*
Pacsin1	protein kinase C and casein kinase substrate in neurons 1	*
Myo1f	myosin IF	*
Notch3	notch 3	*
Pram1	PML-RAR alpha-regulated adaptor molecule 1	*
Pi16	peptidase inhibitor 16	*
TNF alpha	tumor necrosis factor alpha	*
Lta	lymphotoxin A	*
Ltb	lymphotoxin B	*
Tap1	transporter 1, ATP-binding cassette, sub-family B (MDR/TAP)	*
C4b	complement component 4B (Chido blood group)	*
Pglyrp2	peptidoglycan recognition protein 2	*
H2-DMa	histocompatibility 2, class II, locus DMa	*
Ehmt2	euchromatic histone lysine N-methyltransferase 2	*
Stk38	serine/threonine kinase 38	*
Lst1	leukocyte specific transcript 1	*
Cfb	complement factor B	*
Psmb9	proteasome (prosome, macropain) subunit, beta type 9 (large multifunctional peptidase 2)	*
Cdkn1a	cyclin-dependent kinase inhibitor 1A (P21)	*
H2-D1	histocompatibility 2, D region locus 1	*
Tapbp	TAP binding protein	*
Rnf8	ring finger protein 8	*
Def6	differentially expressed in FDCP 6	*
H2-Aa	histocompatibility 2, class II antigen A, alpha	*
Pknox1	Pbx/knotted 1 homeobox	*
Abcg1	ATP-binding cassette, sub-family G (WHITE), member 1	*
H2-Ob	histocompatibility 2, O region beta locus	*
H2-Oa	histocompatibility 2, O region alpha locus	*
H2-Q2	histocompatibility 2, Q region locus 2	*
Tap2	transporter 2, ATP-binding cassette, sub-family B (MDR/TAP)	*
Gpsm3	G-protein signalling modulator 3 (AGS3-like, C. elegans)	*
Pim1	proviral integration site 1	*
H2-K1	histocompatibility 2, K1, K region	*
Srsf3	serine/arginine-rich splicing factor 3	*

Rasal3	RAS protein activator like 3	*
Tff2	trefoil factor 2 (spasmolytic protein 1)	*
Psmb8	proteasome (prosome, macropain) subunit, beta type 8 (large multifunctional peptidase 7)	*
Hmga1	high mobility group AT-hook 1	*
Ager	advanced glycosylation end product-specific receptor	*
Aif1	allograft inflammatory factor 1	*
Ppard	peroxisome proliferator activator receptor delta	*
Neu1	neuraminidase 1	*
Ppt2	palmitoyl-protein thioesterase 2	*
Cyp4f14	cytochrome P450, family 4, subfamily f, polypeptide 14	*
Nkx2-5	NK2 homeobox 5	*
Hsf2bp	heat shock transcription factor 2 binding protein	*
Cd320	CD320 antigen	*
Angptl4	angiopoietin-like 4	*
G6b	immunoreceptor tyrosine-based inhibitory motif (ITIM) containing platelet receptor	*
Cpne5	copine V	*
Hspa1b	heat shock protein 1B	*
Cbs	cystathionine beta-synthase	*
Brd2	bromodomain containing 2	*
Spdef	SAM pointed domain containing ets transcription factor	*
Tff3	trefoil factor 3, intestinal	*
Pbx2	pre B cell leukemia homeobox 2	*
Daxx	Fas death domain-associated protein	*
Sik1	salt inducible kinase 1	*
C2	complement component 2 (within H-2S)	*
Ly6g6f	lymphocyte antigen 6 complex, locus G6F	*
Ly6g6e	lymphocyte antigen 6 complex, locus G6E	*
Ly6g6d	lymphocyte antigen 6 complex, locus G6D	*
Actl9	actin-like 9	
Bak1	BCL2-antagonist/killer 1	
Btbd9	BTB (POZ) domain containing 9	
Btnl6	butyrophilin-like 6	
Cbs	cystathionine beta-synthase	
Cyp4f13	cytochrome P450, family 4, subfamily f, polypeptide 13	
Cyp4f17	cytochrome P450, family 4, subfamily f, polypeptide 17	
Ephx3	epoxide hydrolase 3	
Fgd2	FYVE, RhoGEF and PH domain containing 2	
Ggnbp1	gametogenetin binding protein 1	
Gm10045	predicted pseudogene 10045	
Ip6k3	inositol hexaphosphate kinase 3	

Itpr3	inositol 1,4,5-triphosphate receptor 3	
Mdga1	MAM domain containing glycosylphosphatidylinositol anchor 1	
Morc2b	microrchidia 2B	
Pnpla1	patatin-like phospholipase domain containing 1	
Rab44	RAB44, member RAS oncogene family	
Ubash3a	ubiquitin associated and SH3 domain containing, A	
Uhrf1bp1	UHRF1 (ICBP90) binding protein 1	
Umodl1	uromodulin-like 1	
Wdr4	WD repeat domain 4	
Wiz	widely-interspaced zinc finger motifs	
Zfp870	zinc finger protein 870	

Supplementary Table 3.3. QTLs mapped to the *Cnes2.2* locus.

Symbol	Name	Immune system Related	Respiratory system related
Lmr1	leishmaniasis resistance 1	*	
Lmr7	leishmaniasis resistance 7	*	
Leci2	leukocyte endothelial cell interactions 2	*	
Ceat1	chronic experimental autoimmune thyroiditis 1	*	
Lfnq4	lung function QTL 4		*
Bhr3	bronchial hyperresponsiveness 3		*
Radpf1	radiation pulmonary fibrosis 1		*

Supplementary Table 3.4. QTLs mapped to the *Cnes2.4* locus.

Symbol	Name	Immune system related	Respiratory system related
Hbnr2	Heligmosomoides bakeri nematode resistance 2	*	
Lmr1	leishmaniasis resistance 1	*	
Tir9	trypanosome infection response 9	*	
Char3	P. chabaudi malaria resistance QTL 3	*	
Mbis4	Mycobacterium bovis-induced systemic lupus erythematosus 4	*	
Sles1	systemic lupus erythmatosus suppressor 1	*	
Bbaa28	B.burgdorferi-associated arthritis 28	*	
Asbb3	autoimmune susceptibility in C57BL/6J and BALB/c 3	*	
Sst5	susceptibility to tuberculosis 5	*	
Tir7	trypanosome infection response 7	*	
Ssial4	susceptibility to sialadenitis 4	*	
Lbw1	lupus NZB x NZW 1	*	
Lmr7	leishmaniasis resistance 7	*	
Sm2	susceptibility to Schistosoma mansoni infection 2	*	
Pas2	pulmonary adenoma susceptibility 2		*
Radpf1	radiation pulmonary fibrosis 1		*
Blmpf1	bleomycin-induced pulmonary fibrosis 1		*
Pas19	pulmonary adenoma susceptibility 19		*
Lfnq4	lung function QTL 4		*
Pas2	pulmonary adenoma susceptibility 2		*
Bhr3	bronchial hyperresponsiveness 3		*

Supplementary Table 3.5: List of variants in the *Cnes2.2* interval with high and moderate impact. A: SNPs and B: indels. Variants with deleterious SIFT score are highlighted in blue.

A

Variant	Location	Consequence	Impact	SYMBOL	BIOTYPE	SIFT
rs46111484	17:17911708-17911708	stop_gained	HIGH	Gm7535	protein_coding	-
rs51820294	17:20355816-20355816	stop_gained	HIGH	Vmn2r107	protein_coding	-
rs47297925	17:20890513-20890513	stop_gained	HIGH	Vmn1r231	protein_coding	-
Variant	**Location**	**Consequence**	**Impact**	**SYMBOL**	**BIOTYPE**	**SIFT**
rs243550800	17:17145276-17145276	missense_variant	MODERATE	Zfp97	protein_coding	tolerated(1)
rs52004897	17:17145501-17145501	missense_variant	MODERATE	Zfp97	protein_coding	tolerated(1)
rs51959128	17:17145505-17145505	missense_variant	MODERATE	Zfp97	protein_coding	deleterious((0.04)
rs46574447	17:17145514-17145514	missense_variant	MODERATE	Zfp97	protein_coding	tolerated(0.09)
rs46228392	17:17145576-17145576	missense_variant	MODERATE	Zfp97	protein_coding	tolerated(0.77)
rs108126182	17:17265852-17265852	missense_variant	MODERATE	LOC102640673	protein_coding	-
rs237332378	17:17378510-17378510	missense_variant	MODERATE	Chd1	protein_coding	deleterious((0.02)
rs237332378	17:17378510-17378510	missense_variant	MODERATE	Riok2	protein_coding	deleterious((0.02)
rs49928915	17:17387327-17387327	missense_variant	MODERATE	Chd1	protein_coding	tolerated(0.81)
rs49928915	17:17387327-17387327	missense_variant	MODERATE	Riok2	protein_coding	tolerated(0.81)
rs47492665	17:17387329-17387329	missense_variant	MODERATE	Chd1	protein_coding	tolerated(0.97)
rs47492665	17:17387329-17387329	missense_variant	MODERATE	Riok2	protein_coding	tolerated(0.97)
rs257186443	17:17712756-17712756	missense_variant	MODERATE	Vmn2r90	protein_coding	deleterious((0.02)
rs33755033	17:17733625-17733625	missense_variant	MODERATE	Vmn2r90	protein_coding	tolerated(0.43)
rs33755032	17:17733709-17733709	missense_variant	MODERATE	Vmn2r90	protein_coding	tolerated(0.07)
rs248739740	17:17734015-17734015	missense_variant	MODERATE	Vmn2r90	protein_coding	tolerated(0.19)
rs50121023	17:17911058-17911058	missense_variant	MODERATE	Gm7535	protein_coding	tolerated(1)
rs51500948	17:17911367-17911367	missense_variant	MODERATE	Gm7535	protein_coding	tolerated(0.13)
rs49014309	17:17911684-17911684	missense_variant	MODERATE	Gm7535	protein_coding	deleterious((0.02)
rs255396460	17:18021801-18021801	missense_variant	MODERATE	Fpr-rs4	protein_coding	tolerated(0.72)
rs33055109	17:18022309-18022309	missense_variant	MODERATE	Fpr-rs4	protein_coding	deleterious((0.02)
rs46182873	17:18061994-18061994	missense_variant	MODERATE	Vmn2r124	protein_coding	tolerated(0.12)
rs107740022	17:18062778-18062778	missense_variant	MODERATE	Vmn2r124	protein_coding	tolerated(0.83)
rs224621759	17:19380221-19380221	missense_variant	MODERATE	Vmn2r99	protein_coding	deleterious((0.02)
rs107930176	17:19591123-19591123	missense_variant	MODERATE	Vmn2r101	protein_coding	tolerated(1)
rs29532525	17:19793483-19793483	missense_variant	MODERATE	Vmn2r103	protein_coding	tolerated(1)
rs232227301	17:19812441-19812441	missense_variant	MODERATE	Vmn2r103	protein_coding	deleterious((0.01)
rs51044590	17:20113727-20113727	missense_variant	MODERATE	Fpr-rs7	protein_coding	tolerated(0.24)
rs49243834	17:20356660-20356660	missense_variant	MODERATE	Vmn2r107	protein_coding	tolerated(0.32)
rs33502424	17:20462969-20462969	missense_variant	MODERATE	Vmn2r108	protein_coding	tolerated(0.34)
rs50308311	17:20471016-20471016	missense_variant	MODERATE	Vmn2r108	protein_coding	tolerated(0.09)
rs45997263	17:20471360-20471360	missense_variant	MODERATE	Vmn2r108	protein_coding	deleterious((0.04)
rs48082876	17:20502438-20502438	missense_variant	MODERATE	Vmn1r225	protein_coding	deleterious((0.01)
rs33298471	17:20541341-20541341	missense_variant	MODERATE	Vmn2r109	protein_coding	deleterious((0)
rs29505286	17:20555081-20555081	missense_variant	MODERATE	Vmn2r109	protein_coding	tolerated(0.83)
rs234331073	17:20583156-20583156	missense_variant	MODERATE	Vmn2r110	protein_coding	tolerated(0.52)
rs33393752	17:20596214-20596214	missense_variant	MODERATE	Vmn2r110	protein_coding	tolerated(0.47)
rs29499374	17:20596220-20596220	missense_variant	MODERATE	Vmn2r110	protein_coding	tolerated(1)
rs33558668	17:20736079-20736079	missense_variant	MODERATE	Vmn1r227	protein_coding	-
rs250251895	17:21020790-21020790	missense_variant	MODERATE	Zfp160	protein_coding	tolerated(0.24)
rs107665156	17:21094698-21094698	missense_variant	MODERATE	Gm6811	protein_coding	tolerated(1)
rs13479576	17:21990830-21990830	missense_variant	MODERATE	Zfp943	protein_coding	tolerated(1)
rs246813193	17:22339900-22339900	missense_variant	MODERATE	Zfp944	protein_coding	tolerated(0.42)
rs33768715	17:22374870-22374870	missense_variant	MODERATE	Zfp758	protein_coding	deleterious((0.01)

B

Variant	Location	Consequence	IMPACT	SYMBOL	BIOTYPE	SIFT
rs235073749	17:17395081-1739509	splice_donor_variant	HIGH	Gm26873	lincRNA	-
rs235151182	17:20375749-2037575	frameshift_variant	HIGH	Vmn2r107	protein_coding	-
Variant	**Location**	**Consequence**	**IMPACT**	**SYMBOL**	**BIOTYPE**	**SIFT**
rs257608955	17:17970889-1797090	inframe_deletion	MODERATE	Fpr3	protein_coding	-

Supplementary Table 3.6: List of variants in the *Cnes2.4* interval with high and moderate impact. A: SNPs and B: indels. Variants with deleterious SIFT score are highlighted in blue.

A

Variant	Location	Consequence	IMPACT	SYMBOL	BIOTYPE	SIFT
rs33622206	17:27884606-27884606	splice_donor_variant	HIGH	Uhrf1bp1	protein_coding	-
rs46779183	17:29465343-29465343	splice_donor_variant	HIGH	Gm36199	lncRNA	-
rs47347152	17:33909179-33909179	splice_donor_variant	HIGH	BC051226	antisense	-
rs50972829	17:33977869-33977869	splice_donor_variant	HIGH	H2-K2	misc_RNA	-
rs107815810	17:34241132-34241132	start_lost	HIGH	H2-Ob	protein_coding	-
rs47704390	17:34422101-34422101	splice_donor_variant	HIGH	BC051142	protein_coding	-
rs108391400	17:34515435-34515435	stop_gained	HIGH	Btnl6	protein_coding	-
rs245337516	17:34816264-34816264	splice_acceptor_variant	HIGH	C4a	protein_coding	-
rs51170361	17:34856932-34856932	stop_gained	HIGH	Cfb	protein_coding	-
rs225181922	17:35046234-35046234	stop_gained	HIGH	Msh5	protein_coding	-
Variant	**Location**	**Consequence**	**IMPACT**	**SYMBOL**	**BIOTYPE**	**SIFT**
rs33435921	17:27707905-27707905	missense_variant	MODERATE	Pacsin1	protein_coding	tolerated(0.44)
rs47514860	17:27707988-27707988	missense_variant	MODERATE	Pacsin1	protein_coding	tolerated(0.7)
rs33421366	17:27876824-27876824	missense_variant	MODERATE	Uhrf1bp1	protein_coding	tolerated(1)
rs33166239	17:27876949-27876949	missense_variant	MODERATE	Uhrf1bp1	protein_coding	deleterious(0.01)
rs33350456	17:27880171-27880171	missense_variant	MODERATE	Uhrf1bp1	protein_coding	tolerated(0.51)
rs33139124	17:27880297-27880297	missense_variant	MODERATE	Uhrf1bp1	protein_coding	tolerated(1)
rs33278086	17:27886729-27886729	missense_variant	MODERATE	Uhrf1bp1	protein_coding	tolerated(1)
rs13482936	17:28219802-28219802	missense_variant	MODERATE	Def6	protein_coding	tolerated(1)
rs33120907	17:28689906-28689906	missense_variant	MODERATE	Slc26a8	protein_coding	-
rs51672228	17:28818349-28818349	missense_variant	MODERATE	Brpf3	protein_coding	-
rs33095675	17:28829077-28829077	missense_variant	MODERATE	Brpf3	protein_coding	-
rs33610017	17:28881088-28881088	missense_variant	MODERATE	Pnpla1	protein_coding	tolerated_low_confidence(0.57)
rs33145938	17:28881365-28881365	missense_variant	MODERATE	Pnpla1	protein_coding	tolerated_low_confidence(0.66)
rs33296443	17:28881407-28881407	missense_variant	MODERATE	Pnpla1	protein_coding	deleterious_low_confidence(0.01
rs33243088	17:28881418-28881418	missense_variant	MODERATE	Pnpla1	protein_coding	tolerated_low_confidence(0.08)
rs29497282	17:29121002-29121002	missense_variant	MODERATE	Rab44	protein_coding	-
rs48076604	17:29133778-29133778	missense_variant	MODERATE	Rab44	protein_coding	-
rs49898020	17:29138155-29138155	missense_variant	MODERATE	Rab44	protein_coding	deleterious(0)
rs33273699	17:29139234-29139234	missense_variant	MODERATE	Rab44	protein_coding	tolerated(0.12)
rs33315392	17:29159999-29159999	missense_variant	MODERATE	Cpne5	protein_coding	deleterious(0.02)
rs50145963	17:29308142-29308142	missense_variant	MODERATE	Gm10045	protein_coding	-
rs238304027	17:29308232-29308232	missense_variant	MODERATE	Gm10045	protein_coding	-
rs257938869	17:29308393-29308393	missense_variant	MODERATE	Gm10045	protein_coding	-
rs29499072	17:29327435-29327435	missense_variant	MODERATE	Pi16	protein_coding	tolerated_low_confidence(0.31)
rs47046273	17:29363761-29363761	missense_variant	MODERATE	Fgd2	protein_coding	tolerated_low_confidence(0.31)
rs29538028	17:29376181-29376181	missense_variant	MODERATE	Fgd2	protein_coding	-
rs45986438	17:29378336-29378336	missense_variant	MODERATE	Fgd2	protein_coding	tolerated(0.38)
rs33606398	17:29857637-29857637	missense_variant	MODERATE	Mdga1	protein_coding	deleterious(0.03)
rs13482943	17:30299545-30299545	missense_variant	MODERATE	Btbd9	protein_coding	tolerated(0.97)
rs108666242	17:30971916-30971916	missense_variant	MODERATE	Umodl1	protein_coding	deleterious(0)
rs51939115	17:30973738-30973738	missense_variant	MODERATE	Umodl1	protein_coding	tolerated(0.61)
rs49660269	17:31231442-31231442	missense_variant	MODERATE	Ubash3a	protein_coding	-
rs33318475	17:31235548-31235548	missense_variant	MODERATE	Ubash3a	protein_coding	deleterious(0.02)
rs46850399	17:31512174-31512174	missense_variant	MODERATE	Wdr4	protein_coding	tolerated(0.87)
rs29501189	17:31617253-31617253	missense_variant	MODERATE	Cbs	protein_coding	tolerated(0.5)
rs33635352	17:32143568-32143568	missense_variant	MODERATE	Notch3	protein_coding	deleterious(0.05)
rs33175238	17:32144588-32144588	missense_variant	MODERATE	Notch3	protein_coding	tolerated(0.82)
rs47006251	17:32147425-32147425	missense_variant	MODERATE	Notch3	protein_coding	tolerated(1)
rs33375563	17:32158712-32158712	missense_variant	MODERATE	Notch3	protein_coding	tolerated(1)
rs47778998	17:32189403-32189403	missense_variant	MODERATE	Ephx3	protein_coding	tolerated_low_confidence(1)
rs33220232	17:32367917-32367917	missense_variant	MODERATE	Wiz	protein_coding	tolerated(0.42)
rs13482951	17:32527912-32527912	missense_variant	MODERATE	Cyp4f17	protein_coding	deleterious(0.03)
rs50978141	17:32882681-32882681	missense_variant	MODERATE	Zfp870	protein_coding	deleterious_low_confidence(0.01
rs6348359	17:32883762-32883762	missense_variant	MODERATE	Zfp870	protein_coding	deleterious(0.03)
rs6348807	17:32883809-32883809	missense_variant	MODERATE	Zfp870	protein_coding	tolerated(0.11)
rs6349359	17:32883888-32883888	missense_variant	MODERATE	Zfp870	protein_coding	-
rs51550896	17:32884058-32884058	missense_variant	MODERATE	Zfp870	protein_coding	tolerated(1)
rs46149805	17:32925361-32925361	missense_variant	MODERATE	Cyp4f13	protein_coding	deleterious(0.05)

rs48657382	17:32925723-32925723	missense_variant	MODERATE	Cyp4f13	protein_coding	tolerated(1)
rs46720992	17:32929955-32929955	missense_variant	MODERATE	Cyp4f13	protein_coding	tolerated(0.31)
rs108415077	17:32930009-32930009	missense_variant	MODERATE	Cyp4f13	protein_coding	deleterious(0.03)
rs13459151	17:32941145-32941145	missense_variant	MODERATE	Cyp4f13	protein_coding	tolerated(0.35)
rs33295720	17:33065434-33065434	missense_variant	MODERATE	4921501E09Rik	protein_coding	deleterious(0)
rs33705121	17:33065600-33065600	missense_variant	MODERATE	4921501E09Rik	protein_coding	deleterious(0.01)
rs33198676	17:33065797-33065797	missense_variant	MODERATE	4921501E09Rik	protein_coding	tolerated(1)
rs33635759	17:33065945-33065945	missense_variant	MODERATE	4921501E09Rik	protein_coding	tolerated(0.24)
rs33265776	17:33066010-33066010	missense_variant	MODERATE	4921501E09Rik	protein_coding	tolerated(0.94)
rs49653172	17:33066097-33066097	missense_variant	MODERATE	4921501E09Rik	protein_coding	tolerated_low_confidence(0.61)
rs48883344	17:33066358-33066358	missense_variant	MODERATE	4921501E09Rik	protein_coding	tolerated(0.29)
rs49325851	17:33066460-33066460	missense_variant	MODERATE	4921501E09Rik	protein_coding	deleterious(0.03)
rs48746725	17:33066514-33066514	missense_variant	MODERATE	4921501E09Rik	protein_coding	tolerated(1)
rs47300064	17:33066580-33066580	missense_variant	MODERATE	4921501E09Rik	protein_coding	tolerated(1)
rs51515157	17:33066584-33066584	missense_variant	MODERATE	4921501E09Rik	protein_coding	tolerated(0.43)
rs45754480	17:33066643-33066643	missense_variant	MODERATE	4921501E09Rik	protein_coding	tolerated(0.26)
rs51505881	17:33066767-33066767	missense_variant	MODERATE	4921501E09Rik	protein_coding	tolerated(0.73)
rs51449637	17:33066790-33066790	missense_variant	MODERATE	4921501E09Rik	protein_coding	tolerated(1)
rs46118679	17:33066994-33066994	missense_variant	MODERATE	4921501E09Rik	protein_coding	deleterious(0.02)
rs33123603	17:33067588-33067588	missense_variant	MODERATE	4921501E09Rik	protein_coding	deleterious(0.01)
rs33387399	17:33067615-33067615	missense_variant	MODERATE	4921501E09Rik	protein_coding	tolerated(0.26)
rs33493422	17:33136776-33136776	missense_variant	MODERATE	Morc2b	protein_coding	tolerated_low_confidence(0.25)
rs13482953	17:33137236-33137236	missense_variant	MODERATE	Morc2b	protein_coding	deleterious(0)
rs48346592	17:33302765-33302765	missense_variant	MODERATE	Zfp955b	protein_coding	tolerated(0.4)
rs29519555	17:33335363-33335363	missense_variant	MODERATE	Zfp81	protein_coding	tolerated(1)
rs52049521	17:33335550-33335550	missense_variant	MODERATE	Zfp81	protein_coding	tolerated(0.22)
rs33082684	17:33386458-33386458	missense_variant	MODERATE	Zfp101	protein_coding	tolerated(0.61)
rs33308662	17:33433796-33433796	missense_variant	MODERATE	Actl9	protein_coding	tolerated(0.12)
rs33470805	17:33433799-33433799	missense_variant	MODERATE	Actl9	protein_coding	tolerated(0.71)
rs108153512	17:33594296-33594296	missense_variant	MODERATE	Myo1f	protein_coding	deleterious(0)
rs107636198	17:33602015-33602015	missense_variant	MODERATE	Myo1f	protein_coding	tolerated(1)
rs48088473	17:33640771-33640771	missense_variant	MODERATE	Pram1	protein_coding	tolerated(1)
rs33399614	17:33644700-33644700	missense_variant	MODERATE	Pram1	protein_coding	tolerated(1)
rs108205122	17:33885197-33885197	missense_variant	MODERATE	Kifc1	protein_coding	tolerated(1)
rs108847027	17:33885858-33885858	missense_variant	MODERATE	Kifc1	protein_coding	tolerated(1)
rs33679144	17:33911548-33911548	missense_variant	MODERATE	Daxx	protein_coding	tolerated(0.71)
rs33658005	17:33926106-33926106	missense_variant	MODERATE	Tapbp	protein_coding	tolerated(0.49)
rs50014799	17:33932340-33932340	missense_variant	MODERATE	Rgl2	protein_coding	tolerated(0.92)
rs108172451	17:33933621-33933621	missense_variant	MODERATE	Rgl2	protein_coding	deleterious(0.04)
rs33482449	17:33940933-33940933	missense_variant	MODERATE	Wdr46	protein_coding	tolerated_low_confidence(1)
rs13461486	17:33943386-33943386	missense_variant	MODERATE	Wdr46	protein_coding	tolerated(0.67)
rs6358227	17:33948905-33948905	missense_variant	MODERATE	Wdr46	protein_coding	tolerated(1)
rs46297313	17:33949336-33949336	missense_variant	MODERATE	Wdr46	protein_coding	tolerated(1)
rs49040959	17:33949338-33949338	missense_variant	MODERATE	Wdr46	protein_coding	tolerated(0.56)
rs46278643	17:33958622-33958622	missense_variant	MODERATE	Vps52	protein_coding	tolerated(0.42)
rs108184866	17:33961173-33961173	missense_variant	MODERATE	Vps52	protein_coding	tolerated(0.76)
rs33490761	17:33996613-33996613	missense_variant	MODERATE	H2-K1	protein_coding	-
rs33344611	17:33997122-33997122	missense_variant	MODERATE	H2-K1	protein_coding	-
rs33583118	17:33997124-33997124	missense_variant	MODERATE	H2-K1	protein_coding	tolerated_low_confidence(1)
rs227657521	17:33997127-33997127	missense_variant	MODERATE	H2-K1	protein_coding	tolerated_low_confidence(0.74)
rs33280712	17:33997130-33997130	missense_variant	MODERATE	H2-K1	protein_coding	tolerated_low_confidence(0.13)
rs108394490	17:33997434-33997434	missense_variant	MODERATE	H2-K1	protein_coding	tolerated_low_confidence(1)
rs33293753	17:33997536-33997536	missense_variant	MODERATE	H2-K1	protein_coding	tolerated_low_confidence(0.17)
rs50410315	17:33999279-33999279	missense_variant	MODERATE	H2-K1	protein_coding	tolerated_low_confidence(0.12)
rs47645309	17:33999362-33999362	missense_variant	MODERATE	H2-K1	protein_coding	tolerated_low_confidence(0.26)
rs8237941	17:33999499-33999499	missense_variant	MODERATE	H2-K1	protein_coding	deleterious_low_confidence(0.04
rs8237969	17:33999740-33999740	missense_variant	MODERATE	H2-K1	protein_coding	tolerated_low_confidence(1)
rs258038992	17:33999758-33999758	missense_variant	MODERATE	H2-K1	protein_coding	tolerated_low_confidence(0.39)
rs220276184	17:33999807-33999807	missense_variant	MODERATE	H2-K1	protein_coding	tolerated_low_confidence(0.62)
rs108811653	17:33999859-33999859	missense_variant	MODERATE	H2-K1	protein_coding	tolerated_low_confidence(0.09)

rs51419043	17:33999950-33999950	missense_variant	MODERATE	H2-K1	protein_coding	deleterious_low_confidence(0.03
rs108403127	17:34000034-34000034	missense_variant	MODERATE	H2-K1	protein_coding	tolerated_low_confidence(0.16)
rs49854621	17:34021862-34021862	missense_variant	MODERATE	Ring1	protein_coding	tolerated_low_confidence(0.85)
rs29538025	17:34027482-34027482	missense_variant	MODERATE	H2-Ke6	protein_coding	deleterious(0)
rs13469135	17:34027631-34027631	missense_variant	MODERATE	H2-Ke6	protein_coding	tolerated(1)
rs13482957	17:34030404-34030404	missense_variant	MODERATE	Slc39a7	protein_coding	tolerated(0.68)
rs51544304	17:34051801-34051801	missense_variant	MODERATE	Col11a2	protein_coding	tolerated(0.48)
rs108271195	17:34058912-34058912	missense_variant	MODERATE	Col11a2	protein_coding	deleterious(0.04)
rs107770721	17:34060883-34060883	missense_variant	MODERATE	Col11a2	protein_coding	-
rs52524928	17:34060927-34060927	missense_variant	MODERATE	Col11a2	protein_coding	-
rs50664936	17:34064107-34064107	missense_variant	MODERATE	Col11a2	protein_coding	-
rs13465922	17:34092487-34092487	missense_variant	MODERATE	H2-Oa	protein_coding	tolerated(0.13)
rs107864498	17:34093947-34093947	missense_variant	MODERATE	H2-Oa	protein_coding	deleterious(0.01)
rs29537293	17:34137130-34137130	missense_variant	MODERATE	H2-DMa	protein_coding	tolerated(0.28)
rs46850624	17:34147859-34147859	missense_variant	MODERATE	H2-DMb2	protein_coding	tolerated(1)
rs47444840	17:34148553-34148553	missense_variant	MODERATE	H2-DMb2	protein_coding	tolerated(1)
rs107773684	17:34148580-34148580	missense_variant	MODERATE	H2-DMb2	protein_coding	tolerated(0.37)
rs46675833	17:34153438-34153438	missense_variant	MODERATE	H2-DMb1	protein_coding	tolerated(0.55)
rs50974609	17:34155592-34155592	missense_variant	MODERATE	H2-DMb1	protein_coding	tolerated(1)
rs108028778	17:34157248-34157248	missense_variant	MODERATE	H2-DMb1	protein_coding	tolerated(1)
rs107906207	17:34157275-34157275	missense_variant	MODERATE	H2-DMb1	protein_coding	tolerated(0.3)
rs108371532	17:34159643-34159643	missense_variant	MODERATE	H2-DMb1	protein_coding	tolerated(1)
rs107618331	17:34159932-34159932	missense_variant	MODERATE	H2-DMb1	protein_coding	tolerated(0.95)
rs46967024	17:34183092-34183092	missense_variant	MODERATE	Psmb9	protein_coding	tolerated(1)
rs8242301	17:34189492-34189492	missense_variant	MODERATE	Tap1	protein_coding	tolerated(0.4)
rs8242314	17:34190620-34190620	missense_variant	MODERATE	Tap1	protein_coding	tolerated(0.34)
rs8242352	17:34192956-34192956	missense_variant	MODERATE	Tap1	protein_coding	tolerated(0.12)
rs3023450	17:34193620-34193620	missense_variant	MODERATE	Tap1	protein_coding	deleterious(0)
rs33481450	17:34201249-34201249	missense_variant	MODERATE	Psmb8	protein_coding	tolerated(0.76)
rs48553326	17:34205464-34205464	missense_variant	MODERATE	Tap2	protein_coding	tolerated_low_confidence(1)
rs3023453	17:34205553-34205553	missense_variant	MODERATE	Tap2	protein_coding	deleterious_low_confidence(0.04
rs16797607	17:34211985-34211985	missense_variant	MODERATE	Tap2	protein_coding	tolerated(1)
rs8258631	17:34214091-34214091	missense_variant	MODERATE	Tap2	protein_coding	tolerated(0.21)
rs8258631	17:34214091-34214091	missense_variant	MODERATE	Gm15821	protein_coding	-
rs107815810	17:34241132-34241132	missense_variant	MODERATE	H2-Ob	protein_coding	deleterious(0.04)
rs107918950	17:34243469-34243469	missense_variant	MODERATE	H2-Ob	protein_coding	deleterious(0)
rs51014158	17:34243516-34243516	missense_variant	MODERATE	H2-Ob	protein_coding	tolerated(0.2)
rs33422582	17:34244101-34244101	missense_variant	MODERATE	H2-Ob	protein_coding	-
rs29521642	17:34244102-34244102	missense_variant	MODERATE	H2-Ob	protein_coding	tolerated_low_confidence(0.42)
rs108494306	17:34253888-34253888	missense_variant	MODERATE	H2-Ob	protein_coding	-
rs108650860	17:34263364-34263364	missense_variant	MODERATE	H2-Ab1	protein_coding	tolerated(0.12)
rs108367066	17:34263396-34263396	missense_variant	MODERATE	H2-Ab1	protein_coding	deleterious(0.03)
rs249227964	17:34264772-34264772	missense_variant	MODERATE	H2-Ab1	protein_coding	tolerated(0.08)
rs232662853	17:34264782-34264782	missense_variant	MODERATE	H2-Ab1	protein_coding	tolerated(1)
rs243195174	17:34264788-34264788	missense_variant	MODERATE	H2-Ab1	protein_coding	deleterious(0.05)
rs251232353	17:34264823-34264823	missense_variant	MODERATE	H2-Ab1	protein_coding	tolerated(0.07)
rs107595512	17:34264866-34264866	missense_variant	MODERATE	H2-Ab1	protein_coding	tolerated(1)
rs108861703	17:34264886-34264886	missense_variant	MODERATE	H2-Ab1	protein_coding	tolerated(0.82)
rs243280705	17:34264947-34264947	missense_variant	MODERATE	H2-Ab1	protein_coding	deleterious(0.02)
rs212127444	17:34265000-34265000	missense_variant	MODERATE	H2-Ab1	protein_coding	tolerated(0.25)
rs230460846	17:34265001-34265001	missense_variant	MODERATE	H2-Ab1	protein_coding	tolerated(0.41)
rs107916351	17:34265013-34265013	missense_variant	MODERATE	H2-Ab1	protein_coding	tolerated(0.16)
rs46283069	17:34267345-34267345	missense_variant	MODERATE	H2-Ab1	protein_coding	tolerated(0.21)
rs50772011	17:34267943-34267943	missense_variant	MODERATE	H2-Ab1	protein_coding	tolerated(0.33)
rs108782685	17:34284329-34284329	missense_variant	MODERATE	H2-Aa	protein_coding	tolerated(0.43)
rs245673796	17:34284344-34284344	missense_variant	MODERATE	H2-Aa	protein_coding	tolerated(0.55)
rs231861612	17:34284347-34284347	missense_variant	MODERATE	H2-Aa	protein_coding	tolerated(0.07)
rs245766111	17:34284348-34284348	missense_variant	MODERATE	H2-Aa	protein_coding	tolerated(0.47)
rs47178192	17:34284376-34284376	missense_variant	MODERATE	H2-Aa	protein_coding	tolerated(0.62)
rs220983219	17:34284395-34284395	missense_variant	MODERATE	H2-Aa	protein_coding	tolerated(0.08)

rs108109771	17:34284522-34284522	missense_variant	MODERATE	H2-Aa	protein_coding	tolerated(1)
rs51434336	17:34305957-34305957	missense_variant	MODERATE	H2-Eb1	protein_coding	deleterious(0.04)
rs33342125	17:34309660-34309660	missense_variant	MODERATE	H2-Eb1	protein_coding	tolerated(0.43)
rs50132005	17:34309834-34309834	missense_variant	MODERATE	H2-Eb1	protein_coding	tolerated(0.65)
rs33173284	17:34309841-34309841	missense_variant	MODERATE	H2-Eb1	protein_coding	tolerated(0.36)
rs33420323	17:34309852-34309852	missense_variant	MODERATE	H2-Eb1	protein_coding	tolerated(0.2)
rs29518325	17:34325755-34325755	missense_variant	MODERATE	H2-Eb2	protein_coding	deleterious(0)
rs45786693	17:34334376-34334376	missense_variant	MODERATE	H2-Eb2	protein_coding	tolerated(1)
rs49941515	17:34334413-34334413	missense_variant	MODERATE	H2-Eb2	protein_coding	tolerated(1)
rs51319403	17:34336426-34336426	missense_variant	MODERATE	H2-Eb2	protein_coding	-
rs49265145	17:34338878-34338878	missense_variant	MODERATE	H2-Eb2	protein_coding	deleterious_low_confidence(0)
rs29502799	17:34343714-34343714	missense_variant	MODERATE	H2-Ea-ps	protein_coding	-
rs48758718	17:34347462-34347462	missense_variant	MODERATE	H2-Ea-ps	protein_coding	-
rs33281739	17:34358084-34358084	missense_variant	MODERATE	Btnl2	protein_coding	deleterious(0.04)
rs33666306	17:34358117-34358117	missense_variant	MODERATE	Btnl2	protein_coding	deleterious(0.04)
rs50071031	17:34363519-34363519	missense_variant	MODERATE	Btnl2	protein_coding	tolerated(0.56)
rs46192952	17:34363537-34363537	missense_variant	MODERATE	Btnl2	protein_coding	deleterious(0.03)
rs107609151	17:34377959-34377959	missense_variant	MODERATE	Btnl1	protein_coding	tolerated(0.5)
rs13482958	17:34381084-34381084	missense_variant	MODERATE	Btnl1	protein_coding	tolerated(0.16)
rs33426892	17:34457450-34457450	missense_variant	MODERATE	BC051142	protein_coding	-
rs49977333	17:34460076-34460076	missense_variant	MODERATE	BC051142	protein_coding	deleterious_low_confidence(0)
rs50218359	17:34472368-34472368	missense_variant	MODERATE	Btnl4	protein_coding	tolerated(1)
rs48488783	17:34472624-34472624	missense_variant	MODERATE	Btnl4	protein_coding	tolerated(1)
rs46085868	17:34472636-34472636	missense_variant	MODERATE	Btnl4	protein_coding	deleterious(0)
rs33389488	17:34472696-34472696	missense_variant	MODERATE	Btnl4	protein_coding	tolerated(0.42)
rs33550576	17:34474205-34474205	missense_variant	MODERATE	Btnl4	protein_coding	tolerated(1)
rs108319426	17:34507948-34507948	missense_variant	MODERATE	Btnl6	protein_coding	deleterious_low_confidence(0.01
rs108769382	17:34507987-34507987	missense_variant	MODERATE	Btnl6	protein_coding	tolerated_low_confidence(0.6)
rs107934067	17:34508035-34508035	missense_variant	MODERATE	Btnl6	protein_coding	tolerated(0.59)
rs48141160	17:34508068-34508068	missense_variant	MODERATE	Btnl6	protein_coding	tolerated(0.23)
rs47867628	17:34508228-34508228	missense_variant	MODERATE	Btnl6	protein_coding	tolerated(0.75)
rs47289933	17:34508368-34508368	missense_variant	MODERATE	Btnl6	protein_coding	tolerated(0.51)
rs108106217	17:34508396-34508396	missense_variant	MODERATE	Btnl6	protein_coding	tolerated(0.6)
rs229345218	17:34508899-34508899	missense_variant	MODERATE	Btnl6	protein_coding	tolerated(0.79)
rs108213795	17:34513643-34513643	missense_variant	MODERATE	Btnl6	protein_coding	tolerated(0.27)
rs49003639	17:34513661-34513661	missense_variant	MODERATE	Btnl6	protein_coding	tolerated(1)
rs257003719	17:34514047-34514047	missense_variant	MODERATE	Btnl6	protein_coding	tolerated(0.24)
rs51696402	17:34514077-34514077	missense_variant	MODERATE	Btnl6	protein_coding	tolerated(1)
rs48992697	17:34514128-34514128	missense_variant	MODERATE	Btnl6	protein_coding	tolerated(0.51)
rs217260305	17:34514155-34514155	missense_variant	MODERATE	Btnl6	protein_coding	tolerated(1)
rs46505847	17:34514402-34514402	missense_variant	MODERATE	Btnl6	protein_coding	tolerated(1)
rs214685089	17:34514414-34514414	missense_variant	MODERATE	Btnl6	protein_coding	deleterious(0.02)
rs247407291	17:34514496-34514496	missense_variant	MODERATE	Btnl6	protein_coding	tolerated(0.58)
rs50576946	17:34515429-34515429	missense_variant	MODERATE	Btnl6	protein_coding	tolerated(1)
rs215934976	17:34515434-34515434	missense_variant	MODERATE	Btnl6	protein_coding	tolerated(0.52)
rs48119293	17:34515443-34515443	missense_variant	MODERATE	Btnl6	protein_coding	tolerated(0.71)
rs107737212	17:34515477-34515477	missense_variant	MODERATE	Btnl6	protein_coding	tolerated(0.07)
rs49770915	17:34515478-34515478	missense_variant	MODERATE	Btnl6	protein_coding	tolerated(1)
rs107892072	17:34515500-34515500	missense_variant	MODERATE	Btnl6	protein_coding	deleterious(0.02)
rs108657364	17:34515563-34515563	missense_variant	MODERATE	Btnl6	protein_coding	tolerated(1)
rs48586867	17:34515624-34515624	missense_variant	MODERATE	Btnl6	protein_coding	tolerated(0.81)
rs48704884	17:34515698-34515698	missense_variant	MODERATE	Btnl6	protein_coding	tolerated(0.15)
rs51562827	17:34572591-34572591	missense_variant	MODERATE	Notch4	protein_coding	-
rs33072025	17:34580964-34580964	missense_variant	MODERATE	Notch4	protein_coding	deleterious(0.03)
rs33223511	17:34584417-34584417	missense_variant	MODERATE	Notch4	protein_coding	tolerated(1)
rs107832161	17:34587708-34587708	missense_variant	MODERATE	Notch4	protein_coding	tolerated(0.06)
rs33423464	17:34598180-34598180	missense_variant	MODERATE	Ager	protein_coding	deleterious(0)
rs33423464	17:34598180-34598180	missense_variant	MODERATE	Ager	protein_coding	-
rs33157988	17:34630599-34630599	missense_variant	MODERATE	Prrt1	protein_coding	-
rs29498176	17:34645276-34645276	missense_variant	MODERATE	Fkbpl	protein_coding	tolerated_low_confidence(0.4)

rs48411423	17:34651106-34651106	missense_variant	MODERATE	Atf6b	protein_coding	tolerated(0.12)
rs47461796	17:34672069-34672069	missense_variant	MODERATE	Tnxb	protein_coding	deleterious(0.05)
rs33247838	17:34672522-34672522	missense_variant	MODERATE	Tnxb	protein_coding	tolerated(1)
rs33887584	17:34682106-34682106	missense_variant	MODERATE	Tnxb	protein_coding	-
rs50824235	17:34683532-34683532	missense_variant	MODERATE	Tnxb	protein_coding	tolerated(0.54)
rs223248303	17:34689359-34689359	missense_variant	MODERATE	Tnxb	protein_coding	tolerated(0.32)
rs108790018	17:34693761-34693761	missense_variant	MODERATE	Tnxb	protein_coding	tolerated(1)
rs50308114	17:34694352-34694352	missense_variant	MODERATE	Tnxb	protein_coding	tolerated(0.14)
rs48988536	17:34695630-34695630	missense_variant	MODERATE	Tnxb	protein_coding	deleterious(0.01)
rs245260158	17:34703455-34703455	missense_variant	MODERATE	Tnxb	protein_coding	-
rs49006161	17:34709518-34709518	missense_variant	MODERATE	Tnxb	protein_coding	-
rs260552814	17:34710124-34710124	missense_variant	MODERATE	Tnxb	protein_coding	-
rs108524409	17:34710213-34710213	missense_variant	MODERATE	Tnxb	protein_coding	-
rs215968816	17:34710292-34710292	missense_variant	MODERATE	Tnxb	protein_coding	-
rs223786883	17:34710802-34710802	missense_variant	MODERATE	Tnxb	protein_coding	-
rs214302533	17:34710976-34710976	missense_variant	MODERATE	Tnxb	protein_coding	-
rs237623628	17:34710979-34710979	missense_variant	MODERATE	Tnxb	protein_coding	-
rs222521826	17:34711526-34711526	missense_variant	MODERATE	Tnxb	protein_coding	deleterious(0.01)
rs254813008	17:34711565-34711565	missense_variant	MODERATE	Tnxb	protein_coding	tolerated(0.08)
rs232687639	17:34711722-34711722	missense_variant	MODERATE	Tnxb	protein_coding	deleterious(0.02)
rs247770320	17:34711745-34711745	missense_variant	MODERATE	Tnxb	protein_coding	tolerated(0.24)
rs50011751	17:34713138-34713138	missense_variant	MODERATE	Tnxb	protein_coding	tolerated(0.33)
rs13475137	17:34738895-34738895	missense_variant	MODERATE	C4b	protein_coding	tolerated(0.43)
rs229274524	17:34809558-34809558	missense_variant	MODERATE	C4a	protein_coding	-
rs263370288	17:34809929-34809929	missense_variant	MODERATE	C4a	protein_coding	-
rs48033609	17:34810525-34810525	missense_variant	MODERATE	C4a	protein_coding	-
rs250181651	17:34814356-34814356	missense_variant	MODERATE	C4a	protein_coding	-
rs49335403	17:34815201-34815201	missense_variant	MODERATE	C4a	protein_coding	-
rs29534851	17:34817927-34817927	missense_variant	MODERATE	C4a	protein_coding	-
rs242420196	17:34817939-34817939	missense_variant	MODERATE	C4a	protein_coding	-
rs107766228	17:34818477-34818477	missense_variant	MODERATE	C4a	protein_coding	-
rs233772097	17:34818501-34818501	missense_variant	MODERATE	C4a	protein_coding	-
rs255631719	17:34819332-34819332	missense_variant	MODERATE	C4a	protein_coding	-
rs29538739	17:34819619-34819619	missense_variant	MODERATE	C4a	protein_coding	-
rs33337700	17:34819799-34819799	missense_variant	MODERATE	C4a	protein_coding	-
rs33451789	17:34819905-34819905	missense_variant	MODERATE	C4a	protein_coding	-
rs259699493	17:34820557-34820557	missense_variant	MODERATE	C4a	protein_coding	-
rs33339277	17:34820752-34820752	missense_variant	MODERATE	C4a	protein_coding	-
rs248198580	17:34821967-34821967	missense_variant	MODERATE	C4a	protein_coding	-
rs228700718	17:34821982-34821982	missense_variant	MODERATE	C4a	protein_coding	-
rs246675350	17:34823402-34823402	missense_variant	MODERATE	C4a	protein_coding	-
rs49916438	17:35026737-35026737	missense_variant	MODERATE	Sapcd1	protein_coding	tolerated(1)
rs49916438	17:35026737-35026737	missense_variant	MODERATE	Sapcd1	protein_coding	-
rs33379909	17:35027454-35027454	missense_variant	MODERATE	Sapcd1	protein_coding	deleterious(0.01)
rs33379909	17:35027454-35027454	missense_variant	MODERATE	Sapcd1	protein_coding	-
rs241547476	17:35027954-35027954	missense_variant	MODERATE	Sapcd1	protein_coding	-
rs33561826	17:35028832-35028832	missense_variant	MODERATE	Msh5	protein_coding	tolerated(1)
rs33493455	17:35046753-35046753	missense_variant	MODERATE	Msh5	protein_coding	-
rs222125752	17:35071610-35071610	missense_variant	MODERATE	Ly6g6d	protein_coding	deleterious(0.04)
rs33600239	17:35078214-35078214	missense_variant	MODERATE	Ly6g6e	protein_coding	deleterious(0.03)
rs50058341	17:35102426-35102426	missense_variant	MODERATE	Abhd16a	protein_coding	-
rs108182678	17:35124285-35124285	missense_variant	MODERATE	Gpank1	protein_coding	tolerated(0.54)
rs250626341	17:35135577-35135577	missense_variant	MODERATE	Bag6	protein_coding	tolerated_low_confidence(0.56)
rs214263558	17:35140422-35140422	missense_variant	MODERATE	Bag6	protein_coding	tolerated(0.16)
rs33415727	17:35161042-35161042	missense_variant	MODERATE	Prrc2a	protein_coding	-
rs107937947	17:35186961-35186961	missense_variant	MODERATE	Lst1	protein_coding	tolerated(0.4)
rs108850060	17:35187027-35187027	missense_variant	MODERATE	Lst1	protein_coding	tolerated(1)
rs236829512	17:35195159-35195159	missense_variant	MODERATE	Ltb	protein_coding	tolerated(0.27)
rs8252733	17:35195179-35195179	missense_variant	MODERATE	Ltb	protein_coding	tolerated(0.08)
rs8252734	17:35195296-35195296	missense_variant	MODERATE	Ltb	protein_coding	tolerated(0.43)

rs232119196	17:35220881-35220881	missense_variant	MODERATE	Nfkbil1	protein_coding	-
rs108700197	17:35263430-35263430	missense_variant	MODERATE	H2-D1	protein_coding	tolerated_low_confidence(1)
rs224134401	17:35263575-35263575	missense_variant	MODERATE	H2-D1	protein_coding	tolerated_low_confidence(0.47)
rs8237985	17:35265826-35265826	missense_variant	MODERATE	H2-D1	protein_coding	tolerated_low_confidence(0.17)
rs108347677	17:35266015-35266015	missense_variant	MODERATE	H2-D1	protein_coding	tolerated_low_confidence(1)
rs246308437	17:35266502-35266502	missense_variant	MODERATE	H2-D1	protein_coding	tolerated(0.43)
rs246308437	17:35266502-35266502	missense_variant	MODERATE	H2-D1	protein_coding	tolerated_low_confidence(0.4)
rs229505720	17:35320758-35320758	missense_variant	MODERATE	H2-Q1	protein_coding	-
rs250846213	17:35321437-35321437	missense_variant	MODERATE	H2-Q1	protein_coding	tolerated_low_confidence(0.07)
rs243912932	17:35344958-35344958	missense_variant	MODERATE	H2-Q2	protein_coding	tolerated_low_confidence(0.42)
rs226420083	17:35345176-35345176	missense_variant	MODERATE	H2-Q2	protein_coding	tolerated_low_confidence(0.76)
rs257404728	17:35345471-35345471	missense_variant	MODERATE	H2-Q2	protein_coding	deleterious(0.02)
rs221666791	17:35345474-35345474	missense_variant	MODERATE	H2-Q2	protein_coding	deleterious_low_confidence(0.03
rs48809372	17:35383016-35383016	missense_variant	MODERATE	H2-Q4	protein_coding	tolerated_low_confidence(1)
rs218228737	17:35383094-35383094	missense_variant	MODERATE	H2-Q4	protein_coding	tolerated_low_confidence(0.16)

B

Variant	Location	Consequence	IMPACT	SYMBOL	BIOTYPE	SIFT
rs223987942	17:32701878-32701883	splice_acceptor_variant	HIGH	Cyp4f15	protein_coding	-
rs222438566	17:35188379-35188380	frameshift_variant	HIGH	Lst1	protein_coding	-
rs239381499	17:35345698-35345699	frameshift_variant	HIGH	H2-Q2	protein_coding	-
Variant	**Location**	**Consequence**	**IMPACT**	**SYMBOL**	**BIOTYPE**	**SIFT**
rs218848588	17:28905681-28905684	inframe_deletion	MODERATE	4930539E08Rik	protein_coding	
rs235277251	17:33065334-33065337	inframe_deletion	MODERATE	4921501E09Rik	protein_coding	
rs241036860	17:33912659-33912662	inframe_deletion	MODERATE	Daxx	protein_coding	
rs220101824	17:34092468-34092477	inframe_deletion	MODERATE	H2-Oa	protein_coding	
rs244364491	17:35150280-35150283	inframe_deletion	MODERATE	Prrc2a	protein_coding	

Chapter 4

Essential role of IL-1RI signaling in protection against *Cryptococcus neoformans* infection

Manuscript under revision

Mitra Shourian[1,2], Ben Ralph[3,4], Isabelle Angers[2,5], Donald C. Sheppard[3,4,6], Salman T. Qureshi[1,2,5,6] *

[1] Division of Experimental Medicine, McGill University, Montréal, Québec, Canada

[2] Meakins-Christie Laboratories, McGill University, Montréal, Québec, Canada.

[3] Program in Infectious Diseases and Immunology in Global Health, Centre for Translational Biology, The Research Institute of the McGill University Health Center (RI-MUHC), Montréal, Québec, Canada.

[4] Department of Microbiology and Immunology, McGill University, Montréal, Québec, Canada

[5] Program in Translational Research in Respiratory Diseases and Department of Critical Care, The Research Institute of the McGill University Health Center (RI-MUHC), Montréal, Québec, Canada

[6] Department of Medicine, McGill University, Montréal, Québec, Canada

* **Corresponding author:** Dr. Salman T. Qureshi, salman.qureshi@mcgill.ca.

Running Title: IL-I signaling and cryptococcal infection.

Keywords: *Cryptococcus neoformans*, fungal pneumonia, IL-1, IL-1R, lung inflammation, cytokines, macrophage polarization, lymphocyte differentiation

Preface to Chapter 4

In chapter 2 of my thesis, I showed that IL-1β is one of the proinflammatory cytokines that is highly induced in resistant *Cnes2* congenic mice following infection. Previous work in our lab also has reported higher expression of this cytokine in the lungs of resistant SJL/J compared to susceptible C57BL/6 mice following *C. neoformans* 52D infection. Although production of IL-1β in our and other studies has been associated with protection against cryptococcal infection, there is no study that has demonstrated a causal effect. Genetically engineered deficiency of IL-1RI, a common signaling receptor for both Il-1α and IL-1β, on the C57BL/6 genetic background did not significantly alter host susceptibility to *Cryptococcus* H99 infection; however, a caveat of this study is the fact that wild type C57BL/6 mice with intact IL-1RI function are extremely susceptible to H99 infection. Therefore, to rigorously examine the effect of IL-1R signaling on *Cryptococcus* infection, we generated IL-1R knockout mice on the resistant BALB/c background and analyzed the host susceptibility phenotype and immune response following *C. neoformans* 52D infection.

4.1. Abstract

Interleukin-1 alpha (IL-1α) and IL-1 beta (IL-1β) are pro-inflammatory cytokines that are induced following *Cryptococcus. neoformans* infection and activate the IL-1 Receptor type I (IL-1RI). To establish the role of IL-1RI signaling in cryptococcal infection, we analyzed wild type (WT) and IL-1RI-deficient (IL-1RI$^{-/-}$) mice on the BALB/c background. IL-1RI$^{-/-}$ mice had significantly reduced survival compared to WT mice after intratracheal challenge with *C. neoformans* 52D. Microbiological analysis showed a significant increase in the lung and brain fungal burden of IL-1RI$^{-/-}$ compared to WT mice beginning at week 1 and 4 post-infection, respectively. Histopathology showed that IL-1RI$^{-/-}$ mice exhibit greater airway epithelial mucus secretion and prominent eosinophilic crystals that were absent in WT mice. Susceptibility of IL-1RI$^{-/-}$ mice was associated with significant induction of a Th2-biased immune response characterized by pulmonary eosinophilia, M2 macrophage polarization, and recruitment of CD4^{+} IL-13^{+} T cells. Expression of pro-inflammatory (IL-1α, IL-1β, IL-6, TNFα, MCP-1), Th1-associated (IFNγ, IL-12) and Th17-associated (IL-17) cytokines was significantly reduced in IL-1RI$^{-/-}$ lungs compared to WT. WT mice also had higher expression of KC/CXCL1 and sustained neutrophil recruitment to the lung; however, antibody-mediated depletion of these cells showed that they were dispensable for lung fungal clearance. In conclusion, our data indicate that IL-1RI signaling is required to activate a complex series of innate and adaptive immune responses that collectively enhance host defense and survival following *C. neoformans* infection.

4.2. Introduction

Cryptococcus neoformans is an encapsulated yeast that is estimated to cause approximately 1 million cases of meningitis throughout the world each year (32). In healthy individuals, inhalation of infectious propagules is usually contained in the lung, but among those with a defective immune response, uncontrolled replication may result in dissemination to other parts of the body with a tropism for the brain (15, 17). Severe cryptococcal disease occurs primarily in patients with uncontrolled HIV/AIDS and is also found in solid organ transplant recipients, those receiving exogenous immunosuppression, patients with primary or acquired immunodeficiency, and increasingly among immunologically normal hosts (14, 195, 280, 339).

The pattern of cytokine expression is a crucial determinant of the pathogenesis of cryptococcal infection (17, 115, 116, 340, 341). Th1-type cytokines (IL-12 and IFNγ) promote phagocytosis by dendritic cells and polarize macrophages towards a classically activated phenotype (M1), thereby increasing fungal clearance (262, 289, 342, 343). On the other hand, Th2-type cytokines (IL-4, IL-5, and IL-13) are associated with a significant eosinophil chemotaxis to the lungs and induction of alternatively activated (M2) macrophages that facilitate cryptococcal proliferation and dissemination (267, 298, 344). Finally, there is accumulating evidence that Th17-type cytokines (IL-17 and IL-23) also contribute to protection against *C. neoformans* infection (269, 294, 345, 346).

The mechanisms that initiate and regulate the innate immune response against *C. neoformans* infection are not fully understood. The interaction of *C. neoformans* with host cells triggers production of several pro-inflammatory cytokines including TNFα, IL-6, and IL-1 (347-350). Both IL-1α and IL-1β are induced during cryptococcal infection *in vitro* (210, 347, 348, 351-353) and *in vivo* (139, 191, 264, 354-356) in a NLRP3-dependent manner, and internalization of opsonized encapsulated cryptococci has been shown to activate the canonical NLRP3–ASC–caspase-1 and non-canonical NLRP3–ASC–caspase-8 inflammasome (353, 357). The magnitude of IL-1 expression between inbred mice with different genetic backgrounds has also been associated with natural resistance or susceptibility to progressive cryptococcal infection (354). Following intratracheal infection with *C. neoformans* 52D, the level of IL-1β expression was 11-fold higher in the lungs of resistant SJL/J inbred mice compared to the susceptible C57BL/6 inbred strain. A subsequent analysis of wild type and IL-1R deficient mice on the C57BL/6 genetic background

did not identify significant differences in survival or fungal dissemination following intranasal infection with *C. neoformans* H99; however, at day 12 post-infection the IL-1R$^{-/-}$ mice had a modest elevation of lung fungal burden (264).

Given the essential role for cytokine-mediated inflammation and the evidence for IL-1α and IL-1β induction in response to *C. neoformans,* we hypothesized that the contribution of IL-1R-dependent signaling to host defense may have been underestimated by infection of wild type and IL-1R$^{-/-}$ mice on the susceptible C57BL/6 genetic background with a highly virulent *C. neoformans* strain. To test this hypothesis, we performed intratracheal inoculation of inbred BALB/c mice and IL-1R$^{-/-}$ mice on the same genetic background with *C. neoformans* 52D and analyzed fungal burden and immune responses at serial time points. This approach was chosen to model the process of natural infection in a relatively resistant host with a moderately virulent cryptococcal strain. Our findings demonstrate that IL-1RI$^{-/-}$ mice had a significantly higher fungal burden in the lungs and brains as well as a significantly higher mortality compared to BALB/c mice. In IL-1RI$^{-/-}$ mice, *C. neoformans* 52D infection was associated with heightened lung eosinophilia, elevated airway mucus secretion, and greater recruitment of M2 macrophages and CD4^{+} Th2 cells along with significantly fewer lung neutrophils, DCs, Th1, and Th17 cells. Taken together, this study shows that IL-1R-dependent signaling plays an essential role in protection against lethal *C. neoformans* infection by triggering a complex innate and adaptive immune response and raises the possibility that modulation of this signaling axis could be a potential therapeutic strategy.

4.3. Materials and Methods

Mice. Inbred BALB/c mice were purchased from Charles River and maintained in our facility. IL-1RI$^{-/-}$ mice were purchased from Jackson Labs and backcrossed to BALB/c for 10 generations. Mice were provided with sterile food and water, and cared for according to the Canadian Council on Animal Care guidelines. All experiments were performed using 7- to 9-week old male mice. Mice were humanely euthanized with CO_2 upon completion of experiments, and every effort was made to minimize suffering. All experimental protocols were reviewed and approved by the McGill University Animal Care Committee.

C. neoformans. *C. neoformans* 52D (ATCC 24067) was grown and maintained on Sabouraud dextrose agar (SDA) (BD, Becton Dickinson and Company). To prepare an infectious dose, a single colony was suspended in Sabouraud dextrose broth (BD) and grown to early stationary phase (48 h) at room temperature on a rotator. The stationary phase culture was then washed with sterile phosphate-buffered saline (PBS), counted on a hemocytometer, and diluted to 2×10^5 CFU per ml in sterile PBS. The fungal concentration of the experimental dose was confirmed by plating a dilution of the inoculum on SDA and counting the CFU after 72 h of incubation at room temperature.

Intratracheal infection with *C. neoformans*. For intratracheal administration of *C. neoformans*, mice were anesthetized with 150 mg/kg of ketamine (Ayerst Veterinary Laboratories) and 10 mg/kg of xylazine (Bayer) intraperitoneally. A small skin incision was made below the jaw along the trachea, and the underlying glands and muscle were separated. Infection was performed by intratracheal injection of 10^4 *C. neoformans* in 50µl PBS through a 22-gauge catheter via a 1-ml tuberculin syringe. The incision was closed using the 9-mm EZ clip wound closing kit (Stoelting CO), and mice were monitored daily following surgery.

Tissue isolation and CFU assay. After mice were euthanized with CO_2, their lungs, spleen, and brain were excised and placed in sterile, ice-cold PBS. Tissues were then homogenized using a glass tube and pestle attached to a mechanical tissue homogenizer (Glas-Col), and plated at various dilutions on Sabouraud dextrose agar. Plates were incubated at 37°C for 72 h, and CFU were counted. For survival analyses, mice were inoculated as stated above and monitored twice daily for up to 110 days post-infection.

Histopathological analysis. Following euthanasia, lungs were perfused with ice-cold PBS via the right ventricle of the heart. Using 10% buffered formalin acetate (Fisher Scientific), the lungs were inflated to a pressure of 25 cm H_2O and fixed overnight. Subsequently, lungs were embedded in paraffin, sectioned at 5µm, and stained with hematoxylin-eosin (H&E), periodic acid-Schiff (PAS), or mucicarmine reagents at the Histology Facility of the Goodman Cancer Research Centre (McGill University). Representative photographs of lung sections were taken using a BX51 microscope (Olympus), QICAM Fast 1394 digital charge-coupled device (CCD) camera (QImaging), and Image-Pro Plus software version 7.0.1.658 (Media Cybernetics).

Flow cytometry. Lungs were excised using sterile technique and placed in RPMI (Gibco, Invitrogen) supplemented with 10% fetal bovine serum (Wisent). Subsequently lungs were minced using surgical blades and incubated with 1 mg/ml collagenase (Sigma) at 37°C for 1 h. Following incubation, lung pieces were passed through a 16-gauge needle and filtered through a 70µm cell strainer (BD). Red blood cells were removed using ACK lysis buffer before the cells were counted using a Beckman Coulter Z1 particle counter. Fc receptors were blocked with the addition of unlabeled anti-CD16/32 antibodies (93; eBioscience), and single-cell suspensions were stained with the following fluorescence-conjugated anti-mouse monoclonal antibodies purchased from eBioscience (eBio), BD, and BioLegend (BL): CD45 (30-F11), B220 (RA3-6B2), CD3e (145-2C11), CD4 (GK1.5), CD8 (53-6.7), CD49b (DX5), γδ TCR (GL3), CD11b (M1/70), CD11c (N418), MHCII (M5/114.15.2), Ly6G (1A8), F4/80 (BM8), CD86 (GL1), CD40 (3/23), CD80 (16-10A1), Nos2 (CXNFT), CD206 (C068C2). Non-viable cells were excluded using fixable viability dye reagent (eBio). Data were acquired using a LSR-II flow cytometer (BD) and analyzed using Flow Jo software.

Intracellular flow cytometry. For intracellular cytokine staining of T-cells, lungs were processed as described above. Cells were plated in 96 well plates and stimulated for 4 h with phorbol 12-myristate 13-acetate (PMA) and calcium ionophore (Ionomycin) in the presence of brefeldin A (GolgiPlug) for the final 3 h. Cells were then washed, blocked with anti-CD16/32 antibodies, and stained with a surface antibody cocktail consisting of anti-CD3 (145-2C11), anti-CD4 (GK1.5;), anti-CD8(53-6.7), and anti-CD45(30- F11). Cells were then fixed, permeabilized, and stained with IL-13 (eBio13A), IFNγ (XMG1.2), and IL-17(17B7). Data were acquired using a LSR-II flow

cytometer with gating determined by fluorescence-minus-one (FMO) controls and analyzed using FlowJo software.

Total lung cytokine and chemokine production. Mice were euthanized and lungs flushed with 10 ml of ice-cold PBS. Whole lungs were homogenized in 2 ml PBS with Halt protease and phosphatase inhibitor cocktail (Fisher Scientific) using a sterilized glass tube and pestle attached to a mechanical tissue homogenizer (Glas-Col) and spun at 12,000 rpm for 20 min. Supernatants were collected, and aliquots were stored at -80°C for further analysis. The following cytokines and chemokines in whole-lung protein samples were analyzed using DuoSet enzyme-linked immunosorbent assay (ELISA) kits (R&D Systems): TNFα (DY410), IL-6 (DY406), IL-1β (DY401), IL-1α (DY400), MCP-1 (MJE00), IL-12/IL-23P40 (DY2398), IFNγ (DY485), CXCL1/KC (DY453), IL- 17A (DY421) and IL-13 (DY413).

Neutrophil depletion. BALB/c mice received an intratracheal inoculum of 1×10^4 CFU of *C. neoformans* strain 52D. Mice were treated with control or anti-1A8 antibody (Bio X Cell) one day prior to infection and daily during the study. At day 12 post-infection, lungs were excised and fungal burden were analyzed.

Statistical analysis. To test the significance of single comparisons, an unpaired Student t test was applied (with a threshold P value of ≤ 0.05), unless otherwise stated. For all experiments, the mean and standard error of the mean (SEM) is shown. Survival curves were analysed by the log-rank test. All statistical analysis was performed with GraphPad Prism software version 6 (GraphPad Software Inc.)

4.4. Results

IL-1RI$^{-/-}$ mice have impaired survival and an increased fungal burden in the lung, brain, and spleen following *C. neoformans* infection.

To investigate the role of IL-1RI-mediated signaling following *C. neoformans* 52D infection, we constructed IL-1RI$^{-/-}$ mice on the BALB/c background by repeated backcrossing. We challenged mice with *C. neoformans* 52D and measured the survival rate and tissue fungal burden. No deaths were observed in WT mice; however, IL-1RI$^{-/-}$ mice started to die at 40 days post-infection and had an 100% mortality rate at 72 days post-infection (Figure 1A). Microbiological analysis also showed a significant increase of fungal burden in IL-1RI$^{-/-}$ mice compared to the WT strain at all time points tested (Figure 1B). Importantly, a significant difference in lung fungal burden was observed at 7 days post-infection, suggesting that the IL-1RI signaling affects the initial host response to *C. neoformans* infection. At 35 days post-infection, there was almost a 20-fold increase of lung CFU in the IL-1RI$^{-/-}$ compared to the WT strain. Analysis of the spleen showed a trend towards higher CFU in the IL-1RI$^{-/-}$ mice compared to the WT strain that reached statistical significance at day 14 post-infection (Figure 1C). Analysis of the brain showed comparable CFU in both strains at 14 days post-infection; however, at 35 days post-infection all of the WT mice had cleared the infection while 10/16 (62%) of IL-1RI$^{-/-}$ mice still had detectable fungal growth (Figure 1D). Taken together, these data establish an essential role for IL-1R-mediated signaling in the innate and adaptive control of *C. neoformans* 52D pulmonary growth and organ dissemination.

An altered pattern of pulmonary inflammation is present in IL-1RI$^{-/-}$ lungs following *C. neoformans* infection.

The significant differences in survival and fungal burden between WT and IL-1RI$^{-/-}$ mice prompted us to investigate the effect of IL-1RI signaling on lung pathology following infection with *C. neoformans* 52D. Histopathological analysis was conducted at 35 days post-infection to correspond with the greatest difference in fungal burden prior to the onset of mortality (Figure 2A-C). H&E staining revealed that WT mice displayed abundant lung leukocyte infiltration that was almost absent in the IL-1RI$^{-/-}$ strain. Notably, eosinophilic crystals that have been associated with alternatively activated macrophages in *C. neoformans* infection were clearly observed in IL-1RI$^{-/-}$

lung sections but were absent in the WT. Mucicarmine staining of the cryptococcal cell wall showed that most fungi were located within WT phagocytes with only a few visible extracellular organisms in the parenchyma or airways. In contrast, IL-1RI$^{-/-}$ sections showed lung parenchyma that was filled with heavily encapsulated extracellular cryptococci. PAS staining revealed exuberant mucus secretion by airway epithelial cells in IL-1RI$^{-/-}$ mice; however, this was not observed in the airways of WT mice. Taken together, this histopathological analysis confirmed the results of the lung fungal burden studies and demonstrated reduced inflammation with signs of Th2 polarization in IL-1RI$^{-/-}$ mice compared to the WT strain.

Inflammatory cytokine and chemokine expression is decreased in the lungs of IL-1RI$^{-/-}$ mice following *C. neoformans* infection.

To determine the effect of IL-1RI signaling on the production of soluble inflammatory mediators, WT and IL-1RI$^{-/-}$ mice were infected with *C. neoformans* 52D and the concentration of pro-inflammatory cytokines (IL-1α, IL-1β, TNFα, IL-6), chemokines (MCP-1, KC), Th1-associated cytokines (IFNγ, IL-12), and representative Th2-associated (IL-13) and Th17-associated (IL-17) cytokines was measured in whole lung homogenates at serial time points (Figure 3). No significant differences in the expression of these mediators was observed between two strains prior to infection (data not shown). In WT mice, expression of both IL-1α and IL-1β was induced in the lungs at day 7 post-infection and continued to rise until day 14 post-infection. Compared to WT, IL-1RI$^{-/-}$ mice had stable and significantly lower induction of these two cytokines at day 7 and day 14 post-infection. The expression of TNFα, IL-6, MCP-1, and KC was significantly higher in WT compared to IL-1RI$^{-/-}$ mice at day 7 and day 14 post-infection. Significantly greater induction of IFNγ, IL-12, and IL-17 was also observed in the lungs of WT mice compared to IL-1RI$^{-/-}$ at day 7 and day 14 post-infection. IL-13 production did not differ between strains at day 7 and day 14 post-infection, although a modest increase was observed in IL-1R$^{-/-}$ mice compared to WT at day 21 post-infection. In summary, WT mice exhibited significantly greater induction of pro-inflammatory, Th1, and Th17 cytokines, as well as chemokines, compared to IL-1RI$^{-/-}$ mice; these findings demonstrate a broad effect of IL-1RI signaling on the lung inflammatory response following *C. neoformans* infection.

IL-1RI$^{-/-}$ mice exhibit reduced neutrophil and increased eosinophil recruitment to the lungs following *C. neoformans* infection

To characterize the effect of IL-1RI signaling on the cellular immune response following *C. neoformans* infection, flow cytometry analysis of whole-lung digests was performed on WT and IL-1RI$^{-/-}$ mice at serial time points post-infection. Prior to infection, no significant difference was observed in the total number of lung leukocytes between the two strains. The total number of CD45^{+} cells peaked at day 14 in both strains; however, it was significantly higher in WT compared to IL-1RI$^{-/-}$ mice at 14 and 21 days post-infection (Figure 4). At 7 days post-infection neutrophils (CD11c^{-}, CD11b^{+}, Ly6G^{high}) were the most frequent leukocyte subset in both strains; however, their frequency and total number was significantly higher in the WT compared to the IL-1RI$^{-/-}$ strain and this pattern was maintained until 21 days post-infection. Conversely, the frequency and number of lung eosinophils (CD11c^{-}, CD11b^{+}, Siglec F^{+}, SSC^{high}) was significantly higher in IL-1RI$^{-/-}$ mice compared to the WT strain at 7 days post-infection and this pattern was even more pronounced at 14 and 21 days post-infection. This data suggests that IL-1R signaling plays an important role in recruitment of neutrophils during the innate and adaptive phases of the host response to *C. neoformans* 52D infection. In the absence of IL-1R, mice develop significant and sustained lung eosinophilia that is associated with a higher fungal burden.

To evaluate the functional significance of early and sustained neutrophil recruitment to the lungs of BALB/c mice following infection with *C. neoformans* 52D, the effect of antibody-mediated depletion on tissue fungal burden and lung cell infiltration was characterized. Briefly, WT mice received 200 µg of anti-Ly6G antibody (clone 1A8) in a volume of 100 µl via intraperitoneal injection 24 hours prior to infection and every other day thereafter. To capture the overall effect of neutrophil depletion during the innate and adaptive phases of immunity, lung fungal burden was determined at 12 days post-infection. Interestingly, this analysis showed that neutrophil-depleted mice had a significantly lower cryptococcal burden in the lungs compared to control mice (Figure 4G-H).

IL-1RI$^{-/-}$ mice recruit fewer inflammatory DC and M1 polarized macrophages to the lung following *C. neoformans* infection.

Inflammatory monocyte-derived macrophages (ExMs) and dendritic cells (DCs) are important for protection against *C. neoformans* infection (142, 296). We investigated the effect of IL-1RI signaling on recruitment of ExMs and DCs by harvesting lungs at different times post-infection and analyzing cells by flow cytometry. As both ExMs and DCs express CD11b, CD11c and MHCII, we used auto-fluorescence to distinguish macrophages from DCs (296, 303) (Figure 4A). This analysis showed comparable recruitment of both cell types between the two strains at day 7 post-infection; however, WT mice had a significantly higher number of inflammatory DCs (day 14 and 21) and ExMs (day 21) compared to IL-1RI$^{-/-}$ mice (Figure 5B, C). The macrophage polarization pattern is also important for protection against cryptococcal infection (111, 116). Classically activated macrophages (M1) that express high levels of pro-inflammatory cytokines, produce high levels of reactive nitrogen and oxygen intermediates, and promote strong IL-12-mediated Th1 responses are efficient killers of *C. neoformans*. In contrast, alternatively activated macrophages (M2) that express chitinase-like 3 (Ym1), found in inflammatory zone (FIZZ1), mannose receptor (CD206) and arginase-1 (Arg1) have reduced pro-inflammatory cytokine secretion and are less microbicidal (8, 17, 115, 358, 359). As the number of recruited macrophages peaked at day 14 post-infection in both strains, we characterized polarization at this time point using iNOS and CD206 as representative markers for M1 and M2 macrophages, respectively (Figure 5D). At 14 days post-infection, the frequency of M1 macrophages was significantly greater in WT mice compared to IL-1R$^{-/-}$ mice while the frequency of M2 macrophages was greater in IL-1R$^{-/-}$ compared to WT mice (Figure 5E). Notably, IL-1RI$^{-/-}$ macrophages showed greater upregulation of CD206 compared to WT macrophages at 14 days post-infection (Figure 5F). There was no significant difference in the total number of AMs between two strains, although there was a trend towards a higher number of AMs in WT mice compared to IL-1R$^{-/-}$ mice at day 7 post-infection (data not shown). Taken together, these results indicate that IL-1RI signaling has an important role in recruitment of inflammatory DCs and macrophages and increases the ratio of M1/M2-polarized macrophages following *C. neoformans* infection.

T cells are the predominant sources of IL-17 and IFNγ in WT lungs infected with *C. neoformans* 52D

To characterize the mechanism of differential IL-17 and IFNγ expression between WT and IL-1RI$^{-/-}$ lungs, we identified the main sources of these cytokines following *C. neoformans* 52D infection. Using intracellular cytokine staining, we first measured the total number of IL-17 producing cells in the lungs of WT and IL-1RI$^{-/-}$ mice at early (day 7) and late (day 14 and day 21) phases of infection. Compared to IL-1RI$^{-/-}$ mice, WT mice showed significantly more IL-17 producing cells at 7, 14, and 21 days post-infection and a higher number of IFNγ-producing cells at day 7 post-infection (Figure 6A-C). Several immune cell types including CD4^{+} (Th17), CD8^{+} T (Tc17) cells, NK cells, and iNKT cells have been shown to produce IL-17 during fungal infection (360, 361). At day 7 post-infection, intracellular cytokine staining of WT lymphocytes showed that CD4^{+} and γδT cells were the most common IL-17^{+} subsets (Figure 6D). A similar pattern was observed at day 21 post-infection with CD4^{+} T cells and γδT cells accounting for 60% and 20%, respectively of IL-17^{+} cells. At day 7 and day 21 post-infection, CD4^{+} T and NK cells were the predominant IFNγ-producing subsets (Figure 6E).

Effect of IL-1RI signaling on the lung lymphocyte infiltration following *C. neoformans* infection

As lymphocytes are necessary for effective clearance of *C. neoformans,* we compared the recruitment of CD4^{+} or CD8^{+} T cells, γδT cells, and B cells to the lungs of WT and IL-1RI$^{-/-}$ mice at different time points following infection. Flow cytometry analysis showed that WT mice recruit a significantly higher number of CD4^{+} cells compared to the IL-1RI$^{-/-}$ strain at 14 and 21 days post-infection (Figure 7A). Recruitment of CD8^{+} T cells was comparable between the two strains at all time points, although WT mice showed a trend towards a higher number of CD8^{+} T cells at day 21 compared to IL-1RI$^{-/-}$ mice (Figure 7B). WT mice demonstrated increased recruitment of γδT cells at day 14 and day 21 post-infection compared to uninfected mice; in contrast, there was no significant increase of this cell type in IL-1RI$^{-/-}$ mice during infection (Figure 7D). No differences in the number of B cells recruited to the lungs during infection were observed between the two strains (Figure 7C). Taken together, this analysis demonstrates that IL-1RI signaling selectively

regulates T lymphocyte recruitment to the lungs during the adaptive phase of immunity against *C. neoformans* 52D infection**.**

Pulmonary CD4$^+$ T cells from IL-1RI$^{-/-}$ mice display diminished Th17 and increased Th2 cytokine production following *C. neoformans* infection

It has been clearly shown that a Th1/Th17 response is protective and a Th2 response is detrimental, respectively, against *C. neoformans* infection (62). To analyze the effect of IL-1R signaling on T cell differentiation during infection, we harvested lungs at serial time points, restimulated the cells with PMA/Ionomycin, and stained for intracellular IFNγ, IL-13, and IL-17 as representative cytokines for Th1, Th2, and Th17 polarization states, respectively (Figure 8). The results demonstrate a significantly higher frequency and total number of CD4$^+$ IFNγ$^+$ cells in the lungs of WT compared to IL-1RI$^{-/-}$ mice at 7 days post-infection with a non-significant trend towards more CD4$^+$ IFNγ$^+$ cells at day 14 and 21. Compared to the IL-1RI$^{-/-}$ strain, WT mice showed a trend towards more CD4$^+$ IL-17$^+$ cells at day 7 with a significant increase of this cell type at day 14 and 21. In contrast, IL-1RI$^{-/-}$ lungs contained a significantly higher number of CD4$^+$ IL13$^+$ cells compared to WT lungs at 14 and 21 days post-infection. In summary, these findings demonstrate that following *C. neoformans* infection, IL-1RI signaling significantly increased Th1 differentiation during the early phase of infection and strongly promoted Th17 differentiation during the late phase of infection.

4.5. Discussion

Induction of IL-1α/β during mouse cryptococcal infection has been reported but a clear role for IL-1R-dependent signaling in the host immune response has not been demonstrated (264, 347, 352-354). Here we provide evidence that IL-1RI deficiency has deleterious effects on the outcome of pulmonary cryptococcal infection. The most significant findings of this study are: 1) IL-1RI$^{-/-}$ mice cannot clear moderately virulent *C. neoformans* 52D and develop progressive infection of the lungs and brain resulting in death starting at day 40 post-infection, 2) Susceptibility of IL-1RI$^{-/-}$ mice is associated with reduced levels of proinflammatory, Th1, and Th17 cytokines, 3) IL-1RI signaling in response to *C. neoformans* infection regulates the recruitment of inflammatory DCs to the lung, contributes to M1 polarization of macrophages, and promotes Th1/Th17 differentiation of CD4^{+} T cells, 4) Lung neutrophil recruitment associated with IL-1R signaling is dispensable for protection against cryptococcal infection. Taken together, these data clearly demonstrate that IL-1R-dependent signaling plays a complex and essential role in the control of progressive cryptococcal infection.

Previously, intranasal infection of C57BL/6 and IL-1RI$^{-/-}$ mice with 2 x 10^4 CFU of the virulent *C. neoformans* H99 strain was shown to cause >90% mortality in both groups (264). In the same report, mice lacking MyD88, an intracellular adaptor for IL-1RI, IL-18R, and several Toll-like receptors, had a trend towards reduced survival but no significant difference in fungal burden compared to WT mice after *C. neoformans* challenge (264). Notably, two earlier studies showed that MyD88$^{-/-}$ mice have a significantly shorter survival time and a higher lung fungal burden compared to WT, TLR2$^{-/-}$ and TLR4$^{-/-}$ mice following *C. neoformans* infection (254, 255). These differences may be attributable, at least in part, to variation in the experimental methods that were used including the dose, route, and strain of *C. neoformans* (62, 64, 362, 363). Furthermore, inbred mouse strains also display marked differences in resistance or susceptibility to a standardized cryptococcal infection, highlighting the importance of the host genetic background in disease pathogenesis (253, 291, 321). Our data is consistent with other studies showing that BALB/c mice have a naturally resistant phenotype following respiratory infection with the moderately virulent *C. neoformans* 52D strain. Specifically, BALB/c mice progressively clear pulmonary *C. neoformans* 52D infection in association with numerous hallmarks of a protective Th1 response including tight mononuclear cell infiltrates and classically activated macrophages and do not

develop central nervous system dissemination (256, 291, 298, 316). Our observation that both IL-1α and IL-1β were strongly induced in the lungs of BALB/c mice following intratracheal infection with *C. neoformans* 52D is also consistent with earlier reports that associated the induction of IL-1β in lung and brain with resistance to cryptococcal infection (354, 364, 365).

IL-1 is a central mediator of inflammation and links innate and adaptive immune response mechanisms (366). Binding of IL-1α or IL-1β to IL-1RI is followed by the recruitment of the IL-1 receptor accessory protein (IL-1RAcP) and activation of signal transduction pathways that induce the expression of IL-1 responsive genes including IL-6, monocyte chemoattractant protein 1 (MCP-1), and TNFα (367-370). Induction of pro-inflammatory cytokines followed by generation of a Th1 adaptive immune response is critical for control of cryptococcosis (116, 176, 341). Compared to the BALB/c strain, IL-1RI$^{-/-}$ mice had significantly reduced expression of IL-6, KC, TNFα, and MCP-1 that was associated with increased lung fungal burden at day 7 after infection. TNFα is one of the main target genes of the IL-1 signaling cascade (369, 370) and both mediators share downstream pathways that induce pro-inflammatory gene expression (371, 372). TNFα signaling in the afferent phase of cryptococcal infection is associated with optimal DC activation and induction of Th1/Th17 polarization and protective immunity (176, 177, 373-375). MCP1/CCR2 signaling is also responsible for the recruitment of inflammatory DCs and macrophages following cryptococcal infection (142, 257, 296). Thus, the reduced expression of proinflammatory cytokines and chemokines is one mechanism that could explain the susceptibility of IL-1RI$^{-/-}$ mice to progressive cryptococcosis.

Following *C. neoformans* infection, DCs phagocytose and kill cryptococci by oxidative and non-oxidative mechanisms, play an important role in antigen presentation, and drive protective immune responses by secreting cytokines and chemokines (128, 129, 376, 377). Compared to other innate cell types, lung DCs express a high level of IL-1RI (78)(78)(77)(76)(77) and signaling via this receptor has been shown to promote the maturation and survival of pulmonary DCs and their CCR7-dependent migration to lymph nodes after Influenza A infection (378). At 14 and 21 days post-infection with *C. neoformans*, the total number of CD11b^{+} DCs in the lung was significantly lower in IL-1RI$^{-/-}$ compared to WT mice, suggesting that recruitment and activation of DCs in the LALNs may be regulated by IL-1R signaling in this model. The significant reduction of IL-12 expression in the lungs of IL-1RI$^{-/-}$ mice compared to WT at 14 days post-infection is also

consistent with this possibility. In addition to DCs, inflammatory macrophages that strongly express microbicidal enzymes such as iNOS play a significant role in fungal clearance (142, 256, 296, 311). Following *C. neoformans* 52D infection we observed that lung macrophages of IL-1R$^{-/-}$ mice had reduced expression of the classical activation marker iNOS and increased expression of the alternative activation marker CD206 compared to WT, a pattern that is associated with reduced fungal killing capacity. Our findings are similar to a recent study in BALB/c mice infected with *C. neoformans* 52D that correlated an elevated ratio of Arg1/iNOS expression with an increase in fungal burden and showed a reversal of this ratio during the subsequent period of fungal clearance (111).

Significantly greater neutrophil recruitment was observed in WT compared to IL-1R$^{-/-}$ lungs beginning at an early phase of infection and continuing until day 14. Both IL-1α and IL-1β can promote neutrophil migration (379-382), and diminished neutrophil recruitment to the site of infection due to IL-1R deficiency has been associated with increased susceptibility to several bacterial and fungal infections including *Legionella pneumophila,* Group B *Streptococcus, Citrobacter rodentium,* and *Candida albicans* (361, 383-387). Inbred mouse strains including SJL/J, CBA/J, and BALB/c are naturally resistant to pulmonary cryptococcal infection and exhibit substantial neutrophil recruitment the lungs; however, the importance of these cells in host protection is not clear (253, 321, 354). For example, an early study of BALB/c mice given a single injection of anti-Gr-1 (anti-Ly6C/6G) antibody showed less inflammatory damage and significantly longer survival compared to controls after *C. neoformans* 52D infection (148). A subsequent study of BALB/c mice that had undergone prior immunization with *C. neoformans* strain H99γ showed that neutrophil depletion with a specific anti-Ly6G antibody did not affect pulmonary fungal burden (147). Finally, a recent report showed that profound neutrophilia in type 2–deficient STAT6$^{-/-}$ mice on a C57BL/6 background was associated with immunopathology and exacerbation of cryptococcal disease (388). To specifically analyze the contribution of neutrophils to resistance against *C. neoformans* 52D, we used anti-Ly6G to deplete these cells in WT BALB/c mice throughout the course of infection (389, 390). In the absence of neutrophil recruitment we observed a significantly lower lung fungal burden at 12 days post-challenge compared to controls. This finding suggests that, despite their abundance in the lung, neutrophils may have a detrimental effect on host defense against moderately virulent *C. neoformans* 52D (148). Several mechanisms may explain this observation, including competition for cryptococcal antigen between neutrophils

and antigen-presenting cells, neutrophil secretion of the immunosuppressive cytokine TGFβ1, or production of IL-1 receptor antagonist, a molecule that inhibits IL-1R signaling (387, 391-395). Further research is necessary to precisely establish the physiological mechanisms that control neutrophil recruitment during cryptococcal infection and to determine whether these cells make a positive contribution to host resistance.

In addition to reduced proinflammatory cytokines, IL-1R$^{-/-}$ mice showed diminished levels of lung IFNγ compared to WT mice at the early (day 7) and late (day 14 and 21) phases of infection. Intracellular cytokine staining identified CD4^{+} lymphocytes as the most prominent IFNγ-producing cell type. As very few studies have identified IL-1R expression on Th1 cells (396), induction of IFNγ expression by CD4^{+} T cells appears to be an indirect effect of IL-1RI signaling on DCs and possibly other cell types (378). IFNγ plays a central role in host defence against cryptococci by enhancing the fungal internalization and killing by phagocytes (176, 177). An important role for early IFNγ secretion and the development of a Th1 response against *C. neoformans* 52D infection was previously shown in resistant C.B-17 mice (a BALB/c strain congenic for C57BL/6 immunoglobulin heavy chain gene segment), whereas the absence of this response in the C57BL/6 strain correlated with susceptibility (341).

IL-1 is known to regulate the expression of the transcription factors IRF4 and RORγt, both of which play a major role in the induction of CD4^{+}IL-17^{+} (Th17) cells in mice and humans (397-399). IL-1 signaling has been shown to be essential for development of Th17 immunity to infection with *Coccidioides sp* (400), and mice with deletions of IL-17 or IL-17R are susceptible to candidiasis, pulmonary aspergillosis, and histoplasmosis (361). The role of IL-17 during cryptococcal infection has been analyzed using mice with a C57BL/6 genetic background. In one study, IL-17RA deficiency did not impair pulmonary clearance of *C. neoformans* 52D at 1 or 6 weeks post-infection, nor did it alter survival compared to WT mice (180). Another study using IL-17A-deficient mice showed that this cytokine does contribute to fungal clearance from the lung but was not essential for 8-week survival (269). In contrast, administration of IL-23, which is essential for the differentiation of Th17 lymphocytes, led to prolonged survival and reduced fungal burden in C57BL/6 mice (346). A Th17-polarized immune response appears to facilitate the resolution of *C. neoformans* 52D infection through several mechanisms including lung recruitment of activated DCs and inflammatory macrophages, induction of IFNγ-producing CD4^{+} and CD8^{+} T

cells, and enhanced fungal containment within macrophages (269, 294, 345, 346). Compared to BALB/c, IL-1R$^{-/-}$ mice display several phenotypes that may be attributable to a diminished Th17 response including reduced recruitment of DCs and inflammatory macrophages and increased recruitment of eosinophils and CD4^{+}IL-13^{+} cells to the lungs. Based on the marked difference between WT and IL-1R$^{-/-}$ mice we speculate that IL-17 plays a non-redundant role in survival following *C. neoformans* 52D infection; however, studies of BALB/c mice that are deficient for IL-17 or IL-17RA would be required to formally test this hypothesis.

In mouse models, IL-1 signaling is protective against infection with a wide spectrum of intracellular pathogens including *Leishmania amazonensis*, *Mycobacterium avium*, *Toxoplasma gondii*, and *Listeria monocytogenes* (401-405). IL-1RI deficient mice are also highly susceptible to pulmonary challenge with *Aspergillus fumigatus*; in this model, IL-1α has been shown to be crucial for optimal leukocyte recruitment and IL-1β has been shown to be essential for optimal activation of macrophage anti-fungal activity (406). It has been suggested that polymorphisms in the IL-1 gene cluster might be important in susceptibility or resistance to invasive pulmonary aspergillosis in humans (407, 408). Both IL-1α and IL-1β have also been shown to play an important role in disseminated candidiasis (409-412) and IL-1 signaling has shown to contribute to host resistance against pulmonary histoplasmosis and *Coccidioides sp.* infection (400, 413). The current study expands the role of IL-1 in host defense by demonstrating that IL-1R$^{-/-}$ mice are highly susceptible to progressive *C. neoformans* infection of the lungs and brain. IL-1R deficiency in BALB/c mice results in impaired Th1/Th17 responses and the development of a Th2-biased adaptive immune response. As IL-1α and IL-1β are equally potent activators of IL-1RI signaling yet have different tissue distribution and activation kinetics, future studies that characterize mice that are deficient in either IL-1α or IL-1β could define the specific contribution of each cytokine in the development of protective immunity against *C. neoformans* infection.

Figures

Figure 4. 1. IL-1RI signaling is required for survival and control of pulmonary fungal burden following infection with *C. neoformans*. WT and IL-1RI$^{-/-}$ mice were infected intratracheally with 10^4 CFU of *C. neoformans* strain 52D. **(A)** Mice were observed for up to 110 days for survival analysis (n=12 mice/strain using a log-rank test). **(B-D)** Fungal burden in the lung, brain, and spleen at serial time intervals was determined by plating tissue homogenates on SDA. CFU data are shown as mean ± SEM and representative of 2 independent experiments. *, $P \leq 0.05$; **, $P \leq 0.01$; ***, $P \leq 0.001$, using an unpaired Student's t-test (B) and Mann–Whitney U test (C, D).

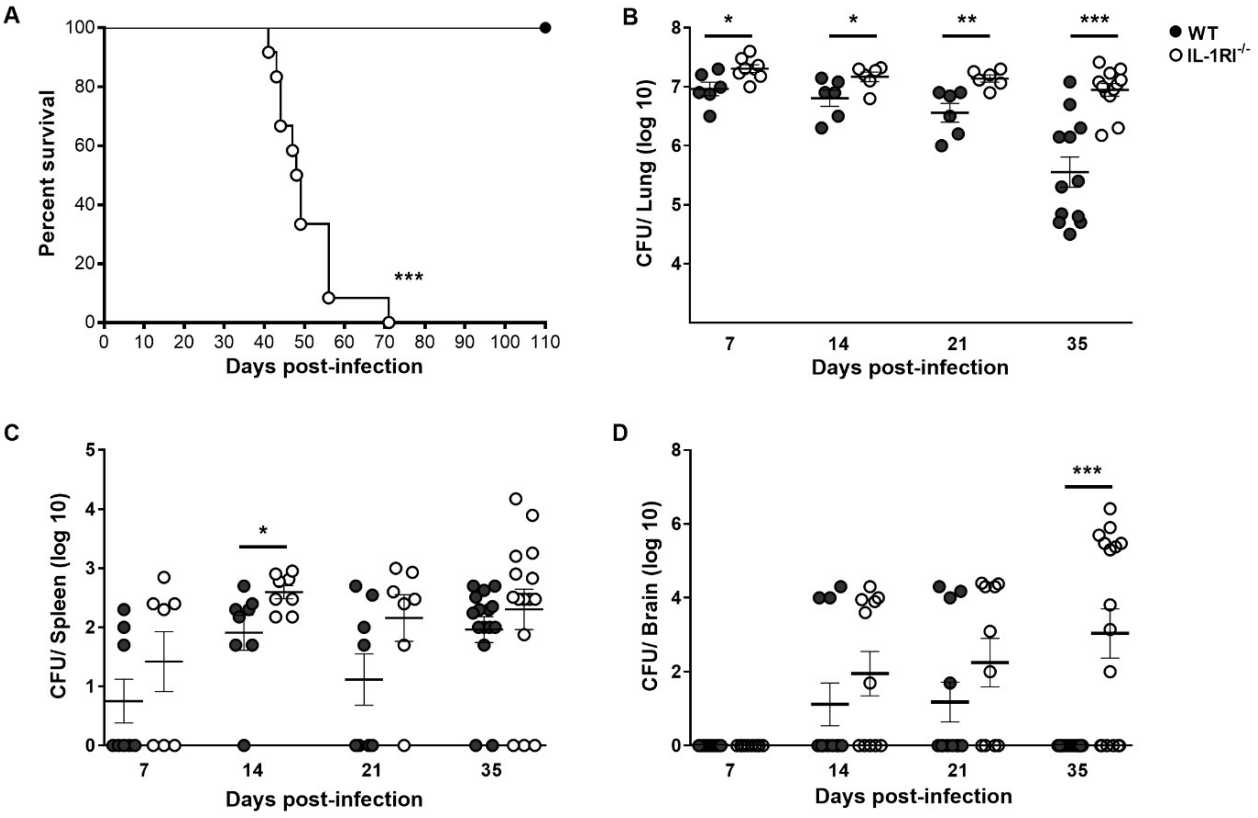

Figure 4. 2. Decreased inflammation in the lungs of IL-1RI$^{-/-}$ mice following infection with *C. neoformans*. WT and IL-1RI$^{-/-}$ mice were infected intratracheally with 10^4 CFU of *C. neoformans* 52D. Lungs were harvested at day 35 post-infection, perfused with PBS, embedded in paraffin and stained with H&E, mucicarmine, and PAS. Representative H&E images **(A)** show a significant reduction of inflammation in IL-1RI$^{-/-}$ compared to WT mice; black arrow indicates the eosinophilic crystals in IL-1R$^{-/-}$ lung. Mucicarmine staining **(B)** shows numerous heavily encapsulated extracellular *C. neoformans* in the airspaces of IL-1RI$^{-/-}$ mice compared to WT mice. Representative images of lungs stained with PAS **(C)** show goblet cell hyperplasia and exuberant mucus in the airways of infected IL-1RI$^{-/-}$ mice compared to WT mice. Each image is representative of 2 independent experiments.

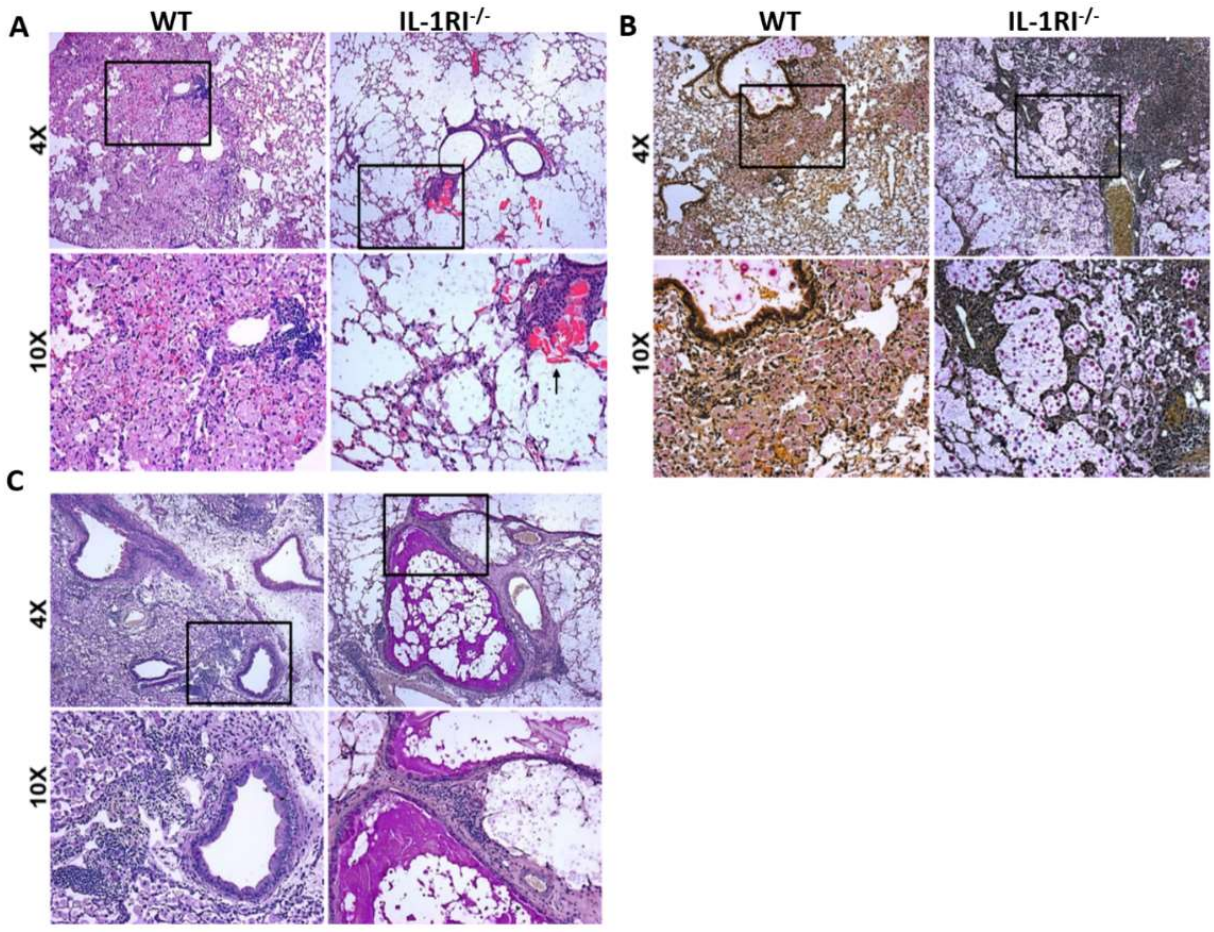

Figure 4. 3. IL-1RI$^{-/-}$ lungs have decreased inflammatory cytokine and chemokine expression following *C. neoformans* infection. Whole lung protein was collected at 7, 14 and 21 days post-infection with 10^4 CFU of *C. neoformans* 52D. ELISA was performed to determine the level of pro-inflammatory cytokines, chemokines, and Th1/Th2/Th17-type cytokines. Data are shown as mean ± SEM and representative of 2 independent experiments (n= 4 mice/strain/time point). *, P ≤ 0.05; **, P ≤ 0.01; ***, P ≤ 0.001.

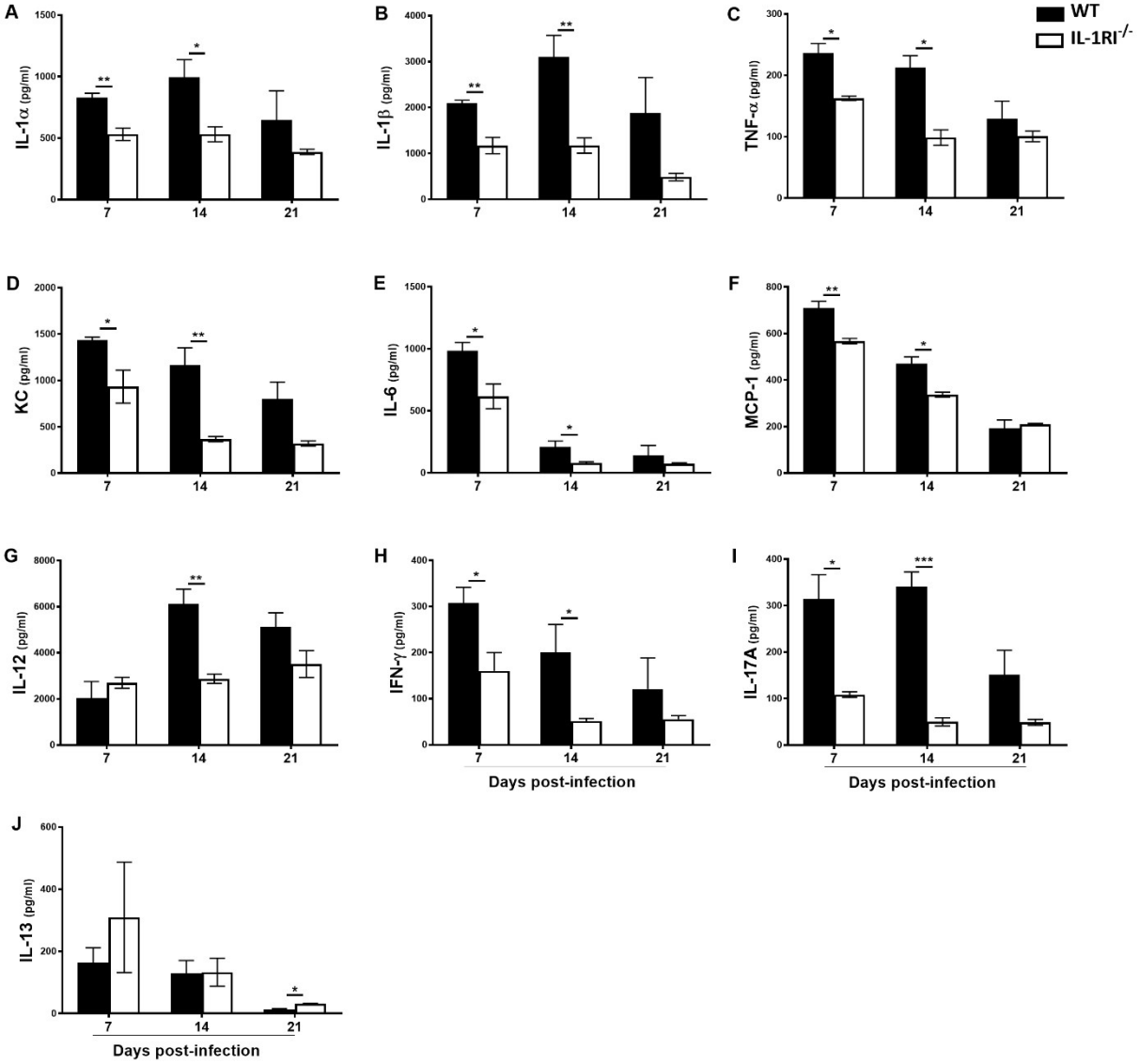

Figure 4. 4. IL-1RI$^{-/-}$ mice have decreased neutrophil and increased eosinophil recruitment to the lungs following *C. neoformans* infection. Lung cell suspensions from uninfected and infected WT and IL-1RI$^{-/-}$ mice were stained with fluorochrome-labeled antibodies and analyzed by flow cytometry as described in Materials and Methods. **(A)** Absolute numbers of total CD45^{+} cells in the lungs at 0, 7, 14, 21 days post-infection, **(B)** representative plots of gating for neutrophils (CD11c^{-}, CD11b^{+}, Ly6G^{high}) and eosinophils (CD11c^{-}, CD11b^{+}, Ly6G low/negative, SSC^{high}), **(C-F)** Frequency and total number of neutrophils and eosinophils at day 0, 7, 14, and 21 post-infection is shown. Data are shown as mean ± SEM and representative of 2 independent experiments (n = 4 mice/strain/time point). *, P ≤ 0.05; **, P ≤ 0.01; ***, P ≤ 0.001. **(G-H)** BALB/c mice underwent intratracheal infection with 1 × 10^{4} CFU of *C. neoformans* strain 52D. Mice were treated with control or with anti-Ly6G antibody one day prior to infection and daily thereafter for 12 days. Lungs were excised for analysis of neutrophil recruitment and CFU. **(G)** The number of neutrophils and **(H)** fungal burden is shown (n = 8 mice/group). ***, P ≤ 0.001.

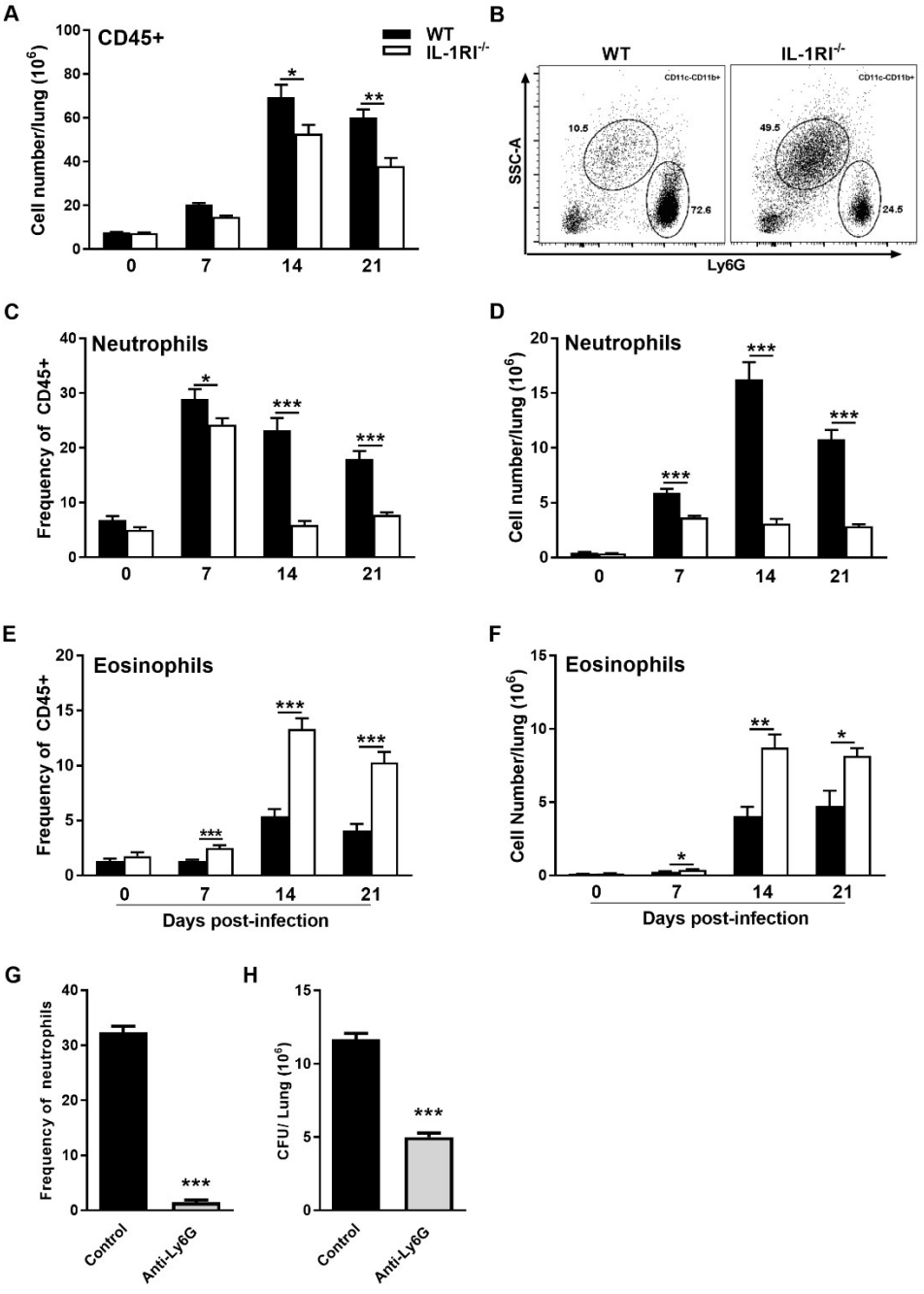

Figure 4. 5. IL-1RI$^{-/-}$ mice have fewer inflammatory DCs and M1 polarized macrophages in lung following *C. neoformans* infection. Lung cell suspensions from uninfected and infected mice were stained with fluorochrome-labeled antibodies and analyzed by flow cytometry as described in Materials and Methods. **(A)** Gating strategy to distinguish AMs (CD11c^{+}, MHCII low, AF^{+}, CD11b^{-}), ExMs (CD11c^{+}, CD11b^{+}, AF^{+}) and DCs (CD11c^{+}, MHCII^{+}, CD11b^{+}, AF^{-}) is shown. **(B, C)** Total number of lung DCs and ExMs at 0, 7, 14 and 21 days post-infection is shown. **(D)** Representative plots of M1 (CD11b^{+}, iNOS^{+}) and M2 (CD11b^{+}, CD206^{+}) polarized macrophages in WT and IL-1RI$^{-/-}$ mice at 14 days post-infection. **(E)** Frequency of M1- and M2-polarized macrophages in WT and IL-1RI$^{-/-}$ mice at 14 days post-infection. **(F)** Upregulation of CD206 in AMs and ExMs in IL-1RI$^{-/-}$ compared to WT mice at day 14 post-infection, IL-1RI$^{-/-}$, gray filled lines; WT, white filled solid lines; uninfected mice, dashed lines. **(G)** Mean Fluorescence Intensity of CD206 expression on macrophages in WT compared to IL-1RI$^{-/-}$ mice is shown. Data are shown as mean ± SEM and representative of 2 independent experiments (n=4 mice/strain/time point). *, P ≤ 0.05; **, P ≤ 0.01; ***, P ≤ 0.001.

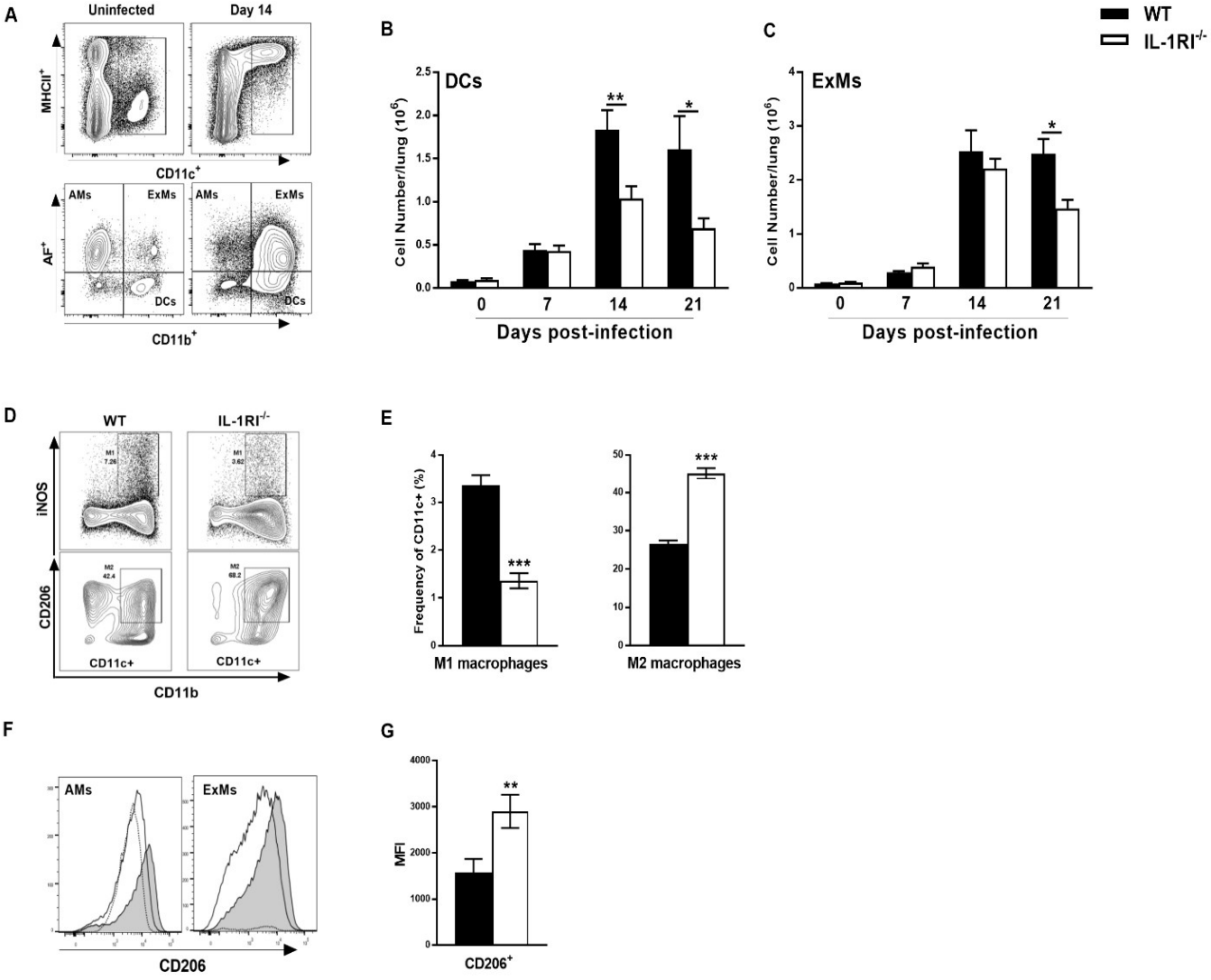

Figure 4. 6. T cells are the predominant sources of IL-17 and IFNγ in BALB/c lungs infected with *C. neoformans*. (A) Lung cell suspensions from uninfected and infected mice were harvested and restimulated with PMA-Ionomycin followed by intracellular staining for IL-17 and IFNγ. **(A, B)** Frequency of total $CD45^{+}IFN\gamma^{+}$ and $CD45^{+}IL\text{-}17^{+}$ cells at 7, 14, and 21 days post-infection. **(C)** Representative flow cytometry plots of lung $CD45^{+}$ cells from individual mice harvested at 21 days post-infection. **(D, E)** Frequency of IL-17 and IFNγ producing cell types in WT mice at 7 and 21 days post-infection is shown. Data are shown as mean ± SEM and representative of 2 independent experiments (n=4 mice/strain/time point). **, $P \leq 0.01$; ***, $P \leq 0.001$.

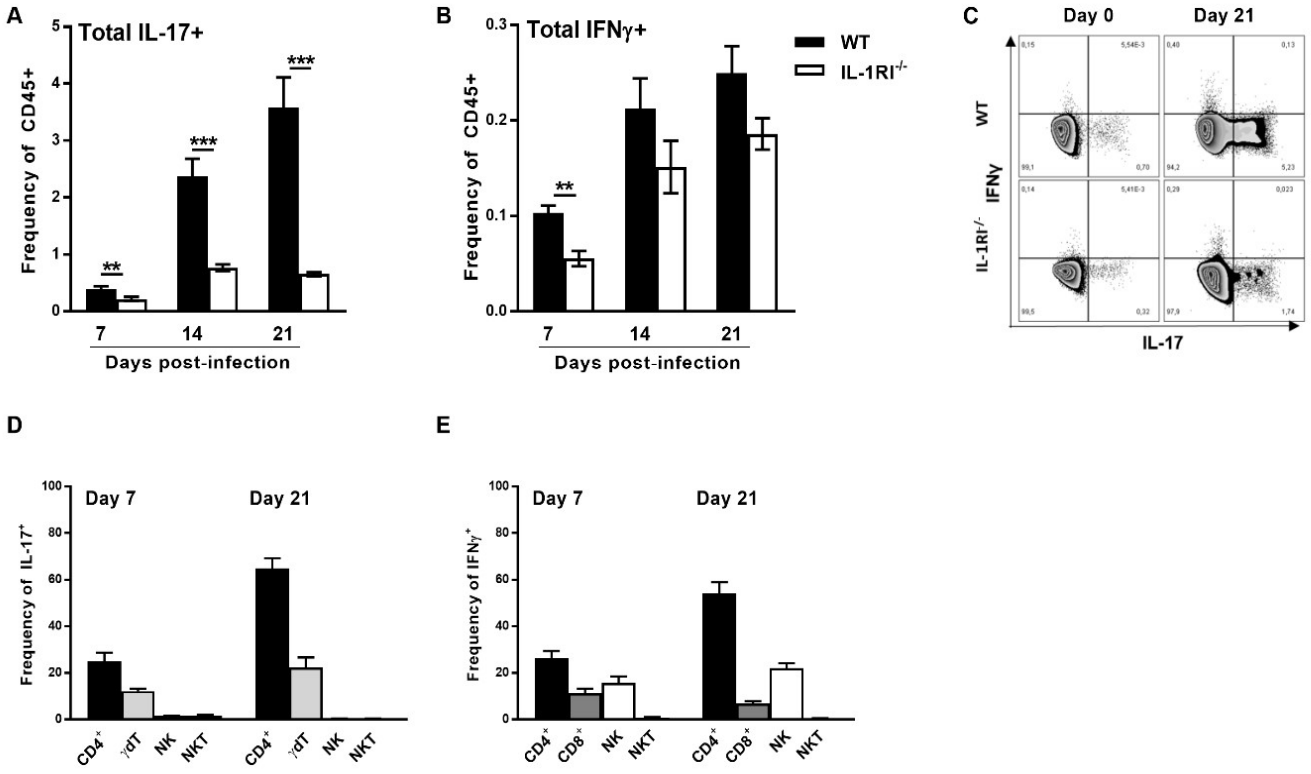

Figure 4. 7. Lungs of IL-1RI$^{-/-}$ mice display fewer CD4^{+} and γδT^{+} lymphocytes during the adaptive phase of immunity following *C. neoformans* infection. Lung cell suspensions from uninfected and infected mice were stained with fluorochrome-labeled antibodies and analyzed by flow cytometry as described in Materials and Methods. **(A-D)** Total number of CD3^{+}CD4^{+}, CD3^{+}CD8^{+}, CD3^{+} γδ^{+} and B220^{+} cells in the lungs at 0, 7, 14 and 21 days post-infection. Data are shown as mean ± SEM and representative of 2 independent experiments (n = 4 mice/strain/time point). **, P ≤ 0.01; ***, P ≤ 0.001.

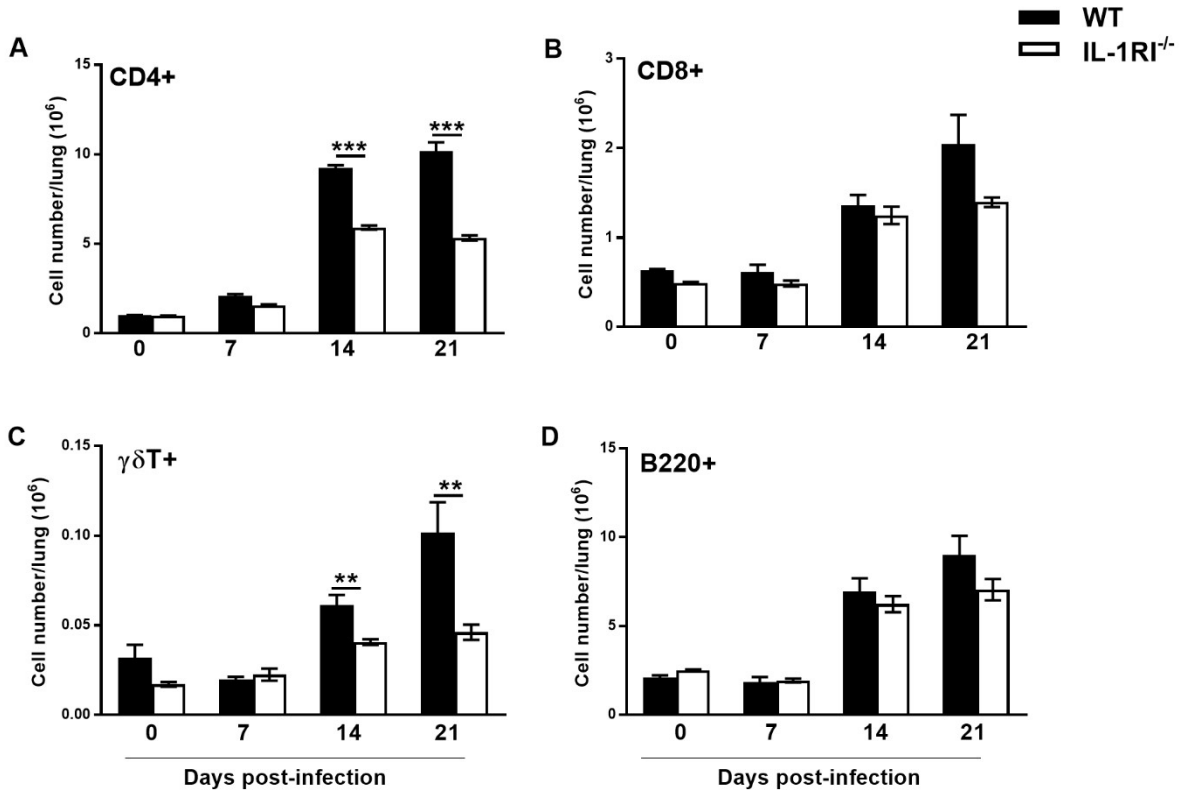

Figure 4. 8. Decreased Th1/Th17 type cytokine expression by CD4$^+$ T cells from IL-1RI$^{-/-}$ lungs infected with *C. neoformans*. (A) Representative flow cytometry plots of lung lymphocytes from individual mice harvested at 14 days post-infection and restimulated with PMA-ionomycin, followed by intracellular staining for IFNγ, IL-17, and IL-13. **(B)** Frequency and **(C-E)** total numbers of CD4$^+$IFN$^+$, CD4$^+$IL-17$^+$ and CD4$^+$IL13$^+$ cells are shown. Data are shown as mean ± SEM and representative of 2 independent experiments (n = 4 mice/strain/time point). *, P ≤ 0.05; **, P ≤ 0.01; ***, P ≤ 0.001.

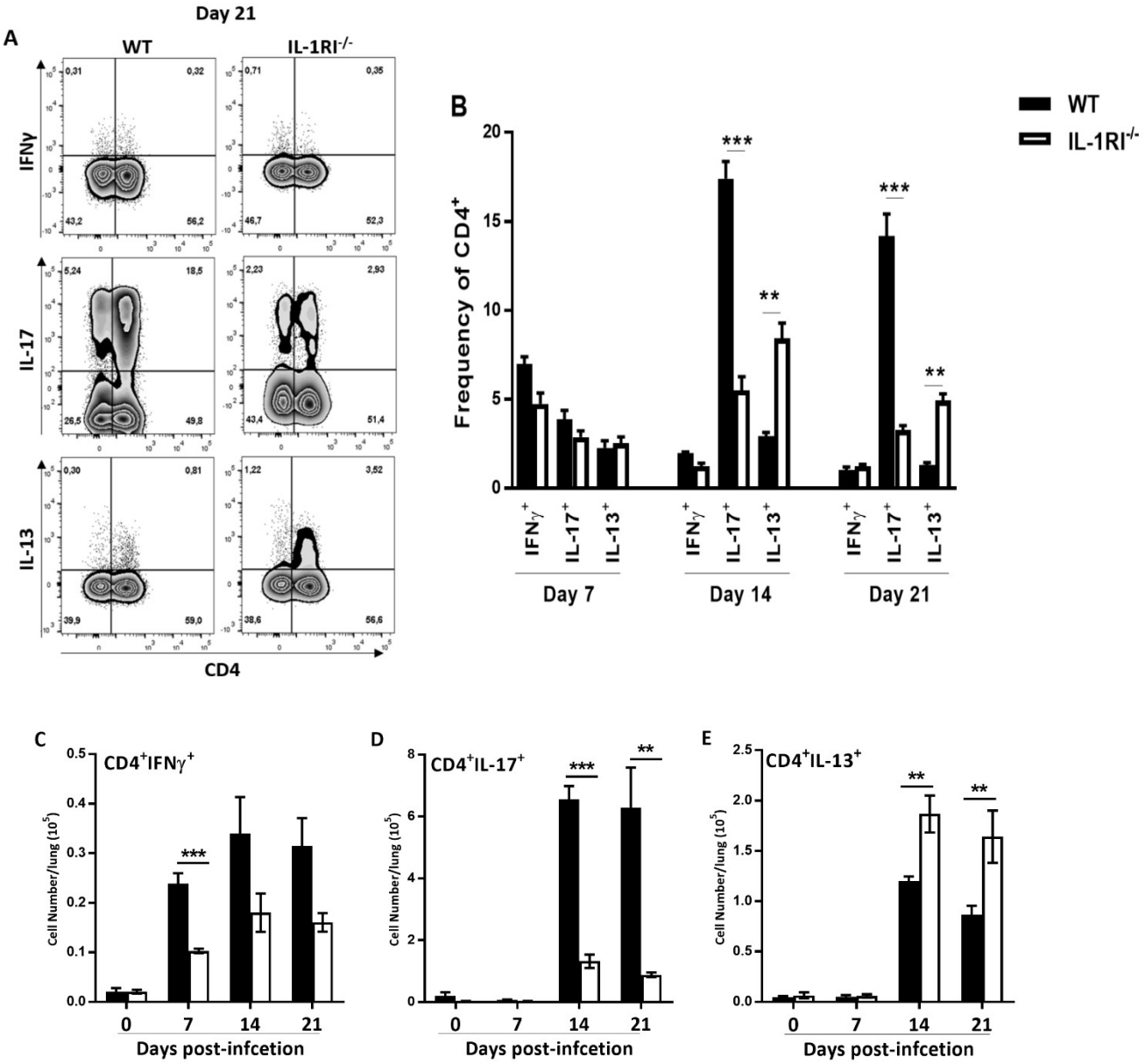

Supplementary Figure 4.1: Decreased Th17 and increased Th2 transcription factors expression by CD4+ T cells from IL-1RI-/- lungs infected with *C. neoformans*. (A) Representative flow cytometry plots of lung lymphocytes from individual mice harvested at 14 dpi followed by intracellular staining for RORγt, GATA3 and FOXP3. **(B-C)** Frequency and total numbers of CD4+RORγt+, CD4+GATA3+ and CD4+FOXP3+ cells are shown. Data are representative of two independent experiment and expressed as mean ± SEM (n = 4-6 mice/time/strain). ***, $P \leq 0.001$.

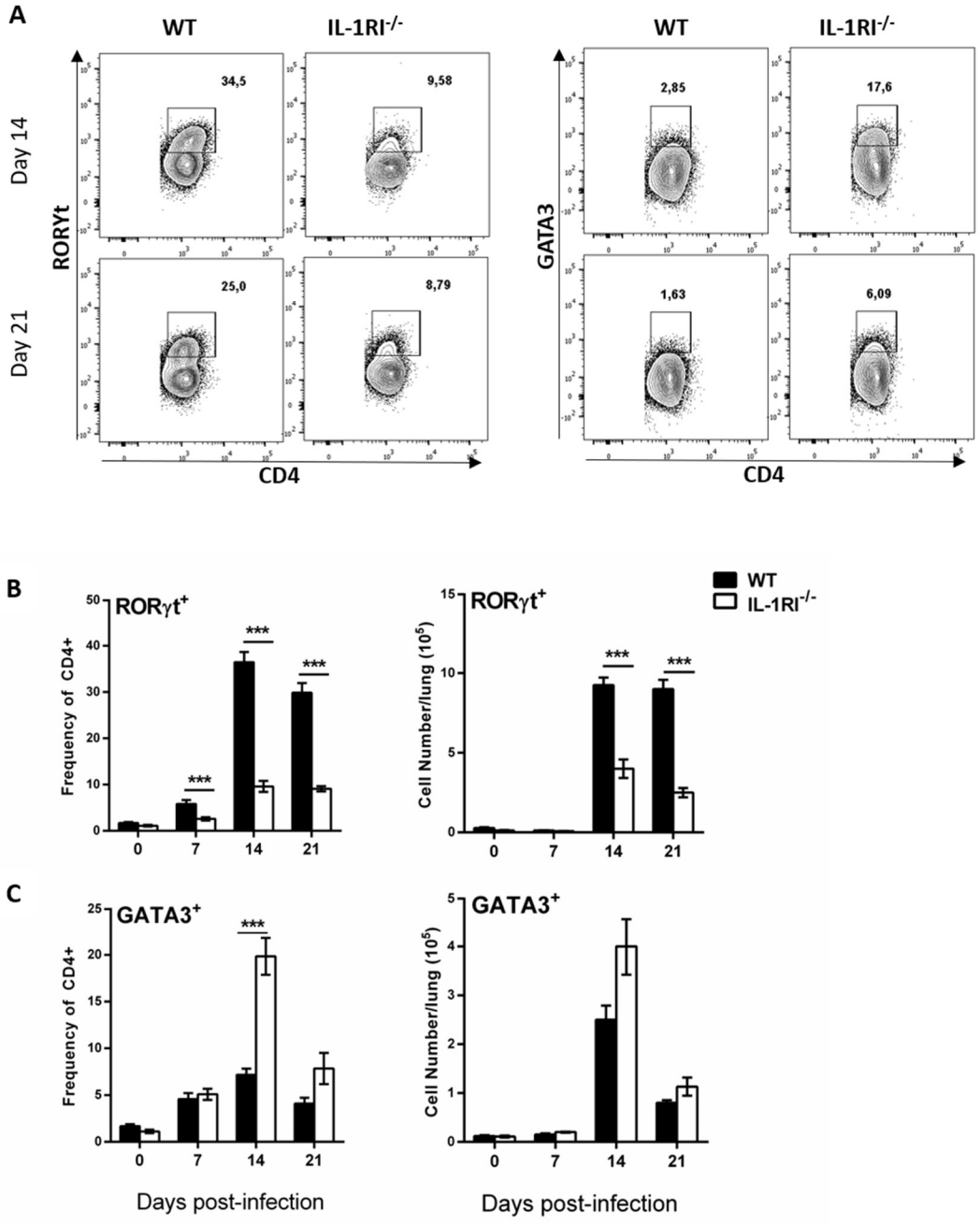

Chapter 5

Final Conclusion

I have investigated genetic and immunological factors that control the host response to *C. neoformans* infection by applying both forward and reverse genetic approaches in mice. My results are based on a well-established experimental model of infection based on direct intratracheal injection of the 52D strain (ATCC 24067) which accurately models the pathogenesis of human disease (167, 414).

5.1. Summary

In chapter 2 of my thesis, I validated the involvement of the *Cnes2* locus on mouse chromosome 17 with host susceptibility to *C. neoformans* infection. The *Cnes2* interval was previously identified by QTL mapping between C57BL/6 and CBA parental strains using lung fungal burden as a phenotypic trait. Microbiological analysis revealed a significant effect of *Cnes2* on lung fungal clearance. Furthermore, the role of *Cnes2* on host susceptibility was confirmed by additional phenotypic assays including histology and detailed analysis of the host response. The main conclusion taken from this study was that the strong effect of *Cnes2* on host susceptibility was mediated by development of a sterilizing immune response characterized by increased expression of proinflammatory and Th1 cytokine/chemokines and increased recruitment of myeloid and lymphoid cells. Therefore, this study not only confirmed the biological effect of *Cnes2* on host susceptibility, but also revealed that *Cnes2* is a pleiotropic regulatory locus.

Since *Cnes2* spans a 31.1Mb interval and contains numerous genes, the resistant phenotype observed in B6.CBA-*Cnes2* mice could be regulated by more than one gene. As the next step, which is presented in chapter 3 of my thesis, I continued this study by generating and phenotyping a series of sub-congenic lines to narrow the critical interval and uncover regions or genes associated with susceptibility to *C. neoformans* infection. As in chapter 2, the effect of each interval on tissue fungal burden and lung immune response was investigated following infection. This work yielded two major findings: First, the size of *Cnes2* interval was reduced by excluding the *Cnes2.1* and *Cnes2.3* sub-intervals based on their neutral effect on fungal burden and host immune response; and second, two independent sub-intervals, *Cnes2.2* and *Cnes2.4*, were associated with enhanced lung fungal clearance and host immune responsiveness following infection.

In chapter 4 of my thesis, I investigated the role of interleukin 1 signaling on host susceptibility to *C. neoformans* infection by a reverse genetic approach. Our previous data and other studies showed that both IL-1α and IL-1β are induced in mouse strains that are resistant to cryptococcal infection; however, their role in host protection had not been definitively studied. My current data reveals the critical role of IL-1 signaling on host resistance against *C. neoformans* infection through induction of proinflammatory cytokines and the development of a Th1 and Th17 immune response.

5.2. Significance of Findings

5.2.1. Significance of the forward genetic studies

1) Recruitment of monocyte derived DCs and ExMs to the lung following cryptococcal infection was strongly associated with the resistant phenotype of *Cnes2* and its effective sub-congenic intervals (*Cnes2.2* and *Cnes2.4*). This result is consistent with other studies that have demonstrated the critical role of DCs and ExMs in protection against *C. neoformans* infection. I believe that gene(s) in the *Cnes2* interval have a potentially important direct or indirect effect on myeloid cell recruitment/activation following infection, possibly through induction of pro-inflammatory cytokines/chemokines. Consistent with this hypothesis, I have shown significant induction of MCP-1, the critical mediator for recruitment of monocyte-derived DCs and macrophages, in infected lungs of *Cnes2* mice.
2) I observed a 13 and 30 percent mortality rate in *Cnes2* and *Cnes2.4* strains infected with *C. neoformans* 52D, respectively, although both strains showed a significantly lower lung fungal burden with no significant difference in brain dissemination compared to control mice. In cryptococcal infection, excessive inflammation can result in severe lung pathology and ultimately death; therefore, it is important for the host to mount an appropriately regulated immune response to the pathogen (8, 93, 270, 326, 335, 415). In general, very high levels of chemokines and cytokines have been correlated with a fatal outcome (192, 416-418). The heightened inflammation in *Cnes2* and *Cnes2.4* mice may be a result of altered function of proteins that regulate host responsiveness to infection. Thus, I believe that the sub-congenic

strains that I have generated will be interesting and useful models for further investigations of an excessive and dysregulated immune response against *C. neoformans* infection.

3) The current study provides strong evidence for the contribution of two sub-congenic loci on mouse chromosome 17 in host susceptibility to *C. neoformans* infection. Although the causative mouse genes and their orthologs remain to be identified, in the future their role in human disease could be established using association or case control studies. Our data advances the understanding of genetic regulation of disease pathogenesis and could unravel pathways involved in the human response to cryptococcal disease in the future (246, 419).

5.2.2. Significance of the reverse genetic studies

1) The significantly decreased proinflammatory cytokines and higher fungal burden in the lungs of IL-1R$^{-/-}$ mice during the early phase of infection confirms the critical role of IL-1 signaling in innate immune protection against cryptococcal infection. This study highlights the important effect of the cytokine milieu on macrophage polarization during the early phase of infection and the subsequent development of an effective Th1/Th17 immune response. In the absence of IL-1 signaling, mice with pulmonary cryptococcal infection develop a non-protective Th2 immune response.
2) In addition to important role of proinflammatory cytokines and early induction of a Th1 response, this study provides strong evidence for a heightened Th17 immune response in the resistant BALB/c strain. As discussed in chapter 4, the role of a Th17 response in cryptococcal infection is not clear; therefore, this model could be useful in defining its contribution to the immune response against *C. neoformans* infection.
3) Fungal burden analysis in the brain and survival data indicate the important role of IL-1 signaling on *C. neoformans* brain dissemination.
4) The neutrophil depletion study clearly reveals that these cells are not required for cryptococcal clearance in the lung and brain and their absence is associated with a protective Th1, rather than Th17, immune response.
5) Finally, this study not only demonstrates the essential role of IL-1 signaling in protective immune response against *C. neoformans* infection, but emphasizes the importance of considering the mouse genetic background in cryptococcal studies. As mentioned in chapter 4,

a previous study using IL-1R$^{-/-}$ mice did not clearly demonstrate an important role of IL-1R signaling in *C. neoformans* infection. In addition to the different cryptococcal strains used in these two studies, the divergent observations may be attributable to the genetic background of the mouse strains that were used. It is clearly recognized that a defined mutation can have markedly different phenotypes when placed on different genetic backgrounds owing to different alleles and/or effects of modifier loci in various inbred strains (420).

5.3. Future Directions

5.3.1. Future directions for the forward genetic studies

1) To rigorously investigate the role of *Cnes2* and *Cnes2.4* on brain dissemination, inflammation, and survival after cryptococcal challenge, experiments will be required among larger groups of mice and at serial time points following intratracheal infection. In the future, intravenous or intracerebral injection of *C. neoformans* could also provide insights into intrinsic antifungal host defenses of the central nervous system. To achieve this, lung and/or brain tissue could be harvested form sick animals prior to death and analyzed for fungal burden and immunopathology with specific immunostaining/histological markers. Furthermore, myeloid cell recruitment, activation/polarization, cytokine/chemokine expression, and the pattern of adaptive immunity could be analyzed in the lungs and/or brain of infected mice. Such data would provide insight into mechanisms of severe and or fatal disease due to lung and/or brain pathology caused by excessive inflammation in *Cnes2* or *Cnes2.4* lines.
2) A direct effect of one or both *Cnes2* sub-congenic intervals on macrophage or DC function could be verified by *in vitro* studies. For example, bone marrow-derived macrophages and DCs from congenic and parental strains could be cultured and stimulated with *C. neoformans* under different experimental conditions. Fungal killing, phagocytosis, and expression of activation or polarization markers by flow cytometry would then be analyzed following infection. In addition, comparative gene expression analysis by microarray or RNAseq on stimulated macrophages and DCs from control and congenic strains could be useful to identify potential candidate genes in each interval.

3) Several other QTLs associated with inflammatory/immune phenotypes have also been mapped to the same *Cnes2* sub-congenic intervals, suggesting that the underlying genes and/or variants may have broad regulatory functions. Therefore, it would be interesting to evaluate the effect of *Cnes2* and its effective sub-congenic intervals on the host immune response against different cryptococcal strains and other fungal pathogens such as *Candida sp.* or *Aspergillus sp.* The information gained from these studies may elucidate a wide-ranging effect of the genes and their associated variants within the *Cnes2* sub-congenic intervals on host antifungal immune responses.
4) Candidate gene analysis: The number of causal genes or variants have been definitively identified by QTL mapping approaches is small; however, this problem is being resolved by improvements in genomic technologies, transcriptomic and proteomic data, and growing databases of sequence variation (230, 240, 244, 245, 421). In fact, forward genetic approaches have been successful in the study of several infectious diseases and have revealed genes, proteins, and signaling pathways that play critical roles in the immune response to important human pathogens (236). Thus far, I have selected the most plausible candidate genes using *in silico* analysis by identifying deleterious variants in the *Cnes2.2* and *Cnes2.4* intervals. As the next step, it would be useful to analyse the differential expression of each gene in the lung tissues from control and sub-congenic mice at different time intervals following *C. neoformans* infection (day 0, 14 and 21) by microarray or RNAseq. In many cases, a QTL will reflect quantitative changes in the expression, rather than sequence variation, of the underlying genes (203, 204, 242).
5) To validate the role of candidate genes chosen by sequence and/or expression analysis in *C. neoformans* infection, generating and phenotyping of mice bearing modifications at individual genes/alleles that may cause a loss- or gain-of-function will be performed (204, 323). Definitive identification of candidate genes or key molecular pathways in mice may lead to the characterization of corresponding human genetic factors that play a role in cryptococcal infection. For example, sequence variation or differential expression of a human gene that is associated with a variable host response to infection or is correlated with the geographical distribution of disease would support a role for that gene in cryptococcal disease and could facilitate disease risk prediction and/or disease management.

5.3.2. Future directions for the reverse genetic studies

1) To confirm a direct effect of IL-1RI signaling on macrophage and dendritic cell activation, polarization, cytokine secretion, and phagocytosis, a preliminary experiment with peritoneal macrophages needs to be confirmed using bone marrow-derived macrophages and dendritic cells in different stimulation conditions. To study the effect of IL-1 signaling on macrophages and DCs *in vivo,* it would be also interesting to adoptively transfer bone marrow derived macrophages (BMMs) and DCs (BMDCs) from WT to IL-1R$^{-/-}$ mice and analyze tissue fungal burden, lung cytokine expression, and cell recruitment following infection.
2) It would be interesting to perform a comparative study of the role of innate lymphoid cell populations in BALB/c and IL-1RI$^{-/-}$ mouse strains since they may function as innate IFN-γ and IL-17-producing cells following *C. neoformans* infection.
3) The effect of Th17 cells on survival and fungal burden could be analyzed by positive selection of CD4^{+}IL17^{+} cells from resistant WT and transferring to IL-1RI deficient mice or by administration of IL-17 to IL-1RI knockout mice. Additional studies using T cells from mice that lack IL-17 could be informative.
4) Fungal burden analysis in the brain and survival data signify the important role of IL-1 signaling on *C. neoformans* brain dissemination; however, an intrinsic effect in the central nervous system could be established by intravenous injection of *C. neoformans* in WT and IL-1RI$^{-/-}$ mice followed by assays of survival, pathology, cytokine/chemokine secretion and inflammatory cell recruitment.
5) As IL-1α and IL-1β are equally potent activators of IL-1RI signaling yet have different tissue distribution and activation kinetics, the availability of mice that are deficient in either IL-1α or IL-1β provides an opportunity to analyze the specific contribution of each cytokine in the development protective immunity against *C. neoformans* infection.
6) Further studies are needed to identify the role of neutrophil recruitment in cryptococcal infection by more detailed phenotyping analysis of neutrophil-depleted mice.

5.4. Final Conclusion

In general, my thesis provides strong evidence for the contribution of genetic factors on mouse chromosome 17 to the immune response against *C. neoformans* infection and shows that an adequate and tightly regulated immune response is important for optimal protection against progressive cryptococcal infection. Furthermore, it clearly demonstrates the essential role of IL-1 signaling in *C. neoformans* infection. These findings may help to guide future immunological studies in the human host during natural infection that are needed to evaluate conserved and/or species-specific immune responses. Ultimately, such knowledge will contribute to the development of more effective antifungal therapy (196).

References

1. CDC. 2015. C. neoformans Infection Statistics. Centers for Disease Control and Prevention.
2. Lin, X., and J. Heitman. 2006. The biology of the Cryptococcus neoformans species complex. *Annu Rev Microbiol* 60: 69-105.
3. Idnurm, A., Y. S. Bahn, K. Nielsen, X. Lin, J. A. Fraser, and J. Heitman. 2005. Deciphering the model pathogenic fungus Cryptococcus neoformans. *Nat Rev Microbiol* 3: 753-764.
4. Pfaller, M. A., P. G. Pappas, and J. R. Wingard. 2006. Invasive fungal pathogens: current epidemiological trends. *Clinical Infectious Diseases* 43: S3-S14.
5. Sciences., R. B. a. H. December 2013. Attacking fungal infection, one of world's major killers. *ScienceDaily*.
6. Brown, G. D., D. W. Denning, N. A. Gow, S. M. Levitz, M. G. Netea, and T. C. White. 2012. Hidden killers: human fungal infections. *Sci Transl Med* 4: 165rv113.
7. Brown, G. D., D. W. Denning, and S. M. Levitz. 2012. Tackling human fungal infections. *Science* 336: 647.
8. May, R. C., N. R. Stone, D. L. Wiesner, T. Bicanic, and K. Nielsen. 2016. Cryptococcus: from environmental saprophyte to global pathogen. *Nat Rev Microbiol* 14: 106-117.
9. Park, B. J., K. A. Wannemuehler, B. J. Marston, N. Govender, P. G. Pappas, and T. M. Chiller. 2009. Estimation of the current global burden of cryptococcal meningitis among persons living with HIV/AIDS. *Aids* 23: 525-530.
10. Rohatgi, S., and L. A. Pirofski. 2015. Host immunity to Cryptococcus neoformans. *Future Microbiol* 10: 565-581.
11. Taylor-Smith, L. M., and R. C. May. 2016. New weapons in the Cryptococcus infection toolkit. *Curr Opin Microbiol* 34: 67-74.
12. Brizendine, K. D., J. W. Baddley, and P. G. Pappas. 2011. Pulmonary cryptococcosis. *Semin Respir Crit Care Med* 32: 727-734.
13. Chang, C. C., T. C. Sorrell, and S. C. Chen. 2015. Pulmonary Cryptococcosis. *Semin Respir Crit Care Med* 36: 681-691.
14. Pappas, P. G. 2013. Cryptococcal infections in non-HIV-infected patients. *Trans Am Clin Climatol Assoc* 124: 61-79.
15. Adams, P. 2016. Cryptococcal meningitis: a blind spot in curbing AIDS. *Lancet* 387: 1605-1606.
16. Jarvis, J. N., and T. S. Harrison. 2007. HIV-associated cryptococcal meningitis. *Aids* 21: 2119-2129.
17. Hole, C., and F. L. Wormley, Jr. 2016. Innate host defenses against Cryptococcus neoformans. *J Microbiol* 54: 202-211.
18. van der Horst, C. M., M. S. Saag, G. A. Cloud, R. J. Hamill, J. R. Graybill, J. D. Sobel, P. C. Johnson, C. U. Tuazon, T. Kerkering, B. L. Moskovitz, W. G. Powderly, and W. E. Dismukes. 1997. Treatment of cryptococcal meningitis associated with the acquired immunodeficiency syndrome. National Institute of Allergy and Infectious Diseases Mycoses Study Group and AIDS Clinical Trials Group. *N Engl J Med* 337: 15-21.
19. Meya, D. B., Y. C. Manabe, B. Castelnuovo, B. A. Cook, A. M. Elbireer, A. Kambugu, M. R. Kamya, P. R. Bohjanen, and D. R. Boulware. 2010. Cost-effectiveness of serum cryptococcal antigen screening to prevent deaths among HIV-infected persons with a CD4+ cell count < or = 100 cells/microL who start HIV therapy in resource-limited settings. *Clin Infect Dis* 51: 448-455.
20. Sloan, D. J., and V. Parris. 2014. Cryptococcal meningitis: epidemiology and therapeutic options. *Clin Epidemiol* 6: 169-182.
21. McKenney, J., R. M. Smith, T. M. Chiller, R. Detels, A. French, J. Margolick, J. D. Klausner, C. Centers for Disease, and Prevention. 2014. Prevalence and correlates of cryptococcal antigen

positivity among AIDS patients--United States, 1986-2012. *MMWR Morb Mortal Wkly Rep* 63: 585-587.
22. Chen, S. C., W. Meyer, and T. C. Sorrell. 2014. Cryptococcus gattii infections. *Clin Microbiol Rev* 27: 980-1024.
23. CDC. 2015. C. gattii Infection Statistics. Centers for Disease Control and Prevention.
24. Kidd, S. E., F. Hagen, R. L. Tscharke, M. Huynh, K. H. Bartlett, M. Fyfe, L. Macdougall, T. Boekhout, K. J. Kwon-Chung, and W. Meyer. 2004. A rare genotype of Cryptococcus gattii caused the cryptococcosis outbreak on Vancouver Island (British Columbia, Canada). *Proc Natl Acad Sci U S A* 101: 17258-17263.
25. Datta, K., K. H. Bartlett, R. Baer, E. Byrnes, E. Galanis, J. Heitman, L. Hoang, M. J. Leslie, L. MacDougall, S. S. Magill, M. G. Morshed, K. A. Marr, and N. Cryptococcus gattii Working Group of the Pacific. 2009. Spread of Cryptococcus gattii into Pacific Northwest region of the United States. *Emerg Infect Dis* 15: 1185-1191.
26. Bartlett, K. H., S. E. Kidd, and J. W. Kronstad. 2008. The emergence of Cryptococcus gattii in British Columbia and the Pacific Northwest. *Curr Infect Dis Rep* 10: 58-65.
27. Kronstad, J. W., R. Attarian, B. Cadieux, J. Choi, C. A. D'Souza, E. J. Griffiths, J. M. Geddes, G. Hu, W. H. Jung, M. Kretschmer, S. Saikia, and J. Wang. 2011. Expanding fungal pathogenesis: Cryptococcus breaks out of the opportunistic box. *Nat Rev Microbiol* 9: 193-203.
28. Pappas, P. G., J. R. Perfect, G. A. Cloud, R. A. Larsen, G. A. Pankey, D. J. Lancaster, H. Henderson, C. A. Kauffman, D. W. Haas, M. Saccente, R. J. Hamill, M. S. Holloway, R. M. Warren, and W. E. Dismukes. 2001. Cryptococcosis in human immunodeficiency virus-negative patients in the era of effective azole therapy. *Clin Infect Dis* 33: 690-699.
29. Bratton, E. W., N. El Husseini, C. A. Chastain, M. S. Lee, C. Poole, T. Sturmer, J. J. Juliano, D. J. Weber, and J. R. Perfect. 2012. Comparison and temporal trends of three groups with cryptococcosis: HIV-infected, solid organ transplant, and HIV-negative/non-transplant. *PLoS One* 7: e43582.
30. McDonald, T., D. L. Wiesner, and K. Nielsen. 2012. Cryptococcus. *Curr Biol* 22: R554-555.
31. Srikanta, D., F. H. Santiago-Tirado, and T. L. Doering. 2014. Cryptococcus neoformans: historical curiosity to modern pathogen. *Yeast* 31: 47-60.
32. Maziarz, E. K., and J. R. Perfect. 2016. Cryptococcosis. *Infect Dis Clin North Am* 30: 179-206.
33. Kwon-Chung, K. J., J. A. Fraser, T. L. Doering, Z. Wang, G. Janbon, A. Idnurm, and Y. S. Bahn. 2014. Cryptococcus neoformans and Cryptococcus gattii, the etiologic agents of cryptococcosis. *Cold Spring Harb Perspect Med* 4: a019760.
34. Chaturvedi, V., and S. Chaturvedi. 2011. Cryptococcus gattii: a resurgent fungal pathogen. *Trends Microbiol* 19: 564-571.
35. Dromer, F., S. Mathoulin-Pelissier, O. Launay, O. Lortholary, and G. French Cryptococcosis Study. 2007. Determinants of disease presentation and outcome during cryptococcosis: the CryptoA/D study. *PLoS Med* 4: e21.
36. Steenbergen, J. N., and A. Casadevall. 2000. Prevalence of Cryptococcus neoformans var. neoformans (Serotype D) and Cryptococcus neoformans var. grubii (Serotype A) isolates in New York City. *J Clin Microbiol* 38: 1974-1976.
37. Kwon-Chung, K. J., J. E. Bennett, B. L. Wickes, W. Meyer, C. A. Cuomo, K. R. Wollenburg, T. A. Bicanic, E. Castaneda, Y. C. Chang, J. Chen, M. Cogliati, F. Dromer, D. Ellis, S. G. Filler, M. C. Fisher, T. S. Harrison, S. M. Holland, S. Kohno, J. W. Kronstad, M. Lazera, S. M. Levitz, M. S. Lionakis, R. C. May, P. Ngamskulrongroj, P. G. Pappas, J. R. Perfect, V. Rickerts, T. C. Sorrell, T. J. Walsh, P. R. Williamson, J. Xu, A. M. Zelazny, and A. Casadevall. 2017. The Case for Adopting the "Species Complex" Nomenclature for the Etiologic Agents of Cryptococcosis. *mSphere* 2.

38. Feldmesser, M., Y. Kress, P. Novikoff, and A. Casadevall. 2000. Cryptococcus neoformans is a facultative intracellular pathogen in murine pulmonary infection. *Infect Immun* 68: 4225-4237.
39. Antinori, S. 2013. New Insights into HIV/AIDS-Associated Cryptococcosis. *ISRN AIDS* 2013: 471363.
40. Litvintseva, A. P., R. Thakur, L. B. Reller, and T. G. Mitchell. 2005. Prevalence of clinical isolates of Cryptococcus gattii serotype C among patients with AIDS in Sub-Saharan Africa. *J Infect Dis* 192: 888-892.
41. Byrnes, E. J., 3rd, W. Li, Y. Lewit, H. Ma, K. Voelz, P. Ren, D. A. Carter, V. Chaturvedi, R. J. Bildfell, R. C. May, and J. Heitman. 2010. Emergence and pathogenicity of highly virulent Cryptococcus gattii genotypes in the northwest United States. *PLoS Pathog* 6: e1000850.
42. Carroll, S. F., L. Guillot, and S. T. Qureshi. 2007. Mammalian model hosts of cryptococcal infection. *Comp Med* 57: 9-17.
43. Lin, X., C. M. Hull, and J. Heitman. 2005. Sexual reproduction between partners of the same mating type in Cryptococcus neoformans. *Nature* 434: 1017-1021.
44. Almeida, F., J. M. Wolf, and A. Casadevall. 2015. Virulence-Associated Enzymes of Cryptococcus neoformans. *Eukaryot Cell* 14: 1173-1185.
45. Rodrigues, M. L., E. S. Nakayasu, D. L. Oliveira, L. Nimrichter, J. D. Nosanchuk, I. C. Almeida, and A. Casadevall. 2008. Extracellular vesicles produced by Cryptococcus neoformans contain protein components associated with virulence. *Eukaryot Cell* 7: 58-67.
46. Rodrigues, M. L., R. M. Godinho, D. Zamith-Miranda, and L. Nimrichter. 2015. Traveling into Outer Space: Unanswered Questions about Fungal Extracellular Vesicles. *PLoS Pathog* 11: e1005240.
47. Oliveira, D. L., C. G. Freire-de-Lima, J. D. Nosanchuk, A. Casadevall, M. L. Rodrigues, and L. Nimrichter. 2010. Extracellular vesicles from Cryptococcus neoformans modulate macrophage functions. *Infect Immun* 78: 1601-1609.
48. Wolf, J. M., J. Espadas-Moreno, J. L. Luque-Garcia, and A. Casadevall. 2014. Interaction of Cryptococcus neoformans extracellular vesicles with the cell wall. *Eukaryot Cell* 13: 1484-1493.
49. Peres da Silva, R., R. Puccia, M. L. Rodrigues, D. L. Oliveira, L. S. Joffe, G. V. Cesar, L. Nimrichter, S. Goldenberg, and L. R. Alves. 2015. Extracellular vesicle-mediated export of fungal RNA. *Sci Rep* 5: 7763.
50. Okagaki, L. H., A. K. Strain, J. N. Nielsen, C. Charlier, N. J. Baltes, F. Chretien, J. Heitman, F. Dromer, and K. Nielsen. 2010. Cryptococcal cell morphology affects host cell interactions and pathogenicity. *PLoS Pathog* 6: e1000953.
51. Zaragoza, O., R. Garcia-Rodas, J. D. Nosanchuk, M. Cuenca-Estrella, J. L. Rodriguez-Tudela, and A. Casadevall. 2010. Fungal cell gigantism during mammalian infection. *PLoS Pathog* 6: e1000945.
52. Crabtree, J. N., L. H. Okagaki, D. L. Wiesner, A. K. Strain, J. N. Nielsen, and K. Nielsen. 2012. Titan cell production enhances the virulence of Cryptococcus neoformans. *Infect Immun* 80: 3776-3785.
53. Alanio, A., F. Vernel-Pauillac, A. Sturny-Leclere, and F. Dromer. 2015. Cryptococcus neoformans host adaptation: toward biological evidence of dormancy. *MBio* 6.
54. Vu, K., J. M. Bautos, and A. Gelli. 2015. The Cch1-Mid1 High-Affinity Calcium Channel Contributes to the Virulence of Cryptococcus neoformans by Mitigating Oxidative Stress. *Eukaryot Cell* 14: 1135-1143.
55. Lev, S., C. Li, D. Desmarini, A. Saiardi, N. L. Fewings, S. D. Schibeci, R. Sharma, T. C. Sorrell, and J. T. Djordjevic. 2015. Fungal Inositol Pyrophosphate IP7 Is Crucial for Metabolic Adaptation to the Host Environment and Pathogenicity. *MBio* 6: e00531-00515.

56. Do, E., G. Hu, M. Caza, D. Oliveira, J. W. Kronstad, and W. H. Jung. 2015. Leu1 plays a role in iron metabolism and is required for virulence in Cryptococcus neoformans. *Fungal Genet Biol* 75: 11-19.
57. Schneider Rde, O., C. Diehl, F. M. dos Santos, A. C. Piffer, A. W. Garcia, M. I. Kulmann, A. Schrank, L. Kmetzsch, M. H. Vainstein, and C. C. Staats. 2015. Effects of zinc transporters on Cryptococcus gattii virulence. *Sci Rep* 5: 10104.
58. Zaragoza, O., C. J. Chrisman, M. V. Castelli, S. Frases, M. Cuenca-Estrella, J. L. Rodriguez-Tudela, and A. Casadevall. 2008. Capsule enlargement in Cryptococcus neoformans confers resistance to oxidative stress suggesting a mechanism for intracellular survival. *Cell Microbiol* 10: 2043-2057.
59. Zaragoza, O., M. L. Rodrigues, M. De Jesus, S. Frases, E. Dadachova, and A. Casadevall. 2009. The capsule of the fungal pathogen Cryptococcus neoformans. *Adv Appl Microbiol* 68: 133-216.
60. Fromtling, R. A., H. J. Shadomy, and E. S. Jacobson. 1982. Decreased virulence in stable, acapsular mutants of cryptococcus neoformans. *Mycopathologia* 79: 23-29.
61. Chang, Y. C., and K. J. Kwon-Chung. 1994. Complementation of a capsule-deficient mutation of Cryptococcus neoformans restores its virulence. *Mol Cell Biol* 14: 4912-4919.
62. Voelz, K., and R. C. May. 2010. Cryptococcal interactions with the host immune system. *Eukaryot Cell* 9: 835-846.
63. Vecchiarelli, A., E. Pericolini, E. Gabrielli, S. Kenno, S. Perito, E. Cenci, and C. Monari. 2013. Elucidating the immunological function of the Cryptococcus neoformans capsule. *Future Microbiol* 8: 1107-1116.
64. Urai, M., Y. Kaneko, K. Ueno, Y. Okubo, T. Aizawa, H. Fukazawa, T. Sugita, H. Ohno, K. Shibuya, Y. Kinjo, and Y. Miyazaki. 2015. Evasion of Innate Immune Responses by the Highly Virulent Cryptococcus gattii by Altering Capsule Glucuronoxylomannan Structure. *Front Cell Infect Microbiol* 5: 101.
65. Kozel, T. R., and R. P. Mastroianni. 1976. Inhibition of phagocytosis by cryptococcal polysaccharide: dissociation of the attachment and ingestion phases of phagocytosis. *Infect Immun* 14: 62-67.
66. van Duin, D., A. Casadevall, and J. D. Nosanchuk. 2002. Melanization of Cryptococcus neoformans and Histoplasma capsulatum reduces their susceptibilities to amphotericin B and caspofungin. *Antimicrob Agents Chemother* 46: 3394-3400.
67. Casadevall, A., A. L. Rosas, and J. D. Nosanchuk. 2000. Melanin and virulence in Cryptococcus neoformans. *Curr Opin Microbiol* 3: 354-358.
68. Wang, Y., P. Aisen, and A. Casadevall. 1995. Cryptococcus neoformans melanin and virulence: mechanism of action. *Infect Immun* 63: 3131-3136.
69. Perfect, J. R. 2006. Cryptococcus neoformans: the yeast that likes it hot. *FEMS Yeast Res* 6: 463-468.
70. Johnston, S. A., K. Voelz, and R. C. May. 2016. Cryptococcus neoformans Thermotolerance to Avian Body Temperature Is Sufficient For Extracellular Growth But Not Intracellular Survival In Macrophages. *Sci Rep* 6: 20977.
71. Kraus, P. R., M. J. Boily, S. S. Giles, J. E. Stajich, A. Allen, G. M. Cox, F. S. Dietrich, J. R. Perfect, and J. Heitman. 2004. Identification of Cryptococcus neoformans temperature-regulated genes with a genomic-DNA microarray. *Eukaryot Cell* 3: 1249-1260.
72. DeLeon-Rodriguez, C. M., and A. Casadevall. 2016. Cryptococcus neoformans: Tripping on Acid in the Phagolysosome. *Front Microbiol* 7: 164.
73. Buchanan, K. L., and J. W. Murphy. 1998. What makes Cryptococcus neoformans a pathogen? *Emerg Infect Dis* 4: 71-83.

74. Levitz, S. M., S. H. Nong, K. F. Seetoo, T. S. Harrison, R. A. Speizer, and E. R. Simons. 1999. Cryptococcus neoformans resides in an acidic phagolysosome of human macrophages. *Infect Immun* 67: 885-890.
75. Olszewski, M. A., M. C. Noverr, G. H. Chen, G. B. Toews, G. M. Cox, J. R. Perfect, and G. B. Huffnagle. 2004. Urease expression by Cryptococcus neoformans promotes microvascular sequestration, thereby enhancing central nervous system invasion. *Am J Pathol* 164: 1761-1771.
76. Cox, G. M., J. Mukherjee, G. T. Cole, A. Casadevall, and J. R. Perfect. 2000. Urease as a virulence factor in experimental cryptococcosis. *Infect Immun* 68: 443-448.
77. Cox, G. M., T. S. Harrison, H. C. McDade, C. P. Taborda, G. Heinrich, A. Casadevall, and J. R. Perfect. 2003. Superoxide dismutase influences the virulence of Cryptococcus neoformans by affecting growth within macrophages. *Infect Immun* 71: 173-180.
78. Chen, S. C., M. Muller, J. Z. Zhou, L. C. Wright, and T. C. Sorrell. 1997. Phospholipase activity in Cryptococcus neoformans: a new virulence factor? *J Infect Dis* 175: 414-420.
79. Cox, G. M., H. C. McDade, S. C. Chen, S. C. Tucker, M. Gottfredsson, L. C. Wright, T. C. Sorrell, S. D. Leidich, A. Casadevall, M. A. Ghannoum, and J. R. Perfect. 2001. Extracellular phospholipase activity is a virulence factor for Cryptococcus neoformans. *Mol Microbiol* 39: 166-175.
80. Aoki, S., S. Ito-Kuwa, K. Nakamura, J. Kato, K. Ninomiya, and V. Vidotto. 1994. Extracellular proteolytic activity of Cryptococcus neoformans. *Mycopathologia* 128: 143-150.
81. Chen, L. C., E. S. Blank, and A. Casadevall. 1996. Extracellular proteinase activity of Cryptococcus neoformans. *Clin Diagn Lab Immunol* 3: 570-574.
82. Goldman, D. L., H. Khine, J. Abadi, D. J. Lindenberg, L. Pirofski, R. Niang, and A. Casadevall. 2001. Serologic evidence for Cryptococcus neoformans infection in early childhood. *Pediatrics* 107: E66.
83. Giles, S. S., T. R. Dagenais, M. R. Botts, N. P. Keller, and C. M. Hull. 2009. Elucidating the pathogenesis of spores from the human fungal pathogen Cryptococcus neoformans. *Infect Immun* 77: 3491-3500.
84. Botts, M. R., and C. M. Hull. 2010. Dueling in the lung: how Cryptococcus spores race the host for survival. *Curr Opin Microbiol* 13: 437-442.
85. Velagapudi, R., Y. P. Hsueh, S. Geunes-Boyer, J. R. Wright, and J. Heitman. 2009. Spores as infectious propagules of Cryptococcus neoformans. *Infect Immun* 77: 4345-4355.
86. Saha, D. C., D. L. Goldman, X. Shao, A. Casadevall, S. Husain, A. P. Limaye, M. Lyon, J. Somani, K. Pursell, T. L. Pruett, and N. Singh. 2007. Serologic evidence for reactivation of cryptococcosis in solid-organ transplant recipients. *Clin Vaccine Immunol* 14: 1550-1554.
87. Visnegarwala, F., E. A. Graviss, C. E. Lacke, A. T. Dural, P. C. Johnson, R. L. Atmar, and R. J. Hamill. 1998. Acute respiratory failure associated with cryptococcosis in patients with AIDS: analysis of predictive factors. *Clin Infect Dis* 27: 1231-1237.
88. Lanternier, F., S. Cypowyj, C. Picard, J. Bustamante, O. Lortholary, J. L. Casanova, and A. Puel. 2013. Primary immunodeficiencies underlying fungal infections. *Curr Opin Pediatr* 25: 736-747.
89. Bowen, L. N., B. Smith, D. Reich, M. Quezado, and A. Nath. 2016. HIV-associated opportunistic CNS infections: pathophysiology, diagnosis and treatment. *Nat Rev Neurol* 12: 662-674.
90. King, J. W. 2016. Cryptococcosis. Medscape, http://emedicine.medscape.com.
91. Perfect, J. R., and T. Bicanic. 2015. Cryptococcosis diagnosis and treatment: What do we know now. *Fungal Genet Biol* 78: 49-54.
92. Loyse, A., H. Thangaraj, P. Easterbrook, N. Ford, M. Roy, T. Chiller, N. Govender, T. S. Harrison, and T. Bicanic. 2013. Cryptococcal meningitis: improving access to essential antifungal medicines in resource-poor countries. *Lancet Infect Dis* 13: 629-637.
93. Coelho, C., and A. Casadevall. 2016. Cryptococcal therapies and drug targets: the old, the new and the promising. *Cell Microbiol* 18: 792-799.

94. Butts, A., and D. J. Krysan. 2012. Antifungal drug discovery: something old and something new. *PLoS Pathog* 8: e1002870.
95. Coker, R. J., M. Viviani, B. G. Gazzard, B. Du Pont, H. D. Pohle, S. M. Murphy, J. Atouguia, J. L. Champalimaud, and J. R. Harris. 1993. Treatment of cryptococcosis with liposomal amphotericin B (AmBisome) in 23 patients with AIDS. *Aids* 7: 829-835.
96. Veringa, A., K. C. van der Elst, J. N. Day, G. E. Thwaites, and J. W. Alffenaar. 2016. Sertraline for HIV-associated cryptococcal meningitis. *Lancet Infect Dis* 16: 1111.
97. Trevino-Rangel Rde, J., H. Villanueva-Lozano, P. Hernandez-Rodriguez, M. F. Martinez-Resendez, J. Garcia-Juarez, H. Rodriguez-Rocha, and G. M. Gonzalez. 2016. Activity of sertraline against Cryptococcus neoformans: in vitro and in vivo assays. *Med Mycol* 54: 280-286.
98. Zhai, B., C. Wu, L. Wang, M. S. Sachs, and X. Lin. 2012. The antidepressant sertraline provides a promising therapeutic option for neurotropic cryptococcal infections. *Antimicrob Agents Chemother* 56: 3758-3766.
99. Rhein, J., B. M. Morawski, K. H. Hullsiek, H. W. Nabeta, R. Kiggundu, L. Tugume, A. Musubire, A. Akampurira, K. D. Smith, A. Alhadab, D. A. Williams, M. Abassi, N. C. Bahr, S. S. Velamakanni, J. Fisher, K. Nielsen, D. B. Meya, D. R. Boulware, and A.-C. S. Team. 2016. Efficacy of adjunctive sertraline for the treatment of HIV-associated cryptococcal meningitis: an open-label dose-ranging study. *Lancet Infect Dis* 16: 809-818.
100. Casadevall, A., W. Cleare, M. Feldmesser, A. Glatman-Freedman, D. L. Goldman, T. R. Kozel, N. Lendvai, J. Mukherjee, L. A. Pirofski, J. Rivera, A. L. Rosas, M. D. Scharff, P. Valadon, K. Westin, and Z. Zhong. 1998. Characterization of a murine monoclonal antibody to Cryptococcus neoformans polysaccharide that is a candidate for human therapeutic studies. *Antimicrob Agents Chemother* 42: 1437-1446.
101. Jarvis, J. N., G. Meintjes, K. Rebe, G. N. Williams, T. Bicanic, A. Williams, C. Schutz, L. G. Bekker, R. Wood, and T. S. Harrison. 2012. Adjunctive interferon-gamma immunotherapy for the treatment of HIV-associated cryptococcal meningitis: a randomized controlled trial. *Aids* 26: 1105-1113.
102. Pappas, P. G., B. Bustamante, E. Ticona, R. J. Hamill, P. C. Johnson, A. Reboli, J. Aberg, R. Hasbun, and H. H. Hsu. 2004. Recombinant interferon- gamma 1b as adjunctive therapy for AIDS-related acute cryptococcal meningitis. *J Infect Dis* 189: 2185-2191.
103. Guillot, L., S. F. Carroll, M. Badawy, and S. T. Qureshi. 2008. Cryptococcus neoformans induces IL-8 secretion and CXCL1 expression by human bronchial epithelial cells. *Respir Res* 9: 9.
104. Merkel, G. J., and B. A. Scofield. 1997. The in vitro interaction of Cryptococcus neoformans with human lung epithelial cells. *FEMS Immunol Med Microbiol* 19: 203-213.
105. Barbosa, F. M., F. L. Fonseca, C. Holandino, C. S. Alviano, L. Nimrichter, and M. L. Rodrigues. 2006. Glucuronoxylomannan-mediated interaction of Cryptococcus neoformans with human alveolar cells results in fungal internalization and host cell damage. *Microbes Infect* 8: 493-502.
106. Misharin, A. V., L. Morales-Nebreda, G. M. Mutlu, G. R. Budinger, and H. Perlman. 2013. Flow cytometric analysis of macrophages and dendritic cell subsets in the mouse lung. *Am J Respir Cell Mol Biol* 49: 503-510.
107. Erwig, L. P., and N. A. Gow. 2016. Interactions of fungal pathogens with phagocytes. *Nat Rev Microbiol* 14: 163-176.
108. Leopold Wager, C. M., C. R. Hole, K. L. Wozniak, and F. L. Wormley, Jr. 2016. Cryptococcus and Phagocytes: Complex Interactions that Influence Disease Outcome. *Front Microbiol* 7: 105.
109. Zhang, M., D. Sun, and M. Shi. 2015. Dancing cheek to cheek: Cryptococcus neoformans and phagocytes. *Springerplus* 4: 410.
110. Bojarczuk, A., K. A. Miller, R. Hotham, A. Lewis, N. V. Ogryzko, A. A. Kamuyango, H. Frost, R. H. Gibson, E. Stillman, R. C. May, S. A. Renshaw, and S. A. Johnston. 2016. Cryptococcus

neoformans Intracellular Proliferation and Capsule Size Determines Early Macrophage Control of Infection. *Sci Rep* 6: 21489.
111. Davis, M. J., T. M. Tsang, Y. Qiu, J. K. Dayrit, J. B. Freij, G. B. Huffnagle, and M. A. Olszewski. 2013. Macrophage M1/M2 polarization dynamically adapts to changes in cytokine microenvironments in Cryptococcus neoformans infection. *MBio* 4: e00264-00213.
112. McQuiston, T. J., and P. R. Williamson. 2012. Paradoxical roles of alveolar macrophages in the host response to Cryptococcus neoformans. *Journal of infection and chemotherapy : official journal of the Japan Society of Chemotherapy* 18: 1-9.
113. Voelz, K., D. A. Lammas, and R. C. May. 2009. Cytokine signaling regulates the outcome of intracellular macrophage parasitism by Cryptococcus neoformans. *Infect Immun* 77: 3450-3457.
114. Martinez, F. O., and S. Gordon. 2014. The M1 and M2 paradigm of macrophage activation: time for reassessment. *F1000Prime Rep* 6: 13.
115. Leopold Wager, C. M., and F. L. Wormley, Jr. 2014. Classical versus alternative macrophage activation: the Ying and the Yang in host defense against pulmonary fungal infections. *Mucosal Immunol* 7: 1023-1035.
116. Arora, S., M. A. Olszewski, T. M. Tsang, R. A. McDonald, G. B. Toews, and G. B. Huffnagle. 2011. Effect of cytokine interplay on macrophage polarization during chronic pulmonary infection with Cryptococcus neoformans. *Infect Immun* 79: 1915-1926.
117. Smith, L. M., E. F. Dixon, and R. C. May. 2015. The fungal pathogen Cryptococcus neoformans manipulates macrophage phagosome maturation. *Cell Microbiol* 17: 702-713.
118. Nicola, A. M., E. J. Robertson, P. Albuquerque, S. Derengowski Lda, and A. Casadevall. 2011. Nonlytic exocytosis of Cryptococcus neoformans from macrophages occurs in vivo and is influenced by phagosomal pH. *MBio* 2.
119. Ma, H., J. E. Croudace, D. A. Lammas, and R. C. May. 2006. Expulsion of live pathogenic yeast by macrophages. *Curr Biol* 16: 2156-2160.
120. Alvarez, M., and A. Casadevall. 2006. Phagosome extrusion and host-cell survival after Cryptococcus neoformans phagocytosis by macrophages. *Curr Biol* 16: 2161-2165.
121. Johnston, S. A., and R. C. May. 2010. The human fungal pathogen Cryptococcus neoformans escapes macrophages by a phagosome emptying mechanism that is inhibited by Arp2/3 complex-mediated actin polymerisation. *PLoS Pathog* 6: e1001041.
122. Alvarez, M., and A. Casadevall. 2007. Cell-to-cell spread and massive vacuole formation after Cryptococcus neoformans infection of murine macrophages. *BMC Immunol* 8: 16.
123. Sorrell, T. C., P. G. Juillard, J. T. Djordjevic, K. Kaufman-Francis, A. Dietmann, A. Milonig, V. Combes, and G. E. Grau. 2016. Cryptococcal transmigration across a model brain blood-barrier: evidence of the Trojan horse mechanism and differences between Cryptococcus neoformans var. grubii strain H99 and Cryptococcus gattii strain R265. *Microbes Infect* 18: 57-67.
124. Tseng, H. K., T. Y. Huang, A. Y. Wu, H. H. Chen, C. P. Liu, and A. Jong. 2015. How Cryptococcus interacts with the blood-brain barrier. *Future Microbiol* 10: 1669-1682.
125. Charlier, C., K. Nielsen, S. Daou, M. Brigitte, F. Chretien, and F. Dromer. 2009. Evidence of a role for monocytes in dissemination and brain invasion by Cryptococcus neoformans. *Infect Immun* 77: 120-127.
126. Poelmans, J., A. Hillen, L. Vanherp, K. Govaerts, J. Maertens, T. Dresselaers, U. Himmelreich, K. Lagrou, and G. Vande Velde. 2016. Longitudinal, in vivo assessment of invasive pulmonary aspergillosis in mice by computed tomography and magnetic resonance imaging. *Lab Invest* 96: 692-704.
127. Shi, M., S. S. Li, C. Zheng, G. J. Jones, K. S. Kim, H. Zhou, P. Kubes, and C. H. Mody. 2010. Real-time imaging of trapping and urease-dependent transmigration of Cryptococcus neoformans in mouse brain. *J Clin Invest* 120: 1683-1693.

128. Syme, R. M., J. C. Spurrell, E. K. Amankwah, F. H. Green, and C. H. Mody. 2002. Primary dendritic cells phagocytose Cryptococcus neoformans via mannose receptors and Fcgamma receptor II for presentation to T lymphocytes. *Infect Immun* 70: 5972-5981.
129. Wozniak, K. L., J. M. Vyas, and S. M. Levitz. 2006. In vivo role of dendritic cells in a murine model of pulmonary cryptococcosis. *Infect Immun* 74: 3817-3824.
130. Hole, C. R., H. Bui, F. L. Wormley, Jr., and K. L. Wozniak. 2012. Mechanisms of dendritic cell lysosomal killing of Cryptococcus. *Sci Rep* 2: 739.
131. Griffin, F. M., Jr. 1981. Roles of macrophage Fc and C3b receptors in phagocytosis of immunologically coated Cryptococcus neoformans. *Proc Natl Acad Sci U S A* 78: 3853-3857.
132. van Asbeck, E. C., A. I. Hoepelman, J. Scharringa, B. L. Herpers, and J. Verhoef. 2008. Mannose binding lectin plays a crucial role in innate immunity against yeast by enhanced complement activation and enhanced uptake of polymorphonuclear cells. *BMC Microbiol* 8: 229.
133. Pirofski, L. A. 2006. Of mice and men, revisited: new insights into an ancient molecule from studies of complement activation by Cryptococcus neoformans. *Infect Immun* 74: 3079-3084.
134. Diamond, R. D., J. E. May, M. A. Kane, M. M. Frank, and J. E. Bennett. 1974. The role of the classical and alternate complement pathways in host defenses against Cryptococcus neoformans infection. *J Immunol* 112: 2260-2270.
135. Yamamoto, H., Y. Abe, A. Miyazato, D. Tanno, M. Tanaka, T. Miyasaka, K. Ishii, and K. Kawakami. 2011. Cryptococcus neoformans suppresses the activation of bone marrow-derived dendritic cells stimulated with its own DNA, but not with DNA from other fungi. *FEMS Immunol Med Microbiol* 63: 363-372.
136. Dan, J. M., R. M. Kelly, C. K. Lee, and S. M. Levitz. 2008. Role of the mannose receptor in a murine model of Cryptococcus neoformans infection. *Infect Immun* 76: 2362-2367.
137. Shoham, S., C. Huang, J. M. Chen, D. T. Golenbock, and S. M. Levitz. 2001. Toll-like receptor 4 mediates intracellular signaling without TNF-alpha release in response to Cryptococcus neoformans polysaccharide capsule. *J Immunol* 166: 4620-4626.
138. Nakamura, K., A. Miyazato, G. Xiao, M. Hatta, K. Inden, T. Aoyagi, K. Shiratori, K. Takeda, S. Akira, S. Saijo, Y. Iwakura, Y. Adachi, N. Ohno, K. Suzuki, J. Fujita, M. Kaku, and K. Kawakami. 2008. Deoxynucleic acids from Cryptococcus neoformans activate myeloid dendritic cells via a TLR9-dependent pathway. *J Immunol* 180: 4067-4074.
139. Nakamura, K., K. Miyagi, Y. Koguchi, Y. Kinjo, K. Uezu, T. Kinjo, M. Akamine, J. Fujita, I. Kawamura, M. Mitsuyama, Y. Adachi, N. Ohno, K. Takeda, S. Akira, A. Miyazato, M. Kaku, and K. Kawakami. 2006. Limited contribution of Toll-like receptor 2 and 4 to the host response to a fungal infectious pathogen, Cryptococcus neoformans. *FEMS Immunol Med Microbiol* 47: 148-154.
140. Bauman, S. K., K. L. Nichols, and J. W. Murphy. 2000. Dendritic cells in the induction of protective and nonprotective anticryptococcal cell-mediated immune responses. *J Immunol* 165: 158-167.
141. Osterholzer, J. J., J. E. Milam, G. H. Chen, G. B. Toews, G. B. Huffnagle, and M. A. Olszewski. 2009. Role of dendritic cells and alveolar macrophages in regulating early host defense against pulmonary infection with Cryptococcus neoformans. *Infect Immun* 77: 3749-3758.
142. Osterholzer, J. J., J. L. Curtis, T. Polak, T. Ames, G. H. Chen, R. McDonald, G. B. Huffnagle, and G. B. Toews. 2008. CCR2 mediates conventional dendritic cell recruitment and the formation of bronchovascular mononuclear cell infiltrates in the lungs of mice infected with Cryptococcus neoformans. *J Immunol* 181: 610-620.
143. Osterholzer, J. J., G. H. Chen, M. A. Olszewski, J. L. Curtis, G. B. Huffnagle, and G. B. Toews. 2009. Accumulation of CD11b+ lung dendritic cells in response to fungal infection results from the

CCR2-mediated recruitment and differentiation of Ly-6Chigh monocytes. *J Immunol* 183: 8044-8053.
144. Kozel, T. R., G. S. Pfrommer, and D. Redelman. 1987. Activated neutrophils exhibit enhanced phagocytosis of Cryptococcus neoformans opsonized with normal human serum. *Clin Exp Immunol* 70: 238-246.
145. Mambula, S. S., E. R. Simons, R. Hastey, M. E. Selsted, and S. M. Levitz. 2000. Human neutrophil-mediated nonoxidative antifungal activity against Cryptococcus neoformans. *Infect Immun* 68: 6257-6264.
146. Miller, M. F., and T. G. Mitchell. 1991. Killing of Cryptococcus neoformans strains by human neutrophils and monocytes. *Infect Immun* 59: 24-28.
147. Wozniak, K. L., J. K. Kolls, and F. L. Wormley, Jr. 2012. Depletion of neutrophils in a protective model of pulmonary cryptococcosis results in increased IL-17A production by gammadelta T cells. *BMC Immunol* 13: 65.
148. Mednick, A. J., M. Feldmesser, J. Rivera, and A. Casadevall. 2003. Neutropenia alters lung cytokine production in mice and reduces their susceptibility to pulmonary cryptococcosis. *Eur J Immunol* 33: 1744-1753.
149. Yamaguchi, H., Y. Komase, M. Ikehara, T. Yamamoto, and T. Shinagawa. 2008. Disseminated cryptococcal infection with eosinophilia in a healthy person. *Journal of infection and chemotherapy : official journal of the Japan Society of Chemotherapy* 14: 319-324.
150. Feldmesser, M., A. Casadevall, Y. Kress, G. Spira, and A. Orlofsky. 1997. Eosinophil-Cryptococcus neoformans interactions in vivo and in vitro. *Infect Immun* 65: 1899-1907.
151. Holmer, S. M., K. S. Evans, Y. G. Asfaw, D. Saini, W. A. Schell, J. G. Ledford, R. Frothingham, J. R. Wright, G. D. Sempowski, and J. R. Perfect. 2014. Impact of surfactant protein D, interleukin-5, and eosinophilia on Cryptococcosis. *Infect Immun* 82: 683-693.
152. Huffnagle, G. B., M. B. Boyd, N. E. Street, and M. F. Lipscomb. 1998. IL-5 is required for eosinophil recruitment, crystal deposition, and mononuclear cell recruitment during a pulmonary Cryptococcus neoformans infection in genetically susceptible mice (C57BL/6). *J Immunol* 160: 2393-2400.
153. Piehler, D., W. Stenzel, A. Grahnert, J. Held, L. Richter, G. Kohler, T. Richter, M. Eschke, G. Alber, and U. Muller. 2011. Eosinophils contribute to IL-4 production and shape the T-helper cytokine profile and inflammatory response in pulmonary cryptococcosis. *Am J Pathol* 179: 733-744.
154. Garro, A. P., L. S. Chiapello, J. L. Baronetti, and D. T. Masih. 2011. Rat eosinophils stimulate the expansion of Cryptococcus neoformans-specific CD4(+) and CD8(+) T cells with a T-helper 1 profile. *Immunology* 132: 174-187.
155. Garro, A. P., L. S. Chiapello, J. L. Baronetti, and D. T. Masih. 2011. Eosinophils elicit proliferation of naive and fungal-specific cells in vivo so enhancing a T helper type 1 cytokine profile in favour of a protective immune response against Cryptococcus neoformans infection. *Immunology* 134: 198-213.
156. Marr, K. J., G. J. Jones, C. Zheng, S. M. Huston, M. Timm-McCann, A. Islam, B. M. Berenger, L. L. Ma, J. C. Wiseman, and C. H. Mody. 2009. Cryptococcus neoformans directly stimulates perforin production and rearms NK cells for enhanced anticryptococcal microbicidal activity. *Infect Immun* 77: 2436-2446.
157. Wiseman, J. C., L. L. Ma, K. J. Marr, G. J. Jones, and C. H. Mody. 2007. Perforin-dependent cryptococcal microbicidal activity in NK cells requires PI3K-dependent ERK1/2 signaling. *J Immunol* 178: 6456-6464.
158. Ma, L. L., C. L. Wang, G. G. Neely, S. Epelman, A. M. Krensky, and C. H. Mody. 2004. NK cells use perforin rather than granulysin for anticryptococcal activity. *J Immunol* 173: 3357-3365.

159. Islam, A., S. S. Li, P. Oykhman, M. Timm-McCann, S. M. Huston, D. Stack, R. F. Xiang, M. M. Kelly, and C. H. Mody. 2013. An acidic microenvironment increases NK cell killing of Cryptococcus neoformans and Cryptococcus gattii by enhancing perforin degranulation. *PLoS Pathog* 9: e1003439.
160. Li, S. S., S. K. Kyei, M. Timm-McCann, H. Ogbomo, G. J. Jones, M. Shi, R. F. Xiang, P. Oykhman, S. M. Huston, A. Islam, M. J. Gill, S. M. Robbins, and C. H. Mody. 2013. The NK receptor NKp30 mediates direct fungal recognition and killing and is diminished in NK cells from HIV-infected patients. *Cell Host Microbe* 14: 387-397.
161. Kawakami, K., Y. Kinjo, K. Uezu, S. Yara, K. Miyagi, Y. Koguchi, T. Nakayama, M. Taniguchi, and A. Saito. 2001. Monocyte chemoattractant protein-1-dependent increase of V alpha 14 NKT cells in lungs and their roles in Th1 response and host defense in cryptococcal infection. *J Immunol* 167: 6525-6532.
162. Kawakami, K., Y. Kinjo, S. Yara, Y. Koguchi, K. Uezu, T. Nakayama, M. Taniguchi, and A. Saito. 2001. Activation of Valpha14(+) natural killer T cells by alpha-galactosylceramide results in development of Th1 response and local host resistance in mice infected with Cryptococcus neoformans. *Infect Immun* 69: 213-220.
163. Lim, T. S., and J. W. Murphy. 1980. Transfer of immunity to cryptococcosis by T-enriched splenic lymphocytes from Cryptococcus neoformans-sensitized mice. *Infect Immun* 30: 5-11.
164. Hill, J. O., and K. M. Aguirre. 1994. CD4+ T cell-dependent acquired state of immunity that protects the brain against Cryptococcus neoformans. *J Immunol* 152: 2344-2350.
165. Mody, C. H., M. F. Lipscomb, N. E. Street, and G. B. Toews. 1990. Depletion of CD4+ (L3T4+) lymphocytes in vivo impairs murine host defense to Cryptococcus neoformans. *J Immunol* 144: 1472-1477.
166. Huffnagle, G. B., J. L. Yates, and M. F. Lipscomb. 1991. T cell-mediated immunity in the lung: a Cryptococcus neoformans pulmonary infection model using SCID and athymic nude mice. *Infect Immun* 59: 1423-1433.
167. Huffnagle, G. B., M. F. Lipscomb, J. A. Lovchik, K. A. Hoag, and N. E. Street. 1994. The role of CD4+ and CD8+ T cells in the protective inflammatory response to a pulmonary cryptococcal infection. *J Leukoc Biol* 55: 35-42.
168. Crowe, S. M., J. B. Carlin, K. I. Stewart, C. R. Lucas, and J. F. Hoy. 1991. Predictive value of CD4 lymphocyte numbers for the development of opportunistic infections and malignancies in HIV-infected persons. *J Acquir Immune Defic Syndr* 4: 770-776.
169. Jarvis, J. N., S. D. Lawn, M. Vogt, N. Bangani, R. Wood, and T. S. Harrison. 2009. Screening for cryptococcal antigenemia in patients accessing an antiretroviral treatment program in South Africa. *Clin Infect Dis* 48: 856-862.
170. Lortholary, O., G. Poizat, V. Zeller, S. Neuville, A. Boibieux, M. Alvarez, P. Dellamonica, F. Botterel, F. Dromer, and G. Chene. 2006. Long-term outcome of AIDS-associated cryptococcosis in the era of combination antiretroviral therapy. *Aids* 20: 2183-2191.
171. Zonios, D. I., J. Falloon, C. Y. Huang, D. Chaitt, and J. E. Bennett. 2007. Cryptococcosis and idiopathic CD4 lymphocytopenia. *Medicine (Baltimore)* 86: 78-92.
172. Netea, M. G., A. E. Brouwer, E. H. Hoogendoorn, J. W. Van der Meer, M. Koolen, P. E. Verweij, and B. J. Kullberg. 2004. Two patients with cryptococcal meningitis and idiopathic CD4 lymphopenia: defective cytokine production and reversal by recombinant interferon- gamma therapy. *Clin Infect Dis* 39: e83-87.
173. Jarvis, J. N., J. P. Casazza, H. H. Stone, G. Meintjes, S. D. Lawn, S. M. Levitz, T. S. Harrison, and R. A. Koup. 2013. The phenotype of the Cryptococcus-specific CD4+ memory T-cell response is associated with disease severity and outcome in HIV-associated cryptococcal meningitis. *J Infect Dis* 207: 1817-1828.

174. Bicanic, T., C. Muzoora, A. E. Brouwer, G. Meintjes, N. Longley, K. Taseera, K. Rebe, A. Loyse, J. Jarvis, L. G. Bekker, R. Wood, D. Limmathurotsakul, W. Chierakul, K. Stepniewska, N. J. White, S. Jaffar, and T. S. Harrison. 2009. Independent association between rate of clearance of infection and clinical outcome of HIV-associated cryptococcal meningitis: analysis of a combined cohort of 262 patients. *Clin Infect Dis* 49: 702-709.
175. Siddiqui, A. A., A. E. Brouwer, V. Wuthiekanun, S. Jaffar, R. Shattock, D. Irving, J. Sheldon, W. Chierakul, S. Peacock, N. Day, N. J. White, and T. S. Harrison. 2005. IFN-gamma at the site of infection determines rate of clearance of infection in cryptococcal meningitis. *J Immunol* 174: 1746-1750.
176. Herring, A. C., J. Lee, R. A. McDonald, G. B. Toews, and G. B. Huffnagle. 2002. Induction of interleukin-12 and gamma interferon requires tumor necrosis factor alpha for protective T1-cell-mediated immunity to pulmonary Cryptococcus neoformans infection. *Infect Immun* 70: 2959-2964.
177. Huffnagle, G. B., G. B. Toews, M. D. Burdick, M. B. Boyd, K. S. McAllister, R. A. McDonald, S. L. Kunkel, and R. M. Strieter. 1996. Afferent phase production of TNF-alpha is required for the development of protective T cell immunity to Cryptococcus neoformans. *J Immunol* 157: 4529-4536.
178. Wiesner, D. L., K. D. Smith, D. I. Kotov, J. N. Nielsen, P. R. Bohjanen, and K. Nielsen. 2016. Regulatory T Cell Induction and Retention in the Lungs Drives Suppression of Detrimental Type 2 Th Cells During Pulmonary Cryptococcal Infection. *J Immunol* 196: 365-374.
179. Kleinschek, M. A., U. Muller, S. J. Brodie, W. Stenzel, G. Kohler, W. M. Blumenschein, R. K. Straubinger, T. McClanahan, R. A. Kastelein, and G. Alber. 2006. IL-23 enhances the inflammatory cell response in Cryptococcus neoformans infection and induces a cytokine pattern distinct from IL-12. *J Immunol* 176: 1098-1106.
180. Szymczak, W. A., R. S. Sellers, and L. A. Pirofski. 2012. IL-23 dampens the allergic response to Cryptococcus neoformans through IL-17-independent and -dependent mechanisms. *Am J Pathol* 180: 1547-1559.
181. Hole, C. R., and F. L. Wormley, Jr. 2012. Vaccine and immunotherapeutic approaches for the prevention of cryptococcosis: lessons learned from animal models. *Front Microbiol* 3: 291.
182. van de Veerdonk, F. L., and M. G. Netea. 2010. T-cell Subsets and Antifungal Host Defenses. *Curr Fungal Infect Rep* 4: 238-243.
183. Ma, L. L., J. C. Spurrell, J. F. Wang, G. G. Neely, S. Epelman, A. M. Krensky, and C. H. Mody. 2002. CD8 T cell-mediated killing of Cryptococcus neoformans requires granulysin and is dependent on CD4 T cells and IL-15. *J Immunol* 169: 5787-5795.
184. Mody, C. H., G. H. Chen, C. Jackson, J. L. Curtis, and G. B. Toews. 1994. In vivo depletion of murine CD8 positive T cells impairs survival during infection with a highly virulent strain of Cryptococcus neoformans. *Mycopathologia* 125: 7-17.
185. Lindell, D. M., T. A. Moore, R. A. McDonald, G. B. Toews, and G. B. Huffnagle. 2005. Generation of antifungal effector CD8+ T cells in the absence of CD4+ T cells during Cryptococcus neoformans infection. *J Immunol* 174: 7920-7928.
186. Uezu, K., K. Kawakami, K. Miyagi, Y. Kinjo, T. Kinjo, H. Ishikawa, and A. Saito. 2004. Accumulation of gammadelta T cells in the lungs and their regulatory roles in Th1 response and host defense against pulmonary infection with Cryptococcus neoformans. *J Immunol* 172: 7629-7634.
187. Szymczak, W. A., M. J. Davis, S. K. Lundy, C. Dufaud, M. Olszewski, and L. A. Pirofski. 2013. X-linked immunodeficient mice exhibit enhanced susceptibility to Cryptococcus neoformans Infection. *MBio* 4.
188. Rohatgi, S., and L. A. Pirofski. 2012. Molecular characterization of the early B cell response to pulmonary Cryptococcus neoformans infection. *J Immunol* 189: 5820-5830.

189. Subramaniam, K. S., K. Datta, M. S. Marks, and L. A. Pirofski. 2010. Improved survival of mice deficient in secretory immunoglobulin M following systemic infection with Cryptococcus neoformans. *Infect Immun* 78: 441-452.
190. Rivera, J., O. Zaragoza, and A. Casadevall. 2005. Antibody-mediated protection against Cryptococcus neoformans pulmonary infection is dependent on B cells. *Infect Immun* 73: 1141-1150.
191. Subramaniam, K. S., K. Datta, E. Quintero, C. Manix, M. S. Marks, and L. A. Pirofski. 2010. The absence of serum IgM enhances the susceptibility of mice to pulmonary challenge with Cryptococcus neoformans. *J Immunol* 184: 5755-5767.
192. Haddow, L. J., R. Colebunders, G. Meintjes, S. D. Lawn, J. H. Elliott, Y. C. Manabe, P. R. Bohjanen, S. Sungkanuparph, P. J. Easterbrook, M. A. French, D. R. Boulware, and H. I. V. a. I. International Network for the Study of. 2010. Cryptococcal immune reconstitution inflammatory syndrome in HIV-1-infected individuals: proposed clinical case definitions. *Lancet Infect Dis* 10: 791-802.
193. Boulware, D. R., D. B. Meya, C. Muzoora, M. A. Rolfes, K. Huppler Hullsiek, A. Musubire, K. Taseera, H. W. Nabeta, C. Schutz, D. A. Williams, R. Rajasingham, J. Rhein, F. Thienemann, M. W. Lo, K. Nielsen, T. L. Bergemann, A. Kambugu, Y. C. Manabe, E. N. Janoff, P. R. Bohjanen, G. Meintjes, and C. T. Team. 2014. Timing of antiretroviral therapy after diagnosis of cryptococcal meningitis. *N Engl J Med* 370: 2487-2498.
194. Scriven, J. E., J. Rhein, K. H. Hullsiek, M. von Hohenberg, G. Linder, M. A. Rolfes, D. A. Williams, K. Taseera, D. B. Meya, G. Meintjes, D. R. Boulware, and C. Team. 2015. Early ART After Cryptococcal Meningitis Is Associated With Cerebrospinal Fluid Pleocytosis and Macrophage Activation in a Multisite Randomized Trial. *J Infect Dis* 212: 769-778.
195. Panackal, A. A., S. C. Wuest, Y. C. Lin, T. Wu, N. Zhang, P. Kosa, M. Komori, A. Blake, S. K. Browne, L. B. Rosen, F. Hagen, J. Meis, S. M. Levitz, M. Quezado, D. Hammoud, J. E. Bennett, B. Bielekova, and P. R. Williamson. 2015. Paradoxical Immune Responses in Non-HIV Cryptococcal Meningitis. *PLoS Pathog* 11: e1004884.
196. Williamson, P. R. 2015. Post-infectious inflammatory response syndrome (PIIRS): Dissociation of T-cell-macrophage signaling in previously healthy individuals with cryptococcal fungal meningoencephalitis. *Macrophage (Houst)* 2.
197. Lionakis, M. S. 2012. Genetic Susceptibility to Fungal Infections in Humans. *Curr Fungal Infect Rep* 6: 11-22.
198. Galanis, E., L. Macdougall, S. Kidd, M. Morshed, and G. British Columbia Cryptococcus gattii Working. 2010. Epidemiology of Cryptococcus gattii, British Columbia, Canada, 1999-2007. *Emerg Infect Dis* 16: 251-257.
199. Maskarinec, S. A., M. D. Johnson, and J. R. Perfect. 2016. Genetic Susceptibility to Fungal Infections: What is in the Genes? *Curr Clin Microbiol Rep* 3: 81-91.
200. Krick, J. A. 1981. Familial cryptococcal meningitis. *J Infect Dis* 143: 133.
201. Yinnon, A. M., B. Rudensky, E. Sagi, G. Breuer, C. Brautbar, I. Polacheck, and J. Halevy. 1997. Invasive cryptococcosis in a family with epidermodysplasia verruciformis and idiopathic CD4 cell depletion. *Clin Infect Dis* 25: 1252-1253.
202. Vilchez, R. A., W. Irish, J. Lacomis, P. Costello, J. Fung, and S. Kusne. 2001. The clinical epidemiology of pulmonary cryptococcosis in non-AIDS patients at a tertiary care medical center. *Medicine (Baltimore)* 80: 308-312.
203. Schadt, E. E., S. A. Monks, T. A. Drake, A. J. Lusis, N. Che, V. Colinayo, T. G. Ruff, S. B. Milligan, J. R. Lamb, G. Cavet, P. S. Linsley, M. Mao, R. B. Stoughton, and S. H. Friend. 2003. Genetics of gene expression surveyed in maize, mouse and man. *Nature* 422: 297-302.
204. Mackay, T. F., E. A. Stone, and J. F. Ayroles. 2009. The genetics of quantitative traits: challenges and prospects. *Nat Rev Genet* 10: 565-577.

205. Cookson, W., L. Liang, G. Abecasis, M. Moffatt, and M. Lathrop. 2009. Mapping complex disease traits with global gene expression. *Nat Rev Genet* 10: 184-194.
206. Blackstock, R., and J. W. Murphy. 2004. Age-related resistance of C57BL/6 mice to Cryptococcus neoformans is dependent on maturation of NKT cells. *Infect Immun* 72: 5175-5180.
207. Carroll, S. F., J. C. Loredo Osti, L. Guillot, K. Morgan, and S. T. Qureshi. 2008. Sex differences in the genetic architecture of susceptibility to Cryptococcus neoformans pulmonary infection. *Genes Immun* 9: 536-545.
208. Jirapongsananuruk, O., V. Luangwedchakarn, J. E. Niemela, P. Pacharn, N. Visitsunthorn, C. Thepthai, P. Vichyanond, S. Piboonpocanun, and T. A. Fleisher. 2012. Cryptococcal osteomyelitis in a child with a novel compound mutation of the IL12RB1 gene. *Asian Pac J Allergy Immunol* 30: 79-82.
209. Chen, S., T. Sorrell, G. Nimmo, B. Speed, B. Currie, D. Ellis, D. Marriott, T. Pfeiffer, D. Parr, and K. Byth. 2000. Epidemiology and host- and variety-dependent characteristics of infection due to Cryptococcus neoformans in Australia and New Zealand. Australasian Cryptococcal Study Group. *Clin Infect Dis* 31: 499-508.
210. Marroni, M., E. Pericolini, E. Cenci, F. Bistoni, and A. Vecchiarelli. 2007. Functional defect of natural immune system in an apparent immunocompetent patient with pulmonary cryptococcosis. *J Infect* 54: e5-8.
211. Akinosoglou, K., M. Melachrinou, D. Siagris, E. Koletsis, M. Marangos, C. A. Gogos, and E. E. Solomou. 2014. Good's syndrome and pure white cell aplasia complicated by cryptococcus infection: A case report and review of the literature. *J Clin Immunol* 34: 283-288.
212. Spinner, M. A., L. A. Sanchez, A. P. Hsu, P. A. Shaw, C. S. Zerbe, K. R. Calvo, D. C. Arthur, W. Gu, C. M. Gould, C. C. Brewer, E. W. Cowen, A. F. Freeman, K. N. Olivier, G. Uzel, A. M. Zelazny, J. R. Daub, C. D. Spalding, R. J. Claypool, N. K. Giri, B. P. Alter, E. M. Mace, J. S. Orange, J. Cuellar-Rodriguez, D. D. Hickstein, and S. M. Holland. 2014. GATA2 deficiency: a protean disorder of hematopoiesis, lymphatics, and immunity. *Blood* 123: 809-821.
213. Hajjeh, R. A., M. E. Brandt, and R. W. Pinner. 1995. Emergence of cryptococcal disease: epidemiologic perspectives 100 years after its discovery. *Epidemiol Rev* 17: 303-320.
214. Jo, E. K., H. S. Kim, M. Y. Lee, M. Iseki, J. H. Lee, C. H. Song, J. K. Park, T. J. Hwang, and H. Kook. 2002. X-linked hyper-IgM syndrome associated with Cryptosporidium parvum and Cryptococcus neoformans infections: the first case with molecular diagnosis in Korea. *J Korean Med Sci* 17: 116-120.
215. Malheiro, L., D. Lazzara, S. Xerinda, M. D. Pinheiro, and A. Sarmento. 2014. Cryptococcal meningoencephalitis in a patient with hyper immunoglobulin M (IgM) syndrome: a case report. *BMC Res Notes* 7: 566.
216. Tabone, M. D., G. Leverger, J. Landman, C. Aznar, L. Boccon-Gibod, and G. Lasfargues. 1994. Disseminated lymphonodular cryptococcosis in a child with X-linked hyper-IgM immunodeficiency. *Pediatr Infect Dis J* 13: 77-79.
217. Gupta, S., M. Ellis, T. Cesario, M. Ruhling, and B. Vayuvegula. 1987. Disseminated cryptococcal infection in a patient with hypogammaglobulinemia and normal T cell functions. *Am J Med* 82: 129-131.
218. Winkelstein, J. A., M. C. Marino, H. Ochs, R. Fuleihan, P. R. Scholl, R. Geha, E. R. Stiehm, and M. E. Conley. 2003. The X-linked hyper-IgM syndrome: clinical and immunologic features of 79 patients. *Medicine (Baltimore)* 82: 373-384.
219. Iseki, M., M. Anzo, N. Yamashita, and N. Matsuo. 1994. Hyper-IgM immunodeficiency with disseminated cryptococcosis. *Acta paediatrica* 83: 780-782.
220. Rezai, M. S., G. Khotael, M. Kheirkhah, T. Hedayat, M. Geramishoar, and F. Mahjoub. 2008. Cryptococcosis and deficiency of interleukin12r. *Pediatr Infect Dis J* 27: 673.

221. Van Dam, M. G., R. A. Seaton, and A. J. Hamilton. 1998. Analysis of HLA association in susceptibility to infection with Cryptococcus neoformans var. gattii in a Papua New Guinean population. *Med Mycol* 36: 185-188.
222. Ou, X. T., J. Q. Wu, L. P. Zhu, M. Guan, B. Xu, X. P. Hu, X. Wang, and X. H. Weng. 2011. Genotypes coding for mannose-binding lectin deficiency correlated with cryptococcal meningitis in HIV-uninfected Chinese patients. *J Infect Dis* 203: 1686-1691.
223. Meletiadis, J., T. J. Walsh, E. H. Choi, P. G. Pappas, D. Ennis, J. Douglas, G. A. Pankey, R. A. Larsen, R. J. Hamill, and S. Chanock. 2007. Study of common functional genetic polymorphisms of FCGR2A, 3A and 3B genes and the risk for cryptococcosis in HIV-uninfected patients. *Med Mycol* 45: 513-518.
224. Hu, X. P., J. Q. Wu, L. P. Zhu, X. Wang, B. Xu, R. Y. Wang, X. T. Ou, and X. H. Weng. 2012. Association of Fcgamma receptor IIB polymorphism with cryptococcal meningitis in HIV-uninfected Chinese patients. *PLoS One* 7: e42439.
225. Hu, X. P., R. Y. Wang, X. Wang, Y. H. Cao, Y. Q. Chen, H. Z. Zhao, J. Q. Wu, X. H. Weng, X. H. Gao, R. H. Sun, and L. P. Zhu. 2015. Dectin-2 polymorphism associated with pulmonary cryptococcosis in HIV-uninfected Chinese patients. *Med Mycol* 53: 810-816.
226. Rohatgi, S., S. Gohil, M. H. Kuniholm, H. Schultz, C. Dufaud, K. L. Armour, S. Badri, R. B. Mailliard, and L. A. Pirofski. 2013. Fc gamma receptor 3A polymorphism and risk for HIV-associated cryptococcal disease. *MBio* 4: e00573-00513.
227. (NIAID), N. I. o. A. a. I. D. August 31, 2016. Evaluation and Follow-up of Patients With Cryptococcosis.
228. Peters, L. L., R. F. Robledo, C. J. Bult, G. A. Churchill, B. J. Paigen, and K. L. Svenson. 2007. The mouse as a model for human biology: a resource guide for complex trait analysis. *Nat Rev Genet* 8: 58-69.
229. Lipoldova, M., and P. Demant. 2006. Genetic susceptibility to infectious disease: lessons from mouse models of leishmaniasis. *Nat Rev Genet* 7: 294-305.
230. Williams, E. G., and J. Auwerx. 2015. The Convergence of Systems and Reductionist Approaches in Complex Trait Analysis. *Cell* 162: 23-32.
231. Malo, D., and E. Skamene. 1994. Genetic control of host resistance to infection. *Trends Genet* 10: 365-371.
232. Dietrich, W. F. 2001. Using mouse genetics to understand infectious disease pathogenesis. *Genome Res* 11: 325-331.
233. Buer, J., and R. Balling. 2003. Mice, microbes and models of infection. *Nat Rev Genet* 4: 195-205.
234. Waterston, R. H., K. Lindblad-Toh, E. Birney, J. Rogers, J. F. Abril, P. Agarwal, R. Agarwala, R. Ainscough, M. Alexandersson, P. An, S. E. Antonarakis, J. Attwood, R. Baertsch, J. Bailey, K. Barlow, S. Beck, E. Berry, B. Birren, T. Bloom, P. Bork, M. Botcherby, N. Bray, M. R. Brent, D. G. Brown, S. D. Brown, C. Bult, J. Burton, J. Butler, R. D. Campbell, P. Carninci, S. Cawley, F. Chiaromonte, A. T. Chinwalla, D. M. Church, M. Clamp, C. Clee, F. S. Collins, L. L. Cook, R. R. Copley, A. Coulson, O. Couronne, J. Cuff, V. Curwen, T. Cutts, M. Daly, R. David, J. Davies, K. D. Delehaunty, J. Deri, E. T. Dermitzakis, C. Dewey, N. J. Dickens, M. Diekhans, S. Dodge, I. Dubchak, D. M. Dunn, S. R. Eddy, L. Elnitski, R. D. Emes, P. Eswara, E. Eyras, A. Felsenfeld, G. A. Fewell, P. Flicek, K. Foley, W. N. Frankel, L. A. Fulton, R. S. Fulton, T. S. Furey, D. Gage, R. A. Gibbs, G. Glusman, S. Gnerre, N. Goldman, L. Goodstadt, D. Grafham, T. A. Graves, E. D. Green, S. Gregory, R. Guigo, M. Guyer, R. C. Hardison, D. Haussler, Y. Hayashizaki, L. W. Hillier, A. Hinrichs, W. Hlavina, T. Holzer, F. Hsu, A. Hua, T. Hubbard, A. Hunt, I. Jackson, D. B. Jaffe, L. S. Johnson, M. Jones, T. A. Jones, A. Joy, M. Kamal, E. K. Karlsson, D. Karolchik, A. Kasprzyk, J. Kawai, E. Keibler, C. Kells, W. J. Kent, A. Kirby, D. L. Kolbe, I. Korf, R. S. Kucherlapati, E. J. Kulbokas, D. Kulp, T. Landers, J. P. Leger, S. Leonard, I. Letunic, R. Levine, J. Li, M. Li, C. Lloyd, S. Lucas, B. Ma, D. R.

Maglott, E. R. Mardis, L. Matthews, E. Mauceli, J. H. Mayer, M. McCarthy, W. R. McCombie, S. McLaren, K. McLay, J. D. McPherson, J. Meldrim, B. Meredith, J. P. Mesirov, W. Miller, T. L. Miner, E. Mongin, K. T. Montgomery, M. Morgan, R. Mott, J. C. Mullikin, D. M. Muzny, W. E. Nash, J. O. Nelson, M. N. Nhan, R. Nicol, Z. Ning, C. Nusbaum, M. J. O'Connor, Y. Okazaki, K. Oliver, E. Overton-Larty, L. Pachter, G. Parra, K. H. Pepin, J. Peterson, P. Pevzner, R. Plumb, C. S. Pohl, A. Poliakov, T. C. Ponce, C. P. Ponting, S. Potter, M. Quail, A. Reymond, B. A. Roe, K. M. Roskin, E. M. Rubin, A. G. Rust, R. Santos, V. Sapojnikov, B. Schultz, J. Schultz, M. S. Schwartz, S. Schwartz, C. Scott, S. Seaman, S. Searle, T. Sharpe, A. Sheridan, R. Shownkeen, S. Sims, J. B. Singer, G. Slater, A. Smit, D. R. Smith, B. Spencer, A. Stabenau, N. Stange-Thomann, C. Sugnet, M. Suyama, G. Tesler, J. Thompson, D. Torrents, E. Trevaskis, J. Tromp, C. Ucla, A. Ureta-Vidal, J. P. Vinson, A. C. Von Niederhausern, C. M. Wade, M. Wall, R. J. Weber, R. B. Weiss, M. C. Wendl, A. P. West, K. Wetterstrand, R. Wheeler, S. Whelan, J. Wierzbowski, D. Willey, S. Williams, R. K. Wilson, E. Winter, K. C. Worley, D. Wyman, S. Yang, S. P. Yang, E. M. Zdobnov, M. C. Zody, and E. S. Lander. 2002. Initial sequencing and comparative analysis of the mouse genome. *Nature* 420: 520-562.

235. Bradley, A. 2002. Mining the mouse genome. *Nature* 420: 512-514.
236. Vidal, S. M., D. Malo, J. F. Marquis, and P. Gros. 2008. Forward genetic dissection of immunity to infection in the mouse. *Annu Rev Immunol* 26: 81-132.
237. Gruenheid, S., and P. Gros. 2010. Forward genetic dissection of innate response to infection in inbred mouse strains: selected success stories. *Clin Exp Immunol* 162: 393-401.
238. Justice, M. J., L. D. Siracusa, and A. F. Stewart. 2011. Technical approaches for mouse models of human disease. *Dis Model Mech* 4: 305-310.
239. Rosenthal, N., and S. Brown. 2007. The mouse ascending: perspectives for human-disease models. *Nat Cell Biol* 9: 993-999.
240. Miles, C. W., M. 2008. Quantitative trait locus (QTL) analysis. *Nature Education* 1.
241. Shao, H., D. S. Sinasac, L. C. Burrage, C. A. Hodges, P. J. Supelak, M. R. Palmert, C. Moreno, A. W. Cowley, Jr., H. J. Jacob, and J. H. Nadeau. 2010. Analyzing complex traits with congenic strains. *Mamm Genome* 21: 276-286.
242. Rogner, U. C., and P. Avner. 2008. Use of Congenic Mouse Strains for Candidate Disease Gene Identification in Complex Traits. In *Sourcebook of Models for Biomedical Research*. P. M. Conn, ed. Humana Press, Totowa, NJ. 575-581.
243. Markel, P., P. Shu, C. Ebeling, G. A. Carlson, D. L. Nagle, J. S. Smutko, and K. J. Moore. 1997. Theoretical and empirical issues for marker-assisted breeding of congenic mouse strains. *Nat Genet* 17: 280-284.
244. Rogner, U. C. 2011. Use of Congenic Mouse Strains for Gene Identification in Type 1 Diabetes, Type 1 Diabetes In *Pathogenesis, Genetics and Immunotherapy*. P. D. Wagner, ed.
245. Flint, J., W. Valdar, S. Shifman, and R. Mott. 2005. Strategies for mapping and cloning quantitative trait genes in rodents. *Nat Rev Genet* 6: 271-286.
246. Rogner, U. C., and P. Avner. 2003. Congenic mice: cutting tools for complex immune disorders. *Nat Rev Immunol* 3: 243-252.
247. Rhodes, J. C., L. S. Wicker, and W. J. Urba. 1980. Genetic control of susceptibility to Cryptococcus neoformans in mice. *Infect Immun* 29: 494-499.
248. Marquis, G., S. Montplaisir, M. Pelletier, S. Mousseau, and P. Auger. 1985. Genetic resistance to murine cryptococcosis: increased susceptibility in the CBA/N XID mutant strain of mice. *Infect Immun* 47: 282-287.
249. Lovchik, J. A., J. A. Wilder, G. B. Huffnagle, R. Riblet, C. R. Lyons, and M. F. Lipscomb. 1999. Ig heavy chain complex-linked genes influence the immune response in a murine cryptococcal infection. *J Immunol* 163: 3907-3913.

250. McClelland, E. E., D. L. Granger, and W. K. Potts. 2003. Major histocompatibility complex-dependent susceptibility to Cryptococcus neoformans in mice. *Infect Immun* 71: 4815-4817.
251. Cauley, L. K., and J. W. Murphy. 1979. Response of congenitally athymic (nude) and phenotypically normal mice to Cryptococcus neoformans infection. *Infect Immun* 23: 644-651.
252. Marquis, G., S. Montplaisir, M. Pelletier, S. Mousseau, and P. Auger. 1985. Genetic resistance to murine cryptococcosis: the beige mutation (Chediak-Higashi syndrome) in mice. *Infect Immun* 47: 288-293.
253. Carroll, S. F., E. I. Lafferty, A. Flaczyk, T. M. Fujiwara, R. Homer, K. Morgan, J. C. Loredo-Osti, and S. T. Qureshi. 2012. Susceptibility to progressive Cryptococcus neoformans pulmonary infection is regulated by loci on mouse chromosomes 1 and 9. *Infect Immun* 80: 4167-4176.
254. Yauch, L. E., M. K. Mansour, S. Shoham, J. B. Rottman, and S. M. Levitz. 2004. Involvement of CD14, toll-like receptors 2 and 4, and MyD88 in the host response to the fungal pathogen Cryptococcus neoformans in vivo. *Infect Immun* 72: 5373-5382.
255. Biondo, C., A. Midiri, L. Messina, F. Tomasello, G. Garufi, M. R. Catania, M. Bombaci, C. Beninati, G. Teti, and G. Mancuso. 2005. MyD88 and TLR2, but not TLR4, are required for host defense against Cryptococcus neoformans. *Eur J Immunol* 35: 870-878.
256. Zhang, Y., F. Wang, U. Bhan, G. B. Huffnagle, G. B. Toews, T. J. Standiford, and M. A. Olszewski. 2010. TLR9 signaling is required for generation of the adaptive immune protection in Cryptococcus neoformans-infected lungs. *Am J Pathol* 177: 754-765.
257. Traynor, T. R., W. A. Kuziel, G. B. Toews, and G. B. Huffnagle. 2000. CCR2 expression determines T1 versus T2 polarization during pulmonary Cryptococcus neoformans infection. *J Immunol* 164: 2021-2027.
258. Traynor, T. R., A. C. Herring, M. E. Dorf, W. A. Kuziel, G. B. Toews, and G. B. Huffnagle. 2002. Differential roles of CC chemokine ligand 2/monocyte chemotactic protein-1 and CCR2 in the development of T1 immunity. *J Immunol* 168: 4659-4666.
259. Olszewski, M. A., G. B. Huffnagle, R. A. McDonald, D. M. Lindell, B. B. Moore, D. N. Cook, and G. B. Toews. 2000. The role of macrophage inflammatory protein-1 alpha/CCL3 in regulation of T cell-mediated immunity to Cryptococcus neoformans infection. *J Immunol* 165: 6429-6436.
260. Huffnagle, G. B., L. K. McNeil, R. A. McDonald, J. W. Murphy, G. B. Toews, N. Maeda, and W. A. Kuziel. 1999. Cutting edge: Role of C-C chemokine receptor 5 in organ-specific and innate immunity to Cryptococcus neoformans. *J Immunol* 163: 4642-4646.
261. Zhou, Q., R. A. Gault, T. R. Kozel, and W. J. Murphy. 2007. Protection from direct cerebral cryptococcus infection by interferon-gamma-dependent activation of microglial cells. *J Immunol* 178: 5753-5761.
262. Chen, G. H., R. A. McDonald, J. C. Wells, G. B. Huffnagle, N. W. Lukacs, and G. B. Toews. 2005. The gamma interferon receptor is required for the protective pulmonary inflammatory response to Cryptococcus neoformans. *Infect Immun* 73: 1788-1796.
263. Decken, K., G. Kohler, K. Palmer-Lehmann, A. Wunderlin, F. Mattner, J. Magram, M. K. Gately, and G. Alber. 1998. Interleukin-12 is essential for a protective Th1 response in mice infected with Cryptococcus neoformans. *Infect Immun* 66: 4994-5000.
264. Wang, J. P., C. K. Lee, A. Akalin, R. W. Finberg, and S. M. Levitz. 2011. Contributions of the MyD88-dependent receptors IL-18R, IL-1R, and TLR9 to host defenses following pulmonary challenge with Cryptococcus neoformans. *PLoS One* 6: e26232.
265. Rayhane, N., O. Lortholary, C. Fitting, J. Callebert, M. Huerre, F. Dromer, and J. M. Cavaillon. 1999. Enhanced sensitivity of tumor necrosis factor/lymphotoxin-alpha-deficient mice to Cryptococcus neoformans infection despite increased levels of nitrite/nitrate, interferon-gamma, and interleukin-12. *J Infect Dis* 180: 1637-1647.

266. Hernandez, Y., S. Arora, J. R. Erb-Downward, R. A. McDonald, G. B. Toews, and G. B. Huffnagle. 2005. Distinct roles for IL-4 and IL-10 in regulating T2 immunity during allergic bronchopulmonary mycosis. *J Immunol* 174: 1027-1036.
267. Blackstock, R., and J. W. Murphy. 2004. Role of interleukin-4 in resistance to Cryptococcus neoformans infection. *Am J Respir Cell Mol Biol* 30: 109-117.
268. Grahnert, A., T. Richter, D. Piehler, M. Eschke, B. Schulze, U. Muller, M. Protschka, G. Kohler, R. Sabat, F. Brombacher, and G. Alber. 2014. IL-4 receptor-alpha-dependent control of Cryptococcus neoformans in the early phase of pulmonary infection. *PLoS One* 9: e87341.
269. Murdock, B. J., G. B. Huffnagle, M. A. Olszewski, and J. J. Osterholzer. 2014. Interleukin-17A enhances host defense against cryptococcal lung infection through effects mediated by leukocyte recruitment, activation, and gamma interferon production. *Infect Immun* 82: 937-948.
270. Leopold Wager, C. M., C. R. Hole, K. L. Wozniak, M. A. Olszewski, and F. L. Wormley, Jr. 2014. STAT1 signaling is essential for protection against Cryptococcus neoformans infection in mice. *J Immunol* 193: 4060-4071.
271. Leopold Wager, C. M., C. R. Hole, K. L. Wozniak, M. A. Olszewski, M. Mueller, and F. L. Wormley, Jr. 2015. STAT1 signaling within macrophages is required for antifungal activity against Cryptococcus neoformans. *Infect Immun* 83: 4513-4527.
272. Qiu, Y., J. K. Dayrit, M. J. Davis, J. F. Carolan, J. J. Osterholzer, J. L. Curtis, and M. A. Olszewski. 2013. Scavenger receptor A modulates the immune response to pulmonary Cryptococcus neoformans infection. *J Immunol* 191: 238-248.
273. Nakamura, Y., K. Sato, H. Yamamoto, K. Matsumura, I. Matsumoto, T. Nomura, T. Miyasaka, K. Ishii, E. Kanno, M. Tachi, S. Yamasaki, S. Saijo, Y. Iwakura, and K. Kawakami. 2015. Dectin-2 deficiency promotes Th2 response and mucin production in the lungs after pulmonary infection with Cryptococcus neoformans. *Infect Immun* 83: 671-681.
274. Geunes-Boyer, S., M. F. Beers, J. R. Perfect, J. Heitman, and J. R. Wright. 2012. Surfactant protein D facilitates Cryptococcus neoformans infection. *Infect Immun* 80: 2444-2453.
275. Flaczyk, A., C. U. Duerr, M. Shourian, E. I. Lafferty, J. H. Fritz, and S. T. Qureshi. 2013. IL-33 signaling regulates innate and adaptive immunity to Cryptococcus neoformans. *J Immunol* 191: 2503-2513.
276. Piehler, D., A. Grahnert, M. Eschke, T. Richter, G. Kohler, W. Stenzel, and G. Alber. 2013. T1/ST2 promotes T helper 2 cell activation and polyfunctionality in bronchopulmonary mycosis. *Mucosal Immunol* 6: 405-414.
277. Mershon, K. L., A. Vasuthasawat, G. W. Lawson, S. L. Morrison, and D. O. Beenhouwer. 2009. Role of complement in protection against Cryptococcus gattii infection. *Infect Immun* 77: 1061-1070.
278. Mitchell, T. G., and J. R. Perfect. 1995. Cryptococcosis in the era of AIDS--100 years after the discovery of Cryptococcus neoformans. *Clin Microbiol Rev* 8: 515-548.
279. Li, S. S., and C. H. Mody. 2010. Cryptococcus. *Proceedings of the American Thoracic Society* 7: 186-196.
280. Brizendine, K. D., J. W. Baddley, and P. G. Pappas. 2013. Predictors of mortality and differences in clinical features among patients with Cryptococcosis according to immune status. *PLoS One* 8: e60431.
281. Pyrgos, V., A. E. Seitz, C. A. Steiner, D. R. Prevots, and P. R. Williamson. 2013. Epidemiology of cryptococcal meningitis in the US: 1997-2009. *PLoS One* 8: e56269.
282. Rhodes, J. C. 1985. Contribution of complement component C5 to the pathogenesis of experimental murine cryptococcosis. *Sabouraudia* 23: 225-234.

283. Segre, J. A., J. L. Nemhauser, B. A. Taylor, J. H. Nadeau, and E. S. Lander. 1995. Positional cloning of the nude locus: genetic, physical, and transcription maps of the region and mutations in the mouse and rat. *Genomics* 28: 549-559.
284. Arora, S., and G. B. Huffnagle. 2005. Immune regulation during allergic bronchopulmonary mycosis: lessons taught by two fungi. *Immunologic research* 33: 53-68.
285. Wozniak, K. L., S. Hardison, M. Olszewski, and F. L. Wormley, Jr. 2012. Induction of protective immunity against cryptococcosis. *Mycopathologia* 173: 387-394.
286. Gibson, J. F., and S. A. Johnston. 2014. Immunity to Cryptococcus neoformans and C. gattii during cryptococcosis. *Fungal Genet Biol*.
287. Levitz, S. M. 1994. Macrophage-Cryptococcus interactions. *Immunology series* 60: 533-543.
288. Bauman, S. K., G. B. Huffnagle, and J. W. Murphy. 2003. Effects of tumor necrosis factor alpha on dendritic cell accumulation in lymph nodes draining the immunization site and the impact on the anticryptococcal cell-mediated immune response. *Infect Immun* 71: 68-74.
289. Hoag, K. A., M. F. Lipscomb, A. A. Izzo, and N. E. Street. 1997. IL-12 and IFN-gamma are required for initiating the protective Th1 response to pulmonary cryptococcosis in resistant C.B-17 mice. *Am J Respir Cell Mol Biol* 17: 733-739.
290. Romani, L. 2011. Immunity to fungal infections. *Nat Rev Immunol* 11: 275-288.
291. Chen, G. H., D. A. McNamara, Y. Hernandez, G. B. Huffnagle, G. B. Toews, and M. A. Olszewski. 2008. Inheritance of immune polarization patterns is linked to resistance versus susceptibility to Cryptococcus neoformans in a mouse model. *Infect Immun* 76: 2379-2391.
292. Arora, S., Y. Hernandez, J. R. Erb-Downward, R. A. McDonald, G. B. Toews, and G. B. Huffnagle. 2005. Role of IFN-gamma in regulating T2 immunity and the development of alternatively activated macrophages during allergic bronchopulmonary mycosis. *J Immunol* 174: 6346-6356.
293. Kawakami, K., M. Tohyama, K. Teruya, N. Kudeken, Q. Xie, and A. Saito. 1996. Contribution of interferon-gamma in protecting mice during pulmonary and disseminated infection with Cryptococcus neoformans. *FEMS Immunol Med Microbiol* 13: 123-130.
294. Zhang, Y., F. Wang, K. C. Tompkins, A. McNamara, A. V. Jain, B. B. Moore, G. B. Toews, G. B. Huffnagle, and M. A. Olszewski. 2009. Robust Th1 and Th17 immunity supports pulmonary clearance but cannot prevent systemic dissemination of highly virulent Cryptococcus neoformans H99. *Am J Pathol* 175: 2489-2500.
295. Hidore, M. R., N. Nabavi, C. W. Reynolds, P. A. Henkart, and J. W. Murphy. 1990. Cytoplasmic components of natural killer cells limit the growth of Cryptococcus neoformans. *J Leukoc Biol* 48: 15-26.
296. Osterholzer, J. J., G. H. Chen, M. A. Olszewski, Y. M. Zhang, J. L. Curtis, G. B. Huffnagle, and G. B. Toews. 2011. Chemokine receptor 2-mediated accumulation of fungicidal exudate macrophages in mice that clear cryptococcal lung infection. *Am J Pathol* 178: 198-211.
297. Hardison, S. E., S. Ravi, K. L. Wozniak, M. L. Young, M. A. Olszewski, and F. L. Wormley, Jr. 2010. Pulmonary infection with an interferon-gamma-producing Cryptococcus neoformans strain results in classical macrophage activation and protection. *Am J Pathol* 176: 774-785.
298. Jain, A. V., Y. Zhang, W. B. Fields, D. A. McNamara, M. Y. Choe, G. H. Chen, J. Erb-Downward, J. J. Osterholzer, G. B. Toews, G. B. Huffnagle, and M. A. Olszewski. 2009. Th2 but not Th1 immune bias results in altered lung functions in a murine model of pulmonary Cryptococcus neoformans infection. *Infect Immun* 77: 5389-5399.
299. Guo, L., R. S. Johnson, and J. C. Schuh. 2000. Biochemical characterization of endogenously formed eosinophilic crystals in the lungs of mice. *J Biol Chem* 275: 8032-8037.
300. Drinkwater, N. R., and M. N. Gould. 2012. The long path from QTL to gene. *PLoS genetics* 8: e1002975.

301. Feldmesser, M., Y. Kress, and A. Casadevall. 1998. Effect of antibody to capsular polysaccharide on eosinophilic pneumonia in murine infection with Cryptococcus neoformans. *J Infect Dis* 177: 1639-1646.
302. Lovchik, J., M. Lipscomb, and C. R. Lyons. 1997. Expression of lung inducible nitric oxide synthase protein does not correlate with nitric oxide production in vivo in a pulmonary immune response against Cryptococcus neoformans. *J Immunol* 158: 1772-1778.
303. Guilliams, M., B. N. Lambrecht, and H. Hammad. 2013. Division of labor between lung dendritic cells and macrophages in the defense against pulmonary infections. *Mucosal Immunol* 6: 464-473.
304. Del Poeta, M., and A. Casadevall. 2012. Ten challenges on Cryptococcus and cryptococcosis. *Mycopathologia* 173: 303-310.
305. Yang, Y., and P. Santamaria. 2006. Lessons on autoimmune diabetes from animal models. *Clinical science* 110: 627-639.
306. Nadeau, J. H. 2001. Modifier genes in mice and humans. *Nat Rev Genet* 2: 165-174.
307. Liu, T. B., D. S. Perlin, and C. Xue. 2012. Molecular mechanisms of cryptococcal meningitis. *Virulence* 3: 173-181.
308. Shao, X., A. Mednick, M. Alvarez, N. van Rooijen, A. Casadevall, and D. L. Goldman. 2005. An innate immune system cell is a major determinant of species-related susceptibility differences to fungal pneumonia. *J Immunol* 175: 3244-3251.
309. Price, M. S., and J. R. Perfect. 2011. Host defenses against cryptococcosis. *Immunological investigations* 40: 786-808.
310. Diamond, R. D., R. K. Root, and J. E. Bennett. 1972. Factors influencing killing of Cryptococcus neoformans by human leukocytes in vitro. *J Infect Dis* 125: 367-376.
311. Qiu, Y., S. Zeltzer, Y. Zhang, F. Wang, G. H. Chen, J. Dayrit, B. J. Murdock, U. Bhan, G. B. Toews, J. J. Osterholzer, T. J. Standiford, and M. A. Olszewski. 2012. Early induction of CCL7 downstream of TLR9 signaling promotes the development of robust immunity to cryptococcal infection. *J Immunol* 188: 3940-3948.
312. Hardison, S. E., G. Herrera, M. L. Young, C. R. Hole, K. L. Wozniak, and F. L. Wormley, Jr. 2012. Protective immunity against pulmonary cryptococcosis is associated with STAT1-mediated classical macrophage activation. *J Immunol* 189: 4060-4068.
313. He, W., A. Casadevall, S. C. Lee, and D. L. Goldman. 2003. Phagocytic activity and monocyte chemotactic protein expression by pulmonary macrophages in persistent pulmonary cryptococcosis. *Infect Immun* 71: 930-936.
314. Lindell, D. M., M. N. Ballinger, R. A. McDonald, G. B. Toews, and G. B. Huffnagle. 2006. Diversity of the T-cell response to pulmonary Cryptococcus neoformans infection. *Infect Immun* 74: 4538-4548.
315. Rivera, J., and A. Casadevall. 2005. Mouse genetic background is a major determinant of isotype-related differences for antibody-mediated protective efficacy against Cryptococcus neoformans. *J Immunol* 174: 8017-8026.
316. Zaragoza, O., M. Alvarez, A. Telzak, J. Rivera, and A. Casadevall. 2007. The relative susceptibility of mouse strains to pulmonary Cryptococcus neoformans infection is associated with pleiotropic differences in the immune response. *Infect Immun* 75: 2729-2739.
317. Cooper, G. M., and J. Shendure. 2011. Needles in stacks of needles: finding disease-causal variants in a wealth of genomic data. *Nat Rev Genet* 12: 628-640.
318. Shen, Y., F. Yue, D. F. McCleary, Z. Ye, L. Edsall, S. Kuan, U. Wagner, J. Dixon, L. Lee, V. V. Lobanenkov, and B. Ren. 2012. A map of the cis-regulatory sequences in the mouse genome. *Nature* 488: 116-120.
319. Morris, K. V., and J. S. Mattick. 2014. The rise of regulatory RNA. *Nat Rev Genet* 15: 423-437.

320. Pai, A. A., J. K. Pritchard, and Y. Gilad. 2015. The genetic and mechanistic basis for variation in gene regulation. *PLoS genetics* 11: e1004857.
321. Shourian, M., A. Flaczyk, I. Angers, B. C. Mindt, J. H. Fritz, and S. T. Qureshi. 2015. The Cnes2 locus on mouse chromosome 17 regulates host defense against cryptococcal infection through pleiotropic effects on host immunity. *Infect Immun* 83: 4541-4554.
322. DiPetrillo, K., X. Wang, I. M. Stylianou, and B. Paigen. 2005. Bioinformatics toolbox for narrowing rodent quantitative trait loci. *Trends Genet* 21: 683-692.
323. Abiola, O., J. M. Angel, P. Avner, A. A. Bachmanov, J. K. Belknap, B. Bennett, E. P. Blankenhorn, D. A. Blizard, V. Bolivar, G. A. Brockmann, K. J. Buck, J. F. Bureau, W. L. Casley, E. J. Chesler, J. M. Cheverud, G. A. Churchill, M. Cook, J. C. Crabbe, W. E. Crusio, A. Darvasi, G. de Haan, P. Dermant, R. W. Doerge, R. W. Elliot, C. R. Farber, L. Flaherty, J. Flint, H. Gershenfeld, J. P. Gibson, J. Gu, W. Gu, H. Himmelbauer, R. Hitzemann, H. C. Hsu, K. Hunter, F. F. Iraqi, R. C. Jansen, T. E. Johnson, B. C. Jones, G. Kempermann, F. Lammert, L. Lu, K. F. Manly, D. B. Matthews, J. F. Medrano, M. Mehrabian, G. Mittlemann, B. A. Mock, J. S. Mogil, X. Montagutelli, G. Morahan, J. D. Mountz, H. Nagase, R. S. Nowakowski, B. F. O'Hara, A. V. Osadchuk, B. Paigen, A. A. Palmer, J. L. Peirce, D. Pomp, M. Rosemann, G. D. Rosen, L. C. Schalkwyk, Z. Seltzer, S. Settle, K. Shimomura, S. Shou, J. M. Sikela, L. D. Siracusa, J. L. Spearow, C. Teuscher, D. W. Threadgill, L. A. Toth, A. A. Toye, C. Vadasz, G. Van Zant, E. Wakeland, R. W. Williams, H. G. Zhang, F. Zou, and C. Complex Trait. 2003. The nature and identification of quantitative trait loci: a community's view. *Nat Rev Genet* 4: 911-916.
324. Kumar, P., S. Henikoff, and P. C. Ng. 2009. Predicting the effects of coding non-synonymous variants on protein function using the SIFT algorithm. *Nat Protoc* 4: 1073-1081.
325. AVNER, U. C. R. A. P. 2008. Use of Congenic Mouse Strains for Candidate Disease Gene Identification in Complex Traits. In *Sourcebook of Models for Biomedical Research*. P. M. E. Conn, ed.
326. Pirofski, L. A., and A. Casadevall. 2008. The damage-response framework of microbial pathogenesis and infectious diseases. *Adv Exp Med Biol* 635: 135-146.
327. Casadevall, A., and L. A. Pirofski. 2014. Microbiology: Ditch the term pathogen. *Nature* 516: 165-166.
328. Lin, K. L., Y. Suzuki, H. Nakano, E. Ramsburg, and M. D. Gunn. 2008. CCR2+ monocyte-derived dendritic cells and exudate macrophages produce influenza-induced pulmonary immune pathology and mortality. *J Immunol* 180: 2562-2572.
329. Moore, B. B., R. Paine, 3rd, P. J. Christensen, T. A. Moore, S. Sitterding, R. Ngan, C. A. Wilke, W. A. Kuziel, and G. B. Toews. 2001. Protection from pulmonary fibrosis in the absence of CCR2 signaling. *J Immunol* 167: 4368-4377.
330. Osterholzer, J. J., M. A. Olszewski, B. J. Murdock, G. H. Chen, J. R. Erb-Downward, N. Subbotina, K. Browning, Y. Lin, R. E. Morey, J. K. Dayrit, J. C. Horowitz, R. H. Simon, and T. H. Sisson. 2013. Implicating exudate macrophages and Ly-6C(high) monocytes in CCR2-dependent lung fibrosis following gene-targeted alveolar injury. *J Immunol* 190: 3447-3457.
331. Kechichian, T. B., J. Shea, and M. Del Poeta. 2007. Depletion of alveolar macrophages decreases the dissemination of a glucosylceramide-deficient mutant of Cryptococcus neoformans in immunodeficient mice. *Infect Immun* 75: 4792-4798.
332. Casadevall, A. 2010. Cryptococci at the brain gate: break and enter or use a Trojan horse? *J Clin Invest* 120: 1389-1392.
333. Santangelo, R., H. Zoellner, T. Sorrell, C. Wilson, C. Donald, J. Djordjevic, Y. Shounan, and L. Wright. 2004. Role of extracellular phospholipases and mononuclear phagocytes in dissemination of cryptococcosis in a murine model. *Infect Immun* 72: 2229-2239.

334. Netea, M. G. 2013. Toward identification of the genetic risk profile for cryptococcal disease in HIV-infected patients. *MBio* 4: e00798-00713.
335. Panackal, A. A., K. C. Williamson, D. van de Beek, D. R. Boulware, and P. R. Williamson. 2016. Fighting the Monster: Applying the Host Damage Framework to Human Central Nervous System Infections. *MBio* 7: e01906-01915.
336. Casadevall, A., and L. A. Pirofski. 2003. The damage-response framework of microbial pathogenesis. *Nat Rev Microbiol* 1: 17-24.
337. Sauna, Z. E., and C. Kimchi-Sarfaty. 2011. Understanding the contribution of synonymous mutations to human disease. *Nat Rev Genet* 12: 683-691.
338. Glazier, A. M., J. H. Nadeau, and T. J. Aitman. 2002. Finding genes that underlie complex traits. *Science* 298: 2345-2349.
339. Neofytos, D., J. A. Fishman, D. Horn, E. Anaissie, C. H. Chang, A. Olyaei, M. Pfaller, W. J. Steinbach, K. M. Webster, and K. A. Marr. 2010. Epidemiology and outcome of invasive fungal infections in solid organ transplant recipients. *Transpl Infect Dis* 12: 220-229.
340. Koguchi, Y., and K. Kawakami. 2002. Cryptococcal infection and Th1-Th2 cytokine balance. *Int Rev Immunol* 21: 423-438.
341. Hoag, K. A., N. E. Street, G. B. Huffnagle, and M. F. Lipscomb. 1995. Early cytokine production in pulmonary Cryptococcus neoformans infections distinguishes susceptible and resistant mice. *Am J Respir Cell Mol Biol* 13: 487-495.
342. Kawakami, K., M. H. Qureshi, T. Zhang, Y. Koguchi, K. Shibuya, S. Naoe, and A. Saito. 1999. Interferon-gamma (IFN-gamma)-dependent protection and synthesis of chemoattractants for mononuclear leucocytes caused by IL-12 in the lungs of mice infected with Cryptococcus neoformans. *Clin Exp Immunol* 117: 113-122.
343. Pietrella, D., P. Lupo, F. Bistoni, and A. Vecchiarelli. 2004. An early imbalance of interleukin 12 influences the adjuvant effect of mannoproteins of Cryptococcus neoformans. *Cell Microbiol* 6: 883-891.
344. Muller, U., W. Stenzel, G. Kohler, C. Werner, T. Polte, G. Hansen, N. Schutze, R. K. Straubinger, M. Blessing, A. N. McKenzie, F. Brombacher, and G. Alber. 2007. IL-13 induces disease-promoting type 2 cytokines, alternatively activated macrophages and allergic inflammation during pulmonary infection of mice with Cryptococcus neoformans. *J Immunol* 179: 5367-5377.
345. Valdez, P. A., P. J. Vithayathil, B. M. Janelsins, A. L. Shaffer, P. R. Williamson, and S. K. Datta. 2012. Prostaglandin E2 suppresses antifungal immunity by inhibiting interferon regulatory factor 4 function and interleukin-17 expression in T cells. *Immunity* 36: 668-679.
346. Kleinschek, M. A., U. Muller, N. Schutze, R. Sabat, R. K. Straubinger, W. M. Blumenschein, T. McClanahan, R. A. Kastelein, and G. Alber. 2010. Administration of IL-23 engages innate and adaptive immune mechanisms during fungal infection. *Int Immunol* 22: 81-90.
347. Vecchiarelli, A., C. Retini, D. Pietrella, C. Monari, C. Tascini, T. Beccari, and T. R. Kozel. 1995. Downregulation by cryptococcal polysaccharide of tumor necrosis factor alpha and interleukin-1 beta secretion from human monocytes. *Infect Immun* 63: 2919-2923.
348. Retini, C., A. Vecchiarelli, C. Monari, C. Tascini, F. Bistoni, and T. R. Kozel. 1996. Capsular polysaccharide of Cryptococcus neoformans induces proinflammatory cytokine release by human neutrophils. *Infect Immun* 64: 2897-2903.
349. Delfino, D., L. Cianci, E. Lupis, A. Celeste, M. L. Petrelli, F. Curro, V. Cusumano, and G. Teti. 1997. Interleukin-6 production by human monocytes stimulated with Cryptococcus neoformans components. *Infect Immun* 65: 2454-2456.
350. Levitz, S. M., A. Tabuni, H. Kornfeld, C. C. Reardon, and D. T. Golenbock. 1994. Production of tumor necrosis factor alpha in human leukocytes stimulated by Cryptococcus neoformans. *Infect Immun* 62: 1975-1981.

351. Vecchiarelli, A., C. Retini, C. Monari, C. Tascini, F. Bistoni, and T. R. Kozel. 1996. Purified capsular polysaccharide of Cryptococcus neoformans induces interleukin-10 secretion by human monocytes. *Infect Immun* 64: 2846-2849.
352. Schoffelen, T., M. T. Illnait-Zaragozi, L. A. Joosten, M. G. Netea, T. Boekhout, J. F. Meis, and T. Sprong. 2013. Cryptococcus gattii induces a cytokine pattern that is distinct from other cryptococcal species. *PLoS One* 8: e55579.
353. Chen, M., Y. Xing, A. Lu, W. Fang, B. Sun, C. Chen, W. Liao, and G. Meng. 2015. Internalized Cryptococcus neoformans Activates the Canonical Caspase-1 and the Noncanonical Caspase-8 Inflammasomes. *J Immunol* 195: 4962-4972.
354. Guillot, L., S. F. Carroll, R. Homer, and S. T. Qureshi. 2008. Enhanced innate immune responsiveness to pulmonary Cryptococcus neoformans infection is associated with resistance to progressive infection. *Infect Immun* 76: 4745-4756.
355. Upadhya, R., W. C. Lam, B. Maybruck, C. A. Specht, S. M. Levitz, and J. K. Lodge. 2016. Induction of Protective Immunity to Cryptococcal Infection in Mice by a Heat-Killed, Chitosan-Deficient Strain of Cryptococcus neoformans. *MBio* 7.
356. Uicker, W. C., H. A. Doyle, J. P. McCracken, M. Langlois, and K. L. Buchanan. 2005. Cytokine and chemokine expression in the central nervous system associated with protective cell-mediated immunity against Cryptococcus neoformans. *Med Mycol* 43: 27-38.
357. Lei, G., M. Chen, H. Li, J. L. Niu, S. Wu, L. Mao, A. Lu, H. Wang, W. Chen, B. Xu, Q. Leng, C. Xu, G. Yang, L. An, L. P. Zhu, and G. Meng. 2013. Biofilm from a clinical strain of Cryptococcus neoformans activates the NLRP3 inflammasome. *Cell Res* 23: 965-968.
358. Sica, A., and A. Mantovani. 2012. Macrophage plasticity and polarization: in vivo veritas. *J Clin Invest* 122: 787-795.
359. Murray, P. J., J. E. Allen, S. K. Biswas, E. A. Fisher, D. W. Gilroy, S. Goerdt, S. Gordon, J. A. Hamilton, L. B. Ivashkiv, T. Lawrence, M. Locati, A. Mantovani, F. O. Martinez, J. L. Mege, D. M. Mosser, G. Natoli, J. P. Saeij, J. L. Schultze, K. A. Shirey, A. Sica, J. Suttles, I. Udalova, J. A. van Ginderachter, S. N. Vogel, and T. A. Wynn. 2014. Macrophage activation and polarization: nomenclature and experimental guidelines. *Immunity* 41: 14-20.
360. Veldhoen, M. 2017. Interleukin 17 is a chief orchestrator of immunity. *Nat Immunol* 18: 612-621.
361. Underhill, D. M., and E. Pearlman. 2015. Immune Interactions with Pathogenic and Commensal Fungi: A Two-Way Street. *Immunity* 43: 845-858.
362. Olszewski, M. A., Y. Zhang, and G. B. Huffnagle. 2010. Mechanisms of cryptococcal virulence and persistence. *Future Microbiol* 5: 1269-1288.
363. Montone, K. T. 2009. Regulating the T-cell immune response toward the H99 strain of Cryptococcus neoformans. *Am J Pathol* 175: 2255-2256.
364. Blasi, E., R. Barluzzi, R. Mazzolla, L. Pitzurra, M. Puliti, S. Saleppico, and F. Bistoni. 1995. Biomolecular events involved in anticryptococcal resistance in the brain. *Infect Immun* 63: 1218-1222.
365. Maffei, C. M., L. F. Mirels, R. A. Sobel, K. V. Clemons, and D. A. Stevens. 2004. Cytokine and inducible nitric oxide synthase mRNA expression during experimental murine cryptococcal meningoencephalitis. *Infect Immun* 72: 2338-2349.
366. Garlanda, C., C. A. Dinarello, and A. Mantovani. 2013. The interleukin-1 family: back to the future. *Immunity* 39: 1003-1018.
367. Weber, A., P. Wasiliew, and M. Kracht. 2010. Interleukin-1 (IL-1) pathway. *Sci Signal* 3: cm1.
368. Casanova, J. L., L. Abel, and L. Quintana-Murci. 2011. Human TLRs and IL-1Rs in host defense: natural insights from evolutionary, epidemiological, and clinical genetics. *Annu Rev Immunol* 29: 447-491.

369. O'Neill, L. A., and C. A. Dinarello. 2000. The IL-1 receptor/toll-like receptor superfamily: crucial receptors for inflammation and host defense. *Immunol Today* 21: 206-209.
370. Bethea, J. R., G. Y. Gillespie, and E. N. Benveniste. 1992. Interleukin-1 beta induction of TNF-alpha gene expression: involvement of protein kinase C. *J Cell Physiol* 152: 264-273.
371. Dinarello, C. A. 2001. Anti-cytokine therapies in response to systemic infection. *J Investig Dermatol Symp Proc* 6: 244-250.
372. Saperstein, S., L. Chen, D. Oakes, G. Pryhuber, and J. Finkelstein. 2009. IL-1beta augments TNF-alpha-mediated inflammatory responses from lung epithelial cells. *J Interferon Cytokine Res* 29: 273-284.
373. Kawakami, K., X. Qifeng, M. Tohyama, M. H. Qureshi, and A. Saito. 1996. Contribution of tumour necrosis factor-alpha (TNF-alpha) in host defence mechanism against Cryptococcus neoformans. *Clin Exp Immunol* 106: 468-474.
374. Milam, J. E., A. C. Herring-Palmer, R. Pandrangi, R. A. McDonald, G. B. Huffnagle, and G. B. Toews. 2007. Modulation of the pulmonary type 2 T-cell response to Cryptococcus neoformans by intratracheal delivery of a tumor necrosis factor alpha-expressing adenoviral vector. *Infect Immun* 75: 4951-4958.
375. Xu, J., A. J. Eastman, A. Flaczyk, L. M. Neal, G. Zhao, J. Carolan, A. N. Malachowski, V. R. Stolberg, M. Yosri, S. W. Chensue, J. L. Curtis, J. J. Osterholzer, and M. A. Olszewski. 2016. Disruption of Early Tumor Necrosis Factor Alpha Signaling Prevents Classical Activation of Dendritic Cells in Lung-Associated Lymph Nodes and Development of Protective Immunity against Cryptococcal Infection. *MBio* 7.
376. Leopold Wager, C. M., and F. L. Wormley, Jr. 2015. Is Development of a Vaccine against Cryptococcus neoformans Feasible? *PLoS Pathog* 11: e1004843.
377. Siegemund, S., and G. Alber. 2008. Cryptococcus neoformans activates bone marrow-derived conventional dendritic cells rather than plasmacytoid dendritic cells and down-regulates macrophages. *FEMS Immunol Med Microbiol* 52: 417-427.
378. Pang, I. K., T. Ichinohe, and A. Iwasaki. 2013. IL-1R signaling in dendritic cells replaces pattern-recognition receptors in promoting CD8(+) T cell responses to influenza A virus. *Nat Immunol* 14: 246-253.
379. Dinarello, C. A. 2009. Immunological and inflammatory functions of the interleukin-1 family. *Annu Rev Immunol* 27: 519-550.
380. Lee, P. Y., Y. Kumagai, Y. Xu, Y. Li, T. Barker, C. Liu, E. S. Sobel, O. Takeuchi, S. Akira, M. Satoh, and W. H. Reeves. 2011. IL-1alpha modulates neutrophil recruitment in chronic inflammation induced by hydrocarbon oil. *J Immunol* 186: 1747-1754.
381. Schmitz, N., M. Kurrer, M. F. Bachmann, and M. Kopf. 2005. Interleukin-1 is responsible for acute lung immunopathology but increases survival of respiratory influenza virus infection. *J Virol* 79: 6441-6448.
382. Mascarenhas, D. P., M. S. Pereira, G. Z. Manin, J. I. Hori, and D. S. Zamboni. 2015. Interleukin 1 receptor-driven neutrophil recruitment accounts to MyD88-dependent pulmonary clearance of legionella pneumophila infection in vivo. *J Infect Dis* 211: 322-330.
383. Barry, K. C., M. F. Fontana, J. L. Portman, A. S. Dugan, and R. E. Vance. 2013. IL-1alpha signaling initiates the inflammatory response to virulent Legionella pneumophila in vivo. *J Immunol* 190: 6329-6339.
384. Biondo, C., G. Mancuso, A. Midiri, G. Signorino, M. Domina, V. Lanza Cariccio, M. Venza, I. Venza, G. Teti, and C. Beninati. 2014. Essential role of interleukin-1 signaling in host defenses against group B streptococcus. *MBio* 5: e01428-01414.
385. Lee, Y. S., H. Yang, J. Y. Yang, Y. Kim, S. H. Lee, J. H. Kim, Y. J. Jang, B. A. Vallance, and M. N. Kweon. 2015. Interleukin-1 (IL-1) signaling in intestinal stromal cells controls KC/ CXCL1

secretion, which correlates with recruitment of IL-22- secreting neutrophils at early stages of Citrobacter rodentium infection. *Infect Immun* 83: 3257-3267.
386. Altmeier, S., A. Toska, F. Sparber, A. Teijeira, C. Halin, and S. LeibundGut-Landmann. 2016. IL-1 Coordinates the Neutrophil Response to C. albicans in the Oral Mucosa. *PLoS Pathog* 12: e1005882.
387. Mantovani, A., M. A. Cassatella, C. Costantini, and S. Jaillon. 2011. Neutrophils in the activation and regulation of innate and adaptive immunity. *Nat Rev Immunol* 11: 519-531.
388. Wiesner, D. L., K. D. Smith, S. W. Kashem, P. R. Bohjanen, and K. Nielsen. 2017. Different Lymphocyte Populations Direct Dichotomous Eosinophil or Neutrophil Responses to Pulmonary Cryptococcus Infection. *J Immunol* 198: 1627-1637.
389. Daley, J. M., A. A. Thomay, M. D. Connolly, J. S. Reichner, and J. E. Albina. 2008. Use of Ly6G-specific monoclonal antibody to deplete neutrophils in mice. *J Leukoc Biol* 83: 64-70.
390. Hasenberg, A., M. Hasenberg, L. Mann, F. Neumann, L. Borkenstein, M. Stecher, A. Kraus, D. R. Engel, A. Klingberg, P. Seddigh, Z. Abdullah, S. Klebow, S. Engelmann, A. Reinhold, S. Brandau, M. Seeling, A. Waisman, B. Schraven, J. R. Gothert, F. Nimmerjahn, and M. Gunzer. 2015. Catchup: a mouse model for imaging-based tracking and modulation of neutrophil granulocytes. *Nat Methods* 12: 445-452.
391. Barquero-Calvo, E., A. Martirosyan, D. Ordonez-Rueda, V. Arce-Gorvel, A. Alfaro-Alarcon, H. Lepidi, B. Malissen, M. Malissen, J. P. Gorvel, and E. Moreno. 2013. Neutrophils exert a suppressive effect on Th1 responses to intracellular pathogen Brucella abortus. *PLoS Pathog* 9: e1003167.
392. Yang, C. W., B. S. Strong, M. J. Miller, and E. R. Unanue. 2010. Neutrophils influence the level of antigen presentation during the immune response to protein antigens in adjuvants. *J Immunol* 185: 2927-2934.
393. Eken, C., O. Gasser, G. Zenhaeusern, I. Oehri, C. Hess, and J. A. Schifferli. 2008. Polymorphonuclear neutrophil-derived ectosomes interfere with the maturation of monocyte-derived dendritic cells. *J Immunol* 180: 817-824.
394. Gasser, O., and J. A. Schifferli. 2004. Activated polymorphonuclear neutrophils disseminate anti-inflammatory microparticles by ectocytosis. *Blood* 104: 2543-2548.
395. Bourke, E., A. Cassetti, A. Villa, E. Fadlon, F. Colotta, and A. Mantovani. 2003. IL-1 beta scavenging by the type II IL-1 decoy receptor in human neutrophils. *J Immunol* 170: 5999-6005.
396. Santarlasci, V., L. Cosmi, L. Maggi, F. Liotta, and F. Annunziato. 2013. IL-1 and T Helper Immune Responses. *Front Immunol* 4: 182.
397. Chung, Y., S. H. Chang, G. J. Martinez, X. O. Yang, R. Nurieva, H. S. Kang, L. Ma, S. S. Watowich, A. M. Jetten, Q. Tian, and C. Dong. 2009. Critical regulation of early Th17 cell differentiation by interleukin-1 signaling. *Immunity* 30: 576-587.
398. Sutton, C., C. Brereton, B. Keogh, K. H. Mills, and E. C. Lavelle. 2006. A crucial role for interleukin (IL)-1 in the induction of IL-17-producing T cells that mediate autoimmune encephalomyelitis. *J Exp Med* 203: 1685-1691.
399. Sims, J. E., and D. E. Smith. 2010. The IL-1 family: regulators of immunity. *Nat Rev Immunol* 10: 89-102.
400. Hung, C. Y., P. Jimenez-Alzate Mdel, A. Gonzalez, M. Wuthrich, B. S. Klein, and G. T. Cole. 2014. Interleukin-1 receptor but not Toll-like receptor 2 is essential for MyD88-dependent Th17 immunity to Coccidioides infection. *Infect Immun* 82: 2106-2114.
401. Xin, L., Y. Li, and L. Soong. 2007. Role of interleukin-1beta in activating the CD11c(high) CD45RB- dendritic cell subset and priming Leishmania amazonensis-specific CD4+ T cells in vitro and in vivo. *Infect Immun* 75: 5018-5026.

402. Hunter, C. A., R. Chizzonite, and J. S. Remington. 1995. IL-1 beta is required for IL-12 to induce production of IFN-gamma by NK cells. A role for IL-1 beta in the T cell-independent mechanism of resistance against intracellular pathogens. *J Immunol* 155: 4347-4354.
403. Denis, M., and E. Ghadirian. 1994. Interleukin-1 is involved in mouse resistance to Mycobacterium avium. *Infect Immun* 62: 457-461.
404. Chen, W., E. A. Havell, L. L. Moldawer, K. W. McIntyre, R. A. Chizzonite, and A. G. Harmsen. 1992. Interleukin 1: an important mediator of host resistance against Pneumocystis carinii. *J Exp Med* 176: 713-718.
405. Juffermans, N. P., S. Florquin, L. Camoglio, A. Verbon, A. H. Kolk, P. Speelman, S. J. van Deventer, and T. van Der Poll. 2000. Interleukin-1 signaling is essential for host defense during murine pulmonary tuberculosis. *J Infect Dis* 182: 902-908.
406. Caffrey, A. K., M. M. Lehmann, J. M. Zickovich, V. Espinosa, K. M. Shepardson, C. P. Watschke, K. M. Hilmer, A. Thammahong, B. M. Barker, A. Rivera, R. A. Cramer, and J. J. Obar. 2015. IL-1alpha signaling is critical for leukocyte recruitment after pulmonary Aspergillus fumigatus challenge. *PLoS Pathog* 11: e1004625.
407. Sainz, J., E. Perez, S. Gomez-Lopera, and M. Jurado. 2008. IL1 gene cluster polymorphisms and its haplotypes may predict the risk to develop invasive pulmonary aspergillosis and modulate C-reactive protein level. *J Clin Immunol* 28: 473-485.
408. Wojtowicz, A., M. S. Gresnigt, T. Lecompte, S. Bibert, O. Manuel, L. A. Joosten, S. Rueger, C. Berger, K. Boggian, A. Cusini, C. Garzoni, H. H. Hirsch, M. Weisser, N. J. Mueller, P. R. Meylan, J. Steiger, Z. Kutalik, M. Pascual, C. van Delden, F. L. van de Veerdonk, P. Y. Bochud, S. Swiss Transplant Cohort, and S. Swiss Transplant Cohort Study. 2015. IL1B and DEFB1 Polymorphisms Increase Susceptibility to Invasive Mold Infection After Solid-Organ Transplantation. *J Infect Dis* 211: 1646-1657.
409. Romani, L. 2004. Immunity to fungal infections. *Nat Rev Immunol* 4: 1-23.
410. Mayer-Barber, K. D., and B. Yan. 2017. Clash of the Cytokine Titans: counter-regulation of interleukin-1 and type I interferon-mediated inflammatory responses. *Cell Mol Immunol* 14: 22-35.
411. Van't Wout, J. W., J. W. Van der Meer, M. Barza, and C. A. Dinarello. 1988. Protection of neutropenic mice from lethal Candida albicans infection by recombinant interleukin 1. *Eur J Immunol* 18: 1143-1146.
412. Vonk, A. G., M. G. Netea, J. H. van Krieken, Y. Iwakura, J. W. van der Meer, and B. J. Kullberg. 2006. Endogenous interleukin (IL)-1 alpha and IL-1 beta are crucial for host defense against disseminated candidiasis. *J Infect Dis* 193: 1419-1426.
413. Deepe, G. S., Jr., and M. McGuinness. 2006. Interleukin-1 and host control of pulmonary histoplasmosis. *J Infect Dis* 194: 855-864.
414. Huffnagle, G. B., and M. F. Lipscomb. 1992. Pulmonary cryptococcosis. *Am J Pathol* 141: 1517-1520.
415. Casadevall, A., and L. A. Pirofski. 2009. Virulence factors and their mechanisms of action: the view from a damage-response framework. *J Water Health* 7 Suppl 1: S2-S18.
416. Wiesner, D. L., and D. R. Boulware. 2011. Cryptococcus-Related Immune Reconstitution Inflammatory Syndrome(IRIS): Pathogenesis and Its Clinical Implications. *Curr Fungal Infect Rep* 5: 252-261.
417. D'Elia, R. V., K. Harrison, P. C. Oyston, R. A. Lukaszewski, and G. C. Clark. 2013. Targeting the "cytokine storm" for therapeutic benefit. *Clin Vaccine Immunol* 20: 319-327.
418. Boulware, D. R., D. B. Meya, T. L. Bergemann, D. L. Wiesner, J. Rhein, A. Musubire, S. J. Lee, A. Kambugu, E. N. Janoff, and P. R. Bohjanen. 2010. Clinical features and serum biomarkers in HIV

immune reconstitution inflammatory syndrome after cryptococcal meningitis: a prospective cohort study. *PLoS Med* 7: e1000384.
419. Kincaid, E. 2016. Of mice and interaction: A new way to investigate complex genetic traits. *Nat Med* 22: 1065-1066.
420. Erickson, R. P. 1996. Mouse models of human genetic disease: which mouse is more like a man? *Bioessays* 18: 993-998.
421. Mott, R., and J. Flint. 2013. Dissecting quantitative traits in mice. *Annu Rev Genomics Hum Genet* 14: 421-439.